AUTONOMA UNIVERSITY OF MADRID

BIOCHEMISTRY DEPARMENT

Generation and characterization of a K-*Ras* model of Noonan syndrome

DOCTORAL THESIS

Isabel Hernández Porras

Madrid, 2014

BIOCHEMISTRY DEPARMENT

Faculty of Medicine

AUTONOMA UNIVERSITY OF MADRID

Generation and characterization of a K-*Ras* model of Noonan syndrome

Isabel Hernández Porras

Graduated in Biology and Biochemistry

Directors: Dr. Mariano Barbacid and Dr. María del Carmen Guerra

Spanish National Cancer Center (CNIO)

Madrid, 2014

A mis padres, hermana y a Pedro

Parafraseando a Ortega y Gasset " *Yo soy yo y mis circunstancias*". Nuestra vida es inconcebible sin las personas y las situaciones que nos rodean en todo momento. Utilizando esta cita puedo decir que esta tesis no hubiese sido posible sin la ayuda de todas las personas que han puesto, a lo largo de estos 6 años, su granito de arena y las que me gustaría que tuvieran su protagonismo en estas páginas.

En primer lugar me gustaría agradecer a Mariano por abrirme las puertas de su laboratorio y por darme la oportunidad de desarrollar este maravilloso proyecto. Por confiar en mis posibilidades y por enseñarme la importancia de los pequeños detalles que son los que al final hacen que un trabajo sea excelente.

También me gustaría a agradecer a Carmen por toda su ayuda, sus múltiples ideas y sus valiosos consejos. Por apostar por mi después de mis prácticas de verano, por tener siempre la puerta abierta de su despacho para poder consultarle tanto un problema científico como personal y por todo lo que me ha enseñado. Además, creo que nunca olvidaré nuestro viaje a Chicago, el éxito de mi charla no hubiera sido posible sin su apoyo y sin esos maravillosos momentos de relajación que tuvimos.

Por su puesto no querría olvidarme de nuestros colaboradores, Xosé Bustelo y Salvatore Fabbiano (CIC de Salamanca), Manuel Desco y Lorena Cussó (Instituto de Investigación Sanitaria Gregorio Marañón), Isabel Valera y Raquel Martínez (Servicio de Evaluación Neurofuncional no Invasiva. Instituto Biomédicas Alberto Sols CSIC-UAM. Servicio de Evaluación Funcional de Animales de Laboratorio, CIBERER, ISCII) y Christopher Heeschen y Alexandra Aicher (CNIO), sin ellos hubiese sido imposible analizar algunas de las múltiples alteraciones que íbamos encontrando en nuestro modelo. Muchas gracias por vuestra ayuda y paciencia. Tampoco querría olvidarme de todas las unidades del CNIO que en algún momento han estado involucradas en este proyecto. Gracias a la unidad de imagen, en especial a Paqui Mulero por su disposición y ayuda y a Juanan, por todas las horas que ha pasado con las mediciones de mis ratones y por las reconstrucciones tan chulas que ha hecho. Gracias a todas las chicas de histología, por todos los cortes, tinciones, por las seriaciones de embriones que "tanto" les han gustado y por ser pacientes con todos mis errores. A Marta Cañamero, por todas esas horas pegadas al microscopio volviéndonos locas con los bazos de los ratones y por su interés y ayuda con el tema de mis vértigos. Gracias a la unidad de transgénicos en especial a Sagrario, Marta y Jaime y la unidad de citometría. Y por último quería dar las gracias a Isabel Blanco y a mis chicas del animalario, Isabel Aragón, Isabel Agudo y May por cuidar tan bien de mis ratones. Agudo, muchas gracias por todos los tratamientos de fin de semana, no se lo que hubiera hecho sin ti. Y May, muchas gracias por seguirme en todas las cosas locas que te he propuesto, en el fondo nos lo hemos pasado bien haciéndoles perrerías a los ratones y sobre todo muchas gracias por tu apoyo y por escucharme en mis malos momentos. Por último,

muchas gracias a Arantxa por enseñarme el complejo mundo de la citometría y José Ligos (CNIC) por salvarnos con el experimento de proliferación.

También quiero agradecer a todos mis compañeros de Oncología Experimental, los que estaban aquí cuando llegué, Mikel, Jelena, Marta, Antonio, Javier, Alberto, Rafa, Sara y Sarah (espero que no se me haya olvidado nadie) y a todos los que están ahora. Muchas gracias Alberto por iniciar este proyecto, por todo lo que me has enseñado, por tus ánimos y por esos piropos que me han alegrado muchos días. Gracias Rafa, por ayudarme con las infecciones. Muchas gracias a mis vecinas Magdy y Lucía, a Matthias, Harrys, Cathy, Teresa, Mónica, David, Chiara, Patri y Raquel García por toda vuestra ayuda y apoyo. Muchas gracias a Rasky por todo su trabajo, aunque tengo que decirte que aún tienes pendiente la visita a Salamanca y eso tienes que intentar solucionarlo lo antes posible. A Nuria, por toda su ayuda mientras estuviste de prácticas y por todos los miles de cortes que te pido. A Lechuga por estar siempre dispuesta a ayudar, por todo lo que me has enseñado, por tener siempre una sonrisa en la cara y por estar pendiente de mí para animarme. A Marta por todo lo que me has ayudado, por todas nuestras charlas, momentos de investigaciones y cotilleos, por compartir nuestra "buena mala salud" y por estar siempre que he necesitado un consejo. Finalmente, Bea, creo que no tengo palabras suficientes para agradecerte todo lo que me ayudas, eres mis segundas manos, un trocito importante de esta tesis es tuya. Muchas gracias por tus ánimos, tu optimismo, tus locuras, por los cafés, compras, las visitas a Salamanca, los conciertos y por todos los momentos que nos quedan, ahora que tendré más tiempo empieza la diversión.

Muchas gracias a tod@s mis estudiantes de prácticas. Sois muchos lo que habéis pasado por aquí en estos años. Gracias a Álvaro, Patri, Eva, Almudena, Rocío, Cristina, Renz, Ruth, Sara, Inma y a mis últimas estudiantes Gema y Fanni por vuestra ayuda. Gracias a Paulita, no sólo por todas las cosas con las que me has ayudado en este proyecto, sino por estar ahí, por tus "A ver Isa vamos a organizarnos", por tu apoyo, por saber escuchar, por tu alegría e ilusión, por las compras, las excursiones y por los buenos momentos que me has hecho y me harás pasar.

Gracias a Silvia, por compartir conmigo todos estos años, por sufrir juntas durante la carrera y seguir sufriendo, aunque por separado, durante mi tesis. Por todos los buenos momentos que hemos pasado juntas y por alegrarte tanto de las cosas que consigo.

Gracias a mis padres, por enseñarme a ser como soy, por inculcarme lo importante que es el trabajo, los estudios y ser humilde, por vuestro apoyo, por sufrir cuando yo sufro y reír cuando yo río. Siempre habéis estado a mi lado, desde el principio, en los malos y buenos momentos. Gracias por ayudarme a no tirar la toalla, por entender que aún estando sólo a dos horas y media de distancia no podíamos vernos nada más que una vez cada tres meses y por vuestro sacrificio. Gracias a mi abuela, simplemente por ser la mejor abuela que existe. Gracias a mi hermana, por ser también mi amiga, por todos tus ánimos, tus locuras y tu manera de ver la vida. Parece mentira que aún siendo la pequeña tengas tantas cosas que enseñarme. Gracias por

todos esos “monitos” y mensajes que me mandas cuando estoy triste, por todos los buenos momentos que hemos pasado juntas, por todas esas tardes de hermanas y por estar ahí siempre que te necesito.

Por último, y no menos importante, muchas gracias a mi compañero, amigo y a la persona con la que comparto mi vida, Pedro. Podría llenar hojas enteras agradeciéndote todo lo que me has ayudado durante la tesis, nadie como tú sabe el sacrificio que nos ha costado ésto y nadie como tú ha sabido entenderlo. Muchas gracias por sacarme una y otra vez del pozo, por aguantar mis inseguridades, por escuchar mis charlas una y otra vez y por entender lo importante que era ésto para mí. Han sido seis años de muchas horas de trabajo, de fines de semana en el laboratorio o en casa delante del ordenador, de vacaciones reducidas a la mínima expresión, de planes que al final no hemos podido hacer y de horas que no hemos pasado juntos y en ningún momento te has quejado. Muchas gracias por cuidarme, por preocuparte de mí, por hacerme reír y por estar siempre a mi lado.

Resumen/Summary

El síndrome Noonan (SN) es un síndrome autosómico dominante caracterizado por dismorfia facial, baja estatura, alteraciones cardiacas, anomalías esqueléticas y retraso mental, presentando además una predisposición moderada a desarrollar desórdenes proliferativos, como la leucemia juvenil mielomonocítica y el desorden mieloproliferativo. Seis genes de la ruta de señalización RAS-MAPK, entre los que se incluyen *PTPN11*, *SOS1*, K-*RAS*, N-*RAS*, *RAF1* y B-*RAF*, se han asociado con el SN (1). Recientemente, se han encontrado mutaciones en *RIT1*, un miembro perteneciente a la subfamilia de RAS, en pacientes con SN (2). Aunque K-*RAS* se encuentra mutado en un pequeño porcentaje de pacientes (<2%), estas mutaciones se asocian a con un fenotipo más severo. Se han descrito 14 mutaciones del gen K-*RAS* en pacientes con SN. Todas ellas resultan en una activación intermedia de la proteína en comparación con la mutaciones típicamente oncogénicas y son distintas a las descritas en tumores humanos (3).

En este trabajo, hemos generado un modelo knock-in que expresa la mutación de K-*RAS* más frecuentemente asociada a pacientes con SN, la sustitución V14I (4). Estos ratones desarrollan muchas de las alteraciones típicas del SN, como retraso en el crecimiento, dismorfia facial, alteraciones cardiacas y desorden mieloproliferativo. Además, los ratones homocigotos presentan letalidad perinatal cuya penetrancia depende del fondo genético. Aparte del desorden mieloproliferativo, los ratones mutantes muestran una predisposición al desarrollo tumoral, presentando una reducción de su supervivencia debido al desarrollo de múltiples neoplasias como leucemias, sarcomas histiocíticos y carcinomas. Así mismo, esta mutación coopera con genes supresores de tumores (*p16Ink4a/p19Arf* y *Trp53*) y con eventos de tipo no genético que causan daño tisular y/o respuesta inflamatoria, como la pancreatitis, inducida por el tratamiento con ceruleína y el tratamiento con nicotina, uno de los principales componentes del tabaco. Finalmente, el tratamiento prenatal con el inhibidor de MEK PD0325901 rescató la letalidad perinatal y previno el retraso en el crecimiento y las alteraciones craneofaciales y cardiacas. Sin embargo, ninguna de estas alteraciones se corrigieron cuando los ratones fueron tratados al destete. El tratamiento este inhibidor tampoco permitió prevenir el desarrollo del desorden mieloproliferativo independientemente del tiempo de inicio del mismo. Sin embargo, retrasó el desarrollo de la enfermedad, incrementando ligeramente la supervivencia.

Referencias:

1. Rauen, K.A. 2013. The RASopathies. *Annu Rev Genomics Hum Genet* 14:355-69

2. Aoki, Y., et al. 2013. Gain-of-function mutations in RIT1 cause Noonan syndrome, a RAS/MAPK pathway syndrome. *Am J Hum Genet* 93**:**173-80.

3. Schubbert, S., et al. 2007. Biochemical and functional characterization of germ line KRAS mutations. *Mol Cell Biol* 27:7765-70.

4. Lo, F.S., et al. 2009. Noonan syndrome caused by germline KRAS mutation in Taiwan: report of two patients and a review of the literature. *Eur J Pediatr* 168:919-23.

Noonan syndrome (NS) is an autosomal dominant disorder characterized by a broad number of alterations including facial dysmorphia, short stature, congenital heart disease, skeletal abnormalities and learning disabilities. Noonan patients are associated with a moderate risk for proliferative disorders such as Juvenile Myelomonocytic Leukemia (JMML) and myeloproliferative disorders (MPD) (1). Six genes of the RAS-MAPK signaling pathway have been associated with NS including *PTPN11*, *SOS1*, K-*RAS*, N-*RAS*, *RAF1* and B-*RAF* (1). Recently, mutations in *RIT1*, a member of the RAS subfamily, have been also described in Noonan patients (2). Although K-*RAS* mutations are found in low percentage of clinical diagnosed patients (<2%), they usually correlate with more severe symptoms. 14 different K-*RAS* mutations have been described in Noonan patients. They result in milder activation of the protein compared to the oncogenic form and have not been identified in human tumors (3).

Here we describe the generation of a K-*Ras* knock-in mouse model induced by the expression of the most frequent K-*RAS* mutations in Noonan patients, the substitution V14I (4). Mutant mice displayed multiple NS-associated developmental defects such as growth delay, craniofacial dysmorphia, cardiac defects and hematological abnormalities, MPD. Homozygous animals had perinatal lethality whose penetrance varied with genetic background. Mutant mice had increased predisposition to tumor development other than MPD. These mice presented reduced life span due to the development of multiple malignancies including lymphomas, sarcomas and carcinomas. Moreover, this mutation cooperated with tumor suppressor genes such as *p16Ink4a/p19Arf* and *Trp53* and with non-genetic events involving tissue damage and/or inflammatory response, like pancreatitis induced by caerulein treatment and nicotine administration. Finally, prenatal exposure to the MEK inhibitor PD0325901 rescued the perinatal lethality and prevented the growth defects, craniofacial dysmorphia and cardiac defects. However, these alterations were not corrected when mice were treated after weaning. Indeed, this MEK inhibitor treatment failed to prevent development of MPD independently of the time of the initiation of the treatment, but slowed the development of the disease since a small benefit in the survival was found.

References:

1. Rauen, K.A. 2013. The RASopathies. *Annu Rev Genomics Hum Genet* 14:355-69

2. Aoki, Y., et al. 2013. Gain-of-function mutations in RIT1 cause Noonan syndrome, a RAS/MAPK pathway syndrome. *Am J Hum Genet* 93**:**173-80.

3. Schubbert, S., et al. 2007. Biochemical and functional characterization of germ line KRAS mutations. *Mol Cell Biol* 27:7765-70.

4. Lo, F.S., et al. 2009. Noonan syndrome caused by germline KRAS mutation in Taiwan: report of two patients and a review of the literature. *Eur J Pediatr* 168:919-23.

1. Index

2. Abbreviations

α–MHC:	*α **M**yosin **H**eavy **C**hain*
ABR:	*Auditory **B**rainstem **R**esponse*
AF6:	*ALL-1 **f**used gene on chromosome **6** protein*
AML:	*Acute **M**yeloid **L**eukemia*
ALL:	*Acute **L**ymphoblastic **L**eukemia*
AP1:	*Activator **P**rotein **1***
APC:	*Allo**p**hyco**c**yanin* (FACS analysis)
APC:	*Adenomatous **P**olyposis **C**oli* (Gen)
ARF:	*ADP **R**ibosylation **F**actors*
BAD:	***B**cl-2 **A**ssociated **D**eath protein*
BM:	***B**one **M**arrow*
BMC:	***B**one **M**ineral **C**ontent*
BMD:	***B**one **M**ineral **D**ensity*
BSA:	***B**ovine **S**erum **A**lbumin*
CAPRI:	***Ca**$^{2+}$ **P**romoted **R**AS **I**nactivator*
CBL:	***C**asitas **B**-Lineage **L**ymphoma*
CFC:	***C**ardio-**F**acio-**C**utaneous syndrome*
CFU-F:	***C**olony **F**orming **U**nits- **F**ibroblast*
CFU-GM:	***C**olony **F**orming **U**nit-**G**ranulocyte **M**acrophage*
CLP:	***C**ommon **L**ymphoid **P**rogenitors*
CMP:	***C**ommon **M**yeloid **P**rogenitors*
CO:	***C**ardiac **O**utput*
CS:	***C**ostello **S**yndrome*
Ct:	***C**ycle **t**hreshold*
CT:	***C**omputed **T**omography*
DAPI:	*4', 6-**dia**midino-2-**p**hen**y**ldole*
DORV:	***D**ouble **O**utlet **R**ight **V**entricle*
DMEM:	***D**ulbecco's **M**odified **E**agle **M**edium*

DMSO:	***D**imethyl **S**ulfoxide*
CMV-Cre:	***C**yto**m**egalo**v**irus Cre*
ECL:	***E**nhanced **C**hemiluminiscence **S**ystem*
EDTA:	***E**thylene **D**iamine **T**etraacetic **A**cid*
EDV:	***E**nd-**d**iastolic **v**olume*
EF:	***E**jection **F**raction*
EGFR:	***E**pidermal **G**rowth **F**actor **R**eceptor*
EGTA:	***E**thylene **G**lycol **T**etraacetic **A**cid*
ELK1:	*ETS domain-containing transcription factor*
ER:	***E**strogen **R**eceptor*
ERBB:	*v-erb-b2 avian Erythroblastic Leukemia Viral Oncogen Homolog*
ERK:	***E**xtracellular Signal **R**egulated **K**inase*
ESV:	***E**nd-**S**ystolic **V**olume*
ETS:	***E**26 **T**ransformation-specific **S**equence*
FACS:	***F**luorescence **A**ctivated **C**ell **S**orting*
FBS:	***F**etal **B**ovine **S**erum*
FCS:	***F**etal **C**alf **S**erum*
FITC:	***F**luorescein **I**so**th**yo**c**yanate*
FKHR:	*Forkhead Transcription Factor*
FOS:	*FBJ murine osteosarcoma viral oncogene homolog*
FOXO:	*Forhead box class O transcription factors*
FMO:	***F**lourescense **M**inus **O**ne*
FS:	***F**ractional **S**hortening*
GAP:	***G**TPase **A**ctivating **P**rotein*
GDP:	***G**uanosine **Dip**hosphate*
GEF:	***G**uanine **E**xchange **F**actor*
GEMM:	***G**enetically **E**ngineered **M**ouse **M**odel*
GH:	***G**rowth **H**ormone*

GM-CSF: ***G**ranulocyte-**M**acrophage **C**olony **S**timulating **F**actor*

GMP: ***G**ranulocyte **M**acrophage **P**rogenitor*

GRB2: ***G**rowth **F**actor **R**eceptor-**b**ound protein **2***

GTP: ***G**uanosine **t**ri**p**hosphate*

HCM: ***H**ypertrophic **C**ardio**m**iopathy*

HIF1α: ***H**ypoxia-**I**nducible **F**actor 1α*

HMG-CoA: *3-**H**ydroxy-3-**M**ethylglutamyl **Co**enzyme **A***

HR: ***H**eart **R**ate*

HSC: ***H**ematopoietic **S**tem **C**ell*

Hyg: ***Hyg**romicin*

H&E: ***H**ematoxylin and **E**osin*

IL3: ***I**nter**l**eukin 3*

IL6: ***I**nter**l**eukin 6*

IMDM: ***I**scove's **M**odified **D**ulbecco's **M**edium*

JMML: ***J**uvenile **M**yelo**m**onocytic **L**eukemia*

LIF: ***L**eukemia **I**nhibitory **F**actor*

LOH: ***L**oss **Of** **H**eterozygosity*

LS: ***L**EOPARD **S**yndrome*

LSK: ***L**ineage^{-}/**S**ca-1^{+}/c-**K**it^{+}*

LSL: ***L**ox-**S**TOP-**L**ox*

LVM: ***L**eft **V**entricle **M**ass*

MAP: ***M**itogen **A**ctivating **P**rotein*

MAPK: ***M**itogen **A**ctivating **P**rotein **K**inase*

MDS: ***M**yelo**d**isplastic **S**yndrome*

MEF: ***M**ouse **E**mbryonic **F**ibroblast*

MEK: *Mitogen Activating Protein (MAP) kinase kinase*

MEP: ***M**egakaryocyte-**E**rythroid **P**rogenitors*

MKK6: *Mitogen Activated Protein Kinase Kinase 6*

MPD: ***M**yeloproliferative **D**isorder*

MPP: ***M**ultipotent **P**rogenitor **P**opulation*

MRI: ***M**agnetic **R**esonance **I**maging*

NCFC: ***N**euro-**C**ardio- **F**acio-**C**utaneous*

NFR: ***N**uclear **F**ast **R**ed*

NF1: ***N**euro**f**ibromatosis type **1**/ **N**euro**f**ibromin **1***

NF-kB: ***N**uclear **F**actor- kB*

NL/MGCLS: ***N**oonan-**l**ike/ **M**ultiple **G**iant **C**ell **L**esions **S**yndrome*

NS: ***N**oonan **S**yndrome*

NS/LAH: ***N**oonan **S**yndrome-like with **L**oose **A**nagen **H**air*

PanIN: ***P**ancreatic **I**ntraepithelial **N**eoplasias*

PBS: ***P**hosphate **B**uffered **S**aline*

PCR: ***P**olymerase **C**hain **R**eaction*

PDAC: ***P**ancreatic **D**uctal **A**deno**c**arcinoma*

PDK1: *3-**P**hosphoinositide-**D**ependent protein **K**inase 1*

PE: ***P**hyco**e**rythrin*

PerCP: ***Per**idinin **C**hlorophyll **P**rotein*

PGK: ***P**hospho**g**lycerate **K**inase*

PIP2: ***P**hosphat**i**dylinositol-3,4,- Bi**p**hosphate*

PIP3: ***P**hosphat**i**dylinositol-3,4,5- Tri**p**hosphate*

PI3K: ***P**hosphat**i**dylinositol-4,5-bisphosphate **3**-**k**inase*

PS: ***P**hosphatidyl**s**erine*

PTEN: *Phosphatase and Tensin Homolog*

PTP: ***P**rotein **T**yrosine **P**hosphatase*

PTPN11: ***P**rotein **T**yrosine **P**hosphatase **N**on- receptor type **11***

RALBP1: ***R**AL **B**inding **P**rotein 1*

RALGDS: ***R**AL **G**uanine nucleotide **D**issociation **S**timulator*

RASGRF: ***R**AS-specific **G**uanine nucleotide-**R**eleasing **F**actor*

RASGRP1/4: ***RAS Guanyl- Releasing Protein***

RASSF: *RAS association domain-containing family*

RBD: ***RAS Binding Domain***

RIN-1: *RAS interaction/interference protein 1*

RIT: ***RAS like protein In Tissues***

RSK: ***Ribosomal S6 kinase***

RT: ***Room Temperature***

SCC: ***Saline Sodium Citrate***

SDS: ***Sodium Dodecyl Sulfate***

SHC: ***Src Homology 2 domain Containing protein***

SHOC2: *Soc2 Suppresor of Clear Homolog*

SHP-2: ***Src Homology Protein- 2***

SH2: ***Src Homology***

SOS1: ***Son of Sevenless 1***

SPRED1: *Sprouty-related, EVH1 domain-containing protein 1*

STAT3: ***Signal Transducer and Activator of Transcription-3***

TAE: ***Tris Acetate EDTA***

TAM: ***Tamoxifen***

TBS: ***Tris Buffered Saline***

TCEP: ***Tris (2' Carboxyethyl) phosphine***

TE: ***Echo Time***

TGF-α: ***Transforming Growth Factor α***

TIAM1: ***T-cell lymphoma Invasion And Metastasis 1***

TK: ***Thymide Kinase***

TR: ***Repetition Time***

VPR: ***Volume Pressure Recording***

UV: ***Ultraviolet***

WBC: ***White Blood Cell***

WT:	***W**ild **T**ype*
WTd:	***W**all **T**hickness in **d**iastole*
WTn:	*Systolic wall thickening*
WTs:	***W**all **T**hickeness in **s**ystole*
ZONAB:	***ZO**-1 **N**ucleic **A**cid **B**inding protein*
4OHT:	**4**-*Hydroxy-tamoxifen*

3. Introduction

Oncogenic properties of *RAS* genes and RAS signaling pathway have been deeply studied *(132)*. In 1990 germline mutations in *NF1* gene (neurofibromin 1) was associated with the Neurofibromatosis type 1 (NF1) *(34)* and in 2001, *PTPN11* (Protein tyrosine phosphatase non-receptor type 11) was described in more than 50% of patients with Noonan syndrome (NS) *(211)*. These studies provided the first association between activated mutations in RAS signaling members and developmental disorders. In 2005, H-*RAS* oncogene was found mutated in Costello syndrome (CS) patients (*12*). More recently, mutations in the K-*RAS* and N-*RAS* oncogenes have been found in NS patients *(41, 188)*.

These findings provide strong indication that developmental disorders result from the novo germline mutations that alter the RAS/MAPK signaling pathway. These syndromes [Cardio-facio-cutaneous syndrome (CFC), Costello syndrome (CS), LEOPARD syndrome (LS), Neurofibromatosis type 1 (NF1) and Noonan syndrome (NS)] share phenotypic features: facial abnormalities, heart defects, impaired growth, cancer predisposition and neurocognitives alterations. Based on these phenotypic similarities these congenital alterations are known as 'Neuro-Cardio-Facial-Cutaneous' (NCFC) and due to their association with the RAS/MAPK pathway dysregulation they are also called 'RASopathies' *(165)*.

The generation of mouse models expressing different mutations identified in these patients help to understand the developmental and physiological defects associated with each syndrome and to evaluate preventative and therapeutic strategies. This thesis presents the generation and characterization of a K-*Ras* knock-in mouse model for NS.

3.1 RAS PROTEINS

Rat sarcoma (RAS) proteins are signaling switch molecules that regulate proliferation, differentiation and survival in response to extracellular stimuli. RAS proteins are small GTPase proteins that cycle between inactive guanosine diphosphate (GDP)-bound and active guanosinetriphosphate (GTP)-bound conformations (RAS–GDP and RAS–GTP, respectively). In absence of stimuli (including soluble growth factors), the RAS proteins are inactive and bound to GDP. The stimulation takes place when GDP is exchanged by GTP driving by the guanine-exchange factors (GEFs). These proteins displace guanine nucleotides from RAS and permit passive binding to GTP, which is abundant in the cytosol ***(Figure 1)***. In the presence of stimuli, the active receptors create intracellular docking sites for adaptor molecules and signal relay proteins, such as GRB2 and SHC that recruit and activate GEFs, such as SOS1/2, RASGRF and RASGRP1/4 *(132)*. RAS signaling is finished by hydrolysis to RAS-GDP driven by their intrinsic GTPase activity. Several GTPase activating proteins (GAPs) markedly stimulate intrinsic GTPase activity by stabilizing a high-energy transition state that occurs

during the RAS–GTP hydrolysis reaction ***(Figure 1).*** Some of these proteins are NF1, p120GAP, GAP1m, GAPIII and CAPRI *(132).*

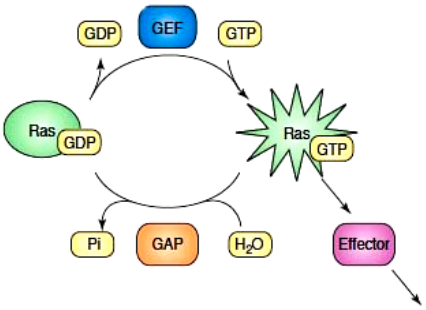

Figure 1. Schematic representation of RAS regulation. RAS cycling between an inactive state bound to GDP and an active state bound to GTP. Guanosine-exchange factors (GEF) promote the exchange of GDP for GTP. GTPase activating proteins (GAPs) catalyze the hydrolysis of GTP. Adapted from Repasky et al., 2004 *(169).*

The RAS wild type forms are called proto-oncogenes due to their oncogenic potential after acquisition of mutations that inhibit the GTPase activity and lock the protein in the active GTP bound conformation. The mutant forms of the *RAS* genes that confer a constitutive active form of the proteins are called *RAS* oncogenes.

3.1.1 The superfamily of RAS proteins

The Ras superfamily comprises over 150 members with evolutionarily conserved orthologs *(44).* This superfamily is divided in 5 families: Rho, Rab, Ran, Arf and Ras *(231).*

The Rho family is involved in signaling networks that regulate actin organization, cell cycle progression and gene expression. In addition they are implicated in hematopoiesis. The Rab family, the largest family of the Ras superfamily, participates in vesicular transport and the trafficking of proteins between different organelles of the endocytic and secretory pathways. In eukaryotas, Ran family only comprises one member, the RAN proteins. By contrast, these proteins are the most abundant and are involved in nuclear transport. Finally, the Arf family is involved in vesicular transport regulation of the exocytic and endocytic pathways *(176).*

Ras family comprises 36 genes, which encode 39 proteins. These members are included in seven subgroups based on the homology of their effector domain: RAP (RAP-1A, RAP-1B, RAP-2A and RAP-2B), R-RAS (R-RAS and TC21/R-RAS2), RIT (RIT1 and RIT2), M-RAS, E-RAS, RAL (RAL and RALB) and RAS *(55, 44, 97).* The subfamily RAS includes 3 genes, which encode 4 small proteins (21 kDa): H-RAS, N-RAS, K-RAS 4A and K-RAS 4B *(124).*

3.1.2 *RAS* proto-oncogenes structure

RAS proto-oncogenes are highly conserved from yeast to human and play a key role in signal transduction. The *RAS* subfamily includes 3 genes: H-*RAS1* (in this thesis H-*RAS*), K-*RAS2* (in this thesis K-*RAS*) and N-*RAS* and 2 pseudogenes: H-*RAS2* y K-*RAS1*. In humans H-

RAS, K-*RAS* y N-*RAS* genes are located in chromosomes 11, 12 and 1, respectively. In mice, H-*Ras*, K-*Ras* and N-*Ras* genes are located in chromosomes 7, 6 and 3, respectively *(17)*.

The structure of the RAS genes is highly conserved, with a first non-coding exon (exon 0) and four coding exons. K-*RAS* presents two alternative forms (4A and 4B), which leads through an alternative splicing to the synthesis of two isoforms, K-RAS 4A and K-RAS 4B, that differ in the last 25 carboxy terminal amino acids *(17, 80)*. However, *RAS* genes differ significantly in the intron sequence and size, resulting in a marked gene length difference: K-*RAS* (35 kb), N-*RAS* (7 kb) and H-*RAS* (3 kb) *(124)*.

3.1.3 RAS proteins structure

The three *RAS* genes encode four highly homologous 21 kDa proteins with 188 amino acids (K-RAS 4B) and 189 amino acids (H-RAS, N-RAS y K-RAS 4A). The N-terminal portion (residues 1–165) of H-RAS, K-RAS and N-RAS comprises a highly conserved G domain that has a common structure. RAS proteins diverge substantially at the C-terminal end, which is known as the hypervariable region (residues 165-188/189).

The first 85 aminoacids of the G domain contain the GDP and GTP binding sites. This region is identical in all the RAS proteins and presents the phosphate-binding loop (P-loop) (residues 10-16) and the nucleotide-sensitive switch I (residues 32–38) and II (residues 59-67) regions. The P-loop is the binding site of the γ phosphate of the GTP. The nucleotide-sensitive switch regions are essential for the control of RAS signaling durations. Switch I controls the binding of GAPs and switch II is involved in the interaction with the GEFs *(93, 160, 235)*. The next 80 amino acids define a second region where mammalian RAS proteins diverge only slightly from each other, exhibiting an 85% homology.

The remaining C-terminal sequence, the hypervariable region, contains sequences that specify post-translational modifications that are essential for targeting RAS proteins to the cellular membranes. All RAS proteins present a CAAX motif, in which C is cysteine, A is usually an aliphatic amino acid and X is residue that contributes to substrate specificity. In the case of H-RAS is a Serine and in the case of K-RAS and N-RAS a Methionine *(72, 234)*. The initial modification is directed by the farnesyl transferase, a cytosolic enzyme that attaches a farnesyl group to the cysteine of the CAAX motif *(71)*. In H-RAS, N-RAS and K-RAS4A, this binding is complemented by palmitoylation on cysteine residues in the hypervariable region of the protein (the so-called ‘second signal’) to anchor the Ras proteins to the membrane. By contrast, K-RAS4B, the predominant splice variant (from now on as K-RAS), contains an alternative second signal composed by a polybasic stretch of lysine residues. In this case, membrane anchoring is mediated by the electropositive lysines that form ionic bonds to the electronegative lipid head groups of the inner leaflet of the plasma membrane *(187)*.

3.2 SIGNALING DOWNSTREAM RAS

GTP–bound RAS, the active form, can interact productively with more than 20 effectors to regulate several cellular responses, including proliferation, differentiation and survival. The most important effectors include RAF, phosphatidylinositol 3-kinase (PI3K) and Ral guanine nucleotide dissociation stimulator (RALGDS) *(53, 187)* ***(Figure 2)***.

The first mammalian effector to be characterized, and the most intensively studied, is the protein serine/threonine kinase RAF. GTP-bound RAS binds to, and contributes to the activation of, the three RAF proteins, A-RAF, RAF1 or C-RAF and B-RAF. This interaction causes RAF to be relocated to the plasma membrane, which seems to be crucial for its activation by serine/threonin phosphorylation *(116, 134)*. Activated RAF subsequently activates by phosphorylation the Mitogen Activating Protein (MAP) kinase kinase 1 and 2 (MEK 1 and MEK 2), which afterward activates by phosphorylation the Extracellular signal-Regulated Kinases 1 and 2 (ERK1 and ERK2). Substrates for ERK1/2 include cytosolic and nuclear factors (such as transcription factors), reflecting that they can be transported into the nucleus after activation. One of this transcription factors is the ETS domain-containing transcription factor (ELK1), an E26 transformation-specific sequence (ETS) family member that forms part of the serum response factor that regulates FOS expression *(242)*. ERK1/2 proteins can also phosphorylate and activate the transcription factor JUN. JUN and FOS proteins form the activator protein 1 (AP1) transcription factor. Activation of these transcriptional regulators can lead to the expression of proteins that control cell-cycle progression, such as cyclin D *(161)*. Hence, RAF activation can promote cell cycle progression. For this reason, the RAF/MEK/ERK pathway is also known as the mitogen or proliferative pathway.

RAS–GTP also binds to the catalytic subunit of type I PI3Ks *(156, 175),* resulting in the translocation of PI3K to the plasma membrane and subsequent activation. PI3K phosphorylates phosphatidylinositol-4,5-bisphosphate (PIP2) to generate phosphatidylinositol-3,4,5-triphosphate (PIP3), a second messenger that binds to a large number of proteins, for instance the kinases PDK1 (3-phosphoinositide-dependent protein kinase 1) and AKT *(16),* controlling their activity. PDK1 is important for the activation of a large number of protein kinases of the AGC family, including AKT, some PKCs, p70 S67K and RSK. AKT promotes survival by inactivation though phosphorylation pro-apoptotic proteins including BAD and Forkhead (FKHR) transcription factors *(79, 227)*. PI3K-AKT signals also control several growth-regulatory transcription factors, including FOXO proteins and nuclear factor-kB (NF-kB) *(16)*. FOXO proteins control the pace of the cell cycle, as well as apoptosis, DNA repair and protection from oxidative damage *(218, 228)*. AKT signaling works as a negative control of these proteins. Whereas FOXO is inactive by AKT, the transcription factor NF-kB is activated, which positively regulates cell survival, proliferation, chemoresistance, angiogenesis, cellular

invasion and oncogenesis *(3, 96)*. The PI3K/PDK1/AKT pathway has a strong anti-apoptotic function and seems to be an important part of the survival signal generated by RAS. In addition PI3K activation leads to stimulation of RAC, a RHO family protein involved in the regulation of the actin cytoskeleton and the transcription factor, such as NF-kB *(109, 131)*.

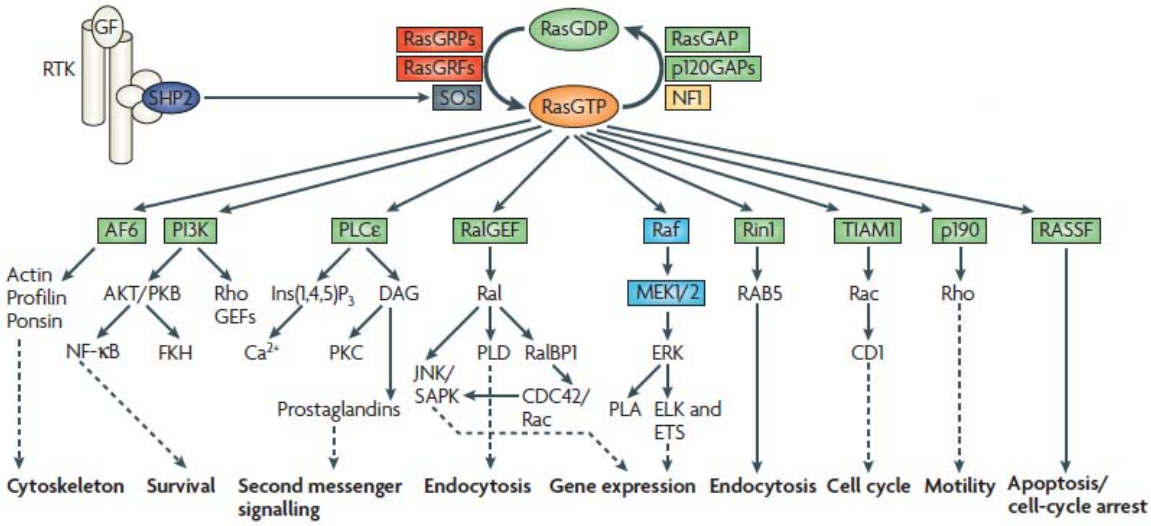

Figure 2. Ras signaling network. RAS proteins are signaling switch proteins that, in response to extracellular stimuli, induce a complex signaling network that control several cellular responses. Adapted from Karnoub et al., 2008 *(97)*.

RALGDS is the third best-studied effector, an ubiquitous protein that present a large number of targets *(59)*. RAL interacts with the phospholipase D1 and ARF mediating vesicle transport and membrane traffic *(88, 125)* and with SEC5, Filamin, RALBP1 and ZONAB regulating endocytosis, exocytosis, actin organization and controlling of gen expression *(142, 22, 58, 173)*. The RAS-GDS-RAL pathway has been shown to be involved in modulation of the activity of transcription factors, like the FOXO family proteins *(50)*.

Although initial studies established a relatively minor role for RAS-RALGDS-RAL pathway in cell transformation *(58, 169)*, recent studies indicated a crucial role *(71)*. RALGDS was required for tumor formation in a mouse model of Ras-dependent skin carcinogenesis *(63)* and the activation of this pathway was necessary and sufficient to induce the growth of non-metastatic prostate cancer cells promoting bone metastasis in xenograft models *(240)*.

Many other effectors are directly coupled to RAS-GTP, several of which have known roles in regulating cellular responses: Phospholipase Cε, which promotes the hydrolysis of PIP2 to diacylglycerol and inositol-1,4,5-triphosphate and the subsequence calcium mobilization and protein kinase C activation *(98, 198, 202)*. RAC exchange factor TIAM1 (T-cell lymphoma invasion and metastasis 1) also binds directly to RAS-GTP, leading to increased levels of RAC and subsequent actin reorganization *(109)*. Other RAS effectors include the RAS

interaction/interference protein-1 (RIN1), ALL-1 fused gene on chromosome 6 protein (AF6) and the RAS association domain-containing family (RASSF) proteins *(97)*.

RAS proteins control several important cellular functions by the interaction with many effectors. Therefore, the correct regulation of this complex signaling pathway is essential for the maintenance of cellular homeostasis.

3.2.1 Aberrant signaling in human tumors

Around 30% of human tumors present activating *RAS* mutations (35). The most frequently mutated isoform is K-*RAS*. These mutations are found in around 22% of tumors and preferentially in pancreatic ductal adenocarcinomas (90%), colorectal cancer (45%) and lung adenocarcinomas (35%) *(60)*. By comparison, the rates of N-*RAS* and H-*RAS* oncogenic mutations are much lower (6% and 3%, respectively) and the tissue distribution is different to K-*RAS* mutations ***(Table 1 in Appendix I).***

In most cases, these somatic missense mutations introduce amino acid substitutions at positions 12, 13 and 61, which impair the intrinsic GTPase activity and confer resistance to GAPs, thereby causing RAS to accumulate in the GTP-bound active form *(24, 217)*. Three-dimensional studies of the RAS structure indicate that oncogenic mutations of Q61 impair the GTP hydrolysis reaction by interfering with the coordination of a water molecule that is required for the nucleophilic attack on the γ-phosphate of GTP *(31, 184)*. Similarly, oncogenic substitutions in residues G12 and G13 prevent the formation of van der Waals bonds between RAS and GAP through steric hindrance and so perturb the proper orientation of the catalytic glutamine (Q61) in RAS, which results in the pronounced attenuation of GTP hydrolysis *(183)*.

RAS can also be activated by alterations in other members of their activating pathway. For instance, in some tumors the activation of the protein is due to loss of GAPs. The most significant example is the NF1, a developmental disorder that is characterized by large number tumors. These tumors are induced by the elimination of both copies of NF1 that encodes the neurofibromin protein, one of the main GAPs of RAS, resulting in the activation of RAS pathway *(see for more details the 2.3.1 section) (230)*.

In some tumors, RAS is activated by the overexpression of the growth factor receptor tyrosine kinases. The most common examples are EGFR and ERBB (HER2/neu), which are frequently activated by their overexpression in breast, ovarian and stomach carcinomas *(140)*. In other tumors like glioblastoma, EGFR is hyperactivated by the expression of a truncated receptor that lacks part of the extracellular domain. This modification promotes a ligand-independent receptor activation and a constitutive activation of the pathway *(106)*. EGFR-family tyrosine kinases are also commonly activated in tumors of epithelial origin by the autocrine production of EGF-like factors such as TGF-α *(106)*.

The constitutive activation of the oncogenic RAS proteins deregulates downstream effector pathways to confer the abnormal functional properties of cancer cells: deregulated cell growth, survival and differentiation. Moreover, oncogenic RAS accelerates the metabolic reprogramming of cancer cells predominantly through the upregulation of hypoxia-inducible factor 1α (HIF1α), which stimulate a glycolytic shift *(162)* and induces non-cell-autonomous changes in the cellular microenvironment that have essential roles in tumor initiation and progression. One example is the induction of angiogenesis *(162)*. The constitutive activation of the pathway also plays a role in the evasion of cancer cells to the immune system *(42, 123)* and contributes to the metastasis process by inducing alterations in cell–cell and cell– matrix interactions and the acquisition of a migratory phenotype *(162)*.

All these effects can be also induced by mutations or amplification of RAS effectors. B-RAF is frequently activated in melanomas (~70%) and colon carcinoma (~15%) *(53)*. The PI3K pathway is activated by the amplification of the p110α genes in a small proportion of ovarian tumors and by the amplification of its downstream target AKT2 in ovarian and breast cancer *(19)*. However, the most significant activation of this pathway comes from the deletion of the negative regulator or the PI3K signaling, the tumor suppressor gene PTEN, which occurs in ~30-40% of human tumors *(16)*.

3.3 RAS IN HUMAN DEVELOPMENTAL DISORDERS

RAS proteins have been intensively studied for more than three decades, since its dysregulation is one of the primary causes of cancer *(132)*. More recent, observations accumulated in the last decade have associated some inherited developmental disorders with germline mutations in *RAS* (H-*RAS*, N-*RAS* and K-*RAS*) or in other upstream (*PTPN11* and *SOS1*) or downstream components (B-*RAF*, C-*RAF*, *MEK*1 and *MEK*2) of the RAS signaling pathway ***(Figure 3)*** *(60, 187, 207, 215)*. Most of these loci (H-*RAS*, K-*RAS*, N-*RAS*, B-*RAF*, *PTPN11* and *NF1*) are also found mutated in human tumors. However, in contrast to the somatic oncogenic mutation, these substitutions are germline mutations that encode less active proteins compared to the cancer-associated mutations, with the exception of H-*RAS*. H-*RAS* mutations that cause CS encode strong gain of function mutations ant it is therefore not surprising that affected individuals are predisposed to benign and malignant tumors *(187)*.

The developmental disorders that result from germline mutations in members of the RAS signaling pathway are known as Neuro-Cardio-Facial-Cutaneous' (NCFC) syndromes or 'RASopathies'. These syndromes share a variable degree of common alterations: facial abnormalities, heart defects, impaired growth, and, in some instances, cancer predisposition and neurocognitives alterations. Cardio-facio-cutaneous syndrome (CFC), Costello Syndrome (CS), LEOPARD Syndrome (LS), Neurofibromatosis type 1 (NF1) and Noonan Syndrome (NS) are

the best-known NCFC syndromes. Legius Syndrome (NF1-like), Noonan syndrome-like with loose anagen, Noonan-like/multiple giant cell lesion syndrome and Noonan-like syndrome have been recently described as complex disease that share some features with NS or NF1 *(165)*.

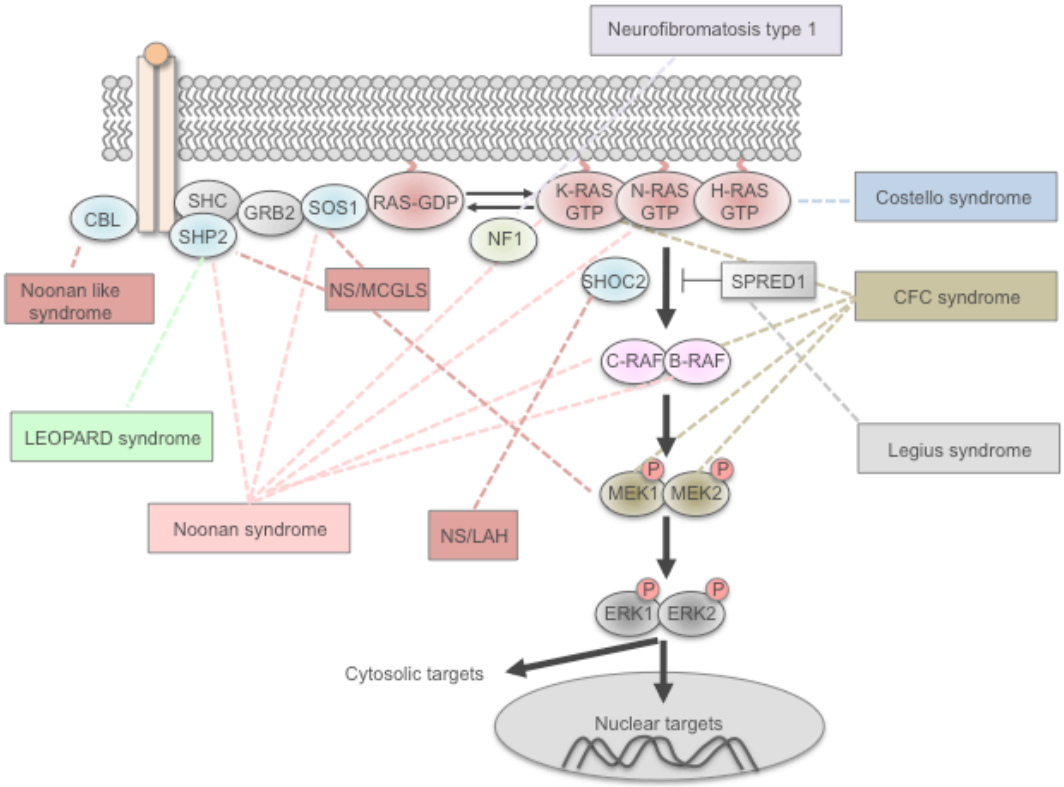

Figure 3. Schematic diagram showing the RAS-MAPK signaling pathway and the components affected in the NCFC syndromes. Adapted from Tidyman et al., 2008 *(215)*.

3.3.1 Neurofibromatosis type 1 (NF1)

Neurofibromatosis type 1 (NF1; OMIM 162200) was the first 'RASopathy' described *(34)*. It is an autosomal dominant disorder affecting approximately 1 in 3000 newborns. Their clinical diagnosis is based on the presence of café-au-lait maculae, axillar or inguinal freckling, neurofibromas and plexiform neurofibromas, iris Lisch nodules, osseous dysplasia and optic pathway glioma. In addition, individuals may have "Noonan-like" faces, mild neurocognitive impairment and a predisposition to developing certain malignancies such as central nervous system tumors (gliomas and astrocytomas), neurofibrosarcomas and juvenile myelomonocytic leukemia (JMML). For this reason, NF1 patients normally have reduced life span *(215)*. Inactivated genetic modification in the *NF1* gene causes this disease. As mentioned before *NF1* encodes neurofibromin 1, a GAP that is a negative regulator of RAS *(see 2.1.1 section)*. The *NF1* missense mutations result in loss-of-function of the protein causing a reduction in RAS-GTPase activity and therefore an increase of the active RAS form.

In mouse, the expression of one copy of a null mutation of the *NF1* locus is associated to an enhanced predisposition to specific tumors including phaeochromocytomas and myeloid leukaemias, tumors that are evident in human NF1 patients *(84)*. However, the expression of two copies of the null mutation is incompatible with the embryonic development. Homozygous null embryos die at mid gestation. Mutant embryos exhibit globular and hypoplastic hearts with significant ventricular septal defects and display double outlet right ventricle *(25, 84)*. Mutant embryos also display hyperplasia of neural crest-derived sympathetic ganglia *(25)*. Besides hematopoietic cells derived from the liver of these embryos display hypersensitivity to Granulocyte/Macrophage Colony-Stimulating Factor (GM-CSF) *(23,111)* and are sufficient to induce a chronic myeloproliferative syndrome in bone marrow (BM) transplanted animals *(111)*.

3.3.2 Cardio-facio-cutaneus (CFC) syndrome

Cardio-facio-cutaneus syndrome (CFC; OMIM 115150) is a sporadic occurrence syndrome. Epidemiological studies that estimate the prevalence of the disease do not exist. Around 60 cases published and 100 unpublished cases are known to the CFC International association *(170)*. This condition is characterized by failure to thrive, severe feeding problems, developmental delay, reduced growth, distinctive dysmorphic facial features, abnormalities of the skin, gastrointestinal tract and central nervous system (seizures are frequently observed), and cardiac defects [most commonly pulmonic stenosis, followed by hypertrophic cardiomyopathy (HCM) and septal defects] *(170)*. CFC syndrome has considerable clinical overlap with NS and CS. In contrast to the other NCFC syndromes, CFC syndrome is believed to have no increased malignancy risk. However, the observation of acute lymphoblastoid leukemia (ALL) in one patient *(151)* raises questions about this matter. Four genes have been associated with this syndrome: K-*RAS* (rare), B-*RAF* (~75%), *MEK1* and *MEK2* (~25%) *(151, 174, 60)*. Due to the phenotypic overlap of CFC syndrome and NS the role of K-*RAS* in the CFC syndrome remains unclear because K-*RAS* mutations were also indentified in Noonan patients.

A genetic modified mouse model for CFC syndrome has been recently generated. This mouse model expresses low levels of expression of B-Raf^{V600E} from germline, a constitutively active mutation first identified in human melanoma. B-$Raf^{+/LSLV600E}$ mice are viable and display several of the characteristic CFC features: reduced life span, small size, facial dysmorphism, cardiomegaly and epileptic seizures. These mice also show up-regulation of catecholamines and cataracts, two features detected in a low percentage in CFC patients. In addition, B-$Raf^{+/LSLV600E}$ mice develop neuroendocrine tumors, a pathology not observed in CFC patients (*223*).

3.3.3 Costello syndrome (CS)

Costello syndrome (CS; OMIM 218040) is a rare developmental disorder, that affects a very few patients (~ 300 around the world) *(67)*. Costello patients develop multiple anomalies, including prenatal overgrowth followed by postnatal feeding difficulties and severe failure to thrive, short stature, distinctive coarse facial features, cardiac defects (most commonly HCM, septal defects, valve thickening and/or dysplasia, and arrhythmias), musculoskeletal and ectodermal abnormalities and neurocognitive delay *(164)*. CS patients have an increased risk of developing neoplasias, including rhabdomyosarcomas, neuroblastomas and bladder cancer. These solid tumors affect approximately to 15% of CS patients. Cutaneous papilloma is a distinctive and common feature of this disorder *(66)*. CS is caused by germline missense mutation in H-*RAS (12)*. The distribution frequency of mutations reveals that more than 80% of individuals have G12S substitution, followed by G12A (9%) and G13D (1.4%) *(67)*. These substitutions disrupt guanine nucleotide binding and cause a reduction in intrinsic and GAP induced GTPase activity. As an exception with the rest of the syndromes, these mutations are frequently found in human tumors. In addition, less frequently observed mutations, such as K117R and A146T may result in an atypical phenotype *(215)*.

Two independent knock-in mouse models involving the expression of the H-Ras^{G12V} mutation have been generated to analyze the molecular mechanisms responsible for the phenotypic defects of CS patients *(40, 189)*. Schuhmacher and colleagues described in 2008 that germline expression of the oncogenic H-Ras^{G12V} allele phenocopies some of the abnormalities observed in CS patients, including facial dysmorphia and cardiomyopathies. These mice also display alterations in the homeostasis of the cardiovascular system, including development of systemic hypertension, extensive vascular remodeling and fibrosis in heart and kidneys. This phenotype is age dependent and is a consequence of the abnormal upregulation of the renin-Ang II system. The expression of the mutation results in hyperplasia of the mammary gland *(189)*. However, development of tumors in these mice is rare. In 2009, Chen and colleagues described that the expression of the same mutation is associated with high perinatal mortality, abnormal cranial dimension, defective dental ameloblast and nasal septal deviation. In contrast to the first mouse model, mice also develop papillomas and angiosarcomas *(40)*. The phenotype differences between these two mice carrying the same mutation, may be explained by gene modifiers, as has been suggested for human patients.

3.3.4 Noonan syndrome (NS)

Noonan syndrome (NS; OMIM 163950) was described by the pediatric cardiologist Jacqueline Noonan 40 years ago. NS is one of the most common developmental disorders, with

estimated incidence of 1:1,000 to 1:2,500 live births, but mild cases may be even more common *(141)*. The typical signs of NS include typical facial feature, chest and spinal deformities, short stature, characteristic heart defects, and learning disabilities with mild mental retardation *(208)*.

The facial appearance of Noonan patients shows considerable change with age, being most striking in the newborn period and most subtle in the adulthood, some adults lack facial alterations *(8)*. In general, NS patients are characterized by ptosis and wide-spaced eyes, low set, posteriorly rotated ears with fleshy helix, inverted triangular face which is broad at the temples and tapers to a small chin and long and broad or webbed neck *(7)*.

The weight and length are also variable with the age. Although patients display normal size and weight at birth, the neonatal feeding problems and failure to thrive (63%) slows the proper development of the children. Even though feeding problems are solved spontaneously later in infancy, the pubertal growth is often attenuated or delayed, resulting in a final adult reduced height. Growth hormone (GH) deficiency and resistance and neurosecretory dysfunction have been described in these patients *(171, 220, 224)*.

NS is the most common syndromic cause of congenital heart disease after the Down's syndrome (OMIM 190685). The frequency of congenital heart disease is estimated between 50% and 90%. The most common are pulmonary stenosis (often with dysplastic valves; 50–60%), HCM (20%), and secundum atrial septal defect (6–10%). Subventricular septal defect, peripheral pulmonary stenosis, atrioventricular canal, aortic stenosis, mitral valve abnormalities, aortic coarctation, tetralogy of Fallot, and coronary artery anomalies are less common alterations. HCM can be mild or severe and can be present from the prenatal period to late childhood. Almost 25% of patients die because of heart failure in the first year *(171, 193)*.

Most NS patients display skeletal abnormalities: chest deformities (90%), scoliosis (13%), various orthopedic defects, such as cubitus valgus (50%) and joint hyperextensibility (50%) *(6, 192)*. Giant cell lesions of the jaw have been reported in several patients *(149)*.

Up to 80% of NS boys have cryptorchidism. Male gonadal dysfunction has been reported due to primary Sertoli cell dysfunction rather than cryptorchidism *(135)*. In both sexes, pubertal development is delayed. But, in contrast to male patients, fertility in females is not impaired *(171)*. Urinary tract malformations are also present in 10% of cases, mostly pyelouretic stenosis and/or hydronephrosis, although treatment is usually not need *(192, 224)*.

Several coagulation defects have been described: factor VII, XI and XII deficiencies, thrombocytopaenia, Von Willebrand's disease, and platelet dysfunction. These manifestations appear individually or in combination and affect about one of third of all individuals *(138, 192)*.

Lymphatic vessels dysplasia, hypoplasia or aplasia (20%), abnormal pigmentation [naevi (25%), café-au-lait spots (10%) and lentigines (3%)], ophthalmic abnormalities, hearing loss and hepatosplenomegaly (25%) are other phenotypic features of NS *(7, 171)*.

Developmental delay and learning problems are less common than in CS and CFC. In most individuals the intelligence is normal and mild retardation, characterized by specific visual and verbal problems, is seen in one-third of patients *(192)*. Prominent behavioral problems are clumsiness, eating problems, fidgety or stubborn spells, echolalia, irritability, social problems and attention deficit. In spite of this wide range of behavioral problems, NS children can be raised with parental support alone *(236)*. Besides, 80% of diagnosed NS, graduated from high school, one-third attended college and 5% had a master degree *(7)*.

3.3.4.1 Molecular pathogenesis

PTPN11 was found mutated in NS ten years ago *(211)*. The *PTPN11* gene product, SHP-2, is a non-receptor tyrosine phosphatase that relays signals from activated growth factor receptors to RAS, SRC family kinases, and other molecules. SHP-2 generally plays a positive role in signal transduction and regulates cellular responses such as proliferation, differentiation, and migration *(148, 155)*. This protein is composed to N-terminal and C-terminal SH2 domains and a catalytic protein tyrosine phosphatase (PTP) domain. Its catalytic function is auto-inhibited through a blocking interaction between the N-SH2 and PTP domains. 50% of cases of NS are caused by missense, gain-of-function, mutations in this gene *(171)*. These mutations cluster in and around the interacting portions of the N-terminal and the catalytic PTP domain, which are involved in switching the protein between its inactive and active conformations. Mutations typically perturb equilibrium, causing constitutive or prolonged activation of the protein. A number of mutations, however, affect residues that also participate in catalysis or in the control of substrate specificity *(209, 210)*. *PTPN11* gene has been recognized as an oncogene. Somatic mutations have been frequently identified in JMML and pediatric acute leukemia. These mutations occurred at the same residues as in NS, but with substitutions that result in a more active protein *(213)*. Vertical transmission of the same mutations in a family is commonly associated with PTPN11 substitutions. PTPN11-associated NS is linked with a high incidence of pulmonary stenosis or atrial septal defects, bleeding diathesis, short stature, and JMML. In contrast the incidence of HCM and coarctation of the aorta is lower in patients with these mutations *(171)*.

Currently, *SOS1* mutations are the second most frequent cause of NS (10%). *SOS1* encodes a RAS-GEF. The majority of the reported mutations were located in residues that are responsible for the stability of the protein in an inhibited conformation. Therefore, these alterations reduce its autoinhibition activity, leading to constitutive activation of the protein with the subsequently constitutive activation of the RAS pathway *(172, 212)*. SOS1-associated NS is characterized by a higher prevalence of ectodermal abnormalites generally associated with lower prevalence intellectual disability, short stature and atrial septal defects *(171)*.

Missense mutations in the *RAF1* gene have also been found in 5-15% of NS patients *(157, 168)*. These mutations are often clustered in two regions: the conserved region 2, flanking the residue S259; and the conserved region 3, in and surrounding the activation segments. In addition, two mutations in the C-terminal domain have also been reported *(157, 168)*. HCM is associated to RAF1-NS (75 vs 20% overall NS patients with other mutated genes) and it seems to be associated with mutations in the Ser259 and Ser621 hotspots. Multiple naevi, lentigines of café-au-lait spots are reported in a third of patients, suggesting a predisposition to hyperpigmented cutaneous lesions *(207)*.

Germline B-*RAF* mutations have been described in a small percentage of patients (<2%) *(180, 154, 168)*. As mentioned before, B-*RAF* has been described as a major gene mutated in CFC syndrome patients. Interestingly, NS and CFC are associated with specific and different B-*RAF* mutations, suggesting a genotype-phenotype correlation. B-RAF-associated NS is related to neonatal growth failure and feeding problems, mild to moderate cognitive deficits, hypotonia and a higher prevalence of multiple nevi and dark colored lentigines. B-*RAF* mutations produce a more severe adult phenotype than *PTPN11* or *SOS1* mutations *(207)*.

K-*RAS* and N-*RAS* germline mutations account for less than 2% of the NS patients. This low number of cases makes impossible to establish a genotype-phenotype correlation. In an analysis of 917 individuals with NS or related disorders, four unrelated individuals (three *de novo* and one familial) had mutations in N-RAS (Cys149Thr or Gly179Ala) *(41)*. K-*RAS* mutations have been described in a small percentage of NS patients, and are usually correlated with more severe symptoms *(26, 33, 46, 99, 104, 115, 118, 122, 147, 153, 167, 188, 243)*. With the exception of a vertical transmission in a family presenting a novel K-RAS mutation (M72L) *(26),* all the cases are sporadic, likely reflecting the decreased reproductive fitness caused by the more frequent and severe intellectual disabilities of these patients. Therefore, several patients display an intermediate phenotype between NS and CFC syndrome *(33, 243)*. Craniosynostosis, a rare finding, was described in four NS patients with K-*RAS* mutations *(26, 104, 188)*.

14 different K-RAS mutations have been described in Noonan patients ***(Table 2 in Appendix I).*** These gain-of-function mutations result in milder activation of the K-RAS protein compared to the typical oncogenic forms and have not been identified in human tumors *(187)*. The position of the mutated amino acid residues altered in NS suggests two distinct pathogenetic mechanisms:

a) The first group of mutations includes the mutant proteins that affect the P-loop (V14I), the Switch I (P34L and P34Q) and II (T58I and G60S) domain or intermediated regions of the G domain (Q22R, M72L, N26I and N116S) ***(Figure 4)***. All these mutations have less GTPase activity, basally and after stimulation with a GAP protein, than wild type K-RAS but more than oncogenic G12D. Thus, these mutants reduced RAS inactivation, resulting in increased RAS signaling *(65, 186, 188)*. Specifically, the intrinsic GTPase activities of the NS-

associated V14I and T58I recombinant proteins are lower than wild type K-RAS, but less impaired that oncogenic G12D. Furthermore, both mutant proteins also show intermediate levels of GTP hydrolysis in response to the GAP-related domains of p120GAP and neurofibromin, compared to the wild type and K-RAS^{G12D}. A particular interesting feature of the T58I mutant protein is its differential responsiveness to p120GAP and neurofibromin. The intermediate phenotypes of NS-associated mutants V14I and T58I are also observed in functional assays. The dose-response curves for hematopoietic progenitor colony formation in response to GM-CSF or erythropoietin are left-shifted in murine fetal liver cells expressing both mutant proteins relative to wild type K-Ras, but these cells are less hypersensitive than cells expressing the G12D form. Macrophage progenitor cultures expressing T58I or G12D K-Ras displayed robust and prolonged activation of Ras and downstream effectors compared to cultures expressing wild type or V14I K-Ras. By contrast, COS-7 cells expressing K-Ras V14I demonstrated elevated basal and serum-starved levels of Ras-GTP and phospho-MEK compared to cells expressing wild type or T58I receptors to the nucleus. These studies show that these alleles are activated, and support the idea that cell context modulates their functional and biochemical effects since the same mutations in different cell types have a different outcome *(188)*.

b) The second group of mutations includes the mutant proteins that alter regions that reside far from the P-loop typically altered in cancer, specifically the α-5 helix of the K-RAS 4B isoform (V152G, D153V and F156I) ***(Figure 4)***. Based on structural modeling, Carta and colleagues indicated that the V152G and D153V substitutions destabilize the conformation of the portions of the G domain that contributes extensively to the interactions of K-RAS with the GTP/GDP guanine ring. They predicted that the mutants will have normal GTPase function but reduced binding to GTP and GPD, permitting GEF-independent activation *(33)*. Although depth biochemical analysis of the V152G and D153V K-RAS mutants has not yet been reported, an F156L substitution in H-RAS results in a rapid rate of nucleotide dissociation, modestly increases of Ras-GTP leves, and transform rodent fibroblast *(186)*. Also, the Val152, Asp153 and Phe156 are encoded by exon 4B, so the mutations only alter K-RAS 4B isoform, providing new evidence that this isoform plays a major role during development.

Finally, it have recently been identified nine missense mutations in *RIT1*, in 17 of 180 NS patients (9%) without described causative mutation. Clinical manifestations of these individuals are consistent with those of NS, but present a high frequency of HCM *(11)*. RIT1 is a RAS subfamily member involved in regulation of the p38 MAPK-dependent signaling cascade related to cellular stress *(32, 196)*. This protein also cooperates with nerve growth factor to promote neuronal development and regeneration *(83, 195)*. This study is the first evidence that other members of the RAS subfamily are implicated in developmental disorders.

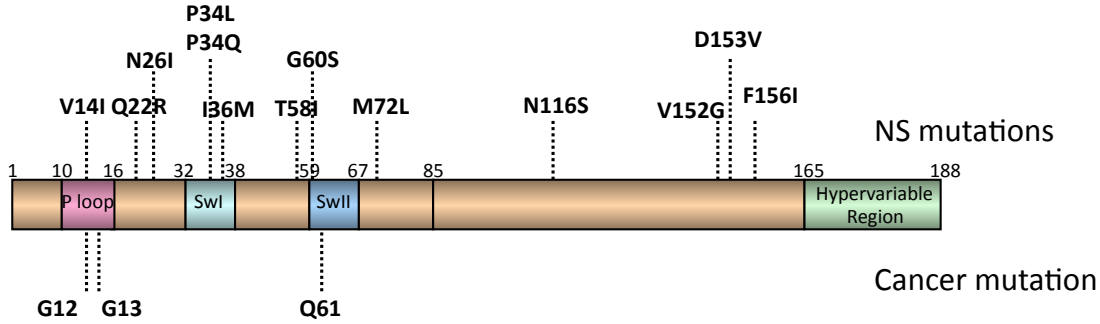

Figure 4. Schematic representation of K-RAS showing the distribution of the amino acid substitution found in Noonan patients (above) and the three amino acids commonly mutated in human tumors (bellow). The P-loop, switch 1 (SwI), switch II (SwII) domains and the hypervariable region are also represented. The position of these domains is represented. Adapted from Schubbert et al., 2007 *(186)*.

3.3.4.2 Cancer in Noonan syndrome

NS is associated with risk for benign and malignant proliferative disorders. Approximately 10% of NS children are affected by a mild myeloproliferative disorder (MPD), which is usually self-limiting. A smaller percentage of patients develop JMML and/or other hematological malignancies, such as myelogenous leukemia and B-cell acute lymphoblastic leukemia *(91)*. There are no good epidemiological studies to establish if NS patients display tumor predisposition. The literature illustrates that 45 of 1,151 NS patients (mutations unkown) developed cancer (3.9%). These tumors include: neuroblastoma (8 patients), acute lymphoblastic leukemia (8 patients), glioma and rhabdomyosarcoma (8 patients), acute myeloid leukemias (3 patients), testicular cancer (3 patients), non-Hodgkin lymphomas (2 patients), and colon cancers (2 patients). Single reports of Wilms tumor, hepatoblastoma, Hodgkin disease, chronic myelomonocytic leukemia, chronic lymphocytic leukemia, breast cancer, malignant schwannoma, and bile duct cancer were also described. The ages of the patients at the time of cancer diagnosis were comparable to the expected for sporadic cancers *(103)*. It has also been reported 40 cases of NS (or Noonan-like syndrome) associated with MPD with a benign course in 16 (40%) and an aggressive course in 6 (15%) cases. By the age of 20, the cumulative incidence of cancer in NS was approximately 4%, lower than the 15% for CS. Both syndromes had a cancer incidence peak in childhood *(103)*.

Furthermore, Jongmans and colleagues published a study of a cohort of 297 Dutch patients with NS with *PTPN11* mutations (mean age 18 years). Twelve patients developed cancer, providing a cumulative risk for developing cancer of 23% up to the age of 55 years (a 3.5 times increased risk). Hematological malignancies were the most frequent neoplasm (4/12, 33%). The non-hematological malignancies observed included three novel cancers in Noonan patients: a malignant epithelioid angiosarcoma, a colon cancer of the sigmoid and a basal cell carcinoma. In conclusion, this study provides the first evidence of an increase tumor risk in PTPN11-NS patients, compared to that in the general population *(91)*.

This study provides evidence that NS patients present increased cancer predisposition. The information is limited, because this disorder is a pediatric disease and no follow up and registry of adult patients exists. Adult patients are healthy or display mild alterations that are treated for the required specialist. Therefore, the study of tumor risk in NS patients is very difficult. However, these studies would provide relevant information for prevention, early detection and treatment of the tumors that seems to have a higher incidence in NS patients.

3.3.5 LEOPARD syndrome

LEOPARD syndrome (LS; OMIM 151100) is an acronym for the more characteristic features of this syndrome: multiple Lentigines, ECG abnormalities, Ocular hypertelorism, Pulmonary valve stenosis, Abnormalities of the genitalia, Retardation of growth and sensorineural Deafness. LS is a rare autosomal dominant disorder, about 200 patients have been reported worldwide but the real incidence of this syndrome has not been assessed and is typically associated with *PTPN11* mutations *(51, 181)*. LS, in contrast to the NS, is caused by *PTPN11* mutations that results in reduced PTP activity. The mutant PTP is then thought to act in a dominant-negative fashion to inhibit SHP-2 expressed from the normal *PTPN11* allele *(51, 62, 64, 74, 101)*. Interestingly, the dysregulated activation of the RAS-MAPK signaling pathway by mutations that have opposing effects upon SHP-2 activity result in the development of two syndromes (NS and LS) that share clinical features *(54, 62)*.

Homozygous *Ptpn*11-null mice die at day 10 of embryonic development due to defective gastrulation *(182)*. However, the elimination of SHP-2 expression in multiple adult tissues results in severe skeletal abnormalities, impaired hematopoiesis, weight loss and lethality *(18)*. Moreover, mice expressing the *Ptpn11*^{Y279C} mutation, one of the most common in LS, recapitulates most of the features of LS. *Ptpn11*$^{+/Y279C}$ mice display short stature, craniofacial dysmorphia, skeletal and chest abnormalities, pathological HCM, abnormal genitalia and macrophage accumulation in the Corti, indicative of sensorineural defects. Biochemical analyses show an increase of the basal and agonist-induced Akt and mTOR activity. Interestingly, the cardiac defects were completely reversed by treatment with rapamycin, an inhibitor of mTOR *(136)*. Similar results are obtained by the overexpression of Q510E, a dominant-negative loss-of-function mutation, in myocardial cells during gestation (under the β–myosin heavy chain promoter). Newborn mice display a heart hypertrophic associated with an impaired contractile function and hyperactivation of the Akt/mTOR pathway. As in the *Ptpn11*^{Y279C} mice *(136),* the HCM is ameliorated by rapamycin treatment *(185)*.

3.3.6 Legius syndrome

Legius syndrome (OMIM 611431), or neufibromatosis type 1-like syndrome, is an autosomal dominant disorder characterized by multiple axillary freckling, café-au-lait spots, macrocephaly, and a NS-like facial dysmorphism in some individuals. Some patients have learning difficulties and/or hyperactive behavior *(207)*. This syndrome presents clinical overlapping with NF1 and NS. The estimated prevalence in the Orphanet webpage is <1 in 1,000,000 newborns. Legius syndrome is caused by heterozygous mutations in *SPRED1 (29)*. *SPRED1* encodes SPRED1, which is a member of the SPROUTY/SPRED family. SPRED1 functions as negative regulator of RAS by inhibiting RAF phosphorylation *(229)*. *SPRED1* mutations associated with Legius syndrome cause truncation of the protein resulting in loss of SPRED1 function, thereby increasing the RAS/MAPK signaling. It is unclear whether individuals with SPRED1 germline mutations have an increased risk for developing cancer.

3.3.7 Noonan syndrome-like with loose anagen hair (NS/LAH)

Although, Noonan syndrome-like with loose anagen hair (NS/LAH; OMIN 607721) shows reminiscent features of NS, the patients are distinguished due to the reduced growth linked to GH deficiency, cognitive deficits, hyperactive behavior and loose anagen hair. Most patients exhibit hairless and darkly pigmented skin with eczema or ichthyosis, and a tendency to pruritus. Ectodermal anomalies also include sparse eyebrows and dystrophic or thin nails. The voice is characteristically hoarse or hypernasal. Cardiac anomalies (dysplasia of the mitral valve and septal defects) are significantly over-represented compared to NS. Estimated prevalence in the Orphanet webpage is <1 in 1,000,000 newborns. NS/LAH is genetically homogeneous, since all patients display the same missense change (Ser2Gly) in *SHOC2*, a scaffold protein required for the efficient signaling transmission from RAS to the MAPK cascade *(45, 139)*.

3.3.8 Noonan-like/multiple giant cell lesion syndrome (NL/MGCLS)

Multiple giant cell lesions (MGCLs) of the jaw and/or other bone/soft tissues are rarely associated to NS. The presence of MGCLs in Noonan patients was originally known as Noonan-like/multiple giant cell lesion syndrome (NL/MGCLS) or Noonan syndrome with cherubism (OMIM 163955) (25). Now, it seems that MGCLs is an associated feature of NS, LS and CFC and that NL/MGCLS is not a separate disorder, since this feature has been documented to occur in different conditions and be caused by mutations affecting *PTPN11*, *SOS1* and *MEK1* genes previously reported mutated in those syndromes *(207)*.

3.3.9 Noonan-like syndrome

It has been recently reported the presence of germline mutations in *CBL* gene in patients with features fitting or partially overlapping NS, characterized by an unusually variable phenotype (developmental delay and reduced growth, facial dysmorphism, café-au-lait spots and predisposition to JMML during childhood), with clinical features that might be quite subtle in some subjects *(137, 150, 158)*. CBL is a member of a small family of E3 ubiquitin ligases that negatively regulate intracellular signaling downstream of receptor tyrosine kinases, but also contribute to signal traffic by its adaptor function *(207)*.

3.4 ANIMAL MODELS OF NOONAN SYNDROME

Several animal models have been generated to study the role of different mutations found in Noonan patients. Animal models help to better understand the molecular and cellular bases of the developmental and physiological defects associated with the NCFCS, as well as to determine their tumor predisposition and to evaluate preventative and therapeutic strategies.

Studies in zebrafish have demonstrated that K-*RAS*, *RAF1* and *PTPN11*, genes mutated in NS, are necessary for the normal development of myocardial and craniofacial structures in the case of K-*RAS*. Zebrafish embryos with morpholino knock-down of these genes display heart malformation *(167, 168)*. Moreover, the expression of the mRNA of Noonan mutant *RIT1 (11), N-RAS (177)* and *PTPN11 (92)* into zebrafish embryos results in craniofacial and cardiac abnormalities, defects reminiscent of NS. Interestingly, MEK inhibitor treatment completely rescues these developmental defects in the embryos that express the mutant N-*RAS (177)*

Araki and colleagues developed the first NS knock-in mouse model in 2004, which expresses one of the most frequent NS-associated mutations, the *Ptpn11*^{D61G}. The expression of one copy of this mutated allele results in high embryonic lethality (around 50%). Surviving *Ptpn11*$^{+/D61G}$ mice have short stature, craniofacial abnormalities and MPD. Severely affected *Ptpn11*$^{+/D61G}$ embryos have multiple cardiac defects: ventricular septal defects, double-outlet right ventricle (DORV) and enlarged valve primordial. These alterations are gene dose dependent since homozygosity results in embryonic lethality at mid-gestation. E13.5 *Ptpn11*$^{D16G/D61G}$ embryos are hemorrhagic and edematous and show smaller and necrotic liver and severe cardiac defects (atrial, atrioventricular or ventricular septal defects, DORV and markedly enlarged outflow tract and atrioventricular valve primordial). Furthermore, *Ptpn11*$^{+/D61G}$ embryos present increased Erk activation in altered regions, such as the endocardial cushions. This hyperactivation is cell and pathway specific, suggesting that Ras-MAPK pathway activation takes place in specific cell types responsible for the abnormalities *(14)*. All these studies were developed in a mix 129S4/SvEv and C57BL6/J background. The

incomplete penetrance of the cardiac defects could reflect the presence of modifier alleles in these strains. To address this possibility *Ptpn11*$^{+/D61G}$ mice were backcrossed to 129S6/SvEv, Balb/c, and C57BL6/J pure backgrounds. No alterations were found in the Balb/c background, although only half of the *Ptpn11*$^{+/D61G}$ expected mice was obtained. On 129S6/SvEv, *Ptpn11*$^{+/D61G}$ mice display nearly normal viability. In contrast, C57BL6/J E13.5 embryos display severe cardiac defects incompatible with life, indicating that there are important strain-specific modifiers of the NS cardiac phenotype *(13)*.

Further characterization of the myeloproliferative phenotype of this model suggests that *Ptpn11*^{D61G} germline mutation accelerates hematopoietic stem cell (HSC) cycling, increases the stem cell pool, and elevates short-term and long-term repopulating capabilities. The later stage myeloid progenitors are also increased. MPD is reproduced in primary and secondary recipient mice suggestive of a stem cell origin. Interestingly, the MPD phenotype is ameliorated by the deletion of Gab2, an interacting protein target of Shp-2 in cell signaling. It indicates that Gab2 is an important mediator for the pathogenic effects of Ptpn11 mutations *(239)*.

In contrast to the *Ptpn11*^{D16G} mice, heterozygous *Ptpn11*$^{+/N308D}$ mice, that express a low activated version of the Shp2, are viable and E13.5 embryos have no apparent cardiac defects. However, 50% of homozygous *Ptpn11*$^{N308D/N308D}$ embryos develop multiple cardiac defects incompatible with life. The other 50% have no apparent cardiac defects and survive, although display growth defects, typical facial appearance and hematologic abnormalities similar to those seen in surviving *Ptpn11*$^{+/D61G}$ mice *(13, 14)*. The abnormalities of *Ptpn11*$^{+/N308D}$ mice are less severe *(13)*. Interestingly, the expression of *Ptpn11*^{D61Y}, other typical NS mutation, in endocardial cells recapitulates the alterations found in *Ptpn11*$^{D16G/D61G}$ mice *(14)*. However, myocardial specific expression, using α myosin heavy chain (α-MHC) promoter, has no obvious cardiac consequences. The specific expression in neural crest produced facial defects similar to the previous reported in mice *(13)*.

Transgenic mice overexpressing the Shp2 Q79R mutant protein (one of the most common NS mutations) under the α-MHC promoter, which allows the expression of the mutation only in myocardial cells after birth, do not display cardiac defects, similar to previous studies *(13, 145)*. In contrast, transgenic mice overexpressing Shp2 Q79R in myocardial cells during the gestation [under the β–myosin heavy chain (β-MHC) promoter], show similar alterations than those reported in the *Ptpn11*^{D16G} mouse model *(145)*. These heart alterations persist postnatally and induce a cardiac hypofunction that ends in congestive heart failure.

These studies indicate that the cardiac defects of NS came from the expression of the mutant protein in endothelia and myocardial cells during the development. The overexpression of the mutation in the same cells in completely developed heart has no effect. Interestingly, as in the *Ptpn11*^{D16G} mice, overexpression of Shp2 Q79R selectively activates Erk1/2. This pathway

is necessary and sufficient to mediate the alterations, since incorporation of the null *Erk1* mice (*Erk1*$^{-/-}$) or the heterozygous *Erk2* mice (*Erk2*$^{+/-}$) completely recue the cardiac phenotype *(145)*.

Mice that overexpress the Shp2 Q79R mutation in neural crest cells, by using the Wnt-1 promoter, develop craniofacial alterations similar to the *Ptpn11*^{D16G} mice *(14, 146)*. These mice show lower body length and weight and typical craniofacial defects (smaller skull lengths, greater inner canthal distances, taller frontal bone heights and reduced mandibular bone length). Therefore, facial abnormalities in Noonan PTPN11-patients reflect aberrant Shp2 action in neural crest-derived cells. Treatment during pregnancy with U0126 (inhibitor of ERK1/2 phosphorylation) abrogates the craniofacial abnormalities. This data illustrate the importance of the Erk1/2 signaling in the neural crest for the craniofacial development (*146*).

Mice overexpressing the Shp2 Q79R mutation only in the endothelial-derived cells die at embryonic day E14.5. Embryos at E13.5 are smaller than control littermates and show edema, smaller and necrotic liver and hemorrhage. The heart displays an increased endocardial cushion size, associated with Erk1/2 activation, suggesting that hyperactivation of this pathway may play a pathogenic role. Erk1 deletion rescues the endocardial phenotype, but embryos still die at E14.5. However, Erk2 deletion does not affect endocardial cushion size *(105)*.

In 2010, Chen and colleagues generated a NS-associated Sos1E846K knock-in mouse model. Heterozygous mice were obtained at Mendelian ratios, whereas homozygous mice are born at significantly lower frequency (2.38%), due to severe cardiovascular problems. The few *Sos1*$^{E846K/E846K}$ mice born have a significant lower life span and display some of the typical NS features: smaller size, facial appearance and multiple cardiac defects; alterations also found in *Sos1*$^{+/E846K}$ mice. These mice also develop hematologic disorder characterized by splenomegaly, leukocytosis, myeloid expansion in BM and spleen and increased sensitivity to IL-3 and GM-CSF. Prenatal treatment with the MEK inhibitor PD0325901 ameliorates embryonic lethality, cardiac defects, and NS features of the homozygous mutant mice, demonstrating that this signaling pathway might represent a promising therapeutic target for Noonan patients *(39)*.

Same phenotype is found in the NS-associated Raf1^{L613V} knock-in mice. *Raf1*$^{+/L613V}$ mice are obtained at Mendelian ratios in a 129S6 × C57BL/6 mixed background. However, similar to *Ptpn11*^{D16G} mice *(14), Raf1*$^{+/L613V}$ mice cannot be backcrossed to C57BL/6 mice for more than 3 generations. Heterozygous mice have short stature, craniofacial dysmorphia and hematologic abnormalities. Valvuloseptal development is normal, but *Raf1*$^{+/L613V}$ mice exhibit eccentric cardiac hypertrophy. Postnatal PD0325901 treatment reduces body length and normalizes the cardiac phenotype, whereas do not improve the facial dysmorphia *(237)*.

4. Objectives

Noonan syndrome (NS) is one of the most common developmental disorders associated with mutations in members of the RAS-MAPK pathway. The broad spectrum of phenotypic alterations and mutations together with the low incidence of some of these mutations, make difficult to establish a good phenoype-genotype correlation. For instance, although K-*RAS* is mutated in a small percentage of patients (<2%), these mutations are associated with a more severe phenotype. However, the low number of patients make impossible to establish the typical spectrum of alterations associated with these mutations.

Moreover, since this disorder is caused by mutations in members of the RAS-MAPK pathway, a signaling pathway frequently mutated in human tumors, it is possible that Noonan patients present an increased risk of tumor development. However, this disorder is managed as a pediatric condition, thus the information about the adult patients is highly limited. For this reason, there is no reliable information about the tumor predisposition of these patients are also limited. Hence, the objectives of this thesis were the following:

1. To generate and characterize a K-*Ras* knock-in mouse model by expressing the most common K-*RAS* mutation found in Noonan patients, the substitution V14I, in order to determine the phenotypic features associated with the expression of this mutation.

2. To study whether germline expression of the K-Ras^{V14I} mutation results in an increased risk of tumor by itself or cooperating with loss of tumor suppressor genes such as *p16Ink4a/p19Arf* and *Trp53*.

3. To determine whether some chronic conditions such as pancreatitis or some leading risk factor such as nicotine administration (tobacco smoking) increases tumor risk in mice that express the K-Ras^{V14I} mutation.

4. To delineate the consequences of the postnatal expression of the K-Ras^{V14I} mutation in all cell types or in specific tissues such as lung or pancreas in order to compare the oncogenic properties of this mutation to the typical K-Ras^{G12V} oncogenic substitution.

5. To determine whether MEK inhibitor treatment is a good therapeutic drug to prevent or ameliorate some of the NS-associated developmental features.

5. Materials and Methods

5.1 GENERATION OF THE CONDITIONAL K-*Ras*^{LSLV14I} KNOCK-IN MOUSE MODEL

5.1.1 Generation of the targeting DNA vector to modify the endogenous locus of K-*Ras*

The first step in the modification of the endogenous locus of K-*Ras* in the 5' region is the generation of a targeting vector that allow the incorporation of the V14I mutation and the cassette *"LoxP-PGK-Hyg-STOP-LoxP"* in the proper region by the homology recombination.

The genomic DNA of K-*Ras* was isolated from a 129Sv/J genomic DNA library (Stratagene) using as a probe a 400 bp SacI-StuI fragment of pCMV-*K-Ras* DNA that contains the human noncoding exon 0 *(117)*. To target the 5´ region of the K-*ras* locus, we mutagenized one nucleotide (underlined) corresponding to codon 14 (GTA [Val] to ATA [Ile]) in a plasmid containing the first *K-Ras* exon within a 700 bp EcoRI DNA fragment. This mutation introduces an isoleucine at the fourteen codon instead of the endogenous valine. The mutagenesis was performed using the QuikChange® single site mutagenesis kit (Stratagene) according to the manufacture's instructions and the specific primers: AJ-KrasV14I-F1: 5'-GTTGGAGCTGGTGGC**A**TAGGCAAGAGCGCC-3' and AJ-KrasV14I-R1: 5'-GGCGCTCTTGCCTA**T**GCCACCAGCTCCAAC-3'. In the primer sequence, nucleotides in bold correspond to nucleotides which have been modified.

The next step was the introduction of the LSL cassette (*PGK-Hyg-STOP* cassette flanked by loxP sites). This cassette was inserted with a 5 Kb NotI-EcoRV DNA fragment at an EcoRI site located 100 bp upstream of the mutagenized exon 1. Finally, we introduced the negative selection cassette (*PGK-TK*) in a KpnI site located at end of the left homology arm. These steps were performed by restriction endonucleases digestion followed by the ligation of the fragments.

During the process, selected clones were sequenced to ensure that only the desired mutations or fragments were introduced. The final targeting vector was called pAJ-34.

5.1.2 Homology recombination in ES cells

The targeting vector was linearized with Eam1105I, an enzyme with a single cutting site in our vector. 20 μg of the vector were electroporated into $5.6x10^6$ R1 ES cell, derived from 129/Sv embryos *(144)* in a final volume of 0.8 ml at 240 V and 500 μF using the Genepulser (Biorad). This step was performed by the Transgenic Mice Unit of the CNIO.

After the electroporation, the ES cells were maintained in culture in Dulbecco's Modified Eagle Medium (DMEM, Sigma-Aldrich) supplemented with 15% of heating

inactivated fetal bovine serum (FBS) and 10^3 U/ml of leukemia inhibitory factor (LIF). During this culture time the positive and negative selection was performed.

The targeting vector contains a hygromycin (*Hyg*) resistance gene whose expression is driven by the phosphoglycerate kinase (*PGK*) promoter. This gene encodes a kinase that inactivates the antibiotic by phosphorylation. Therefore only clones in which the targeting vector was introduced can inactivate the hygromycin and survive in a medium containing the antibiotic. This positive selection was performed by culturing the ES cells 7 days in a medium supplemented with 200 μg/ml of hygromycin. In this medium only the cells that have the targeting vector by recombination can survive.

The targeting vector also contains the thymidine kinase (*TK*) gene under the control of the *PGK* promoter located far from the homology recombination sites. The TK catalyzes the phosphorilation of deoxithymidine in a pathway leading to DNA synthesis. Gancyclovir is an analogous of nucleoside 2´deoxiguanosine. The TK can phosphorilate and transform this molecule in its bioactive form. This form is a competitive inhibitor of DNA polymerase and competes with the deoxiguanosine triphosphate (dGTP) for the active site of the enzyme, blocking its activity and thereby the cell replication. Therefore, clones in which the targeting vector was introduced randomly, not by the homology recombination, will have all the construction, including the *TK* gene, and die in a medium that contain gancyclovir. This negative selection was performed by growing the ES cells 7 days in a medium supplemented with 2 μM of gancyclovir.

Positive and negative selection was performed at the same time by culturing the ES cell in a medium with hygromycin and gancyclovir. Hence only the clones in which the targeting vector was introduced in the proper place by the homology recombination event can survive. DNA from the double resistant clones was isolated and submitted to Southern blot analysis to ensure that the LSL cassette and the V14I mutation were introduced.

5.1.3 Identification of the homologous recombinant clones by Southern blot

5.1.3.1 Genomic DNA isolation

To isolate the DNA from the double resistance clones, cells were incubated in a lysis buffer (pH8.0) that contains 1M Tris-HCl, 5M NaCl, 10% Sodium Dodecyl Sulfate (SDS), 0.5M Ethylenediaminetetraacetic acid (EDTA) and 400 μg/ml of K proteinase at 55ºC over night. Next, a NaCl saturated water solution was added to each sample, which after short ice incubation and centrifugation at maximum speed allows precipitation of proteins and cell debris, leaving the DNA in the supernatant. This supernatant was transferred to a fresh tube and DNA was precipitated adding an equal volume of isopropanol. Pellet was washed twice with

70% ethanol, dried and finally resuspended in TE (10 mM Tris-HCl pH 8.0 and 1mM EDTA pH 8.0).

5.1.3.2 Genomic analysis by Southern blot

20 µg of genomic DNA was digested with a specific restriction enzyme during 12 hours at 37ºC. XbaI was the restriction enzyme chosen according to the Southern blot strategy. After XbaI incubation, DNA restriction fragments were loaded onto a 0.7% agarose (Seckem LE) gel and the fragments were separated by electrophoresis according to size. 1X Tris-Acetate-EDTA (TAE) was the buffer used for the agarose gel electrophoresis and etidium bromide was the dye used for the DNA detection.

A radioactively labeled nucleic acid probe was previously designed to complementary bind to a specific DNA region. This region differs in size depending on the presence or not of the construction with the LSL cassette and the V14I mutation. In our strategy, the external probe (probe a) recognized a specific EcoRV-XbaI DNA fragment located in the 3´region of K-*Ras* locus. The expected size will be 5 Kbp for the ES cell clones carrying the wild type (WT) allele and 3.5 Kbp for the clones carrying the recombinant allele (LSLV14I) ***(Figure 5).***

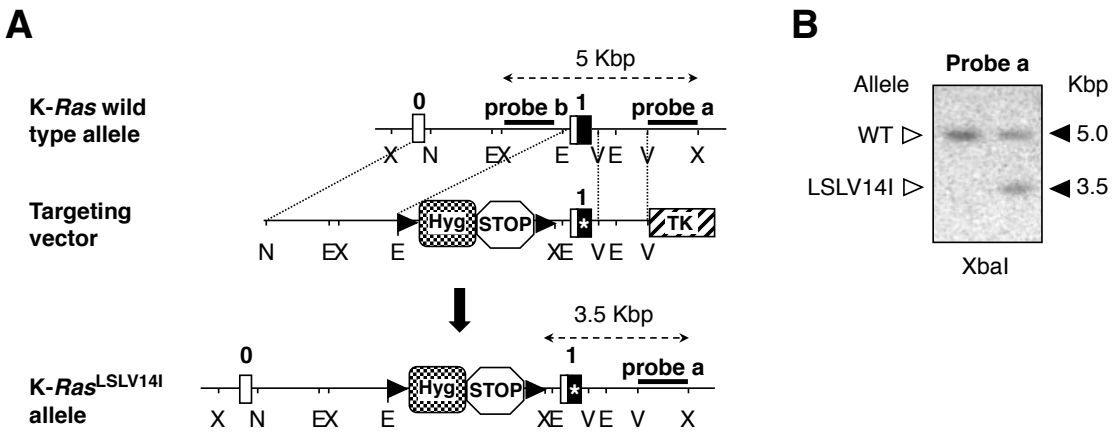

Figure 5. Gene targeting strategy. (A) Homologous recombination at the 5´region of the K-Ras locus. White box represents the K-Ras noncoding exon 0; black box, K-Ras coding exon 1; checkered box, PGK-Hygromycin (Hyg) resistance cassette; octagonal box (STOP), transcriptional inhibitory sequences; triangle, loxP sites; asterisk, mutation in codon 14 (V14I). The position of the external probes used in the Southern blot analysis is indicated. Representative restriction enzyme cleavage sites are in indicated (X, XbaI; E, EcoRI; V, EcoRV; N, NotI). **(B)** Southern blot analysis of DNA isolated from recombinant ES cells clones carrying the wild type (WT) allele and the expected homologous recombinant event (+/LSLV14I) after digestion with XbaI. The size of the wild type (5 Kbp) and targeted (3.5 Kpb) alleles is indicated.

The nucleic acid probe is a DNA fragment with a sequence complementary to a specific region of the locus. Therefore it is necessary that both, the probe and the genomic DNA

fragments were denatured, in a single-stranded DNA to the complementary binding. For this reason, the DNA gel was placed into an alkaline solution (1.5M NaCl and 0.5N NaOH) for 20 minutes at room temperature (RT) to denature the double-stranded DNA. For DNA fragments larger than 15 Kbp, prior to denaturalization, the gel must be treated with an acid solution to depurinate the DNA fragments, breaking the DNA into smaller pieces that are easily transfered from the gel to the membrane. To this aim agarose gel was treated with an acid solution (0.25N HCl) for 15 minutes at RT. Finally, since the transfer needs a pH lower than 9, the gel was incubated in a neutralizing solution (0.5M Tris HCl pH 7.4 and 1.5M NaCl) during 30 minutes at RT to equilibrate the pH. All these steps were performed on a rotary platform.

After the gel treatment, the DNA fragments were transferred to nylon membrane (Hybond-N^+, Amershand) by capillary action using 10X Saline Sodium Citrate (SSC) as a buffer transfer from 12 to 24 hours. Ion exchange interactions bind the DNA to the membrane due to the negative charge of the DNA and the positive charge of the membrane. Then the membrane was exposed to $1.2x10^5$ μJ of ultraviolet radiation using a UV Stratalinker 1800 (Strategene) to permanently attach the DNA to the membrane by covalent interactions.

After that, the DNA within the membrane was exposed to hybridization with the specific probe. Before that, the membrane was blocked during 4 hours with the hybridization solution that contains salmon sperm DNA, formamide and detergents such as SDS to reduce non-specific binding of the probe and the probe was radioactively labeled. 20 μg of purified probe was denatured by heat (5 minutes boiling) and labeled with 50 μCi of α^{32}P-CTP according to the manufacture's instructions (Amersham Rediprime II Random primer). The membrane was incubated with labeled probe in the hybridization buffer (5mM Polyvinylpyrrolidone, 2mM Ficoll, 0.1M Dextran Sulfate, 25mM Na_2HPO_4, 20mM NaH_2PO_4, 0,9M NaCl, 35mM SDS, 2.5M EDTA pH 8, 10 mg/ml of salmon sperm DNA, 13M formamide and water) for 24 hours at 42ºC.

After hybridization, excess probe was washed from the membrane using first 2X SSC/0.1% SDS, second 1X SSC/0.1% SDS and third 0.1X SSC/0.1% SDS incubations for 20 minutes at 42ºC.

Finally, the pattern of hybridization was visualized by exposing the membrane to the Phosphoimager screen for 24 hours and scanning the screen afterward (Molecular Dynamics).

5.1.4 Generation of chimeric mice

ES clones carrying the homologous recombination event were submitted to cytogenetic analysis and two of them among those exhibiting normal morphology, growing, karyotype and absence of mycoplasm were used to generate chimeric mice by microinjection into C57BL/6J blastocysts. This step was performed by the Transgenic Mice Unit of the CNIO.

Tissues from the chimeric mice have been developed from the injected ES cells (129/Sv) and the recipient blastocyst cells (C57BL/6J). This mixture of starter cells is shown in the mouse's coat, which exhibits patches of coat color from the host embryo (black) and patches from the injected ES clones (agouti). Coat color percentage was determined, and male with 50% or higher ES cell contribution (agouti) were backcrossed to C57BL/6J females to test for germline transmission of the targeted allele. To check for germline transmission, the tail DNA from the agouti offspring was analyzed by Southern blot, following the same strategy explained before *(see 3.1.3.2 section)*. Moreover, the exon 1 of the K-*Ras* allele was amplified from tail genomic DNA by PCR. The PCR product was sequenced to verify the presence of G→A transition ***(Figure 6).*** Mice born from the chimeras that display germline transmission of the homologous recombinant event were called K-*Ras*$^{+/LSLV14I}$ mice.

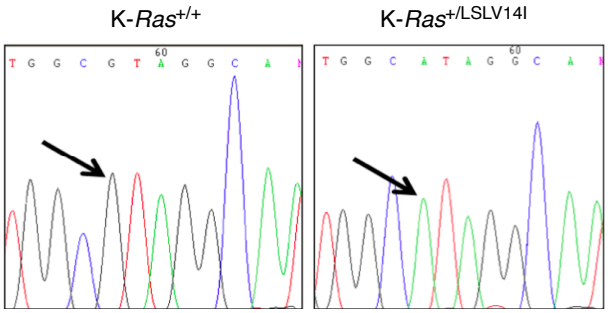

Figure 6. Detection of the V14I mutation. Sequencing of exon 1 of the K-*Ras* allele from tail genomic DNA of the K-*Ras*$^{+/+}$ (left) and K-*Ras*$^{+/LSLV14I}$ (right) agouti animals. Black arrow points to the modified nucleotide transversion G → A. G (guanine) in black and A (adenine) in green.

5.1.5 Germline K-*Ras*^{V14I} expression

K-*Ras*$^{+/LSLV14I}$ mice were crossed with the transgenic mice *EIIaCre (108)* that express the Cre recombinase at the zygote stages to allow the efficient cleavage of the LSL cassette in the germline. The tail DNA from the offspring was analyzed by Southern blot to test the cleavage of the LSL cassette. For this aim, an external probe was designed to recognized an XbaI-EcoRI fragment located upstream of the LSL cassette. The expected size will is of 5 Kbp for wild type mice and 1.9 Kbp for the mice that express the K-*Ras*^{V14I} mutation (V14) after XbaI digestion ***(Figure 7)***. Mice in which the STOP cassette is eliminated will express the mutant allele but still maintain one of the loxP. These mice were called K-*Ras*$^{+/LV14I}$, for simplicity, were called only K-*Ras*$^{+/V14I}$.

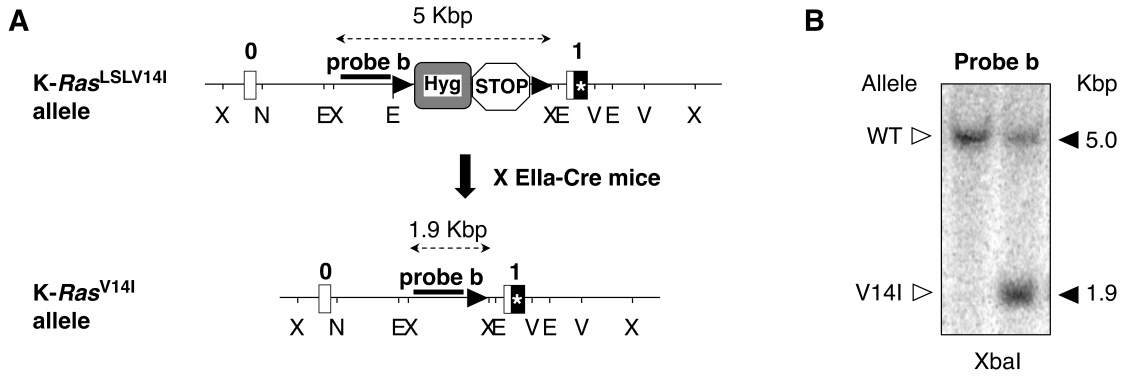

Figure 7. Excision of the LSL cassette strategy. (A) K-*Ras*^{V14I} allele results from crossing K-*Ras*$^{+/LSLV14I}$ mice to EIIaCre transgenic animals to excise the LSL cassette. White box represents the K-Ras noncoding exon 0; black box, K-Ras coding exon 1; checkered box, PGK-Hygromycin (Hyg) resistance cassette; octagonal box (STOP), transcriptional inhibitory sequences; triangle, loxP sites; asterisk, mutation in codon 14 (V14I). The position of the external probes used in the Southern blot analysis is indicated. Representative restriction enzyme cleavage sites are indicated (X, XbaI; E, EcoRI; V, EcoRV; N, NotI). **(B)** Southern blot analysis of DNA isolated from tails of mice carrying the wild type (+/+) and K-*Ras*^{V14I} (+/LV14I) allele after digestion with XbaI. Size of the wild type (5 Kbp) and K-*Ras*^{V14I} (1.9 Kbp) alleles is indicated.

Mice that express the mutation in all the cells, including germline cells, were crossed to C57BL/6J.OlaHsd to eliminate the *EIIaCre* transgene. The offspring of these crosses presented a mixed C57BL/6J.OlaHsd;129S2/SvPasCrl background (from now on C57BL;129S2/Sv).

5.2 MICE: MAINTENANCE AND GENOTYPING

5.2.1 Maintenance of mice

Animals were maintained in the animal facility of the CNIO (Centro Nacional de Investigaciones Oncológicas) according with the animal care standards established by the European Union. All the experiments were reviewed and approved by the Animal Care Committee of the Institute of Health Carlos III and the University of Salamanca. In the CNIO's animal facility the animals were subjected to cycles of light and dark of 12 hours each with the temperature and humidity of the rooms controlled.

Mice were maintained in a mixed C57BL/6J;129S2/Sv background (from now on B6/129) or were backcrossed up to seven generation into 129S2/Sv (from now on 129S2/Sv) or C57BL/6J (from now on C57BL/6J) background. Other strains of mice used in this study include the *p16Ink4a/p19Arf*$^{-/-}$ *(191)*, *Trp53*$^{-/-}$ *(52),* α myosin heavy chain (α*–MHC*)-Cre *(2),* *Rosa26*^{LSLLacZ} *(133),* Mx1-Cre *(107),* *Elas*-tTA/*tetO*-Cre *(70),* K-*Ras*$^{+/-}$ mice (developed by Carmen Guerra in our laboratory), *RERTn (69)* and *Pi3kca*^{LmgLH1047R} (provided by the Experimental Therapeutic Unit of the CNIO).

5.2.2 PCR genotyping

For routine genotyping of K-*Ras*^{LSLV14I} and K-*Ras*^{V14I} alleles, tail DNA was extracted as explained before *(see 3.1.3.1 section)*. We submitted tail DNA to PCR analysis at 94ºC for 5 min, followed by 30 cycles of 94ºC denaturing for 1 min, 60ºC annealing for 1 min, and 72ºC extension for 1 min, followed by an elongation cycle of 72ºC for 10 min with the following primers: 5´forward primer (5IO_2: 5'-TACCGCAAGGGTAGGTGTTGG-3', reverse wild type primer (3Ex1_2: 5'-ACCAGCTCCAACCACCACAAG-3') and reverse mutant primer (130rev-2: 5'-CTGCTCTTTACTGAAGGCTC-3'). The sizes of the diagnostic PCR products are 403 bp for the K-*Ras* wild type allele and 621 bp for the targeted K-*Ras*^{LSLV14I} allele. Samples in which the floxed STOP cassette was excised, primers 5I0 and 3Ex1 yield a DNA fragment of 669 bp.

5.3 BODY WEIGHT AND SIZE ANALYSIS

For growth curves, body length and body weight were measured every fifteen days. Mice were anesthetized with continuous flow of 1% to 3% isoflurane/oxygen mixture and the anal-nasal length was determined using a digital caliber.

5.4 BLOOD EXTRACTION AND NECROPSY

5.4.1 Blood extraction and analysis

To obtain blood from living animals, mice were anesthetized with continuous flow of 1% to 3% isoflurane/oxygen mixture and around 100 μl of blood was collected from the orbital sinus. Blood collection from the renal vein was used like a terminal method of blood extraction during the necropsy. In both cases, the blood was obtained using EDTA-tubes and blood populations were quantified using a blood analyzer (Abacus Junior Vet).

5.4.2 Necropsy

For the necropsy of adult animals, mice were sacrificed in CO_2 chamber and several tissue samples were collected including bone (femur), brain, heart, kidney, large intestine, liver, lung, pituitary gland, sex organs, skin, small intestine, spleen, stomach, thymus and urinary bladder. All the tissues samples were fixed in formalin and processed by the Comparative Pathology Unit at CNIO. Embryos at the different analyzed time points (E13.5 and E18.5) were extracted from the uterus of the mother, fixed in formalin and processed by the Comparative Pathology Unit at CNIO.

5.5 HISTOPATHOLOGY AND IMMUNOHISTOCHEMISTRY

5.5.1 Histopathology

Embryos and tissues were fixed in 10% buffered formalin and embedded in paraffin. Embryos, pancreata and lungs were serially sectioned (3 μm) and every 10 sections stained with hematoxylin and eosin (H&E). Sections (3 μm) of bone marrow (femur), brain, heart, kidney, large intestine, liver, lung, pituitary gland, sex organs, skin, small intestine, spleen, stomach, thymus and urinary bladder were stained with H&E for histopathological examination.

5.5.2 Blood smear preparation and staining

Blood smears were prepared using the Wedge technique. A small drop of blood about 3 mm of diameter was placed at one end of a glass slide. A second slide (pusher slide) was hold in front of the drop at a 30-45º angle to the smear slide. The pusher slide was pulled back into the blood drop and hold in that position until the blood spread across the width of the slide. It was then quickly and smoothly pushed forward to the end of the smear slide, creating a wedge smear. The slides were air-dried for 20 minutes and stained using May-Grünwald/Giemsa. Blood smears were covered with May-Grünwald solution (Merck) and incubated for 1 minute. After this time, the solution was washed carefully by adding destilled water and the slides were covered and incubated for 20 minutes with 1:10 Giemsa (Merk). Finally, the Giemsa solution was washing using destilled water and the blood smears were air-dried.

5.5.3 X-Gal staining on cryosections

X-Gal staining provides a visual assay of LacZ activity. LacZ gene encodes the β-galactosidase enzyme. This enzyme cleaves X-Gal into galactose and 5-bromo-4-chloro-3-hydroxyndole. This second compound is then oxidized into 5, 5-dibromo-4,4-dichloro-indigo. As its name suggests, this final product has a blue color.

To detect β-galactosidase activity, hearts were included in O.C.T^{TM} (Sakura) and frozen at -80ºC. The samples were cut in 10 μm sections using a cryostat (Vacutomer, Dako) and X-Gal staining was performed as described (Hogan et al., 1994). Sections were stored at 4ºC over night or 1 hour at RT. Next, they were fixed using a fixation solution that contains 0.2% glutaraldehyde (Sigma-Aldrich), 2mM $MgCl_2$, 5mM Ethylene Glycol Tetraacetic acid (EGTA) and 0.1M phosphate buffer pH 7.2 for 15 minutes at RT. The fixation solution was washed 3 times, 20 minutes, with a washing solution that contains 2mM $MgCl_2$, 0.02% NP40, 0.01% sodium deoxycolate (Sigma-Aldrich) and 0.1M phosphate buffer pH 7.2. After the washes, the

sections were incubated in a staining solution (0.1M pH 7.2, 2mM $MgCl_2$, 0.02% NP40, 0.01% sodium deoxycolate, 5mM $K_3Fe(CN)_6$, 5mM $K_4Fe(CN)_6$ and 1mg/ml X-Gal) at 37ºC over night. The following day, the sections were washed 3 times with the washing solution previously described, and thereafter rinsed once with 1X PBS and after with water. Finally, the counterstaining was performed with Nuclear Fast Red (NFR). The sections were stained with NFR for 1 minute. This staining was stopped with H_2O and after that the sections were dehydratated. To this aim, sections were washed for 2 minutes with 70% Ethanol, then 2 minutes with 100% Ethanol and were rinsed with Xilol (Merck) for 1 minute. Finally the sections were mounted with the mounting media (DAKO).

5.5.4 Immunohistochemistry

The immunohistochemistry was performed by the Comparative Pathology Unit of the CNIO using standard procedures. Antibodies used for immunohistochemistry analysis included goat polyclonal anti-CD3 antibody (1:250; M-20; Santa Cruz 1127), rabbit polyclonal anti-CD31 (1:50: ABCAM), rat monoclonal anti-F4/80 (1:10; D10; Monoclonal Antibodies CNIO core unit), prediluted rabbit monoclonal Ki67 (SP6; Master Diagnóstica 000311OQD), goat polyclonal anti-Pax5 (1:500; Santa Cruz 1974) and rabbit polyclonal anti-pErk (1:15; 9101, Cell signaling Technology)

5.5.5 Ki67 and cardiomyocyte quantification

The number of Ki67 positive cells was quantified using Axiovision Release 4.8.2 software. Cardiomyocyte area and relative cardiomyocyte numbers were quantified in heart H&E stained sections using Metamorph-Metaview software (Universal Imaging).

5.6 MOLECULAR ANALYSIS OF THE K-*Ras*^{V14I} MUTATION

5.6.1 Protein extraction

To extract proteins, small pieces of tissues (heart, lung and spleen) and pellets of mouse embryonic fibroblasts (MEFs) were incubated in an extraction buffer solution that contains 50mM Tris-HCl (pH 7.4), 150mM NaCl and 0.5% NP-40. To avoid the possible degradation of protein and to maintain the phosphate groups during the process, a cocktail of proteases inhibitors (Complete Mini, Roche) and phosphatase inhibitors (Sigma-Aldrich) were added to the extraction solution. In this solution, the tissues were homogenized on ice using a mini-homogenizer. After that, cells debris and chromosomal DNA were removed by 30 minutes

centrifugation at maximum speed (13,500 rpm). Finally, the supernatant was transferred to a fresh tube.

5.6.2 Protein quantification

Total protein amount in tissues and cells extract was determined using the Bradford protein quantification method. The Bradford assay is a colorimetric protein assay based on the formation of a complex between the dye, Coomassie Brilliant Blue G-250, and proteins under acidic conditions. The protein-dye complex causes a shift in the absorption maximum of the dye from 465 to 595 nm. The amount of absorption at 595 nm is proportional to the to the amount of proteins present in the sample. 1 μl of the protein sample was added to 1 ml of 1X Bradford solution (Bio-Rad) and the 595 nm absorbance was read on a spectrophotometer (Amersham Biosciences). A protein standard (growing concentration of Bovine Serum Albumin, BSA) was used to calculate the protein concentration on each sample.

5.6.3 Western blot: identification of Ras proteins and members of the Ras signaling pathway

Western blot method was used to determine the levels of expression of Ras proteins and its downstream effectors. The Western blot is an analytic technique used to identify proteins separated by electrophoresis and transfered to a membrane, using specific antibodies. 40 μg protein extracts obtained from E13.5 embryo, heart, lung, MEFs and spleen were separated using gel electrophoresis by molecular weight. The proteins were resolved by SDS-polyacrylamide gel electrophoresis (SDS-PAGE). Therefore, the samples were separated using 4-12% Bis-Tris polyacrilamide gels (Criterion XT Precast gel, Bio-Rad) and loaded with 1X XT Sample buffer (Bio-Rad) and 1X XT Reducing agent (Bio-Rad). The second buffer provided SDS and Tris-(2-Carboxyethyl)-phosphine (TCEP) as reducing agent. The SDS is an anionic detergent that maintains polypeptides in a denatured state and imparts a negative charge to the proteins. Heat treatment of the proteins in the presence of SDS and reducing agent (TCEP) effectively linearized the proteins. Thus, negative charged proteins in their denatured state moved to the positively charged electrode through the polyacrylamide mesh of the gel. In these conditions the proteins were separated by electrophoresis according to size. 1X MES (Bio-Rad) was the buffer used for the electrophoresis.

Then, the proteins were transferred to a nitrocellulose membrane (GE Healthcare) by semi-dry transfer method using 1X Tris-Glycine/20% methanol as buffer transfer at 0.35 mA for 45 minutes. The efficiency of the transfer was checked by staining the membrane with Ponceau solution (Sigma-Aldrich-Aldrich). Ponceau staining was completely removed by

continued water washing. After that, the membrane was incubated in 5% BSA in 1X Tris-Buffered Saline (TBS) solution with a 0.1% of Tween-20 at RT during 1 hour to block non-specific bindings. Subsequently the membrane was blotted with antibodies against Akt (1:1000; Cell Signaling Technology), phosphorylated Akt (1:1000; phosphoresidues Ser473; Cell Signaling Technology), Erk1 (1:1000; G262-118, BD Pharmigen), Erk2 (1:2000; 33, BD Pharmigen), phosphorylated Erk1/2 (1:500; phosphoresidues Thr202 and Tyr204; Cell Signaling Technology), Mek 1 (1:1000; C-18; Santa Cruz Biotechnology Inc.), phosphorylated Mek1 (1:500; phosphoresidues Ser217 and Ser211; Cell Signaling Technology), Pan-Ras (1:250; Ab-3, Calbiochem) and GAPDH (1:20000; Sigma-Aldrich-Aldrich) for loading control. The antibodies were diluted in 5% BSA/1X TBS/0.1% Tween-20 or 5% non-fat milk/1X TBS/0.1% Tween-20 according to the manufacture's protocols. The incubations were performed at 4ºC over-night.

After the incubation, unbound primary antibodies were washed from the membrane using four incubations of 10 minutes each with 1X TBS/0.1% Tween-20 at RT. Finally the membrane was incubated with the corresponding polyclonal goat horseradish peroxidase-linked secondary antibody against mouse or rabbit IgG for 1 hour at RT. These secondary antibodies were diluted at 1:1000 in 5% non-fat milk/1X TBS/0.1% Tween-20 and after four washes of 10 minutes each in 1X TBS/0.1% Tween-20 were visualized with an enhanced chemiluminescent system (ECL Plus, Amersham Bioseciences). Horseradish peroxidase catalyzes the oxidation of a cheminescent agent (luminol) in 3-aminophthalate, in a reaction that produces luminescence in proportion to the amount of protein. Therefore, exposure of the membrane to a sensitive photographic film and exposing it to the light of the reaction, we obtained an image corresponding to the band recognized by the primary antibody.

5.6.4 Determination of the Ras activation levels

To measure active GTP-bound K-Ras protein, 4 mg of protein extract from E13.5 embryos and MEFs were incubated with the Raf1 RBD agarose beads at 4ºC for 1 hour with gentle agitation according to manufacture's instruction (Ras activation assay kit, Cell Biolabs). Pulled-down K-Ras protein was detected by Western blot analysis, using the Pan-Ras antibody described above (*see 3.6.3 section*).

5.7 RNA ISOLATION AND QUANTITATIVE REAL TIME RT-PCR

Total RNA was isolated from hearts using trizol (Qiagen). Complementary DNA (cDNA) was synthesized using the NCode VILO microRNA cDNA synthesis kit (Invitrogen). The quantitative real time RT-PCR (qPCR) for microRNA-100 was performed using Express

SYBR GreenER Supermix with premixed ROX (Invitrogen). The Ct (Cycle threshold) values were normalized to SNOR95 (dCt) and relative expression was calculated using the 2^{-dCt} method. Primers for microRNA qPCR for mir-100 were purchased from abm and miScript primer assay (Qiagen) for SNOR95. For quantification of MKK6, Nanog and Smarca 5 expression, TaqMan probes were used according to the manufacturer's protocol (Applied Biosystem) and Ct were normalized to 18S rRNA (dCt).

5.8 MEFS ISOLATION AND IMMORTALIZATION

MEFs were isolated from E13.5 embryos and cultured in DMEM supplemented with 2mM glutamine, 1% penicillin/streptomycin and 10% fetal calf serum (FCS). Immortalization assay were performed using a classical 3T3 protocol *(216).*

5.9 IN-VIVO IMAGING METHODS

5.9.1 Micro X-ray computed tomography (micro-CT)

The CT acquisition was performed by the Molecular Imaging Unit at the CNIO, with an eXplore Vista PET CT (GE Healthcare) using an amperage of 200 μA and a voltage of 35 kV. Four-month old mice were anesthetized with a continuous flow of 1% to 3% isoflurane/oxygen mixture. 3D images of the skeleton were generated and analyzed with MMWS/Vista Software (GE Healthcare). Six measurements were taken using micro-CT images: skull length, skull width, skull height, inner canthal distance, and jaw length and width. The measures were established using anatomical references according to Jackson Laboratory standards protocols and procedures (http://craniofacial.jax.org/standard_protocols.html) ***(Figure 8).*** The skull volume was determined using 3D images.

5.9.2 PIXImus Densitometry

The densitometry acquisition was performed using PIXImus scans (PIXImus, LUNAR, Madison, WI). This scan provided skeletal and body composition data such as Bone Mineral Density (BMD, g/cm^2), Bone Mineral Content (BMC, g), body mass (g), lean content (g), fat content (g) and percentage of fat content. The PIXImus small animal densitometer (DEXA) had a resolution of 0.18 x 0.18 mm pixels and was equipped with software version 1.46. Mice were anesthetized with a continuous flow of 1% to 3% isoflurane/oxygen mixture.

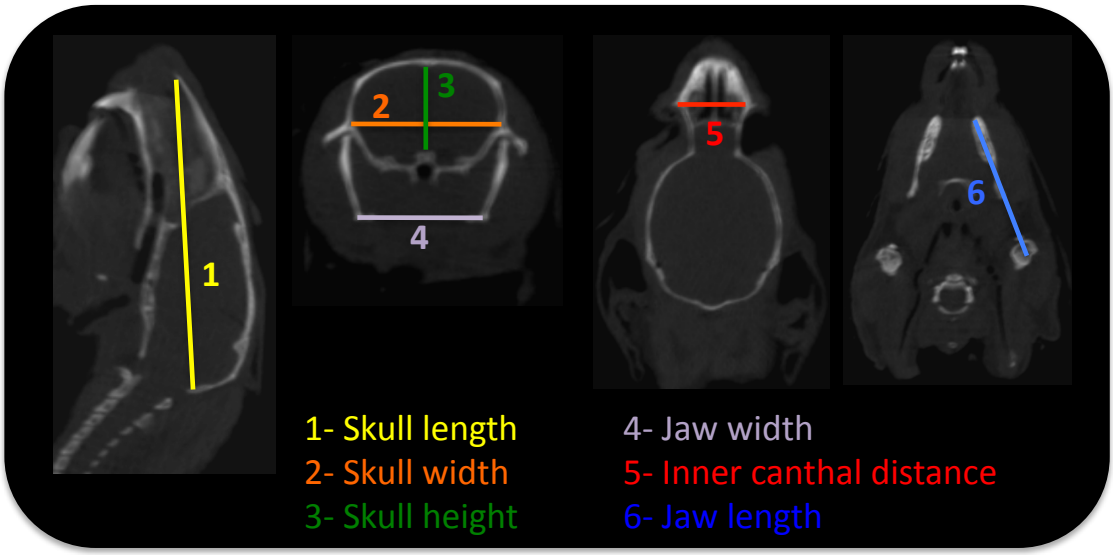

Figure 8. Representation of the anatomical landmarks used for the skull characterization. Four difference CT images were used to determine the six skull parameters analyzed. Each parameter was represented using colored lines and numbers. Yellow represents the skull length (1), orange the skull width (2), green the skull height (3), purple the jaw width (4), red the inner canthal distance (5) and blue the jaw length (6).

5.9.3 Magnetic Resonance Imaging (MRI) study

MRI studies were performed at the 'Gregorio Marañón' hospital. Mice were anaesthetized with a continuous flow of 2% Sevoflurane. MRI was acquired using a intraGateFLASH sequence from the aorta to the heart apex with slice thickness of 0.75 mm, repetition time (TR) 8 ms, echo time (TE) 2.691 ms, field of view (FOV) 6 x 4.13 cm and matrix size 465 x 256 cm. Left-ventricular functionality was evaluated on images in diastole and systole (Segment v1.9, R2354 software). Left ventricular epicardial and endocardial borders were manually delineated on the short-axis of each slide in order to measure the end-diastolic volume (EDV), end-systolic volume (ESV), ejection fraction (EF), left ventricle mass (LVM) and cardiac output (CO). The wall thickness in diastole (WTd) and systole (WTs), systolic wall thickening (WTn) and fractional shortening (FS) were measured in one slide at 3 mm from the apex.

5.10 ANALYSIS OF HEARING PARAMETERS

The analysis of the hearing parameters was performed by the 'Servicio de Evaluación Neurofuncional no Invasiva at the Instituto Biomédicas Alberto Sols CSIC-UAM. Servicio de Evaluación Funcional de Animales de Laboratorio, CIBERER, ISCIII'. 4-months-old mice were anesthetized with an intraperitoneal injection (i.p) of ketamine (75mg/kg)/xilacyne (5mg/kg)

mixture. Mice were exposed to a 'click', a mixture of sounds with different unknown frequencies to determine the hearing threshold, and a pure sounds of 8, 16, 28 and 40 kHz to determine the audiogram. The stimuli response was recording using electrodes placed in a standard position.

5.11 HEMODYNAMIC STUDY

Mean blood pressure was recorded in conscious mice at 4, 5 and 6 months of age with a non-invasive tail-cuff method (CODA, Kent Scientific). Blood pressure was measured in the tail of the mouse using a Volume Pressure Recording (VPR) sensor and an occlusion tail-cuff. Mice were accustomed to procedure for one week before accepting the recorded parameters.

5.12 FLOW CYTOMETRY ANALYSIS

5.12.1 Flow cytometry analysis: spleen

Single-cell suspensions were obtained from spleens using standard procedures. Mice were sacrificed by CO_2 inhalation and spleens were dissected. Splenocytes were obtained by mechanical dissociation of the organ in RPMI 1640 (BioWhittaker, Lonza) and filtration using 40 μm cell strainers. Erythrocytes were lysed after 30 seconds incubations in ACK lysis buffer (BioWhittaker, Lonza) and cells were resuspended in 1X PBS (BioWhittaker, Lonza) containing 0.5% BSA (Sigma-Aldrich-Aldrich) and 2 mM EDTA. Prior to analysis, cells were pre-incubated with purified anti-mouse CD16/32 antibody (1:200; BD Pharmigen, San Jose, CA) for 15 minutes on ice to block nonspecific Fc receptor-mediated binding. Aliquots of $5x10^6$ cells were stained for 30 minutes to 1 hour at RT in the dark with the following monoclonal antibodies from BD Pharmigen, San Jose, CA: APC rat anti-mouse CD19 (1:200; clone 1D3), APC hamster anti-mouse CD3e (1:200; clone 145-2C11), FITC rat anti-mouse CD11b (1:200; clone M1/70), PerCP-Cy5.5 rat anti-mouse CD11b (1:200; clone M1/70), PE-Cy7 rat anti-mouse CD8a (1:200; clone 53-6.7), PE-Cy7 rat anti-mouse Ly-6G and Ly6C (Gr1) (1:100; clone RB6-8C5), PerCP-Cy5.5 rat anti-mouse CD4 (1:200; clone RM 4-5) and PerCP-Cy5.5 mouse anti-mouse CD45.2 (1:100; clone 104). 4',6-diamidino-2-phenylindole (DAPI) was used to discriminate dead cells. Single stained controls were used for the signal compensation in the different channels and flourescense minus one (FMO) was used for setting the gating on control samples. The FMO control contains all the flourochromes in a panel, except the one that is being measured. The absence of signal of this flourochrome allows the setting of the corresponding gating for this color. Samples were processed on FACS CANTO II analyzer (BD Pharmigen, San Jose, CA). A minimum of 10,000 events was acquired. Data was analyzed

using FlowJo (Treestar, Ahskand, OR).

5.12.2 Flow cytometry analysis: bone marrow

Mice were sacrificed by CO_2 inhalation and femur and tibia were dissected. BM cells were freshly harvested by flushing femur and tibias with RPMI 1640 medium (BioWhittaker, Lonza). The end of the bones was cut, the tip of a needle with RPMI 1640 medium was inserted into the BM cavity and the BM was flushed into a tube. Erythrocytes were lysed with 30 seconds ACK lysis buffer (BioWhittaker, Lonza) incubation and Fc receptors were blocked by 30 minutes incubation with 3% BSA (Sigma-Aldrich-Aldrich) on ice.

HSCs were identified as Lin^- $IL7R\alpha^-$ $c\text{-}Kit^+$ $Sca1^+$; CLPs as Lin^- $IL7R\alpha^+$ $c\text{-}Kit^{low}$ $Sca1^{low}$; CMPs as Lin^- $IL7R\alpha^-$ $c\text{-}Kit^+$ $Sca1^+$ $Fc\gamma R^{low}$ $CD34^+$; GMPs Lin^- $IL7R\alpha^-$ $c\text{-}Kit^+$ $Sca1^+$ $Fc\gamma R^{high}$ $CD34^+$; and MEPs as Lin^- $IL7R\alpha^-$ $c\text{-}Kit^+$ $Sca1^+$ $Fc\gamma R^{low}$ $CD34^-$. $5x10^6$ BM cells were stained at RT for 1 hour in the dark with alexa-flour-488 rat anti-mouse CD127 (IL7Rα) (1:200; clone A7R34; eBioscience), APC mouse lineage antibody cocktail (1:100; BD Pharmigen, San Jose, CA), APC-H7 rat anti-mouse CD117 (c-Kit) (1:200; clone 2B8; BD Pharmigen, San Jose, CA), PE rat anti-mouse CD34 (1:250; clone RAM 34; BD Pharmigen, San Jose, CA), PE-Cy7 rat anti-mouse CD16/32 (FcγR) (1:400; clone 93; eBioscience) and PerCP-Cy5.5 rat anti-mouse Ly-6A/E (Sca1) (1:400, clone D7; eBioscience). DAPI was used to discriminate dead cells. Single stained controls were used for the signal compensation and FMOs were used for setting the gating on control tube. Samples were processed on FACS CANTO II analyzer (BD Pharmigen, San Jose, CA). A minimum of 50,000 events was acquired. Data was analyzed using FlowJo (Treestar, Ahskand, OR).

5.12.3 Flow cytometry analysis: blood

Blood was collected as mentioned before *(see 3.4.1 section)*. Erythrocytes were lysed with 15 minutes Erythrocyte Lysis Buffer (10 ml, Qiagen) incubation on ice and after 10 minutes centrifugation at 1200 rpm, cells were resuspended in 1X PBS/0,5% BSA/2 mM EDTA. Non-specific bindings were blocked using 15 minutes purified anti-mouse CD16/32 antibody (1:200; BD Pharmigen, San Jose, CA) incubation on ice. Aliquots of $5x10^6$ cells were stained for 30 minutes to 1 hour at RT in the dark with the following monoclonal antibodies from BD Pharmigen, San Jose, CA: APC rat anti-mouse CD19 (1:200; clone 1D3), APC hamster anti-mouse CD3e (1:200; clone 145-2C11), PerCP-Cy5.5 rat anti-mouse CD11b (1:200; clone M1/70), PE-Cy7 rat anti-mouse CD8a (1:200; clone 53-6.7), PE-Cy7 rat anti-mouse Ly-6G and Ly6C (Gr1) (1:100; clone RB6-8C5), PerCP-Cy5.5 rat anti-mouse CD4 (1:200; clone RM 4-5) and PerCP-Cy5.5 mouse anti-mouse CD45.2 (1:100; clone 104). DAPI

was used to discriminate dead cells. Single stained controls were used for the signal compensation and FMOs were used for setting the gating on control samples. Samples were processed on FACS CANTO II analyzer (BD Pharmigen, San Jose, CA). A minimum of 50,000 events was acquired. Data was analyzed using FlowJo (Treestar, Ahskand, OR).

5.12.4 Flow cytometric analysis and sorting: heart

Hearts were homogenized with Collagenase P (1mg/ml; Roche) for 20 minutes at 37º C and filtered through 40 μm cell strainers to obtain a single cell suspension. Then, cells were stained for 15 minutes on ice with APC rat anti-mouse Ly-6A/E (Sca1) (1:200; clone D7; BD Pharmigen, San Jose, CA), FITC rat anti-mouse CD31 (PECAM-1) (1:50; clone MEC 13.3; BD Pharmigen, San Jose, CA) and PE rat anti-mouse PDGFRα (CD140α) (1:100; clone APA5; eBioscience). Samples were sorted using a BD influx cell sorter (BD Pharmigen, San Jose, CA). DAPI was used to discriminate dead cells. Data was analyzed using FlowJo (Treestar, Ahskand, OR).

5.12.5 Apoptosis assay

Single bone marrow cell suspension was obtained as mentioned in the 3.12.2 section. 5 x 10^6 cells were stained with APC lineage antibody cocktail (1:100; BD Pharmigen, San Jose, CA), APC-H7 rat anti-mouse CD117 (c-Kit) (1:200; clone 2B8; BD Pharmigen, San Jose, CA) and PerCP-Cy5.5 rat anti-mouse Ly-6A/E (Sca1) (1:400; clone D7; eBioscience). Cells were subsequently stained with 5 μl of PE rat anti-mouse Annexin V and DAPI in the dark during 15 minutes at RT using the 1x Annexin V binding buffer [0.1M Hepes/ NaOH (pH 7.4)/ 1.4M NaCl/ 25mM $CaCl_2$] from the BD annexin V-PE apoptosis detection kit I (BD Pharmigen, San Jose, CA). Annexin V is a marker of early apoptotic cells. In apoptotic cells, the membrane phospholipid phosphatidylserine (PS) is translocated from the inner to the outer leaflet of the plasma membrane. Annexin V is a Ca^{2+}-dependent phospholipid-binding protein that has a high affinity for PS and binds to cells with exposed PS. Therefore, Annexin V staining identifies the early apopototic cells. This staining is used in combination with the vital dye DAPI, then viable cells are Annexin V and DAPI negative, cells that are in a early apoptosis are Annexin V positive and DAPI negative, and cells that are in late apoptosis are both Annexin V and DAPI positive. Apoptosis was analyzed by quantification of the Annexin V positive/ DAPI negative cell population by FACs.

5.12.6 Proliferation assay

For the proliferative assay, mice received 150 mg/kg of BrdU (5-bromo-2-deoxyuridine) (BD Pharmigen, San Jose, CA) by intraperitoneal injection 12 hours before euthanasia. BrdU is a synthetic nucleoside that is an analog of thymidine. It is incorporated into the newly synthesized DNA of replicating cells, substituting for thymidine during DNA replication. Using antibodies against this analog, cells that were actively replicating their DNA can be detected. To detect the proliferative HSC, lineage negative fraction was separated using magnetic mouse hematopoietic enrichment method and then cells were incubated with a specific antibody for BrdU.

First, single BM cells suspension was obtained as mentioned in the 3.12.2 section. Cells were enriched in hematopoietic progenitor by lineage depletion using BD IMag^{TM}-streptavidin-conjugated magnetic beads (Mouse Hematopoietic Progenitor (Stem) Cell Enrichment-Set, BD Pharmigen, San Jose, CA). For this aim, BM cells were incubated with the Biotinylated Mouse Lineage Depletion Cocktail (5µl per 1x10^6 cells) on ice for 15 minutes. This cocktail contains biotinylated monoclonal antibodies against mouse CD3e (CD3 ε chain), CD11b (Integrin αM chain), CD45R/B220, Ly6G and Ly6C (Gr-1) and TER-119/erythoroid cells (Ly-76). Therefore, this cocktail reacts with cells from the major hematopoietic cell lineages: T-lymphocytes, B-lymphocytes, monocytes/macrophages, granulocytes and erythrocytes. After washing with a 1X BD IMag^{TM} buffer, cells were incubated with the BD IMag^{TM} Streptavidin Particles Plus-DM (5µl per 1x10^6 cells) for 30 minutes at 6ºC-12ºC. These particles bind the cells bearing the biotinylated antibodies and provide a magnetic bead. The tube containing this labeled cell suspension was then placed within the magnetic field of the BD IMagnet^{TM}. Labeled cells (mature hematopoietic cells) migrate toward the magnet, leaving the unlabeled cells (lineage cells) in suspension. The supernatant, with the unlabeled cells (depleted fraction), were aspirated and placed in a new tube. Additional selections were performed to optimize the process. Finally, the total cell suspension with the depleted fraction was stained with APC rat anti-mouse CD117 (c-Kit) (1:200; clone 2B8; BD Pharmigen, San Jose, CA) and PE rat anti-mouse Ly-6A/E (Sca1) (1:200; clone D7; BD Pharmigen, San Jose, CA).

Cells were subsequently incubated with FITC anti-BrdU (FITC BrdU Flow kit, BD Pharmigen, San Jose, CA). This staining is an intracellular staining, therefore required a permeabilization step to allow the entrance of the antibody inside the cell. Also required the DNA denaturalization to allow the antibody access to the incorporated BrdU residues. For this aim, cells were incubated with BD Cytofix/Cytoperm buffer for 15 minutes at RT. This buffer contains a mixture of the fixative paraformaldehyde and the detergent saponine, hence it preserves the cell morphology, fixes the cellular proteins and permeabilizes the cells. After the incubation, cells were washed with 1 ml of 1X BD Perm/Wash buffer, centrifuged 10 minutes at

300g and the supernatant was discarded. This supernatant was resuspended in with 100 µl of BD Cytoperm Plus buffer for 10 minutes on ice. This buffer is used as a staining enhancer and secondary permeabilization reagent. A re-fixation step was performed by 5 minutes incubation at RT with 100 µl of BD Cytofix/Cytoperm buffer. After washing with 1 ml of 1X BD Perm/Wash buffer, cells were treated with DNase for 1 hour at 37ºC to expose the incorporated BrdU. Then, cells were washed and stained with FITC anti-BrdU antibody (1:50, FITC BrdU Flow kit, BD Pharmigen, San Jose, CA) in 1X BD Perm/Wash buffer for 20 minutes in the dark at RT. Finally, cells were washed and stained with Hoechst for cell cycle analysis. Samples were processed on LSRII/Fortesa analyzer (BD Pharmigen, San Jose, CA). A minimum of 50,000 events was acquired. Data was analyzed using FlowJo (Treestar, Ahskand, OR).

5.13 COLONY FORMING ASSAY

5.13.1 BM colony assay

In the bone marrow, the HSCs produce the hematopoietic progenitors. These progenitors proliferate and differentiate resulting in the generation of the variety of mature blood cells. *In vitro* assay systems have been developed to quantify these progenitors. When cultured in a semi-solid media, such as methylcellulose, supplemented with the proper nutrients and cytokines, individual progenitors called colony-forming cells (CFCs), proliferate to form discrete cell clusters or colonies. Each progenitor forms a type of colonies easily identified based on their different morphology. In our case, BM cells ($2x10^4$) were cultured in the methylcellulose-base media Methocult M3234 (StemCell Technologies) in absence of cytokines or containing recombinant murine GM-CSF (PeproTech) or IL-3 (PeproTech) at growing concentrations to promote the formation of the CFC-granulocyte macrophage (CFU-GM). Methocult M3234 medium contains 1% Methycellulose, 15% FBS, 1% BSA, 10 µg/ml of insulin, 200 µg/ml of human transferrin (iron-saturated), 10^{-4}M 2-Mercaptoethanol and was supplemented with Iscove´s MDM medium (IMDM, StemCell Technologies), 2 mM glutamine and 1% penicillin/streptomycin.

Single BM cell suspension was obtained as mentioned in the 3.12.2 section. A ten-fold higher concentration of cellular suspension ($2x10^5$ cells/ml) was prepared in IMDM (StemCell Technologies) and 300 µl of this suspension was added to 3 ml of Methocult M3234 containing the proper amount of cytokines (0.001, 0.01, 0.1, 1 and 10 ng/ml of IL3 or 0.001, 0.01, 0.1, 1 ng/ml of GM-CSF) or in absence of cytokines. After vortex the mixture and let stand for 2-5 minutes to dissipate the bubbles, 1.1 ml of cells plus Methocult mixture was dispensed using a syringe attached to 18 gauge needle to each of two 35 mm dishes (StemCell Technologies) for

duplicate experiments. The duplicated dishes were placed into a 100 mm culture plate with an uncovered extra 35 mm dish containing 3-4 ml of sterile water to maintain the humidity. Cells were incubated at 37ºC, 5% CO_2 and 95% humidity for 9-12 days. Colonies were counted on day 9 using an inverted microscope.

5.13.2 CFU-F colony assay of cardiac stem cells

For colony forming units-fibroblast (CFU-F) assay, 5,000 Sca-1^+/PDGFRα^+/$CD31^-$ cells were plated on chamber slides (Ibidi) and cultured in αMEM (GIBSO) plus 20% of Fetal Calf Serum (FCS) for two weeks.

5.14 BONE MARROW TRANSPLANTATION

BM cells from K-*Ras*$^{+/+}$ and heterozygous K-*Ras*$^{+/V14I}$ mice backcrossed to the C57BL/6J background for four generations were harvested from femurs and tibias. After eritrocytes lysis, a ten-fold higher concentration of cellular suspension (10^7 cells/ml) was prepared in 1X PBS (BioWhittaker, Lonza). 100 µl of this suspension (10^6 cells) was injected into the lateral tail vein of lethally irradiated (two doses of 550 cGy in a three hours interval) C57BL/6J host mice. A small group of mice was injected only with 1X PBS (BioWhittaker, Lonza) like an irradiation control. Mice were maintained with 2.5 mg/100 ml of Enrofloxacine (broad spectrum antibiotic) in drinking water until the end of the experiment.

5.15 MICE PROTOCOLS TO CONTROL THE CRE RECOMBINASE ACTIVITY

5.15.1 Polyinosinic-polycytidylic acid (pI-pC) treatment

For induction of interferon-inducible Cre (Mx1-Cre) expression, K-*Ras*$^{+/+}$; Mx1-$Cre^{+/T}$ and K-*Ras*$^{+/LSLV14I}$; Mx1-$Cre^{+/T}$ 4- to 5-week-old mice were injected intraperitoneally (i.p) with 10 µg/g body weight of Polyinosinic-polycytidylic acid (pI-pC, Sigma-Aldrich) in 1X PBS every other day for three doses.

5.15.2 Tamoxifen diet treatment

To activate the expression of the K-*Ras*$^{+/LSLV14I}$ and *Pi3kca*$^{+/H1047R}$ in somatic cells in a temporally controlled manner we used the *RERTn*$^{ert/ert}$ strain that express a CreERT2 recombinase which activity is driven by tamoxifen. K-*Ras*$^{+/LSLV14I}$; *RERTn*$^{ert/ert}$ and the K-*Ras*$^{+/LSLV14I}$; *RERTn*$^{ert/ert}$; *Pi3kca*$^{+/H1047R}$ mice were submitted to a tamoxifen diet (Tekland CRD

Tam^{400}/CreER) *ad libitum*. This treatment resulted in the activation of the inducible Cre-ERT2 recombinase, leading the expression of both mutations. The standard diet (28018S, Tekland) contains genistein, a phytoestrogen that belongs to the category of the isoflavones. The genistein has been shown to interact with animal and human estrogen receptors. To avoid the competition between genistein and tamoxifen to bind to the estrogen receptor, 10 days before the TAM-diet administration, mice were maintained with a wash out diet (2019S, Tekland). This diet does not contain alfalfa or soybean meal, thus minimizing the occurrence of natural phytoestrogens. The active metabolite of tamoxifen, 4-hydroxy-tamoxifen (4OHT), was produced in the organism by hydroxylation.

5.15.3 Adenovirus intratracheal infection

Eight-week-old mice were treated once by intratracheal adeno-Cre instillation with $3x10^8$ plaque forming units (pfu)/mouse of virus after anesthesia via i.p injection of ketamine (75mg/kg, Imalgene®) and xylazyne (12 mg/kg, Rompum®) solution. The virus was introduced directly in the trachea through a cannula *(200)*. After inoculation mice were maintained during 10-15 minutes under a heat lamp.

5.16 INDUCTION OF PANCREATITIS BY CAERULEIN TREATMENT

Chronic pancreatitis was induced by treatment with caerulein (Sigma-Aldrich), a cholecystokinin analog *(133, 241)*. Caerulein was administered as a 0.1 ml single daily i.p injection of 50 mg/ml solution in saline, 5 days per week during the time of the study *(70)*.

5.17 NICOTINE TREATMENT

Nicotine at a concentration of 100 µg/ml (Sigma-Aldrich) was provided *ad libitum* in the drinking water with sucrose (2% water/volume) to 4 week-old-mice for 1 year *(203)*.

5.18 MEK INHIBITOR TREATMENT

To determine whether the MEK inhibitor PD0325901 (Wuhan Sunrise Technology Development Company Limited, China) treatment could prevent or ameliorate some of the defects associated with the expression of the K-RasV14I mutation we performed three different treatment protocols ***(Figure 9):***

1. *Prenatal treatment*: MEK inhibitor PD0325901 was resuspended in 0.5% hydroxypropylmethylcellulose (Sigma-Aldrich) with 0.2% Tween80 (Sigma-Aldrich)

and injected i.p (1 mg/kg of body weight) into pregnant female daily, beginning on gestational day 7.5 (E7.5) until P9. Vehicle-injected mice were used as a control. At P10, PD0325901 or vehicle was injected i.p (1mg/kg of body weight) directly into the pups every other day, until 4 weeks after birth.

2. *Postnatal treatment:* PD0325901 was dissolved in DMSO (Sigma-Aldrich), and then resuspended in 0.5% hydroxypropylmethylcellulose with 0.2% Tween80 (in a proportion of 1% DMSO/99% hydroxypropylmethylcellulose; Tween80) and daily injected (i.p, 5 mg/kg of body weight) at P21 for 6 weeks. Control mice were injected only with vehicle.
3. *Adult treatment:* PD0325901 was dissolved in DMSO (Sigma-Aldrich), and then resuspended in 0.5% hydroxypropylmethylcellulose with 0.2% Tween80 (in a proportion of 1% DMSO/99% hydroxypropylmethylcellulose; Tween80) and daily injected (i.p, 5 mg/kg of body weight) into 4-month-old mice 1 month. Control mice were injected only with vehicle.

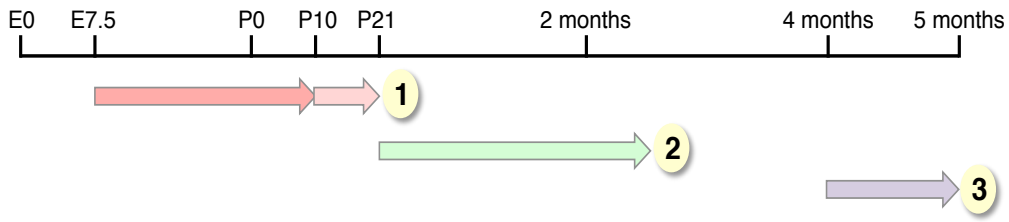

Figure 9. **Treatment protocols.** Arrows indicate the duration of the treatments. Pink arrows: prenatal treatment or treatment 1, green arrow: postnatal treatment or treatment 2, purple arrow: adult treatment or treatment 3.

5.19 STATISTICS

Results were expressed as mean ± SD. K-*Ras*$^{+/V14I}$ and K-*Ras*$^{V14I/V14I}$ mice were compared to K-*Ras*$^{+/+}$ mice using 2-tailed Student´s test. A *P* value less than 0.05 was considered significant. U Mann Whitney test was used in the experiments of the cardiac stem cells. Long rank (Mantel-Cox) test was used to compare the survival curve of mice treated either with the vehicle or with the PD0325901. A *P* value less than 0.05 was considered significant.

6. Results

6.1 GENERATION OF A CONDITIONAL K-*RAS* KNOCK-IN MOUSE MODEL FOR NOONAN SYNDROME

To better understand the developmental and physiological defects associated with the expression of germline K-*RAS* mutations we have generated a knock-in mouse model that expresses the most common K-*RAS* mutations found in Noonan patients, the substitution V14I *(122)*. Furthermore, this mouse model allows to evaluate the tumor predisposition of K-*RAS*-Noonan patients and to test preventative and therapeutic strategies that can prevent or ameliorate the alterations associated with the expression of these activated mutations.

6.1.1 Conditional K-*Ras*^{LSLV14I} knock-in mouse model

To generate a mouse model for Noonan Syndrome (NS), we knocked-in a G→A transition in the first base of the 14th codon of the K-*Ras* locus, a strategy that led to the replacement of the normal GTA sequence (valine) by ATA (isoleucine), the most frequent K-*RAS* mutation observed in NS patients *(122)*. To control the expression of this mutation we introduced a transcriptional STOP sequence upstream of the mutagenized exon flanked by loxP sites *(108)*. The loxP sites are 34 bp of DNA sequences that are specifically recognized by the Cre recombinase, an enzyme that catalyses a recombination event between the two loxP sites. In our strategy, the orientation of the loxP sites allows the elimination of the transcriptional STOP sequence and consequently the expression of the mutations by the recombination event driven by the Cre recombinase. Together with the STOP cassette we also introduced a hygromicin resistant gene (*Hyg*) whose expression is driven by the phosphoglycerate kinase (*PGK*) promoter. Therefore, the resistance sequence can be removed together with the STOP cassette, avoiding interferences with the expression of the mutated allele *(see section 5.1 Material and Methods for detail description)*

The allele that includes all the modifications was called K-*Ras*^{LSLV14I} where "LSL" indicated "LoxP-STOP-LoxP" cassette, a short name for the cassette "LoxP-PGK-Hyg-STOP-LoxP" and V14I indicated the mutation.

Mice lacking the K-*Ras* gene die from E12.5 to E15 *(89, 100)*. Therefore, since the STOP sequence prevents the expression of the K-*Ras* mutated allele; mice homozygous for the LSLV14I sequence are not viable.

6.2 K-*Ras*^{V14I} EXPRESSION IS COMPATIBLE WITH EMBRYO AND POSTNATAL STAGES

Prenatal widespread expression of oncogenic K-*Ras* mutations (G12V or G12D) was not tolerated during the embryonic development and embryos died from E9.5 to E11.5 due to placental, cardiovascular and hematopoietic defects *(69, 193, 221)*.

To address if expression of the K-*Ras*^{V14I} mutation is compatible with embryonic and postnatal development, K-*Ras*$^{+/LSLV14I}$ mice were crossed with the transgenic mice *EIIaCre (108)*. In this mouse, the adenovirus EIIa promoter drives the expression of the Cre recombinase selectively to pre-implantation embryos, at one-cell zygote stage of embryonic development. Promoting, in our mouse model, the expression of the mutation in all cell populations, including gemline cells. Mice carrying the K-*Ras*^{V14I} allele in all the cells were identified by Southern blot *(see 5.1.5 section in Materials and Methods)* and crossed with C57BL/6J mice to eliminate the *EIIaCre* transgene. The resulting K-*Ras*$^{+/V14I}$ mice express the K-*Ras*^{V14I} allele in heterozygosity in all the cells. These mice were in a mixed C57BL/6J;129S2/Sv background (from now on B6/129). All the studies described in this manuscript were carried out with these mice, unless otherwise indicated.

K-*Ras*$^{+/V14I}$ mice were born at the expected Mendelian ratio and reached adulthood. In contrast, homozygous K-*Ras*$^{V14I/V14I}$ mice displayed high perinatal lethality due to cardiovascular problems *(see bellow)*. 10% of homozygous K-*Ras*$^{V14I/V14I}$ animals, obtained from crosses between heterozygous mice, overcame these problems, survived and reached adulthood. Although, K-*Ras*$^{+/V14I}$ and K-*Ras*$^{V14I/V14I}$ mice presented reduced life span with a half-life of 62 and 36 weeks, respectively ***(Figure 10).***

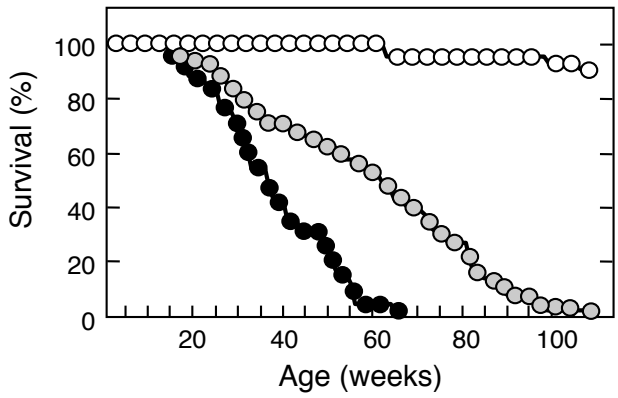

Figure 10. K-*Ras*^{V4I} mice displayed reduced life span. Survival curve of wild type (n=25; open circles), K-*Ras*$^{+/V14I}$ (n=68; gray circles), and K-*Ras*$^{V14I/V14I}$ (n=30; solid circles) mice in mixed B6/129 genetic background.

K-*Ras*$^{+/V14I}$ mice were fertile. Both K-*Ras*$^{V14I/V14I}$ females and males were also fertile, since crosses with K-*Ras*$^{+/V14I}$ and wild type mice succeeded. However, the offspring from crosses with heterozygous K-*Ras*$^{+/V14I}$ mice was smaller (3 to 4 pups) compared to the average litter size (7 pups). Moreover, no mating between K-*Ras*$^{V14I/V14I}$ mice worked. Thus, all these findings suggest that K-*Ras*$^{V14I/V14I}$ mice have some fertility problems.

Male gonadal dysfunction is reported in Noonan patients. In contrast, fertility in females is not affected *(100, 171)*. Therefore, the breeding inefficiency between K-*Ras*$^{V14I/V14I}$ mice could reflect some of the alterations found in NS patients.

6.2.1 Perinatal lethality of K-*Ras*$^{V14I/V14I}$ mice

Analysis of embryos and newborns at different stages revealed that K-*Ras*$^{V14I/V14I}$ mice died early just after birth. At embryonic days E13.5 and E18.5, the number of homozygous embryos appeared as expected and were comparable, in size and morphology, to their wild type littermates. However, daily control of the matings (pregnant females, date of birth, offspring number and genotyped of the death pups) illustrated that high percentage of K-*Ras*$^{V14I/V14I}$ mice were born dead or died shortly after birth ***(Table 1).***

Table 1. Viable progeny from matings between K-Ras$^{+/V14I}$ mice.

Stage	n	K-*Ras*$^{+/+}$	K-*Ras*$^{+/V14I}$	K-*Ras*^{V14I}
E13.5	68	16 (23%)	38 (56%)	14 (21%)
E18.5	46	12 (26%)	21 (46%)	13 (28%)
P0	25	7 (28%)	13 (52%)	5 (20%)
P21	416	159 (38%)	214 (52%)	43 (10%)

Number and the corresponding percentage of embryos and mice at different stages are shown.

Heart characterization revealed that K-*Ras*$^{V14I/V14I}$ neonatal mice showed an enlarged heart already evident at midgestation (E13.5) ***(Figure 11A)***. Although K-*Ras*$^{V14I/V14I}$ mice found dead at P0 were similar in size and morphology to the wild type littermates, careful histological analysis of these homozygous mice (n=5) revealed focal necrosis areas in tissues such as liver and muscle, a result consistent with defects associated to a cardiovascular etiology ***(Figure 11B)***. All together, these results suggest that homozygous mice die at perinatal stages due to cardio-respiratory problems.

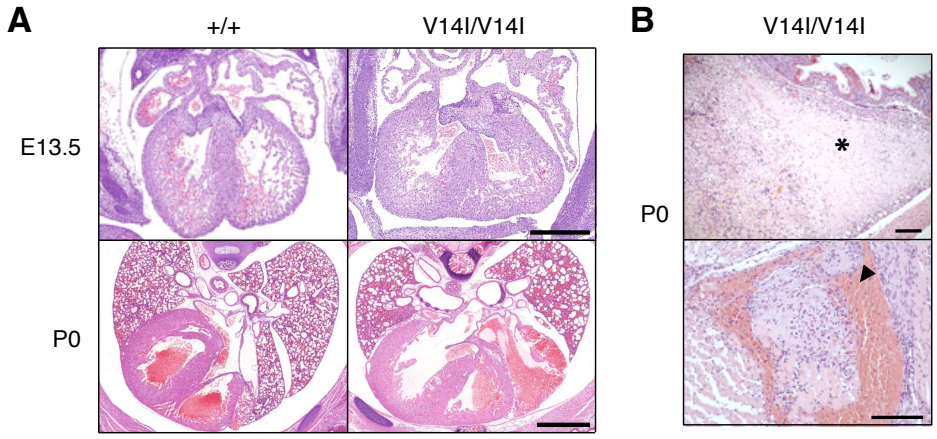

Figure 11. K-*Ras*$^{V14I/V14I}$ mice display perinatal lethality. (A). Top: H&E stained paraffin transverse section of E13.5 wild type (+/+) and K-*Ras*$^{V14I/V14I}$ (V14I/V14I) embryos. Scale bar, 500 μm. Bottom: H&E stained paraffin transverse section of neonate (P0) wild type (+/+) and K-*Ras*$^{V14I/V14I}$ (V14I/V14I) pups. Scale bar, 1000 μm), showing the heart morphology at these stages. **(B).** H&E stained paraffin sections from liver (top) and muscle (bottom) from a representative K-*Ras*$^{V14I/V14I}$ sick P0 mouse. Asterisk indicates the necrotic area in liver. Solid arrowhead points to necrotic area in muscle. Scale bar, 100 μm.

6.3 MOLECULAR ANALYSIS OF THE K-Ras^{V14I} MUTATION AND THE K-Ras SIGNALING PATHWAY

6.3.1 Molecular analysis of the K-Ras^{V14I} mutation

K-RAS^{V14I} mutation is located in the P-loop of the protein and interferes with the guanine nucleotide exchange factor site. Biochemical analysis suggested that this change induces a reduced GTPase activity, basally or after stimulation with GAP proteins, compared to the wild type form of the protein but more than the oncogenic form G12D *(see more detail in 2.3.4.1 section)*. Therefore this modification induces an intermediate increase of the active RAS status compared to the wild type and oncogenic protein *(65, 186, 188)*.

RAS, in their active conformation, can interact with more than 20 effectors to regulate several cellular responses *(53, 187)*. One of these effectors is the RAF protein. GTP-active RAS binds to the RAS-binding domain (RBD) of this protein to control downstream signaling cascade. To quantify the RAS activation of, the GTP-bound status of the protein, we used RAF1-RBD agarose beads. These beads selectively bind to the RAS-GTP allowing its isolation by a pull-down assay.

To this aim, we obtained protein extracts from E13.5 embryos. As expected, the amount of K-Ras-GTP was more abundant in K-*Ras*$^{+/V14I}$ and K-*Ras*$^{V14I/V14I}$ embryos than in wild type littermates. However, the total GTP bound K-Ras^{V14I} protein, even in homozygous embryos, was lower that the amount bound to the oncogenic K-Ras^{G12V} isoform ***(Figure 12)***. This result

confirms that the activation levels of the K-Ras^{V14I} protein are higher than those of the wild type protein, but lower than those of the oncogenic form. Therefore, the K-Ras^{V14I} protein has attenuated biochemical phenotype compatible with embryo and postnatal development.

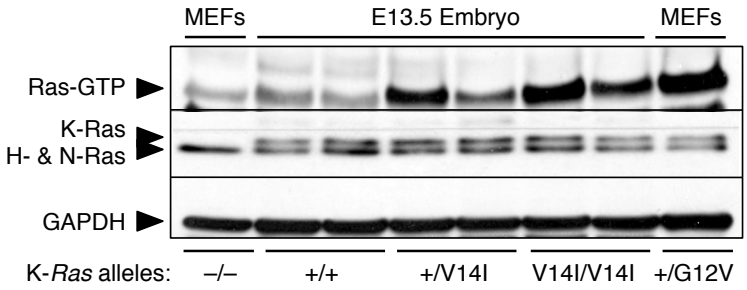

Figure 12. Molecular analysis of the activation status of the K-Ras^{V14I} mutation. Western blot of protein extracts (4 mg) obtained from K-*Ras*$^{+/+}$ (+/+), K-*Ras*$^{+/V14I}$ (+/V14I) and K-*Ras*$^{V14I/V14I}$ (V14/V14I) E13.5 embryos and K-*Ras*$^{-/-}$ (-/-) and K-*Ras*$^{+/G12V}$ (+/G12V) MEFs incubated with the Ras binding domain (RBD) of c-Raf. The resulting complexes, as well as 40 µg of unprocessed protein extracts were resolved by SDS-PAGE, transferred to a nitrocellulose membrane and blotted with a Pan-Ras antibody. GAPDH was used as a loading control. The migration of the RBD-bound Ras proteins, as well as of the individual K-Ras, H-Ras and N-Ras proteins is indicated by arrowheads.

6.3.2 Molecular analysis of the K-*Ras* signaling pathway

To analyze if the enhanced level of GTP-bound K-Ras protein in K-*Ras*$^{+/V14I}$ and K-*Ras*$^{V14I/V14I}$ embryos is associated with an increased signaling activation, we characterized two of the most important signaling pathways (the RAF and the PI3K pathway) by Western blot.

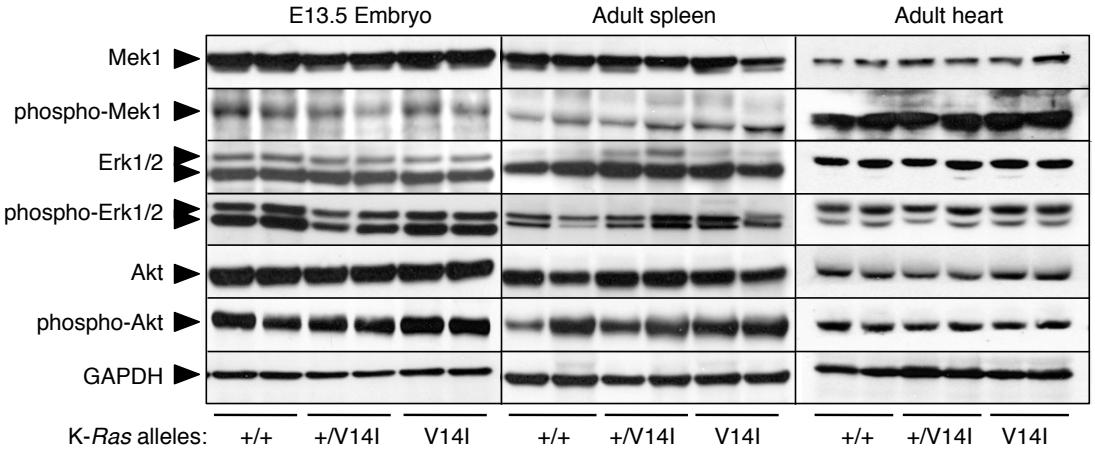

Figure 13. Functional characterization of the K-Ras signaling. Proteins extracts (40 µg) obtained from E13.5 embryos and spleens and hearts of 4-month-old K-*Ras*$^{+/+}$ (+/+), K-*Ras*$^{+/V14I}$ (+/V14I) and K-*Ras*$^{V14I/V14I}$ (V14I/V14I) mice were resolved by SDS-PAGE, transferred to a nitrocellulose membrane and blotted with antibodies against nonphosphorylated and phosphorylated forms of Erk1/2, Mek1 and Akt. GAPDH was used as a loading control. The migration of the corresponding proteins is indicated by arrowheads.

In spite of the accumulation of the K-Ras^{V14I} mutation in the active form, the phosphorylation levels of the Mek, Erk1/2 and Akt downstream kinases were comparable in wild type and mutant E13.5 embryos ***(Figure 13)***. Same results were obtained in adult tissues such as spleen and heart, two of the organs most affected by the expression of the K-Ras^{V14I} isoform *(see bellow)*. According to this result, the total levels of the Erk1, Erk2, Mek1 and Akt protein effectors were similar in wild type and mutant E13.5 embryos and in the studied adult tissues, heart and spleen ***(Figure 13)***. These observations are reminiscent of those previously observed in H-*Ras*^{G12V} Costello mouse model *(189)*, thus suggesting the existence of negative feedback mechanisms that control the levels of Ras signaling. This negative feedback signaling has been previously suggested for K-Ras^{G12D} signaling during embryo development *(194)*. Alternatively, it is possible that Western-blot analysis of phosphorylated downstream effectors may not be sensitive enough to detect subtle differences in the amount of Ras signaling generated in tissues expressing constitutively active K-Ras^{V14I} proteins. In fact, significant levels of pErk were detected by immunohistochemistry in heart of K-*Ras*$^{V14I/V14I}$ embryos and neonate, one of the most affected tissues in these mice ***(Figure 14)***. Similar results were described for other NS mouse models (14).

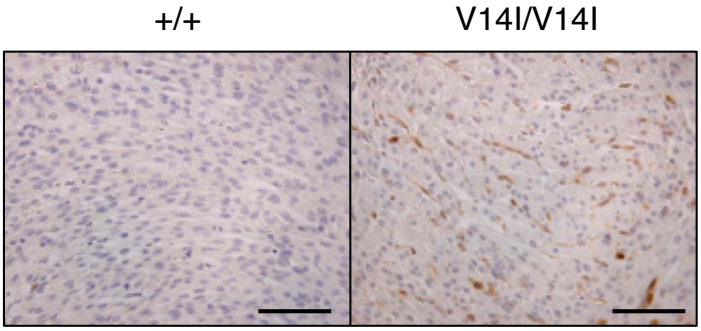

Figure 14. Enhanced Erk activation in heart embryos. pErk1/2 immunostaining in hearts of E18.5 wild type (+/+) and K-*Ras*$^{V14I/V14I}$ (V14I/V14I) embryos. Scale bar, 50 μm.

6.4 ROLE OF K-*Ras*^{V14I} IN PROLIFERATIVE SENESCENCE

Primary mouse embryonic fibroblast (MEFs) expressing the K-*Ras*^{G12V} or K-*Ras*^{G12D} oncogenes do not undergo proliferative senescence and proliferate as immortal cells *(69, 221)*.

To address if MEFs expressing the K-*Ras*^{V14I} mutation became immortalized with the same kinetics of those that express the oncogenic mutations, MEFs were extracted from E13.5 embryos and were immortalized by the standard 3T3 protocol. Unlike K-*Ras* oncogenes, the endogenous expression of the K-*Ras*^{V14I} mutation did not prevent the proliferative senescence. After few passages in culture, K-*Ras*$^{+/V14I}$ (n=6) and K-*Ras*$^{V14I/V14I}$ (n=5) MEFs underwent

proliferative senescence, as well as wild type cells (n=5). However, upon continuous passages, K-*Ras*$^{V14I/V14I}$ MEFs overcame the crisis and became immortal (around passage 14th) faster than wild type MEFs. This process was gene dose dependent since K-*Ras*$^{+/V14I}$ MEFs displayed an intermediate phenotype, overcoming the crisis around passage 17th ***(Figure 15)***.

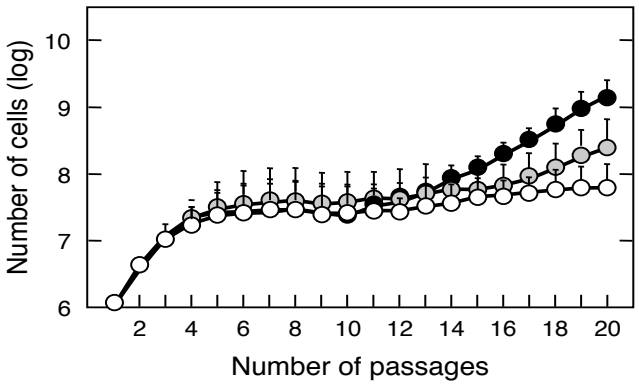

Figure 15. Immortalization properties of MEFs expressing the K-*Ras*^{V14I} mutation. Immortalization of wild type (n=5; open circles), K-*Ras*$^{+/V14I}$ (n=6; gray circles) and K-*Ras*$^{V14I/V14I}$ (n=5; solid circles) MEFs following the 3T3 protocol. Error bars indicate the SD.

This observation indicates that although the expression of the K-*Ras*^{V14I} mutation is not associated with a hyperproliferative phenotype, the expression of this mutation induces a stronger proliferative response, at least in MEFs.

6.4.1 Molecular analysis of the K-Ras^{V14I} mutation in MEFs

We determined the Ras-GTP levels in MEFs following the approach described in *section 6.3.1*. As observed in E13.5 embryos, primary K-*Ras*$^{+/V14I}$ and K-*Ras*$^{V14I/V14I}$ MEFs showed higher levels of activate GTP-bound Ras, than the wild type MEFs. Again, this activation was lower compared to MEFs that express the G12V oncogenic form ***(Figure 16A)***.

We also determined the activation status of the RAS signaling pathway in primary MEFs by Western blot. Like E13.5 embryos and adult tissues, K-*Ras*$^{+/V14I}$ and K-*Ras*$^{V14I/V14I}$ MEFs contained equal phosphorylation and total levels of Mek, Erk1/2 and Akt downstream effectors, compared to the wild type cells ***(Figure 16B)***. Therefore, primary K-*Ras*^{V14I}-expressing MEFs displayed comparable signaling response in their downstream mitogenic (Raf/Mek/Erk) and survival (PI3K/Pdk/Akt) pathways to wild type MEFs.

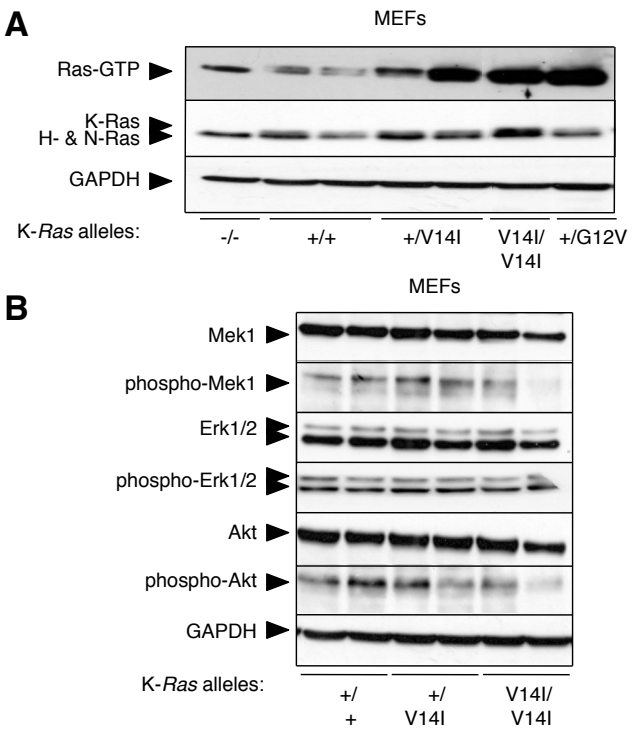

Figure 16. Molecular analysis of the K-Ras^{V14I} mutation in MEFs. (A). Western blot analysis of protein extracts (4 mg) obtained from K-*Ras*$^{-/-}$ (-/-), K-*Ras*$^{+/+}$ (+/+), K-*Ras*$^{+/V14I}$ (+/V14I) and K-*Ras*$^{V14I/V14I}$ (V14/V14I) and K-*Ras*$^{+/G12V}$ (+/G12V) MEFs incubated with the Ras binding domain (RBD) of c-Raf. The resulting complexes, as well as 40 μg of unprocessed protein extracts were resolved by SDS-PAGE, transferred to a nitrocellulose membrane and blotted with a Pan-Ras antibody. GAPDH was used as a loading control**.** The migration of the RBD-bound Ras proteins as well as the individual K-Ras, H-Ras and N-Ras proteins is indicated by arrowheads. **(B)**. Protein extracts (40 μg), from K-*Ras*$^{+/+}$ (+/+), K-*Ras*$^{+/V14I}$ (+/V14I) and K-*Ras*$^{V14I/V14I}$ (V14I/V14I) MEFs, were resolved by SDS-PAGE, transferred to a nitrocellulose membrane and blotted with antibodies against nonphosphorylated and phosphorylated forms of Erk1/2, Mek1 and Akt. GAPDH was used as a loading control. The migration of the corresponding proteins is indicated by arrowheads.

6.5 K-*Ras*^{V14I} DISPLAYED REDUCED BODY SIZE

Noonan patients display normal size and weight at birth. However, adults present smaller height due to a reduction of the pubertal growth *(171, 220, 224)*. This feature was reproduced in all the Noonan mouse models previously generated *(13, 14, 39, 237)*.

As Noonan patients, K-*Ras*$^{+/V14I}$ and K-*Ras*$^{V14I/V14I}$ mice displayed similar weight and body size to wild type animals at birth (data not shown). Nevertheless, K-*Ras*$^{V14I/V14I}$ mice were significantly smaller at weaning. At 4 weeks of age, the body weight of K-*Ras*$^{V14I/V14I}$ male was significantly reduced [11.7±2.22 g (n=18) *vs*. 16.3±3.97 g (n=24)] and the mutant mice were shorter than the controls [(7.1±4.26 cm (n=7) *vs*. 8.2±2.27 cm (n=6)]. These differences became ameliorated with age, mostly in the case of the body weight. At 3 months of age, the body length remains reduced [(9.5±3.14 cm (n=7) *vs*. 10.0±1.45 cm (n=6)]. These differences are gene dose dependent, since K-*Ras*$^{+/V14I}$ displayed smaller size and length only at weaning and these parameters were normalized along the time ***(Figure 17A and B)***.

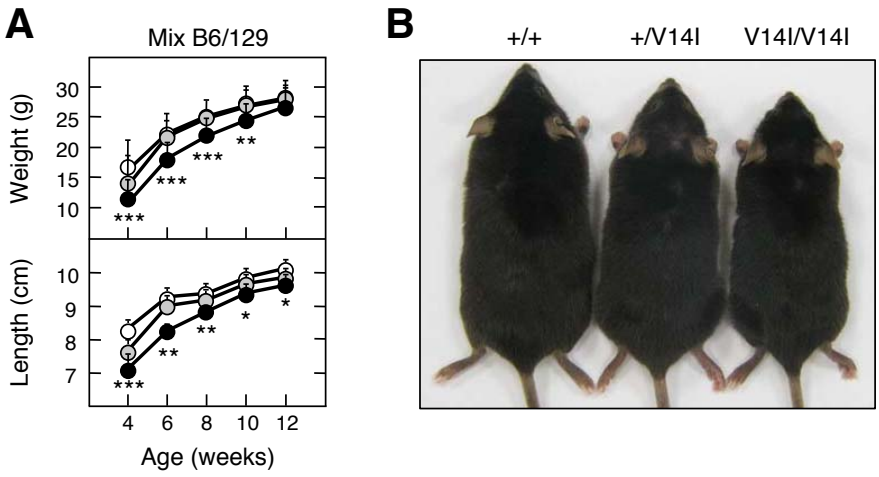

Figure 17. NS-like developmental defects in K-*Ras*^{V14I} mice. (A) Growth curves of male mice. Top: Body weight of wild type (n=24; open circles), K-*Ras*$^{+/V14I}$ (n=36; gray circles) and K-*Ras*$^{V14I/V14I}$ (n=18; solid circles) mice. Bottom: Body length of wild type (n=6; open circles), K-*Ras*$^{+/V14I}$ (n=14; gray circles) and K-*Ras*$^{V14I/V14I}$ (n=7; solid circles) mice. Error bars indicate SD. *P < 0.05; **P < 0.01; ***P < 0.001. **(B)** Representative image of 4-month-old male wild type (+/+), K-*Ras*$^{+/V14I}$ (+/V14I) and K-*Ras*$^{V14I/V14I}$ (V14I/V14I) mice.

We analyzed lean and fat content by densitometer to find an explanation of these differences. At 4 weeks of age, K-*Ras*$^{V14I/V14I}$ male (n=5) presented less lean content than the control mice (n=4). This difference became ameliorated with age, being the lean content comparable at 4 months of age. In the case of fat content, 4-weeks-old K-*Ras*$^{V14I/V14I}$ male (n=5) displayed a small reduction compared to wild type littermates (n=4). This difference disappeared one month later, but increased exponentially at 3 and 4 months of age. No differences were found in K-*Ras*$^{+/V14I}$ mice (n=10) ***(Table 3 in Appendix I)***.

These observations indicate that K-*Ras*^{V14I} mice displayed smaller body weight due to a reduction of lean and fat content at weaning. However, reduction in lean content as well as body weight became ameliorated with age. In contrast, the fat content still remained reduced at 3 and 4 months of age. K-*Ras*^{V14I} mice displayed MPD around 4 months of age *(see bellow, 6.9 section),* thus this loss of the fat content could be an indicative of the illness of the mice.

6.6 K-*Ras*^{V14I} MICE DISPLAYED FACIAL DYSMORPHIA AND NO SKELETAL ABNORMALITIES

6.6.1 K-*Ras*^{V14I} mice displayed normal skeleton

Most Noonan patients develop skeletal alterations such as thoracic deformities and spine abnormalities *(6, 192)*. Using micro X-ray computed tomography (micro-CT) we analyzed the entire skeleton of K-*Ras*$^{+/V14I}$ and K-*Ras*$^{V14I/V14I}$ mice at different ages to determine the presence of alterations. However, as the other Noonan mouse models *(13, 14, 39, 237)* no abnormalities were found in any of the scanned mice (data not shown).

A small percentage of Noonan patients develop osteopenia and/or osteoporosis *(204)*. We determined the bone status in our mouse model analyzing the bone mineral density (BMD) and bone mineral content (BMC) at different ages (1, 2, 3, 4 months) by densitometer ***(Table 3 in Appendix I)***. No alterations were found in K-*Ras*$^{+/V14I}$ mice (n=10). However, at 4 weeks of age, BMC of K-*Ras*$^{V14I/V14I}$ mice (n=5) was significantly reduced compared to wild type mice (n=4). Interestingly, these differences disappeared with age. In addition, no significant differences were found in the BMD of K-*Ras*$^{V14I/V14I}$ mice (n=5) and wild type littermates (n=4). Besides, no bone histological alterations were found in 4-months old and aging mice (data not shown). All these findings together revealed that the K-*Ras*^{V14I} mice displayed normal skeletal structure and normal bone physiology.

6.6.2 K-*Ras*^{V14I} mice displayed facial dysmorphia

Noonan patients display typical facial dysmorphia characterized by ptosis and wide-spaced eyes, low set, posteriorly rotated ears, inverted triangular face and broad or webbed neck *(7)*. Noonan mouse model that express *Ptpn11*, *Raf1* or *Sos1* mutations has a "triangular" facial appearance reminiscence of the facial abnormalities seen in NS patients *(13, 14, 39,146, 237)*.

A

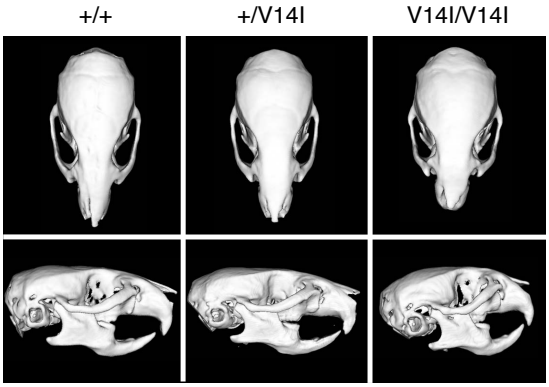

B

	B6/129 mice				
	K-*Ras*$^{+/+}$ (n=6)	K-*Ras*$^{+/V14I}$ (n=7)	K-*Ras*^{V14I} (n=6)	p value +/+ *vs* +/V14I	p value +/+ *vs* V14I
1. Length (mm)	23.34 ± 0.61	23.49 ± 0.33	20.94 ± 1.33	0.5950 NS	0.0034 **
2. Width (mm)	9.66 ± 0.13	9.88 ± 0.24	10.42 ± 0.30	0.0727 NS	0.0028 **
3. Height (mm)	5.44 ± 0.22	5.94 ± 0.31	8.44 ± 1.92	0.0073 **	0.0035 **
4. Volume (mm^3)	411.29 ± 18.9	433.61 ± 25.9	453.77 ± 33.72	0.2478 NS	0.0279 *

Figure 18. Craniofacial dysmorphia of K-*Ras*^{V14I} mice. (A) Representative micro-CT scans of skulls of 4-month-old wild type (+/+), K-*Ras*$^{+/V14I}$ (+/V14I) and K-*Ras*$^{V14I/V14I}$ (V14I/V14I) male mice in mixed B6/129 genetic background. **(B)** Morphometric measurements of 4-month-old wild type, K-*Ras*$^{+/V14I}$ and K-*Ras*$^{V14I/V14I}$ male mice. Numbers shown indicate the media ± SD. Statistical significance was assessed by two-tailed Student's test. *P < 0.05; **P < 0.01; NS: no significant.

K-*Ras*$^{V14I/V14I}$ mice exhibited facial dysmorphia characterized by a more pronounced triangular facial appearance with a shorter distance between the ears and the nose, blunter snout and wider separation between the eyes ***(Figure 18A)***. Analysis of 4-month-old males (n=6) by micro-CT revealed increased skull width and height along with reduced length resulting in a more round skull with bigger volume. Consistent with a gene dose effect, these alterations were less pronounced in heterozygous mice (n=7) ***(Figure 18A and B)***. These features are reminiscent of the facial phenotype of the other NS mouse models *(13, 14, 39,146, 237)* as well as of NS patients *(7)*.

6.7 K-*Ras*^{V14I} MICE DISPLAYED NORMAL AUDITORY PARAMETERS

Hearing loss is found in 10-40% of NS patients due to otitis media complication (15-40%) or sensorineural defects (10-25%) *(224)*. The auditory parameters of 4-months-old K-*Ras*^{V14I} mice were analyzed by ABR (Auditory Brainstem Response) by the "Servicio de Evaluación Neurofuncional no Invasiva. Instituto Biomédicas Alberto Sols CSIC-UAM. Servicio de Evaluación Funcional de Animales de Laboratorio, CIBERER, ISCIII".

The ABR is a neurophysiological technique that measures the brainstem function in response to auditory stimuli. This technique is based on auditory stimulation using known characteristic sounds and the subsequent recording of the electrical activity generated by the auditory neurons using electrodes placed in standard positions. The ABR system allows determining the hearing threshold for click stimulation and for pure tones (audiograms).

K-*Ras*$^{+/V14I}$ (n=7) and K-*Ras*$^{V14I/V14I}$ mice (n=4) displayed similar hearing threshold for click stimulation to the control mice (n=8) ***(Table 5 in Appendix I)***. The values of the three analyzed genotypes were found in the reference values of normal audition. No differences were found in the analysis of the hearing threshold for pure tones (8, 16, 28 and 40 kHz). Moreover, the audiogram of the control mice (n=8) had the typical shape of mice with normal audition [all the hearing thresholds were lower than 45dB SPL (decibel Sound Pressure Levels) and the best values were obtained at the frequency of 16 kHz] and was comparable to the audiogram obtained in mix B6/129 cohort of mice. K-*Ras*$^{+/V14I}$ (n=7) and K-*Ras*$^{V14I/V14I}$ mice (n=4) displayed an audiogram similar to the wild type mice ***(Figure 19)***.

These results indicate that 4-month-old K-*Ras*^{V14I} mice display normal audition. Therefore, the expression of this mutation in mice is not associated with hearing defects under normal conditions. An evaluation in extreme conditions (aging or noisy environment) might be needed to highlight the presence of these defects.

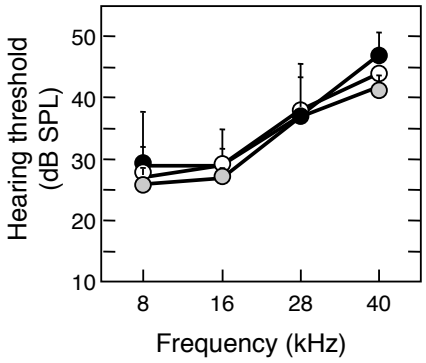

Figure 19. K-*Ras*^{V14I} mice displayed normal audiogram. Hearing threshold for pure tones of 8, 16, 28 and 40 kHz (audiogram) of wild type (n=8; open circles), K-*Ras*$^{+/V14I}$ (n=7; gray circles,) and K-*Ras*$^{V14I/V14I}$ (n=4; solid circles) male mice. Error bars indicate SD.

6.8 K-*Ras*^{V14I} MICE DEVELOPED HEART ABNORMALITIES

One of the most common alterations of Noonan patients is the congenital heart disease (50-90%) that includes pulmonary stenosis, hypertrophic cardiomiopathy (HCM) and secundum atrial septal defects *(171, 193)*. These cardiac alterations have been reproduced in all the mouse models that express mutations found in NS patients, being in many cases incompatible with life *(13, 14, 39, 237)*.

K-*Ras*^{V14I} mice displayed substantially larger hearts already evident in midgestation (E13.5) embryos and neonatal animals. Histological analysis revealed that K-*Ras*^{V14I} embryos and neonatal animals displayed a significant bigger heart, with a significant increase in the size of all chambers ***(Figure 11)***. At 4 months of age, cardiac abnormality was characterized by a significant increase in heart weight and heart/body weight ratio ***(Figure 20A)***. Histological analysis revealed a substantial thickening of all chambers. We did not observe gross alterations in the histological structure of auricles or ventricles or tissue fibrosis. However, the aortic valves were thicker in the mutant mice. Heterozygous animals displayed similar, albeit less pronounced, alterations ***(Figure 20B)***.

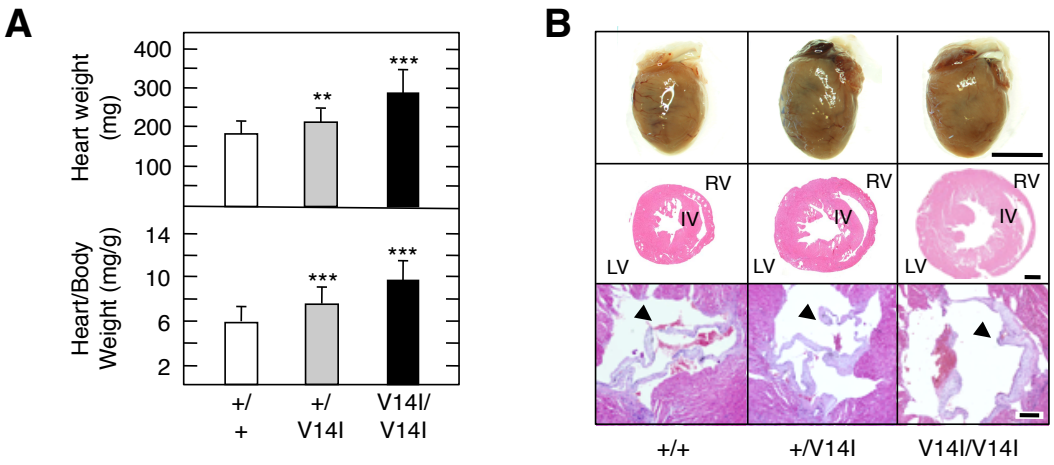

Figure 20. Heart defects in K-*Ras*^{V14I} mice. **(A)** Top: Heart weight and Bottom: heart/body weight ratio of 4-month-old wild type (n=22) (+/+, open bars), K-*Ras*$^{+/V14I}$ (n=30) (+/V14I, gray bars) and K-*Ras*$^{V14I/V14I}$ (n=13) (V14I/V14I, solid bars) male mice. Error bars indicate SD. **P < 0.01; ***P < 0.001. **(B)** Top: Formalin-fixed hearts. Scale bar, 0.5 cm. Middle: H&E stained heart ventricular sections. Interventricular wall (IV), right ventricle (RV) and left ventricle (LV) are indicated. Scale bar, 1 mm. Bottom: H&E stained aortic valves. Solid arrowheads point to aortic valves. Scale bar, 50 μm.

The enlargement of an organ size could be due to an increase in the number of cells (hyperplasia) or an increase in cells size (hypertrophy). We quantified the number of cardiomyocytes and determined the cardiomyocyte size in H&E hearts slides of 4-month-old animals. The cardiomyocyte area was comparable in mutant and control hearts. By contrast, the K-*Ras*$^{+/V14I}$ (n=12) and K-*Ras*$^{V14I/V14I}$ mice (n=3) displayed a significant increase number of cardiomyocytes. This change is gene dose dependent, since K-*Ras*$^{+/V14I}$ mice presented an intermediate phenotype ***(Figure 21A)***. We studied if the increased number of cardiomyocytes was due to an elevated proliferation rate. Hence, we measured the cardiomyocyte proliferation by Ki67 immunostaining. Ki67 positive cells were more abundant in K-*Ras*$^{V14I/V14I}$ hearts compared to control ***(Figure 21B and C)***. Therefore, these results suggest that K-*Ras*^{V14I} mice displayed a heart hyperplasia due to an enhanced proliferation rate.

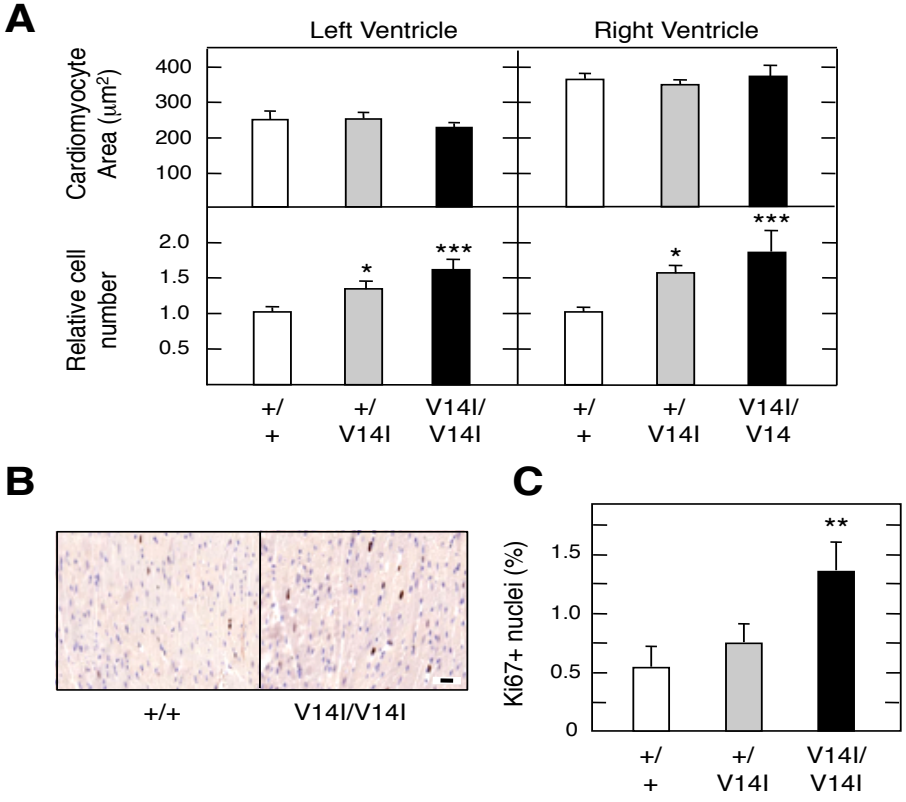

Figure 21. Heart hyperplasia in 4-month-old K-*Ras*^{V14I} male mice. **(A)** Cardiomyocyte area (Top) and relative cardiomyocyte number per ventricle (Bottom) of wild type (n=8) (+/+, open bars), K-*Ras*$^{+/V14I}$ (n=12) (+/V14I, gray bars) and K-*Ras*$^{V14I/V14I}$ (n=3) (V14I, solid bars) mice. **(B)** Ki67 immunostaining of hearts from wild type (+/+) and K-*Ras*$^{V14I/V14I}$ (V14I/V14I) mice. Scale bar, 20 μm. **(D)** Percentage of Ki67-positive cardiomyocytes in wild type (n=5) (+/+, open bars), K-*Ras*$^{+/V14I}$ (n=5) (+/V14I, gray bars) and K-*Ras*$^{V14I/V14I}$ (n=5) (V14I/V14I, solid bars) mice. Error bars indicate SD. *P < 0.05; **P < 0.01; ***P < 0.001.

6.8.1 K-*Ras*^{V14I} mice displayed an expansion of the cardiac stem cells

The longstanding dogma that mammalian heart is postmitotic organ with limited regenerative capacities has been challenged by the discovered of a number of multipotent stem

cell like population and their likely contribution to new cardiomyocytes and vascular lineages after injury *(9, 20, 94, 163)*. Since we found an increase of cycling cardiomyocytes in K-*Ras*^{V14I} mice, we questioned whether the expression of the K-*Ras*^{V14I} might induce also an expansion of the cardiac stem cells.

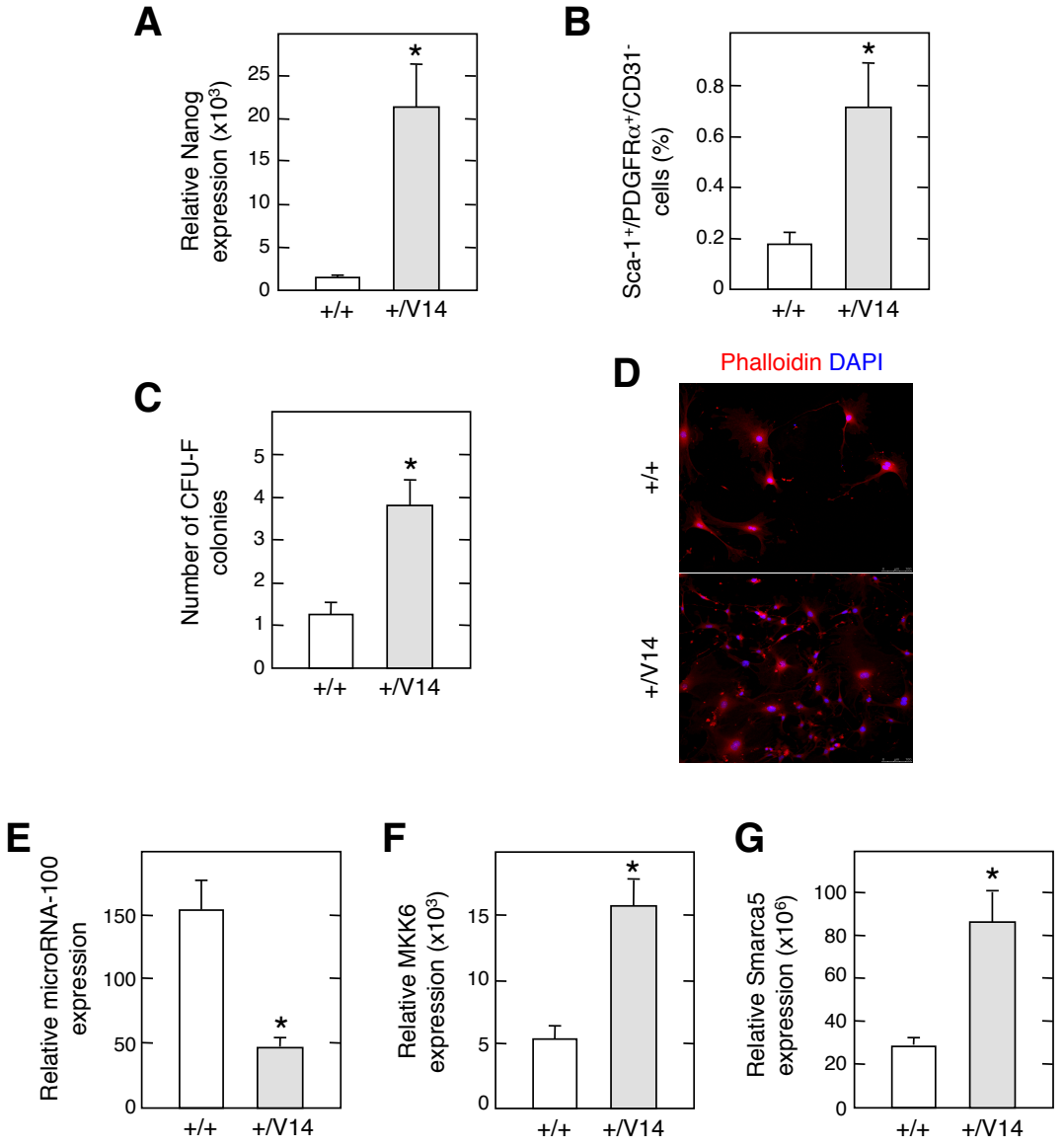

Figure 22. K-*Ras*^{V14I} hearts displayed increased pluripotency and expansion of cardiac stem cell at P10-P14 (A) Relative expression of Nanog in hearts from wild type (n=4) (+/+, open bars) and K-*Ras*$^{+/V14I}$ (n=4) (+/V14I, gray bars) pups. **(B)** Percentage of Sca-1^{+}/PDGFRα^{+}/CD31^{-} cells in hearts from wild type (n=4) (+/+, open bars) and K-*Ras*$^{+/V14I}$ (n=8) (+/V14I, gray bars) pups. **(C)** Number of CFU-F colonies derived from of Sca-1^{+}/PDGFRα^{+}/CD31^{-} cells of wild type (n=4) (+/+, open bars) and K-*Ras*$^{+/V14I}$ (n=6) (+/V14I, gray bars) pups. **(D)** Representative pictures of DAPI (blue) and Phalloidin (red) of CFU-F coloines derived from of Sca-1^{+}/PDGFRα^{+}/CD31^{-} cells of wild type (+/+) and K-*Ras*$^{+/V14I}$ (+/V14I) pups. **(E)** Relative expression of microRNA-100 in hearts from wild type (n=4) (+/+, open bars) and K-*Ras*$^{+/V14I}$ (n=4) (+/V14I, gray bars) pups. **(F)** Relative expression of MKK6 in hearts from wild type (n=4) (+/+, open bars) and K-*Ras*$^{+/V14I}$ (n=4) (+/V14I, gray bars) pups. **(G)** Relative expression of Smarca5 in hearts from wild type (n=4) (+/+, open bars) and K-*Ras*$^{+/V14I}$ (n=4) (+/V14I, gray bars) pups. Error bars indicate SD. *P < 0.05.

We observed that *Nanog* expression, a pluripotency-associated gene, was significantly up-regulated in hearts from K-*Ras*$^{+/V14I}$ mice sacrificed from postnatal day 10 to 14 compared to wild type littermates ***(Figure 22A)***. Next, we analyzed the number of Mesenchymal Stem Cells (MSC)-like Sca-1^{+}/PDGFRα^{+}/CD31^{-} cardiac stem cells in hearts from K-*Ras*$^{+/V14I}$ and wild type mice sacrificed at P10-14 and the capacity of these cells to produce colony forming units-fibroblast (CFU-Fs). Thus, we observed that in hearts from P10-14 K-*Ras*$^{+/V14I}$ mice the number of Sca-1^{+}/PDGFRα^{+}/CD31^{-} cardiac stem cells was increased compared to control mice ***(Figure 22B)*** and the number of CFU-Fs colonies derived from these mutant cardiac stem cell was bigger than those derived from wild type cells ***(Figure 22C and D)***.

Finally, we analyzed the expression of the microRNA-100. This microRNA-100 is required for proper differentiation of mouse embryonic stem cells and is repressed in undifferentiated embryonic stem cells *(206)*. Moreover, down-regulation of this microRNA is essential for the initiation of the dedifferentiation/proliferation process after heart injury in mice *(unpublished data from Aguirre A., Izpisua-Belmonte JC. and Sánchez-Martinez I.)*. In line with these, we observed a down-regulation of the microRNA-100 ***(Figure 22E)***, which results in an up-regulation of two of its targets, MKK6 ***(Figure 22F)*** and Smarca5 ***(Figure 22G)***, in hearts from P10-14 K-*Ras*$^{+/V14I}$ compared to control hearts.

6.8.2 Hemodynamic study, cardiac morphology and function analysis

Non-invasive hemodynamics studies established that mean arterial pressure measured at 4, 5 and 6 months of age was comparable in mutant and control mice ***(Figure 23)***. The absence of hypertension in these mice is in agreement with the lack of heart fibrosis and cardiovascular remodeling (data not shown).

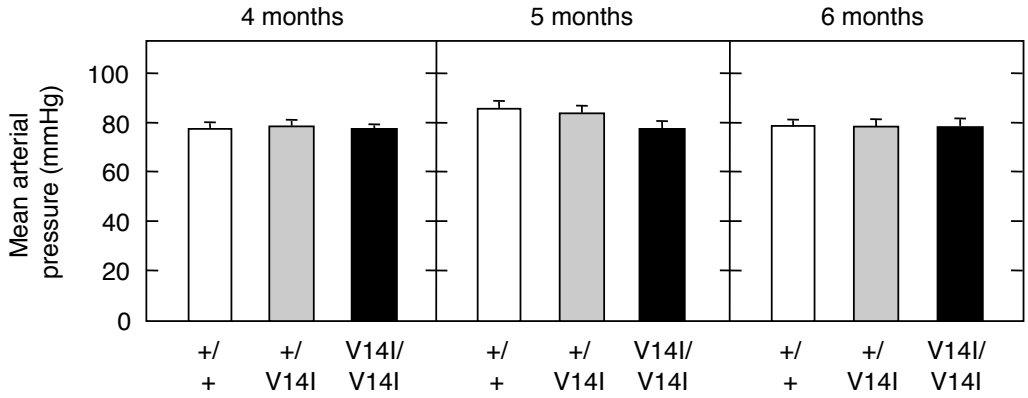

Figure 23. K-*Ras*^{V14I} mice display normal mean arterial pressure. Mean arterial pressure of wild type (+/+, open), K-*Ras*$^{+/V14I}$ (+/V14I, gray bars) and K-*Ras*$^{V14I/V14I}$ (V14I/V14I, solid bars) male mice at 4 months (n=9, n=14, n=6, respectively), 5 months (n=6, n=11, n=3, respectively) and 6 months (n=8, n=4, n=4, respectively). Error bars indicate SD.

To analyze cardiac morphology and function, we performed Magnetic Resonance Imaging (MRI) studies on 4-month-old mice in collaboration with the 'Instituto de Investigación Sanitaria Gregorio Marañón'. As expected, wall thickness in systole (WTs), systolic wall thickening (WTn) and left ventricle mass (LVM) were significantly increased in K-*Ras*$^{V14I/V14I}$ mice (n=3) compared to wild type littermates (n=5). These results were in agreement with the larger heart characteristic of these mutant mice. Accordingly, K-*Ras*$^{V14I/V14I}$ hearts showed enhanced end diastolic volume (EDV), the volume of blood in the left ventricle at the end of diastole, before the contraction. This increase was also in concordance with the bigger heart of mutant mice. Since K-*Ras*$^{V14I/V14I}$ mice displayed enlarged heart, the volume of blood inside of the ventricle was also bigger. Moreover, end systolic volume (ESV), the volume of blood in the left ventricle at the end of the contraction, remained normal indicating preserved or enhanced function. Although the heart of K-*Ras*$^{V14I/V14I}$ mice is larger and the volume of blood inside the heart is bigger, the contractibility function is able to pump all the blood out. Therefore, no volume change was found in K-*Ras*$^{V14I/V14I}$ mice compared to control mice at the end of the systole. Consistent with this interpretation, fractional shortening (FS) and cardiac output (CO) is enhanced in K-*Ras*$^{V14I/V14I}$ mice. The FS is the degree of shortening of the left ventricle diameter between end diastole and end systole and estimates the myocardial contractibility of the left ventricle. Hence, an increase in FS suggests enhanced myocardial contractibility. The CO is the volume of blood being pumped out by the left ventricle per minute. In K-*Ras*$^{V14I/V14I}$ mice the volume of blood inside of the heart is bigger. However, due to the enhanced heart function, the heart is able to pump all the blood out. Therefore, the CO is also bigger ***(Table 6 in Appendix I).***

Other parameters such as wall thickening in diastole (WTd), ejection fraction (EF) and heart rate (HR) were comparable in mutant and control mice.

These results suggest that K-*Ras*^{V14I} mice display an enlarged heart, but the increase of the heart size is not pathological. The cardiac function of K-*Ras*^{V14I} mice is preserved or enhanced and allows the correct function of this bigger heart.

6.8.3 Myocardial expression of the K-*Ras*^{V14I} mutation

To determine if the postnatal expression of the K-*Ras*^{V14I} mutation in myocardial cells have an impact in the heart function, we crossed the conditional K-*Ras*$^{+/LSLV14I}$ mouse model with mice that express the Cre recombinase under the control of the α myosin heavy chain (α–*MHC*) promoter. This promoter allows the expression of the mutation only in myocardial cells after birth. This strain also carried the *Rosa26*^{LSLLacZ} allele to monitor the efficiency of the deletion of the "STOP" cassette by determining the number of LacZ expressing cells.

X-Gal staining revealed an efficient deletion of the "STOP" cassette in myocardial cells. However, the pattern of B-Gal positive cells in mutant mice was comparable to the wild type littermates at 4 months of age ***(Figure 24A)***. Interestingly, the expression of the K-*Ras*^{V14I} mutation in myocardial cells after birth had no obvious consequences. The size and the histology of mutant hearts were similar to the wild type littermates ***(Figure 24A and B)***. These results suggest that the expression of the mutant protein in myocardial cells of completely developed hearts is not associated to cardiac alterations. Therefore, the expression of the mutation during the development and/or in other cell types (for example: endothelial cells) is essential for the development of the heart abnormalities.

These observations are reminiscent of those previously reported in mouse models that express the *Ptpn11*^{D61Y} *(13)* and K-*Ras*^{G12D} mutation *(47)* or overexpress the *Ptpn11*^{Q79R} *(145)* mutation in myocardial cells, using the same promoter.

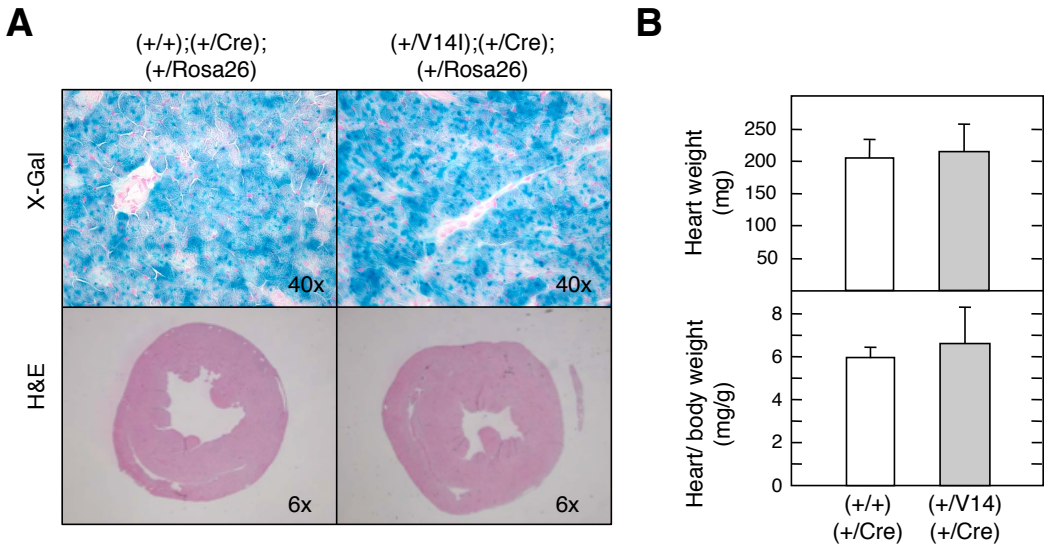

Figure 24. Postnatal myocardial expression of the K-*Ras*^{V14I} mutation does not cause cardiac alterations. **(A)** Top: X-Gal stained transverse section from 4-month-old K-*Ras*$^{+/+}$; *αMHC*-Cre$^{+/T}$; *Rosa26*$^{+/LSLLacZ}$ (+/+, +/Cre, +/Rosa26) and K-*Ras*$^{+/LSLV14I}$; *αMHC*-Cre$^{+/T}$; *Rosa26*$^{+/LSLLacZ}$ (+/V14I, +/Cre, +/Rosa26) mice. Bottom: H&E stained transverse section from 4-month-old K-*Ras*$^{+/+}$; *αMH* -Cre$^{+/T}$; *Rosa26*$^{+/LSLLacZ}$ (+/+, +/Cre, +/Rosa26) and K-*Ras*$^{+/LSLV14I}$; *αMHC*-Cre$^{+/T}$; *Rosa26*$^{+/LSLLacZ}$ (+/V14I, +/Cre, +/Rosa26) mice. **(B)** Heart weight (top) and heart/body weight (bottom) of 4-month-old K-*Ras*$^{+/+}$; *αMHC*-Cre$^{+/T}$ (+/+, +/Cre) and K-*Ras*$^{+/LSLV14I}$; *αMHC*-Cre$^{+/T}$ (+/V14I, +/Cre) mice. Error bars indicate SD.

6.9 HEMATOLOGICAL DEFECTS OF K-*Ras*^{V14I} MICE

Individuals with NS display hepatoesplenomegaly (25%) and have predisposition to proliferative disorders, being the most common the MPD (10%) *(10, 75)*. Noonan mouse models that express *Ptpn11*^{D61G}, *Raf1*^{L613K} or *Sos1*^{E846K} mutations, developed hematological

disorders characterized by splenomegaly, leukocytosis, myeloid expansion and increased IL-3 and GM-CSF sensitivity, reminiscence of the alterations found in NS patients *(14, 39, 237)*.

At 4 months of age, K-*Ras*$^{V14I/V14I}$ animals (n=10) showed leukocytosis in peripheral blood, mainly due to expansion of neutrophil, eosinophil and basophil population. Mutant mice were also anemic and suffered from thrombocytopenia, a reduction of the platelet count ***(Table 7 in Appendix I)***. Blood smear analysis showed the presence of high number of granulocyte immature cells. Heterozygous mice displayed intermediate phenotype. At this time, K-*Ras*$^{V14I/V14I}$ mice (n=12) displayed severe splenomegaly. Heterozygous K-*Ras*$^{+/V14I}$ mice (n=22) also had enlarged spleens albeit to a more limited extent ***(Figure 25A and B)***. H&E staining of spleen sections showed marked congestion and increased extramedullary hematopoiesis with loss of splenic architecture and expansion of the red pulp compartment. Histopathological analysis also revealed perivascular lymphoid and myeloid infiltrates in a variety of organs including liver, kidney and lung ***(Figure 25C).***

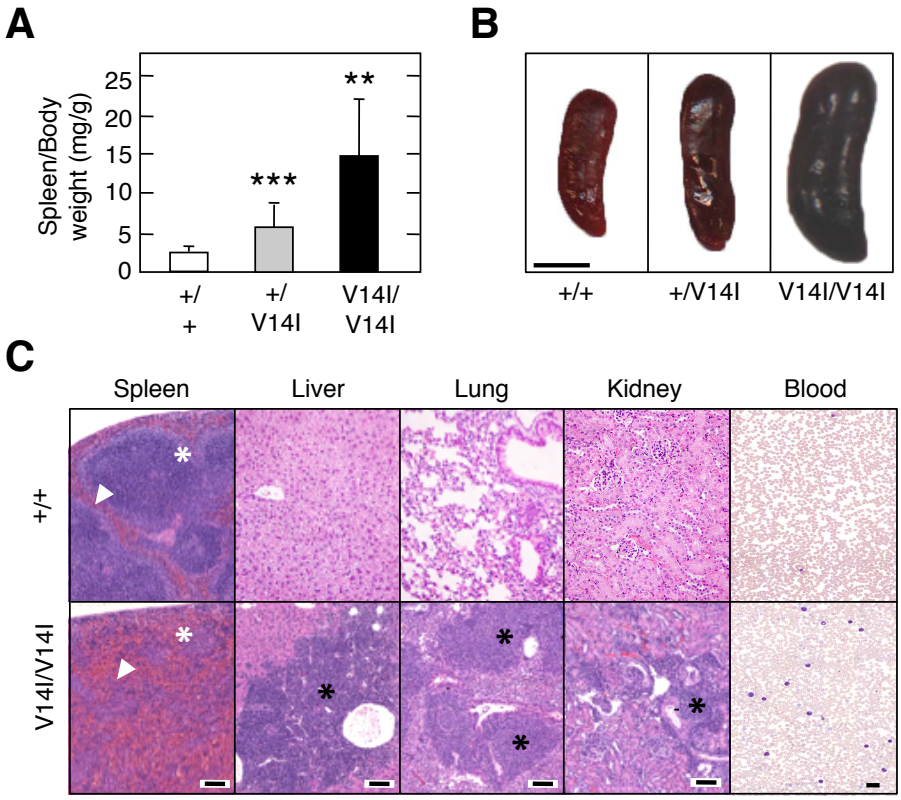

Figure 25. Hematological disorders in 4-month-old K-*Ras*^{V14I} mice. (A) Spleen/body weight ratio in wild type (n=13) (+/+, open bars), K-*Ras*$^{+/V14I}$ (n=22) (+/V14I, gray bars) and K-*Ras*$^{V14I/V14I}$ (n=12) (V14I/V14I, solid bars) mice. **(B)** Representative spleens of wild type (+/+), K-*Ras*$^{+/V14I}$ (+/V14I) and K-*Ras*$^{V14I/V14I}$ (V14I) mice. Scale bar, 5 mm. **(C)** H&E stained paraffin sections of spleen, liver, lung, kidney and peripheral blood smears stained with May-Grünwald/Giemsa of wild type (+/+) and K-*Ras*$^{V14I/V14I}$ (V14I) mice. Spleen, asterisks and arrowheads indicate the white and red pulp, respectively. Solid asterisks indicate immunoinfiltrates. Scale bars, 100 μm for spleen, liver, kidney and lung and 20 μm for blood smears.

Flow cytometry analysis revealed significant expansion of myeloid cells in the spleen of K-*Ras*$^{V14I/V14I}$ (n=14) and K-*Ras*$^{+/V14I}$ (n=18) mutant mice with increased levels of both Gr1^{+}/CD11b^{+} double positive and CD11b^{+} single positive cells ***(Figure 26A and B)***. The expansion of myeloid cells was associated with a concomitant decrease in the percentage of CD3^{+} T-cells, due to a significant decrease of CD8^{+} T-cells. However, the percentage of CD19^{+} B-cells and CD4^{+} T-cells in mutant mice was comparable to wild type littermates ***(Figure 26C).***

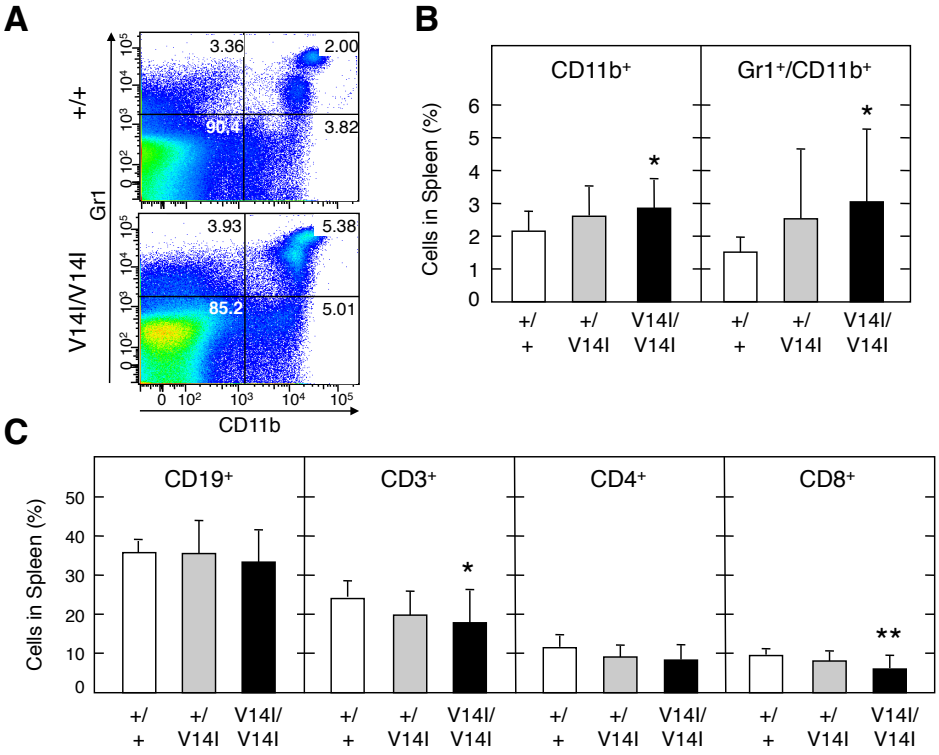

Figure 26. Four month-old K-*Ras*^{V14I} mice display expansion of the myeloid lineage, concomitant with a decrease in the CD8 single-positive cells. (A). Flow cytometry analysis of Gr1^{+} and CD11b^{+} cells in spleens of wild type (+/+) and K-*Ras*$^{V14I/V14I}$ (V14I/V14I) mice. **(B)** Percentages of CD11b^{+} and Gr1^{+}/CD11b^{+} myeloid cells in spleens of wild type (n=12) (+/+, open bars), K-*Ras*$^{+/V14I}$ (n=18) (+/V14I, gray bars) and K-*Ras*$^{V14I/V14I}$ (n=14) (V14I/V14I, solid bars) mice. **(B)** Percentages of CD19^{+} B-cells and CD3^{+}, CD4^{+} and CD8^{+} T-cells in spleens of wild type (n=12) (+/+, open bars), K-*Ras*$^{+/V14I}$ (n=18) (+/V14I, gray bars) and K-*Ras*$^{V14I/V14I}$ (n=14) (V14I/V14I, solid bars) mice. Error bars indicate SD. *P < 0.05; **P < 0.01.

6.9.1 Cytokines response of bone marrow progenitors

The proliferative capacity of bone marrow (BM) progenitors was assayed in methylcellulose cultures in presence of IL-3 and GM-CSF. BM cells of K-*Ras*$^{+/V14I}$ and K-*Ras*$^{V14I/V14I}$ mice, but not those of wild type animals, formed significant number of colonies in absence of exogenous cytokines. These colonies were of smaller size and less differentiated

than colonies that grew in the presence of cytokines. BM progenitors of mutant mice also demonstrated hypersensitivity to GM-CSF and IL-3 ***(Figure 27A)***. In presence of these cytokines, cells of K-*Ras*$^{+/V14I}$ and K-*Ras*$^{V14I/V14I}$ mice form more and bigger colonies than the wild types ***(Figure 27B)***.

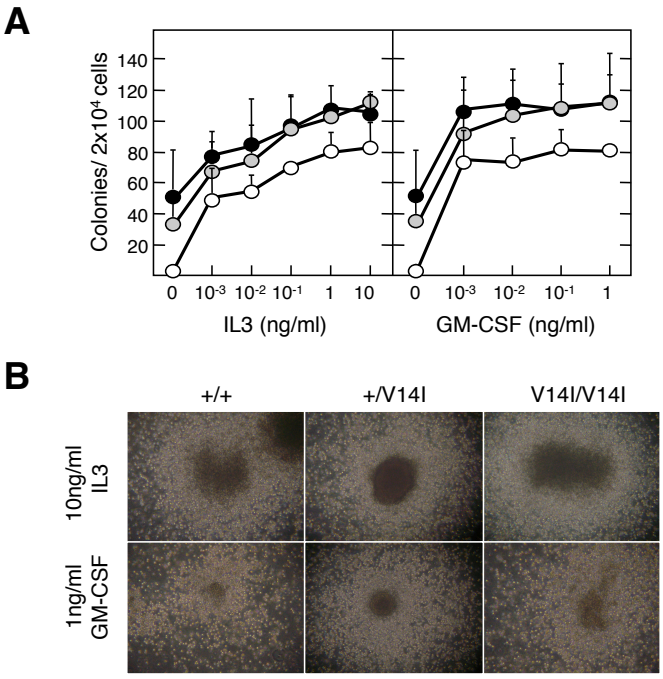

Figure 27. Cytokine response of K-*Ras*^{V14I} BM progenitors (A). Number of colonies formed by BM cells obtained from 4-month-old wild type (n=3) (open circles), K-*Ras*$^{+/V14I}$ (n=3) (gray circles) and K-*Ras*$^{V14I/V14I}$ (n=3) (solid circles) mice in the absence or presence of the indicated concentrations of IL3 and GM-CSF. Error bars indicate the SD. **(B)** Representative pictures of individual colonies formed by BM cells from 4-month-old wild type (+/+), K-*Ras*$^{+/V14I}$ (+/V14I) and K-*Ras*$^{V14I/V14I}$ (V14I/V14I) mice in the presence of 10 ng/ml of IL3 (upper panel) and 1 ng/ml of GM-CSF (lower panel).

The phenotype of the methylcellulose colonies was determined by microscopic visualization of May-Grünwald Giemsa-stained cytospin preparation of colonies after 12 days in culture. The cell morphology of the K-*Ras*$^{V14I/V14I}$ and the wild type colonies was similar. In both cases, the cell appearance resembles granulocyte/macrophages; therefore most of the colonies are CFU-GM (colony forming unit-granulocyte macrophage) colonies ***(Figure 28).***

In conclusion, K-*Ras*^{V14I} developed a hematological disorder characterized by splenomegaly, leukocytosis, myeloid expansion and increased sensitivity to IL-3 and GM-CSF similar to MPD.

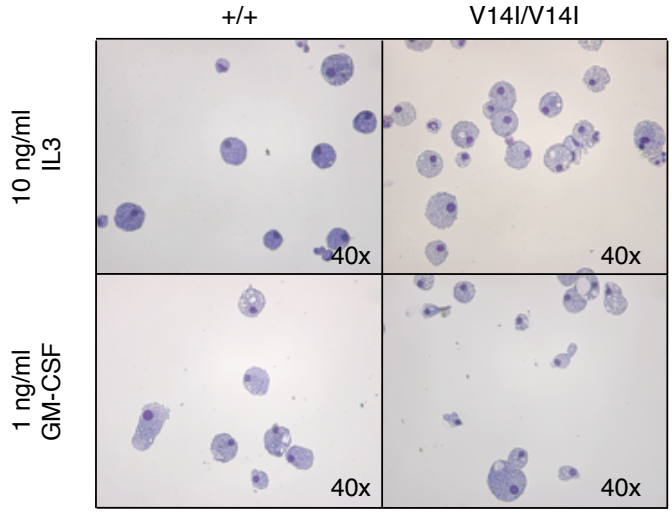

Figure 28. GM-CSF colonies formed by K-*Ras*^{V14I} BM cells. May-Grünwald Giemsa-stained cytospin of individual methylcellulose colonies formed by BM cells obtained from 4-month-old wild type (+/+) and K-*Ras*$^{V14I/V14I}$ (V14I/V14I) mice in presence of 10 ng/ml of IL3 (upper panel) or 1 ng/ml of GM-CSF (lower panel).

6.9.2 Germline K-*Ras*^{V14I} mutation increased HSC and lineage progenitor population

To investigate the mechanism by which expression of the K-Ras^{V14I} protein induced MPD, we analyzed the BM of 4-month-old K-*Ras*^{V14I} mice for the presence of Lineage^{-}/Sca-1^{+}/c-Kit^{+} (LSK) cells, a population known to be enriched for hematopoietic stem cells (HSCs). As illustrated in ***Figure 29***, K-*Ras*$^{V14I/V14I}$ (n=9) and K-*Ras*$^{+/V14I}$ (n=15) mice displayed a significant increase in the frequency and absolute number of LSK cells in bone marrow.

To delineate the mechanism by which K-*Ras*^{V14I} mutation caused HSC expansion, proliferation and apoptosis status of LSK cells of K-*Ras*^{V14I} mice were analyzed and compared with those cells of control mice. The mutant LSK cells had a similar proliferation index, based on BrdU uptake, to that observed in cells obtained from control littermates ***(Figure 30A and B)***. However, the mutant LSK cells had reduced levels of Appendyxin V, a marker for apoptotic cells ***(Figure 30C and D)***. These results indicate that the expansion of HSC population in K-*Ras*^{V14I} mice is due to a decreased programmed cell death rather than to an enhanced cell proliferation.

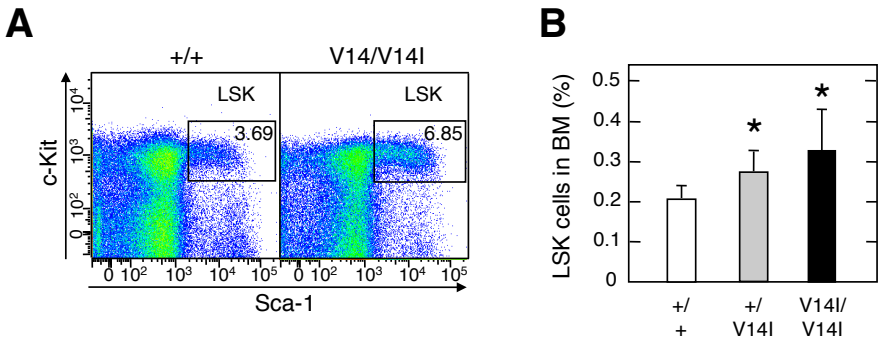

Figure 29. K-*Ras*^{V14I} mice displayed an expansion of HSCs. (A) Flow cytometry analysis of freshly harvested BM cells of 4-month-old wild type (+/+) and K-*Ras*$^{V14I/V14I}$ (V14I/V14I) mice using antibodies against c-Kit and Sca-1. The percentage of Lineage^{-}/Sca-1^{+}/c-Kit^{+} (LSK) cells is indicated. **(B)** Percentage of LSK cells in the BM of 4-month-old wild type (n=11) (+/+, open bars), K-*Ras*$^{+/V14I}$ (n=15) (+/V14I, gray bars) and K-*Ras*$^{V14I/V14I}$ (n=9) (V14I/V14I, solid bars) mice. Error bars indicate SD. *P < 0.05.

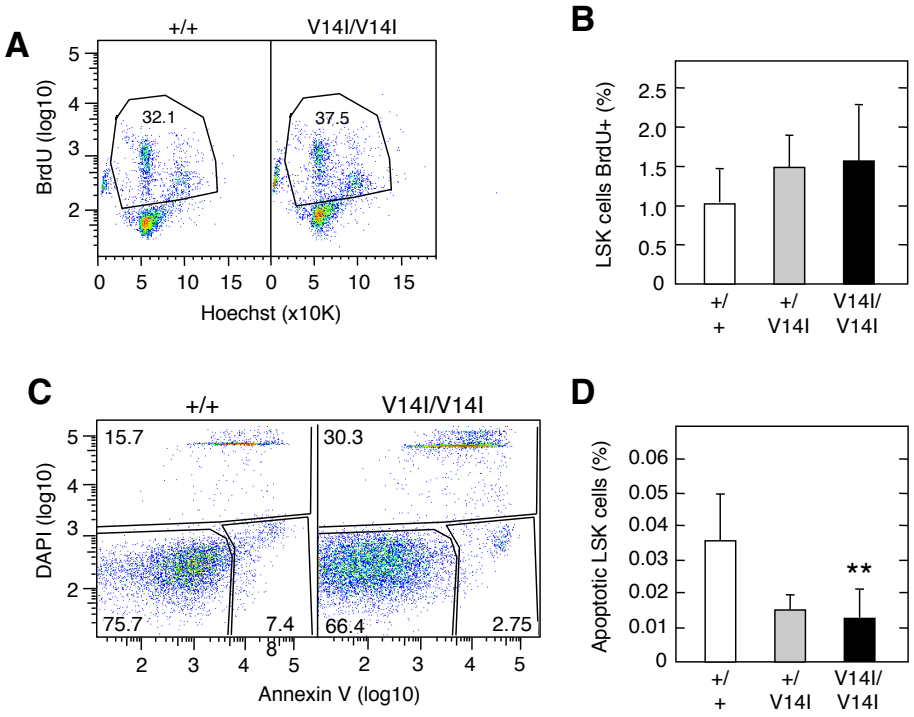

Figure 30. Expansion of LSK cells in BM of 4-month-old K-*Ras*^{V14I} mice. **(A)** Flow cytometry analysis of BrdU^{+} cells in LSK cells of wild type (+/+) and K-*Ras*$^{V14I/V14I}$ (V14I/V14I) mice. **(B)** Percentage of LSK BrdU^{+} cells in BM of wild type (n=6) (+/+, open bars), K-*Ras*$^{+/V14I}$ (n=5) (+/V14I, gray bars) and K-*Ras*$^{V14I/V14I}$ (n=5) (V14I/V14I, solid bars) mice. Error bars indicate SD. **(C)** Flow cytometry analysis of Annexin V^{+} DAPI^{-} cells in LSK cells of wild type (+/+) and K-*Ras*$^{V14I/V14I}$ (V14I/V14I) mice. **(D)** Percentage of LSK apoptotic cells (Annexin V^{+} DAPI^{-} cells) in BM of wild type (n=5) (+/+, open bars), K-*Ras*$^{+/V14I}$ (n=8) (+/V14I, gray bars) and K-*Ras*$^{V14I/V14I}$ (n=8) (V14I/V14I, solid bars) mice. Error bars indicate SD. **P < 0.01.

Using multiparameter flow cytometry analysis, we defined the effects of K-*Ras*^{V14I} mutation on hematopoietic cell development by quantification of the committed progenitors, including common myeloid progenitors (CMPs), common lymphoid progenitors (CLP), granulocyte-macrophage progenitors (GMPs) and megakaryocyte-erythroid progenitors (MEPs). This analysis revealed a significant increase in the absolute numbers of CMPs and GMPs, as well as a slight increase in CLPs. However, the absolute numbers of MEPs did not display significant alterations ***(Figure 31A and B).***

These observations suggest that the expression of the K-Ras^{V14I} protein promotes expansion of the both HSCs and committed precursor of the myeloid lineage.

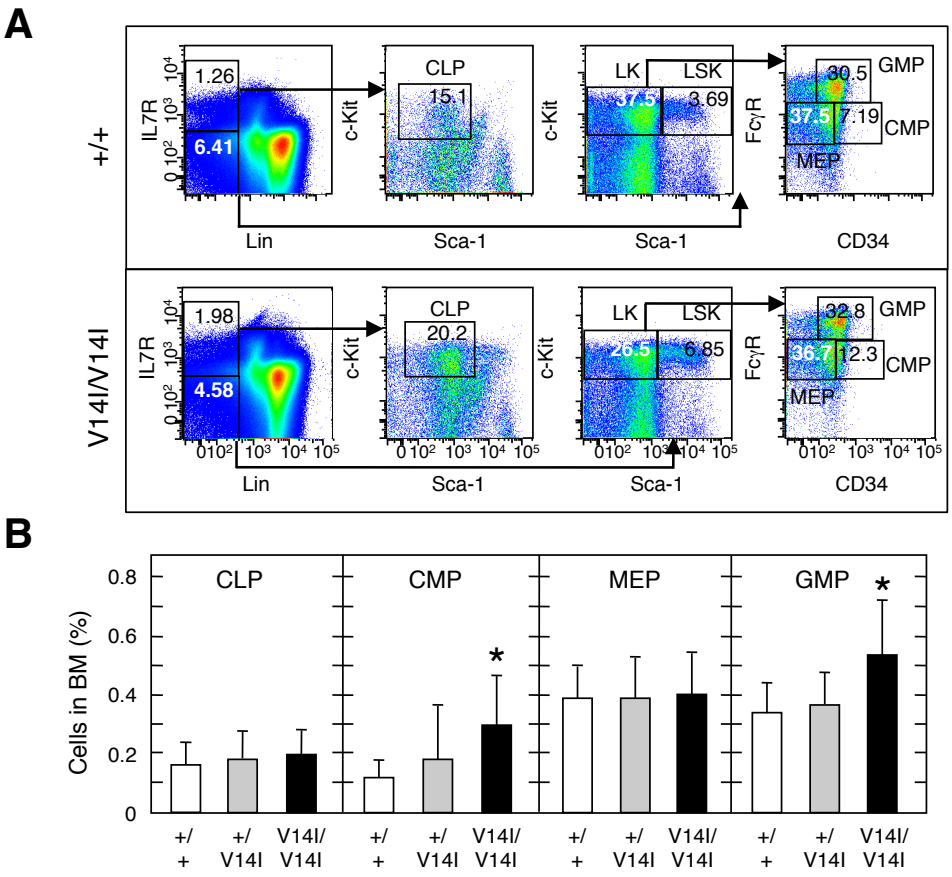

Figure 31. Aberrant hematopoietic cell development in 4-month-old K-*Ras*^{V14I} mice. Staining for LSK cells, common lymphoid progenitors (CLP), common myeloid progenitors (CMP), granulocyte-macrophage progenitors (GMP), and megakaryocyte-erythroid progenitors (MEP) in the BM of wild type (+/+) and K-*Ras*$^{V14I/V14I}$ (V14I/V14I) mice using antibodies against Lin, c-Kit, Sca-1, CD34, FcγR (CD16/32) and IL-7R (CD127). **(D)** Frequencies of CLP, CMP, MEP and GMP populations in BM cells were quantified in wild type (n=11) (+/+, open bars), K-*Ras*$^{+/V14I}$ (n=15) (+/V14I, gray bars) and K-*Ras*$^{V14I/V14I}$ (n=9) (V14I/V14I, solid bars) mice. Error bars indicate SD. *P < 0.05.

6.9.3 Stem cell origin of K-*Ras*^{V14I}-driven MPD

To determine whether the MPD displayed by K-*Ras*^{V14I} mice was due to the observed expansion of HSCs, we transplanted BM cells from wild type K-*Ras*$^{+/+}$ (n=20) and K-*Ras*$^{+/V14I}$ (n=14) mice, backcrossed to the C57BL/6J background for four generations, into lethally irradiated C57BL/6J recipients. In mice, there are two different CD45 alleles: CD45.1 (Ly5.1) and CD45.2 (Ly5.2). The C57BL/6J.OlaHsd strain that we used, expresses the CD45.2 (Ly5.2) isotype. More than 99% of blood cells obtained from K-*Ras*$^{+/V14I}$ mice backcrossed for four generations, expressed the CD45.2 (Ly5.2) allele similar to the original strain (data not shown). For this reason, we chose this generation for the transplantation experiments.

Peripheral blood of recipient mice was analyzed at various intervals after transplantation (2 to 34 weeks). The bone marrow cells, regardless of whether they were obtained from wild

type or K-*Ras*$^{+/V14I}$ mice efficiently reconstituted the entire hematopoietic system in the recipient mice. At 2 weeks after transplantation, all the hematopoietic populations were detected at normal levels in both types of transplanted mice (data not shown). In contrast, mice inoculated only with PBS were defective for blood cells and died between 2 to 4 weeks after irradiation. This is indicative of the efficiency of the irradiation and tail vain inoculation of BM cells.

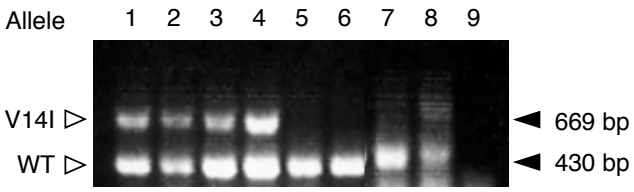

Figure 32. Spleens of reconstituted mice carry the K-*Ras*^{V14I} mutated allele. PCR genotyping for the K-*Ras*^{V14I} allele. Lanes 1-4: DNA isolated from spleen of mice transplanted with BM cells from K-*Ras*$^{+/V14I}$ mice sacrificed 30-34 weeks after transplantation. Lanes 5-6: DNA isolated from spleen of mice transplanted with BM cells from wild type mice sacrificed 30-34 weeks after transplantation. Lane 7: DNA isolated from control wild type MEFs. Lane 8: DNA isolated from control K-*Ras*$^{+/V14I}$ MEFs; Lane 9: water. Size of the wild type (WT, 430 bp) and K-*Ras*^{V14I} (V14I, 669 bp) alleles is indicated by arrowheads.

Regardless of the genotype, the BM cells reconstituted the hematopoietic system. However, only those animals transplanted with cells derived from K-*Ras*$^{+/V14I}$ mice developed MPD between 30 to 34 weeks after transplantation. The presence of the K-*Ras*^{V14I} mutation in the spleen of sacrificed mice was determined by PCR. As expected, spleens of mice inoculated with BM cells derived from K-*Ras*$^{+/V14I}$ mice carried in heterozygosity the K-*Ras*^{V14I} mutation ***(Figure 32)***. In these mice, white blood cell (WBC) counts in their peripheral blood were increased mainly due to expansion of neutrophils, eosinophils and basophils ***(Table 8 in Appendix I)***. Spleens of mice reconstituted with BM cells carrying the K-*Ras*^{V14I} mutation were enlarged ***(Figure 33A and B)***. Histopathological analysis revealed perivascular lymphoid and myeloid infiltrates in liver, kidney and lung ***(Figure 33C)***. Flow cytometry analysis showed an expansion of the myeloid cells CD11b^{+} and Gr1^{+}/CD11b^{+} in spleen ***(Figure 33D and E)***. Finally, the percentage of LSK cells, as well as of CMP and GMP progenitors was also significantly increased in the BM of the reconstituted mice ***(Figure 34)***.

We can conclude that the MPD phenotype was reproduced in primary recipient mice transplanted with K-*Ras*$^{+/V14I}$ BM cells. Therefore, the pathogenic effect of the K-*Ras*^{V14I} mutation initiates at stem cell level.

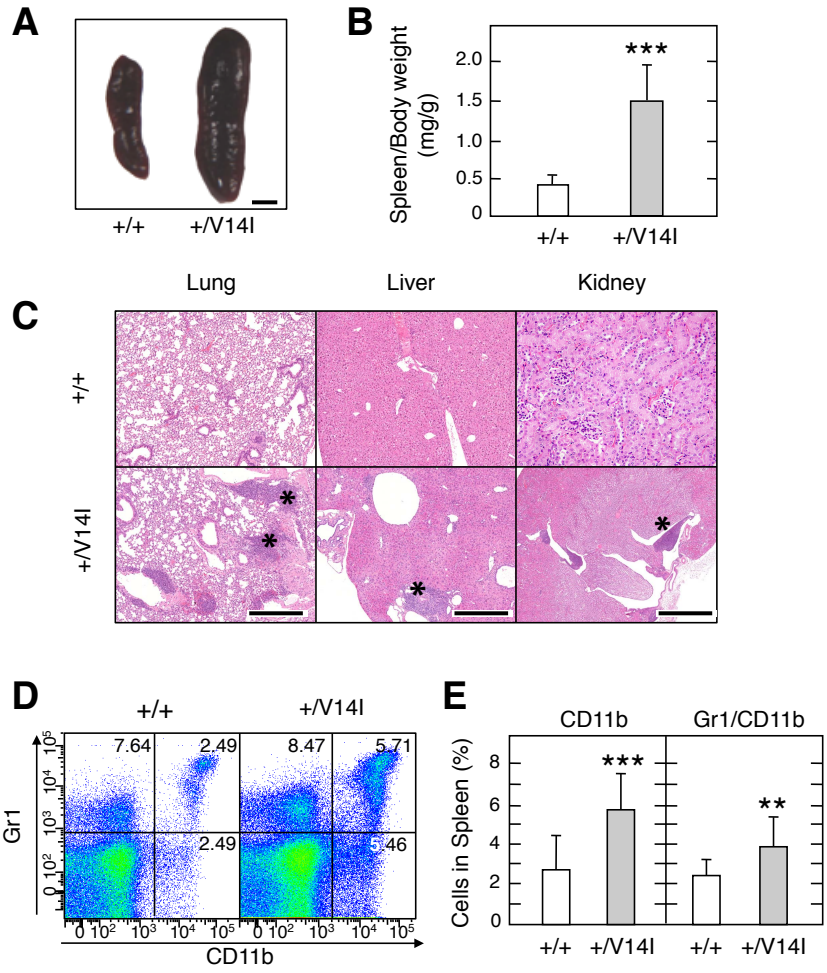

Figure 33. **MPD in mice transplanted with BM from K-*Ras*$^{+/V14I}$ mice**. **(A)** Spleens of mice transplanted with BM cells from wild type (+/+) and K-*Ras*$^{+/V14I}$ (+/V14I) mice sacrificed 30-34 weeks after transplantation. Scale bar, 5 mm. **(B)** Spleen/body weight ratio of mice transplanted with BM cells obtained from wild type (n=20) (+/+, open bars) and K-*Ras*$^{+/V14I}$ (n=14) (+/V14I, gray bars) mice sacrificed 30-34 weeks after transplantation. **(C)** H&E stained paraffin section of lung, liver and kidney of mice transplanted with BM cells obtained from wild type (+/+) and K-*Ras*$^{+/V14I}$ (+/V14I) mice sacrificed 30-34 weeks after transplantation. Solid asterisk indicate immunoinfiltrates. Scale bar, 500 μm. **(D)** Flow cytometry analysis of Gr1^{+} and CD11b^{+} cells in spleens obtained from mice transplanted with BM cells obtained from wild type (+/+) and K-*Ras*$^{+/V14I}$ (+/V14I) mice sacrificed 30-34 weeks after transplantation. **(E)** Frequencies of donor cell-derived myeloid CD11b^{+} and Gr1^{+}/CD11b^{+} cells in mice transplanted with BM cells obtained from wild type (n=20) (+/+, open bars) and K-*Ras*$^{+/V14I}$ (n=14) (+/V14I, gray bars) mice sacrificed 30-34 weeks after transplantation. Error bars indicate SD. **P < 0.01; ***P < 0.001.

6.9.4 Activation of K-*Ras*^{V14I} mutation in hematopoietic cells

N-*RAS* and K-*RAS* mutations are present in approximately 30% of acute myeloid leukemias (AML), MPD and myelodysplastic syndromes (MDS) *(24)*. In mice, the expression of the K-*Ras*^{G12D} mutation in the hematopoietic system, using the interferon (IFN)-inducible Cre (*Mx1*-Cre) rapidly induced a fatal MPD *(27, 37)*. However, mice that expressed the N-*Ras*^{G12D} mutation in the hematopoietic compartment by the same approach developed an indolent MPD, and die due to a diverse spectrum of hematologic alterations that included MPD, a disorder that was reminiscence of human MDS, lymphoid expansion and histiocytic sarcoma *(120)*.

To characterize the biological consequences of expressing the K-*Ras*^{V14I} mutation in hematopoietic cells we crossed the conditional K-*Ras*$^{+/LSLV14I}$ mice with the interferon-inducible Cre (*Mx*1-Cre) line. We performed the same study with the K-*Ras*$^{+/LSLG12V}$ mice in order to compare both mutations. The *Mx1*-Cre transgene directs efficient recombination in BM and in hematopoietic cells with high repopulating potential *(107)*. The *Mx1* promoter can be activated by administration of IFNα, IFN-β or the synthetic double-stranded RNA [polyinosinic-polycydilic acid (pIpC)], an INF inducer *(107)*.

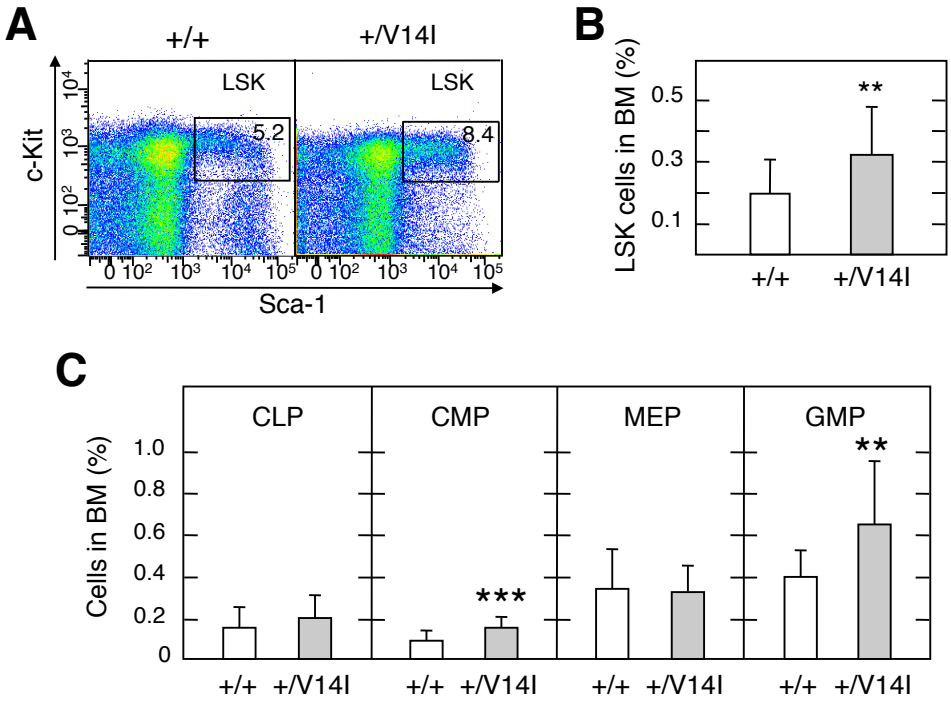

Figure 34. **Aberrant hematopoiesis in mice transplanted with BM from K-*Ras*$^{+/V14I}$ mice**. **(A)** Flow cytometry analysis of BM cells obtained from mice transplanted with BM cells of wild type (+/+) and K-*Ras*$^{+/V14I}$ (+/V14I) mice sacrificed between 30 to 34 weeks after transplantation, using antibodies against c-Kit and Sca-1. The percentage of LSK cells is indicated. **(B)** Percentage of LSK donor-derived cells in mice transplanted with BM cells obtained from wild type (n=20) (+/+, open bar) and K-*Ras*$^{+/V14I}$ (n=14) (+/V14I, gray bar). **(C)** Percentage of CLP, CMP, MEP, and GMP cells in mice transplanted with BM cells obtained from wild type (n=20) (+/+, open bars) and K-*Ras*$^{+/V14I}$ (n=14) (+/V14I, gray bars) mice. Error bars indicate SD. **P < 0.01; ***P < 0.001.

Four to five-weeks-old K-*Ras*$^{+/+}$;*Mx1*-Cre$^{+/T}$ (n=7) and K-*Ras*$^{+/LSLV14I}$;*Mx1*-Cre$^{+/T}$ (n=10) mice were treated with pIpC to induce expression of the Cre recombinase and the subsequent expression of the K-*Ras*^{V14I} allele after excision of the floxed STOP cassette. K-*Ras*^{V14I} mutant and wild type control mice were sacrificed at 9 months (n=4) and 15 months (n=5 and n=3 respectively) of age. One of the K-*Ras*$^{+/LSLV14I}$;*Mx1*-Cre$^{+/T}$ mice succumbed before reaching 15 months of age due to hematological alterations. At the analyzed time points (9 and 15 months) mutant mice developed progressive leukocytosis due to an expansion in the lymphoid, neutrophils, eosinophils and basophils population (data not shown). Mutant 9-month-old mice

displayed a slight increase in the spleen/body weight ratio compared to control mice ***(Figure 35A and B)***. Histological analysis revealed the presence of small perivascular immunoinfiltrates in all tissues analyzed, such as kidney, liver and lung. The progression of the hematological alteration was evident at 15 months of age since spleen of mutant mice was significantly bigger, as well as the area of tissues affected by the immunoinfiltrates, being the lung the more affected ***(Figure 35)***. Similar results we obtained with the oncogenic K-*Ras*^{G12V} mutation, but in this case the development of the disease was faster (data not shown). Most of the mice were sacrificed at humane end point between 6 to 12 months old.

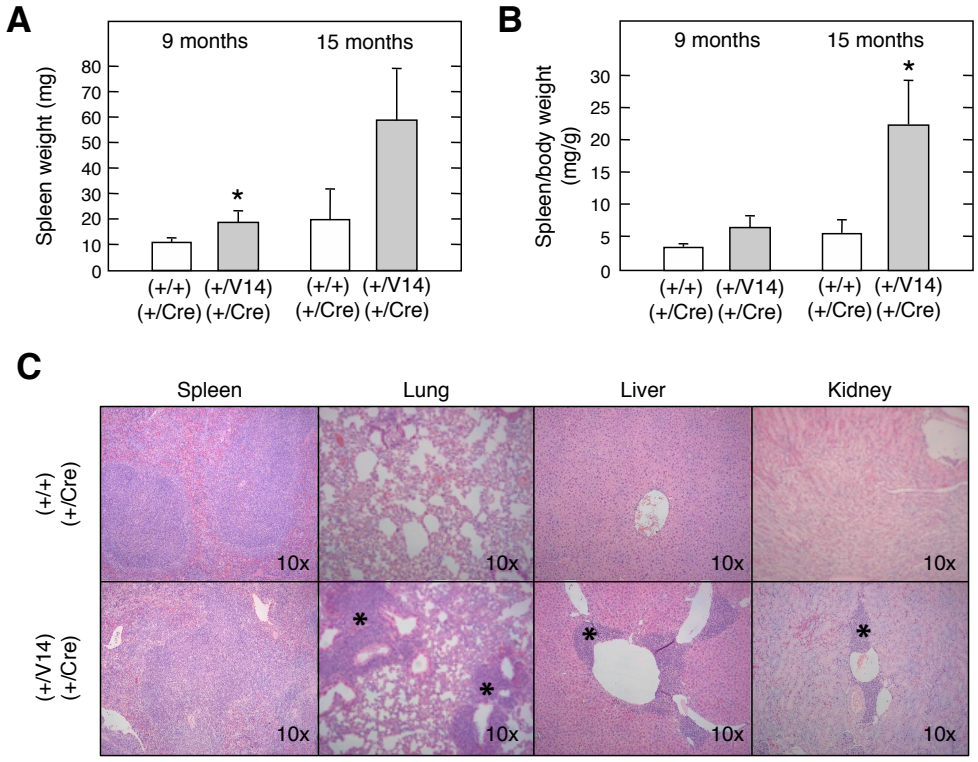

Figure 35. **K-Ras^{V14I} expression induces the development of a hematological disorder**. **(A)** Spleen weight of K-*Ras*$^{+/+}$; *Mx1*-Cre$^{+/T}$ (+/+; +/Cre, gray bar) and K-*Ras*$^{+/LSLV14I}$; *Mx1*-Cre$^{+/T}$ (+/V14I; +/Cre, solid bar) mice at 9 (n=4 and n=4, respectively) and 15 (n=3 and n=5, respectively) months of age. **(B)** Spleen/body weight of K-*Ras*$^{+/+}$; Mx1-Cre$^{+/T}$ (+/+; +/Cre, gray bar) and K-*Ras*$^{+/LSLV14I}$; *Mx1*-Cre$^{+/T}$ (+/V14I; +/Cre, solid bar) mice at 9 (n=4 and n=4, respectively) and 15 (n=3 and n=5, respectively) months of age. Error bars indicate SD. *P < 0.05. **(C)** H&E stained paraffin section of spleen, lung, liver and kidney of K-*Ras*$^{+/+}$; *Mx1*-Cre$^{+/T}$ (+/+; +/Cre) and K-*Ras*$^{+/LSLV14I}$; *Mx1*-Cre$^{+/T}$ (+/V14I; +/Cre) mice sacrificed at 15 months of age. Solid asterisks indicate immunoinfiltrates.

Therefore, we can conclude that the expression of the K-*Ras*^{V14I} mutation in hematopoietic cells is associated with the development of a hematological disorder similar to the MPD induced by the K-*Ras*^{V14I} germline expression and by the expression in the hematopoietic compartment of the oncogenic K-*Ras* isoforms, K-*Ras*^{G12D} and N-*Ras*^{G12D} *(27, 37, 120)*. However, the progression of the disease is slower in the K-*Ras*^{LSLV14I};*Mx1*-Cre$^{+/T}$ mice than in the K-*Ras*^{LSLG12D};*Mx1*-Cre$^{+/T}$ mice, since most of the K-*Ras*$^{+/LSLV14I}$;*Mx1*-Cre$^{+/T}$ mice

were alive at 15 months of age (83%; 5/6 mice), a time at which most of the K-*Ras*$^{+/LSLG12D}$;*Mx1*-Cre$^{+/T}$ *(27, 37)* and K-*Ras*$^{+/LSLG12V}$;*Mx1*-Cre$^{+/T}$ mice succumbed by the progression of the disease.

6.10 EFFECT OF MODIFIER ALLELES: GENETIC BACKGROUND AFFECTS NS PHENOTYPE

K-*Ras*$^{V14I/V14I}$ mice in a mixed B6/129 background displayed significant perinatal lethally due to cardiovascular problems. However, 10% of these mice obtained from crosses between heterozygous mice, overcame these problems and survived. The incomplete penetrance of this perinatal lethality could reflect modifier alleles in one or the other strain or stochastic events. To distinguish between these possibilities, we backcrossed K-*Ras*^{V14I} mice to C57BL/6J and 129S2/Sv backgrounds. Heterozygous mice were viable and were obtained as expected Mendelian ratios in both genetic backgrounds for at least seven generations. However, homozygous mice were no viable when we intercrossed heterozygous mice backcrossed to the C57BL/6J background for five generations. At embryonic days E13.5 and E18.5, homozygous C57BL/6J mice appeared at the expected Mendelian ratio (data not shown). However, no C57BL/6J K-*Ras*$^{V14I/V14I}$ mice were found at P0. In contrast, backcrosses to the 129S2/Sv resulted in a significant perinatal lethality at the fifth generation, similar to the mix B6/129 background. Around 13% of the 129S2/Sv homozygous mice obtained from crosses between heterozygous mice, were born and reached adulthood ***(Table 9 in Appendix 1).***

Therefore, we can conclude that the phenotypic consequences of the C57BL/6J background might be more aggressive, at least during embryonic and/or perinatal development, than those of 129S2/Sv background.

6.10.1 Phenotypic consequences of the genetic backgrounds on the body size and facial dysmorphia

To determine the effect of modifier alleles on mice development, we followed up the body weight and body length of mutant and control mice backcrossed to the C57BL/6J or 129S2/Sv backgrounds for five generations.

The weight and body size of C57BL/6J K-*Ras*$^{+/V14I}$ mice (n=25) was comparable to wild type animals (n=30). Similar to the C57BL/6J background, no differences were found between 129S2/Sv heterozygous (n=21) and control mice (n=14). However, 129S2/Sv K-*Ras*$^{V14I/V14I}$ mice (n=8) displayed significant reduced body size and body length compared to the wild type littermates. These differences persisted for at least 3 months ***(Figure 36)***.

We also studied the effect of modifier alleles on the craniofacial alteration. We analyzed the different skull parameters by micro-CT in 4-month-old mice for five generations to C57BL/6J or 129S2/Sv genetic backgrounds. The skull alterations (increased skull width and height, reduced length and bigger skull volume) were less pronounced in heterozygous mice of pure C57BL/6J and 129S2/Sv genetic backgrounds. However, 129S2/Sv homozygous mice displayed more evident skull alterations than the B6/129 homozygous mice ***(Table 10 in Appendix I).***

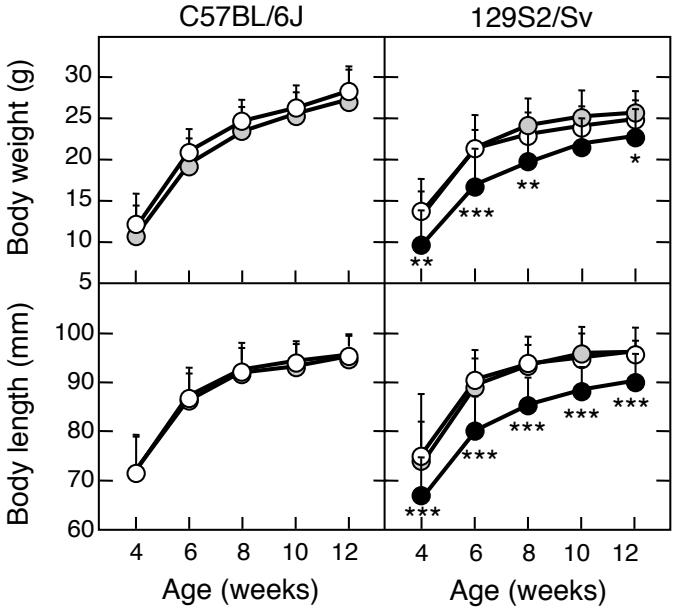

Figure 36. **Phenotypic consequences of the genetic backgrounds on the body size.** Growth curves of male mice backcrossed for five generations to C57BL/6J and 129S2/Sv genetic backgrounds.. Body weight (Top) and body length (bottom) of wild type (n=30 and 14, respectively) (open circles), K-*Ras*$^{+/V14I}$ (n=25 and 21, respectively) (gray circles) and K-*Ras*$^{V14I/V14I}$ (n=8) (solid circles) male mice. Error bars indicate SD. *P < 0.05; **P < 0.01; ***P < 0.001.

These results suggest that the growth and the facial appearance phenotype of heterozygous mice became ameliorated or disappeared in the C57BL/6J or 129S2/Sv pure genetic backgrounds compared to the mix background. However, the phenotype of 129S2/Sv homozygous mice was similar or more dramatic than in the mix B6/129 homozygous mice.

6.10.2 Phenotypic consequences of the genetic backgrounds on cardiac and hematopoietic alterations

To determine the effect of modifier alleles on the cardiac and hematopoietic phenotype, we sacrificed 4 month-old mutant and control mice after the fifth-generation backcross onto C57BL/6J or 129S2/Sv backgrounds.

Heart weight and heart/body weight ratio of C57BL/6J and 129S2/Sv heterozygous mice were bigger compared to the wild type littermates. This increase was similar in both genetic backgrounds and was comparable to the mix B6/129. The heart of K-*Ras*$^{+/V14I}$ mice was 24% heavier in the C57BL/6J background (n=14), 26% in the 129S2/Sv background (n=10) and 16% in the B6/129 mix background (n=30) than control mice. In contrast, cardiac phenotype of

homozygous mice was ameliorated in 129S2/Sv compared to the B6/129 mix background. The heart of 129S2/Sv K-*Ras*$^{V14I/V14I}$ mice (n=5) was 32% heavier than control mice, while heart of homozygous B6/129 mice (n=13) was 57% heavier than the wild type littermates ***(Figure 37A)***.

In the context of the hematopoietic alterations, this phenotype was more dramatic in the C57BL/6J background. Mutant mice showed an increase in the number of leukocytes in peripheral blood, mainly due to expansion of neutrophils, eosinophils and basophils population. They were also anemic and suffered from thrombocytopenia ***(Table 11 in Appendix I)***. The spleen of C57BL/6J heterozygous mice (n=14) was 3 times bigger than the control mice (n=9), while the spleen of B6/129 heterozygous mice (n=22) was only 2 times bigger than the control mice (n=13). Similar results were obtained when we compared the spleen/body weight ratio ***(Figure 37B).*** However, the life span of C57BL/6J heterozygous mice was similar to the B6/129 heterozygous mice (half-life of 64 weeks *vs* 62 weeks) ***(Figure 36)***.

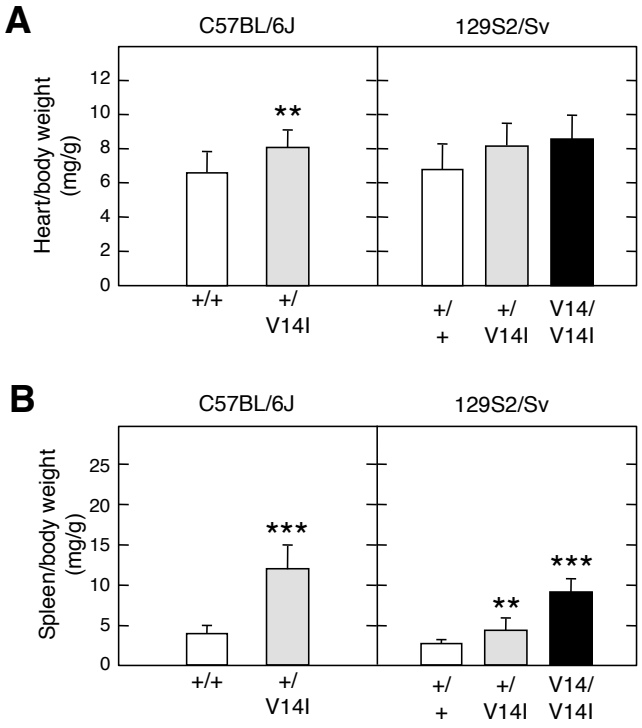

Figure 37. **Phenotypic consequences of the genetic backgrounds on cardiac and hematopoietic phenotype. (A)** Right: Heart/body weight ratio of 4-month-old wild type (n=9) (+/+, open bars) and K-*Ras*$^{+/V14I}$ (n=14) (+/V14I, gray bars) C57BL/6J male mice. Left: Heart/body weight ratio of 4-month-old wild type (n=10) (+/+, open bars), K-*Ras*$^{+/V14I}$ (n=10) (+/V14I, gray bars) and K-*Ras*$^{V14I/V14I}$ (n=5) (V24I/V14I, solid bars) 129S2/Sv male mice. **(B)** Right: Spleen/body weight ratio of 4-month-old wild type (n=9) (+/+, open bars) and K-*Ras*$^{+/V14I}$ (n=14) (+/V14I, gray bars) C57BL/6J male mice. Left: Spleen/body weight ratio of 4-month-old wild type (n=10) (+/+, open bars), K-*Ras*$^{+/V14I}$ (n=10) (+/V14I, gray bars) and K-*Ras*$^{V14I/V14I}$ (n=5) (V14I/V14I, solid bars) 129S2/Sv male mice. Error bars indicate SD. **P < 0.01; ***P < 0.001.

In contrast, this phenotype became ameliorated in the 129S2/Sv genetic background. Homozygous and heterozygous mice displayed a significant increase in spleen weight and spleen/body weight ratio. However, while spleen of B6/129 homozygous mice (n=12) was 5 times bigger than the control mice (n=13), the spleen of 129S2/Sv homozygous mice (n=5) was only 3 times bigger that the wild type mice (n=10). In contrast, the spleen of B6/129 (n=22) and 129S2/Sv (n=10) heterozygous mice was 2 times bigger than their corresponding controls. Similar results were obtained when we compared the spleen/body weight ratio of homozygous and heterozygous mice of both genetic backgrounds ***(Figure 37B)***. Blood count analysis also

confirmed that the MPD is ameliorated in the 129S2/Sv background, at least in homozygous mice. No blood alterations were found at 4 months of age in heterozygous mice and homozygous mice only displayed leukocytosis ***(Table 11 in Appendix I)***. All together resulted in longer life span with a half-life of 82 weeks in K-*Ras*$^{+/V14I}$ mice (a 32% increase in the life span compared to B6/129 heterozygous mice) and of 57 weeks in K-*Ras*$^{V14I/V14I}$ mice (a 58% increase in the life span compared to B6/129 homozygous mice) ***(Figure 38)***.

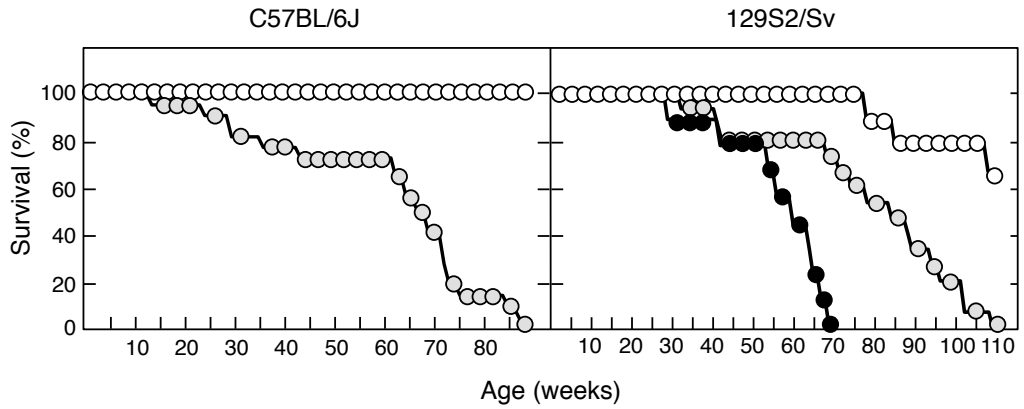

Figure 38. **Phenotypic consequences of the genetic backgrounds on the survival rate.** Left: survival curve of wild type (n=5; open circles) and K-*Ras*$^{+/V14I}$ (n=22; gray circles) C57BL/6J mice. Right: survival of wild type (n=9; open circles), K-*Ras*$^{+/V14I}$ (n=15; gray circles) and K-*Ras*$^{V14I/V14I}$ (n=9; solid circles) 129S2/Sv mice.

Together these results suggest no effect of modifier alleles on the cardiac alterations, since the phenotype observed in the three different backgrounds was similar However, the hematopoietic phenotype is sensitive to the presence of modifier alleles of these genetic backgrounds, being these alterations more remarkable in the C57BL/6J genetic background.

6.11 CANCER RISK IN K-*Ras*^{V14I} mice

Patients with NS have high predisposition for benign and malignant proliferative disorders *(91)*. This study, performed in a large cohort of patients with NS carrying the *PTPN11* mutation, describes that these patients have increased tumor risk *(91)*. Regardless of this study, data on the incidence of malignancies in NS is incomplete, since there is no follow up in the adulthood and there are no studies about the tumor risk of different NS-associated mutations.

Our objective was to estimate the cancer risk and tumor spectrum of K-*Ras*^{V14I} mutant mice. Considering the universal role of RAS-MAPK signaling in oncogenesis, we hypothesized that the K-*Ras*^{V14I} gain of function mutation might confer an increased risk for developing a broad range of malignancies, including tumors in which K-*RAS* is preferentially mutated:

pancreatic ductal adenocarcinomas, colorectal cancer and lung adenocarcinomas *(60)*.

Table 2. Summary of pathological alterations found in K-*Ras*$^{+/V14I}$ and K-*Ras*$^{V14I/V14I}$ mice sacrificed at humane end point

Neoplastic malignancies	K-*Ras*$^{+/V14I}$ (n=26)		K-*Ras*$^{V14I/V14I}$ (n=12)	
Lymphoma	16	(61%)	8	(67%)
B-cell lymphoma	3	(11%)	0	(0%)
Lymphoblastic lymphoma	1	(4%)	0	(0%)
Histiocytic sarcoma	5	(19%)	3	(25%)
Myeloid leukemia	2	(8%)	0	(0%)
Angiosarcoma	1	(4%)	0	(0%)
Adenocarcinoma	4	(12%)	1	(8%)
Lung	2	(8%)	0	(0%)
Liver	2	(8%)	0	(0%)
Adenohypophysis	0	(0%)	1	(8%)
Adenoma	6	(23%)	0	(0%)
Lung	1	(4%)	0	(0%)
Liver	1	(4%)	0	(0%)
Intestine	3	(11%)	0	(0%)
Epipidymis	1	(4%)	0	(0%)

Other pathological alteration	K-*Ras*$^{+/V14I}$ (n=26)		K-*Ras*$^{V14I/V14I}$ (n=12)	
Kidney alterations	2	(8%)	8	(67%)
Hydronephrosis	1	(4%)	3	(25%)
Glomerulonephritis	1	(4%)	1	(8%)
Pyelonephritis	0	(0%)	5	(42%)
Vasculitis	3	(11%)	0	(0%)
Infarctation area in heart	2	(8%)	1	(8%)

Numbers in parentheses indicate tumor incidence. Total percentage > 100% due to the fact that some mice developed more than one tumor type. See table 12 in Appendix I for more details.

As described above, K-*Ras*$^{+/V14I}$ and K-*Ras*$^{V14I/V14I}$ mice presented reduced life span with a half-life of 62 and 36 weeks, respectively (Figure 10) due to the development of

hematopoietic alterations characterized by splenomegaly, leukocytosis and anemia ***(Table 12 in Appendix I)***. Complete histological evaluation of K-*Ras*$^{+/V14I}$ (n=26) and K-*Ras*$^{V14I/V14I}$ mice (n=12) sacrificed at humane end point, revealed the presence of multiple malignancies including lymphomas, sarcomas and carcinomas. Tumor development was slightly more prevalent in K-*Ras*$^{+/V14I}$ (24/26, 92%) than in K-*Ras*$^{V14I/V14I}$ mice (9/12, 75%) possibly due to their longer survival. Among the observed tumors, lymphomas were most frequent followed by sarcomas, preferentially histiocytic sarcomas and adenocarcinomas. Two K-*Ras*$^{+/V14I}$ animals also developed leukemia. Other pathologies included kidney alterations (hydronephrosis, glomerulonephritis and pyelonephritis), possibly as a consequence of the hematological disorders, vasculitis and areas of heart infarctation ***(Table 2 and Table 12 in Appendix I)***.

All these results suggest that K-*Ras*^{V14I} mice develop a MPD that in combination with a diverse spectrum of hematological disorders including lymphomas, histiocytic sarcomas and leukemia ultimately result in the death of the mice. Moreover, germline expression of the K-*Ras*^{V14I} mutation induces the development of some adenomas and adenocarcinomas.

6.11.1 Role of K-*Ras*^{V14I} in lung tumor development

Mutations of the K-*RAS* oncogene are found in 35% of human lung adenocarcinomas *(60)*. In mice, the postnatal/adult expression of one allele of the oncogenic K-*Ras*^{G12D} or K-*Ras*^{G12V} mutation in adults induces the appearance of lung adenomas/adenocarcinomas and pancreatic tumors *(69, 86, 221)*.

The K-*Ras*^{V14I} mutation is a gain of function mutation that results in milder activation of the protein compared to the somatic oncogenic form. This mutation is compatible with embryo development and does not induce the appearance of pancreatic tumors. Moreover, only 8% (2/26) of K-*Ras*$^{+/V14I}$ mice developed lung adenocarcinomas and no lesions were found in K-*Ras*$^{V14I/V14I}$ mice. This mutation, in contrast to the oncogenic ones, is present throughout development in all the cells in the organism. Thus, the cells may have been adapted to these levels of activation, assuming them as normal in some tissues. It is also possible that the mice die of hematologic malignancies without having time to develop other pathologies.

To test this possibility, we used the conditional K-*Ras*$^{+/LSLV14I}$ strain to achieve the induction of the expression of the K-*Ras*^{V14I} mutation in adult stages in lung. We performed an intratracheal infection of two-month old conditional K-*Ras*$^{+/LSLV14I}$ mice with adenoviral vectors expressing the Cre recombinase *(21)*. This strain also carried the *Rosa26*^{LSLLacZ} reporter allele to monitor the efficiency of the infection by determining the number of LacZ expressing cells. In parallel, we infected K-*Ras*$^{+/LSLVG12Vgeo}$ mice as control for tumor development.

X-Gal staining of lungs of K-*Ras*$^{+/LSLV14I}$;*Rosa26*^{LSLLacZ} or K-*Ras*$^{+/+}$;*Rosa26*^{LSLLacZ} infected mice at 5 months of age (n=3) revealed the presence of similar percentages of LacZ

positive cells, indicative of the efficiency of the infection ***(Figure 39)***. However, expression of the K-*Ras*^{V14I} allele in adult lungs did not induce any lesions in K-*Ras*^{V14I} mice at 18 months of age (n=12) ***(Figure 39)***, a time when, as expected *(21)*, all the K-*Ras*$^{+/LSLVG12Vgeo}$ animals had died due to the presence of numerous lung tumors (data not shown). These observations indicate that the K-*Ras*^{V14I} mutation does not have enough oncogenic properties to elicit lung tumors.

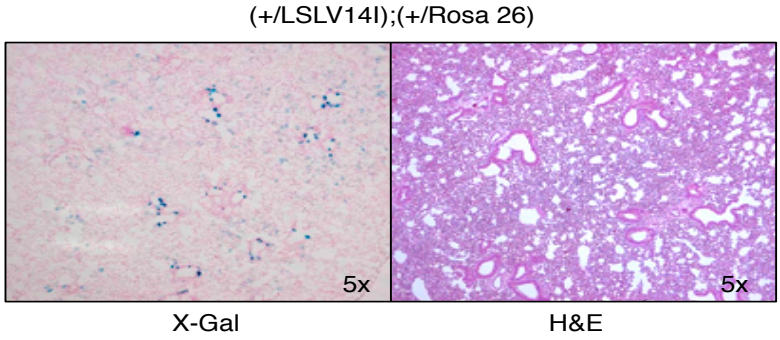

Figure 39. **Expression of the K-*Ras*^{V14I} mutation in lung does not induce tumor development.** Left: X-Gal stained section from 5-month-old K-*Ras*$^{+/LSLV14I}$; *Rosa26*$^{+/LSLLacZ}$ infected intratracheally with adeno-Cre. Right: H&E stained section from 18-month-old K-*Ras*$^{+/LSLV14I}$; *Rosa26*$^{+/LSLLacZ}$ infected intratracheally with adeno-Cre illustrating the absence of lesions.

6.11.2 Role of K-*Ras*^{V14I} in pancreatic tumor development

We interrogated whether the K-*Ras*^{V14I} mutation may increase tumor risk in the context of chronic pancreatitis, a condition that has been shown to cooperate with oncogenic K-*Ras* mutations to induce pancreatic ductal adenocarcinomas (PDAC) *(69, 70)*, one of the human tumors with worst prognosis *(199)*.

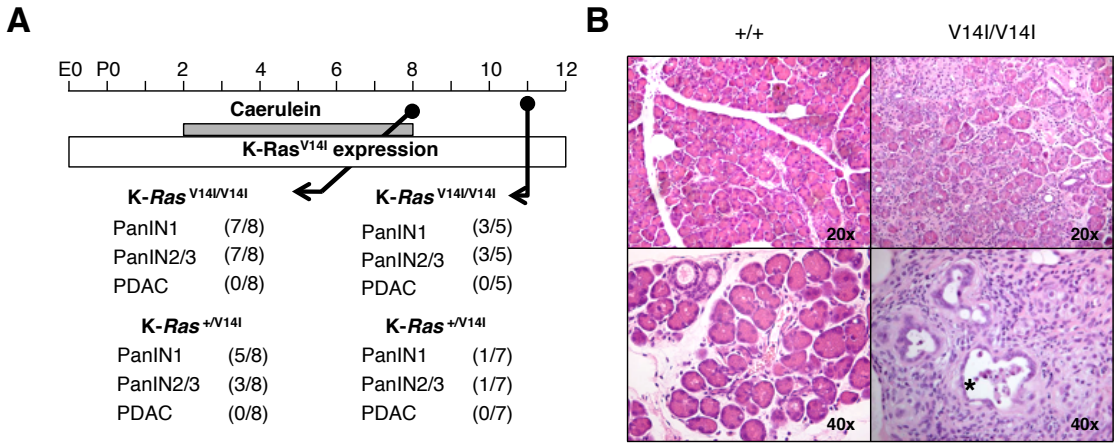

Figure 40. **K-*Ras*^{V14I} expression induced PanIN lesions in pancreatitis context. (A)** K-*Ras*^{V14I} mice were exposed to caerulein (gray box) for 6 months. The open box indicates the time of the K-*Ras*^{V14I} expression. The number of animals positive for low-grade PanIN1 and high-grade PanIN2/3 lesions is indicated for each time point. **(B)** H&E stained paraffin sections of pancreas of wild type (+/+) and K-*Ras*$^{V14I/V14I}$ (V14I/V14I) mice treated with caerulein during 6 months and sacrificed just after the end of the treatment. Asterisk indicates a PanIN3 lesion.

Two-month-old K-*Ras*$^{+/V14I}$ (n=15) and K-*Ras*$^{V14I/V14I}$ (n=13) mice were treated with caerulein for six months and sacrificed either at the end of the treatment or three months later for pathology inspection ***(Figure 40A)***. Just after caerulein treatment, 5 out of 8 K-*Ras*$^{+/V14I}$ mice (62%) and 7 out of 8 K-*Ras*$^{V14I/V14I}$ mice (87%) displayed low-grade pancreatic intraepithelial neoplasias (PanIN1), the early lesions observed during PDAC development. Moreover, 3 out of 8 K-*Ras*$^{+/V14I}$ mice (37%) and 7 out of 8 K-*Ras*$^{V14I/V14I}$ mice (87%) also developed high-grade PanIN2 and PanIN3 lesions ***(Figure 40A)***, the later also called "in situ" carcinomas, the direct PDAC precursors. Yet, no *bona fide* PDAC tumors were identified in K-*Ras*^{V14I} mice. Three months after the caerulein treatment PanIN lesions were also found. 60% (3/5) of K-*Ras*$^{V14I/V14I}$ mice displayed low-grade PanIN lesions and high-grade PanIN lesions could be found in 3 out of 5 mice (60%). Only one mouse out of seven K-*Ras*$^{+/V14I}$ mice displayed low and high-grade PanINs. Again, no *bona fide* PDAC tumors were identified at this time. As expected no lesions were found in wild type animals either just after caerulein treatment (n=3) ***(Figure 40B)*** or three months after the treatment (n=4). Furthermore, the caerulein treatment induced a tissue remodeling at the stroma level and acinar atrophy ***(Figure 40B)*** similar to that observed in K-*Ras*^{LSLG12Vgeo};*Elas*-tTA/*tetO*-Cre mice *(70)*.

These observations indicate that K-Ras^{V14I} protein has oncogenic potential in the context of pancreatic tumor development but at a significant reduced level compared to the *bona fide* oncoproteins K-Ras^{G12D} and K-Ras^{G12V} *(70, 80)*.

Trp53 deficiency cooperated with the oncogenic K-*Ras*^{G12V} mutation to induce metastatic PDAC *(70)*. A small group of K-*Ras*$^{+/V14I}$;*Trp53*$^{-/-}$ mice was used to study cooperation between K-*Ras*^{V14I} expression and *Trp53* loss in PanIN and PDAC development (n=4) in the context of caerulein treatment. These mice were sacrificed at humane end point due to lymphoma and sarcoma development *(see 6.11.5 section)*, during the course of caerulein treatment (around three months after the beginning of the treatment at P30). Pancreata of these mice were removed for pathology inspection. Three out of four mice displayed low and high-grade PanIN lesions and no *bona fide* PDAC tumors were found, similar to the results obtained in K-*Ras*$^{+/V14I}$ mice with wild type *Trp53* (data not shown). These results indicate that loss of *Trp53* did not cooperate with K-*Ras*^{V14I} mutation to induce pancreatic tumor development, in contrast to the K-*Ras*^{G12V} mice. However, K-*Ras*$^{+/V14I}$;*Trp53*$^{-/-}$ mice died around three months after the beginning of the treatment. Therefore, it is possible that the length of the study might not be enough to rule out a possible cooperation. Experiments with heterozygous *Trp53*$^{+/-}$ mice treated with caerulein for six months might help to unveil this issue.

Finally, we generated a K-*Ras*$^{+/LSLV14I}$;*Elas-tTA/tetO*-Cre mice in order to perform a comparative study to the pancreatic tumor model developed in the laboratory, K-*Ras*^{LSLG12Vgeo};*Elas*-tTA/*tetO*-Cre mice *(70)*. Both conditional compound mice carry a bitransgenic strain that expresses the Cre recombinase in acinar cells under the control of the rat *Elastase* promoter

using a tet-off strategy (Tetracycline-controlled transcriptional activation). By this conditional strategy the transcription of the Cre recombinase is activated in the absence of the antibiotic tetracycline or doxycycline (one of its derivates), leading to its expression in acinar cells.

Two-month-old K-*Ras*$^{+/LSLV14I}$;*Elas*-tTA/*tetO*-Cre mice (n=10), maintained in absence of doxycycline, were treated with caerulein for six months and sacrificed just after treatment for histological analysis. This analysis revealed that only three mice (30%) displayed low-grade PanIN lesions. High-grade PanIN lesions were found only in one of them ***(Figure 41)***. Moreover, a group of ten K-*Ras*$^{+/LSLV14I}$;*Elas*-tTA/*tetO*-Cre mice was sacrificed 6 months after the end of the caerulein treatment. In this cohort of mice, only one mouse displayed high-grade PanIN lesions and no mice displayed low-grade PanIN lesions ***(Figure 41)***. Furthermore, one mouse was sacrificed only 4 months after caerulein treatment due to humane end point. This mouse developed a high-grade PanIN3, similar to PDAC.

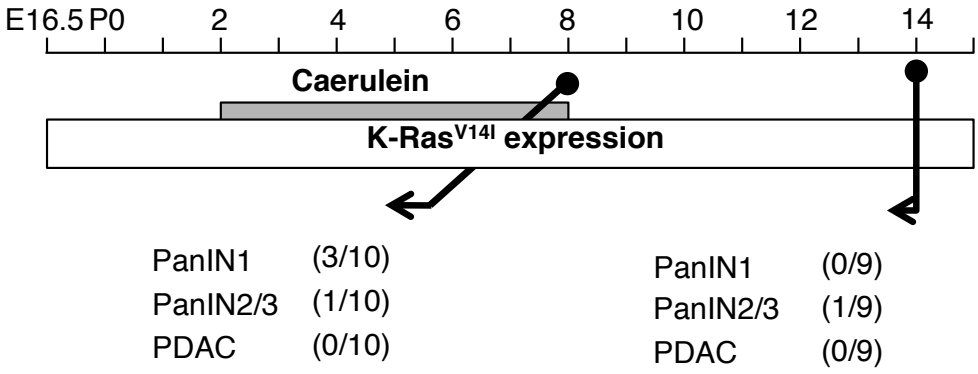

Figure 41. **K-*Ras*^{V14I} expression in acinar cells induced low number of PanIN lesions in the context of pancreatitis.** K-*Ras*$^{+/LSLV14I}$;*Elas*-tTA/*tetO*-Cre mice were exposed to caerulein (gray box) for 6 months. The open box indicates the time of the K-*Ras*^{V14I} expression. The number of animals positive for low-grade PanIN1 and high-grade PanIN2/3 lesions is indicated for each time point.

The number of lesions and the number of K-*Ras*$^{+/LSLV14I}$;*Elas*-tTA/*tetO*-Cre affected mice was much lower than in the case of the K-*Ras*^{LSLG12Vgeo} ;*Elas*-tTA/*tetO*-Cre mice *(68, 70)*. Furthermore, these results suggest that the expression of the K-*Ras*^{V14I} mutation only in acinar cells induces lower incidence of PanIN lesions than the germline expression of this mutation. In the K-*Ras*$^{+/LSLV14I}$;*Elas*-tTA/*tetO*-Cre conditional mice, expression of the K-*Ras* activated mutation takes place in around 30% of acinar cells starting at E16.5 of embryo development. It is a low percentage compared to the K-*Ras*^{V14I} Noonan model in which the expression takes place in all cells since germline. The low transforming capacity of the K-*Ras*^{V14I} mutation and the low percentage of cells expressing the mutation in this model might explain the small number of PanIN lesions found in the K-*Ras*$^{+/LSLV14I}$;*Elas*-tTA/*tetO*-Cre mice.

6.11.3 Nicotine increases tumor risk of K-*Ras*^{V14I} expressing mice

Smoking is the most important risk factor for lung cancer, since 85-90% of the cases can be attributed to tobacco smoking in men *(219)*. Moreover, smoking has been identified as a leading risk factor for PDAC development. Almost one fourth of deaths in patients with PDAC are linked to tobacco use *(130)* and smoking a pack of cigarettes or more a day is associated with a five-to six-fold increased risk of developing pancreatic cancer *(127)*. Among the thousands of substances contained in tobacco smoke, nicotine has been the most widely studied due to its addictive properties. Several *in vitro* studies using cancer cell lines have demonstrated that nicotine increases cell proliferation, migration and survival by activating components of the MAPK, PI3K and Src pathway *(48, 232)*. Moreover, nicotine administration promotes tumor growth in lung and pancreatic cancer mouse models *(49, 77, 143)*.

We interrogated whether nicotine administration may increase tumor risk of K-*Ras*^{V14I} mice. To this aim, we exposed mutant and wild type mice at 2 months of age to continuous treatment of nicotine in the drinking water. K-*Ras*$^{V14/V14I}$ mice were sacrificed at humane end point due to development of hematological disorders *(see 6.11 section)* after 4 months (n=1) and 10 months (n=2) of nicotine treatment. Pancreata and lungs of these mice were histologically analyzed. Two out of three mice displayed adenocarcinomas in lung and one out of three displayed a sarcomatoid PDAC ***(Figure 1 in Appendix I).*** Interestingly, these lesions appeared independently of the length of nicotine treatment (Figure 42). In contrast, no lesions were found in wild type mice exposed to nicotine for 12 months (n=3). Although nicotine treatment promoted tumor development in K-*Ras*$^{V14/V14I}$ mice, the effect was less aggressive than in the case of K-*Ras*$^{+/LSLG12Vgeo}$;*Elas*-tTA/*tetO*-Cre mice, which pancreas were severely affected by high numbers of PanIN lesions (Hermann PC and Heeschen Ch, unpublished data).

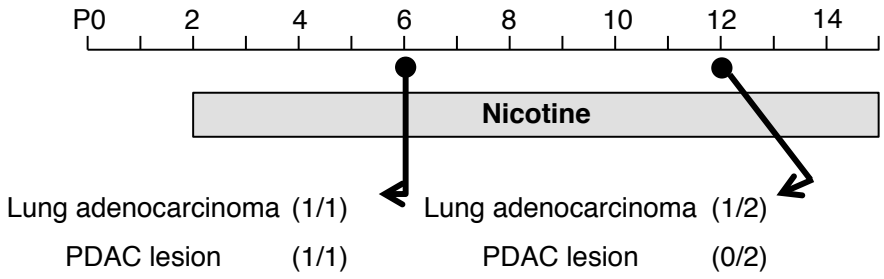

Figure 42. **Nicotine increases tumor risk in K-*Ras*^{V14I} mice.** K-*Ras*^{V14I} mice were exposed at 2 months of age to continuous nicotine administration (gray box). The number of mice affected by lung adenocarcinomas and PDAC lesions and the sacrifice time point are indicated.

These preliminary studies suggest that nicotine administration enhanced the oncogenic properties of the K-*Ras*^{V14I} mutation. Therefore, tobacco smoking in patients that express K-Ras-NS-associated mutation might increase the risk of lung and pancreatic tumor development.

6.11.4 Loss of heterozygosity (LOH)

Loss of heterozygosity (LOH) or deletion of the wild type allele is a common secondary event detected in advanced tumors. In mice, loss of one wild type K-*Ras* allele increases lung tumor development by carcinogens *(244)*. Furthermore, data of our laboratory also indicates that the elimination of the wild type allele in mice that express one copy of the oncogenic K-*Ras*^{G12V} mutation results in earlier onset and fast progression of lung tumors and reduced life span *(33)*. These observations suggest that loss of the wild type K-*Ras* allele may facilitate transformation and tumorigenesis mediated by the oncogenic Ras mutations.

To address if the elimination of the wild type allele increases the oncogenic potential of the K-*Ras*^{V14I} expression, we crossed our K-*Ras*$^{+/V14I}$ mice with heterozygous K-*Ras* deficient mice, K-*Ras*$^{+/-}$, developed in our laboratory. Hemizygous K-*Ras*$^{V14I/-}$ mice (n=14 out of 61 mice obtained from crosses between K-*Ras*$^{+/V14I}$ and K-*Ras*$^{+/-}$ mice, 23%) were born at expected Mendelian ratio and at 4 months of age (n=12) displayed enlarged heart and splenomegaly mimicking the phenotype of the K-*Ras*^{V14I} mice (data not shown). K-*Ras*$^{V14I/-}$ mice (n=29) died due to the development of hematological disorders and the survival rate was similar to the K-*Ras*$^{+/V14I}$ mice (n=68), with a small not significant reduction of the half-life (54 weeks *vs.* 62 weeks), which is still far from the half-life of K-*Ras*$^{V14I/V14I}$ mice (n=30; 36 weeks) ***(Figure 43)***. Therefore, the elimination of the wild type allele did not affect the progression of the hematological disorder, since the survival of mice that express one copy of the K-*Ras*^{V14I} allele with or without the wild type allele is similar ***(Figure 43)***. Furthermore, we did not observe any other pathology in K-*Ras*$^{V14I/-}$ mice different from the previously described in K-*Ras*$^{+/V14I}$ or K-*Ras*$^{V14I/V14I}$ mice (data not shown).

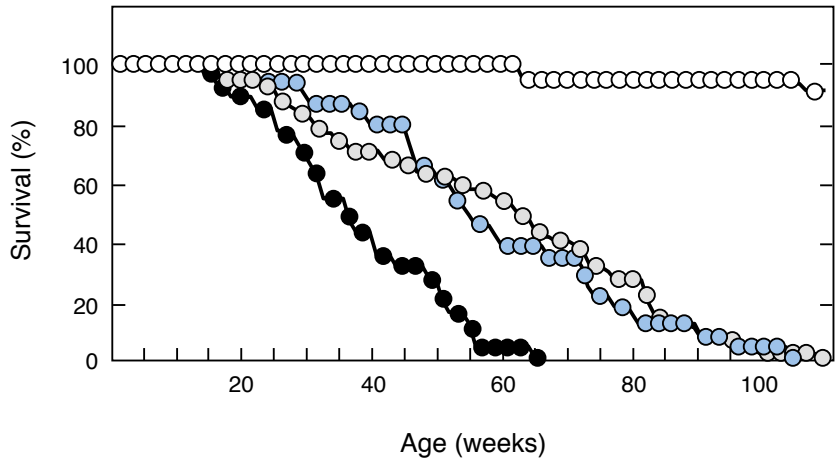

Figure 43. **Loss of the wild type copy of K-*Ras* had no effects in the survival rate.** Survival curve of wild type (n=; 25open circles), K-*Ras*$^{+/V14}$ (n=68; gray circles), K-*Ras*$^{V14I/V14I}$ (n=30; solid circles) and K-*Ras*$^{V14I/-}$ (n=29; blue circles) mice.

6.11.5 Cooperation between K-*Ras*^{V14I} mutation and tumor suppressors genes

Next, we examined whether the K-*Ras*^{V14I} mutation cooperated with other oncogenic mutations such as loss of tumor suppressor genes including *p16Ink4a/p19Arf* and *Trp53*.

p16Ink4a/p19Arf deficient mice developed spontaneous tumors at early age including lymphomas and sarcomas, mainly fibrosarcoma *(191)*. Elimination of *p16Ink4a/p19Arf* in K-*Ras*$^{V14I/V14I}$ mice (n=9), but not in their heterozygous littermates (n=13), led to a 15% reduction in life span ***(Figure 44)***. K-*Ras*$^{V14I/V14I}$;*p16Ink4a/p19Arf* $^{-/-}$ mice died due to a faster development of hematopoietic malignancies, mainly lymphomas (3 out of 8 histological analyzed mice) and histiocytic sarcomas (7 out of 8 histological analyzed mice) spreading to different organs ***(Table 13 in Appendix I, Figure 45 and Figure 2 and 3 in Appendix I)***. All these tumors are characteristic of the *p16Ink4a/p19Arf* deficient mice *(191)*. However, the incidence of these tumors was different. Only one histiocityc sarcoma (11%; 1 out of 9) was reported in *p16Ink4a/p19Arf* deficient mice *(191)*. This is a very low percentage compared to the incidence of this malignance in K-*Ras*$^{V14I/V14I}$;*p16Ink4a/p19Arf* $^{-/-}$ mice (87%; 7 out of 9). Interestingly, no fibrosarcomas were found in the K-*Ras*$^{V14I/V14I}$;*p16Ink4a/p19Arf*$^{-/-}$ mice. Therefore, these results suggest that the elimination of *p16Ink4a/p19Arf* in mice that express two copies of the K-*Ras*^{V14I} mutation promotes the development of hematological abnormalities, preferentially histiocytic sarcomas, more than mesenchymal tumors like fibrosarcomas.

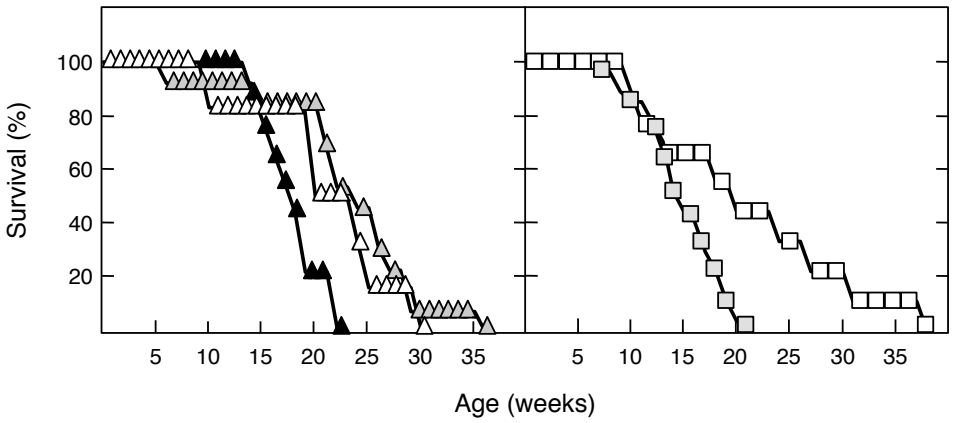

Figure 44. **K-*Ras*^{V14I} cooperates with loss of tumor suppressor genes.** Left: survival curve of K-*Ras*$^{+/+}$; *p16Ink4a/p19Arf* $^{-/-}$ (n=6, open triangles), K-*Ras*$^{+/V14I}$; *p16Ink4a/p19Arf* $^{-/-}$ (n=13, gray triangles) and K-*Ras*$^{V14I/V14I}$; *p16Ink4a/p19Arf* $^{-/-}$ (n=9, solid triangles) mice. Right: survival curve of K-*Ras*$^{+/+}$;*Trp53*$^{-/-}$ (n=9, open squares) and K-*Ras*$^{+/V14I}$;*Trp53*$^{-/-}$ (n=27, gray squares) mice.

The K-*Ras*^{V14I} mutation also cooperated with loss of *Trp53*. K-*Ras*$^{+/V14I}$;*Trp53*$^{-/-}$ mice (n=27) died significantly faster (50% survival at 15 *vs.* 20 weeks, a 25% reduction in life-span) than *Trp53 null* animals (n=9) ***(Figure 44)***. *Trp53* deficient mice spontaneously developed a variety of neoplasm at 6 months of age, including lymphomas and sarcomas *(52)*. These tumors had also been found in the K-*Ras*$^{+/V14I}$;*Trp53*$^{-/-}$ mice ***(Table 14 in Appendix I, Figure 45)***.

Therefore, the reduction in life span was not due to the appearance of different tumor types. Histological examination of K-*Ras*$^{+/V14I}$;*Trp53*$^{-/-}$ mice (n=10) revealed the presence of more aggressive tumors. Lymphomas spread to more organs ***(Figure 4 in Appendix I)*** and the angiosarcomas were multicentric ***(Figure 5 in Appendix I)***. Furthermore, most of the mice (7/10) were affected by more than one tumor. These results suggest that this survival reduction is due to an increase in the number of tumors as well as to their more aggressive nature.

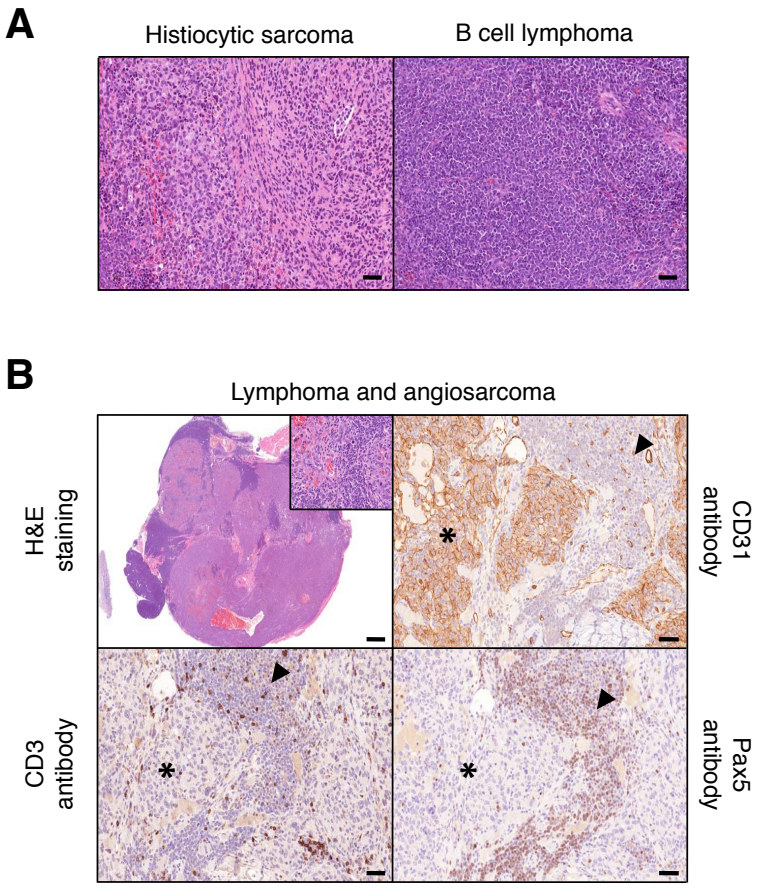

Figure 45. **Tumors of K-*Ras*^{V14I};*p16Ink4a/p19Arf*$^{-/-}$ and K-*Ras*$^{+/V14I}$;*Trp53*$^{-/-}$ mice. (A)** H&E stained paraffin sections of representative histiocytic sarcoma (left) and B cell lymphoma (right) of a K-*Ras*^{V14I};*p16Ink4a/p19Arf*$^{-/-}$ mouse sacrificed at humane end point. Scale bars, 50 μm. **(B)** H&E stained paraffin section and CD31, CD3 and Pax5 immunostaining of an abdominal mass found in a K-*Ras*$^{+/V14I}$;*Trp53*$^{-/-}$ mouse with a representative lymphoma and angiosarcoma. Inset shows detail of the area affected by both tumors. Arrowheads point to the lymphoma and asterisks indicate the angiosarcoma. H&E scale bar, 1000 μm. Immunostaining scale bars, 50 μm.

Thus far, we were not able to obtain K-*Ras*$^{V14I/V14I}$;*Trp53*$^{-/-}$ mice. From crosses between K-*Ras*$^{+/V14I}$;*Trp53*$^{-/-}$ and K-*Ras*$^{+/V14I}$;*Trp53*$^{+/-}$ mice, only rests of two pups were found just after birth and the genotype by PCR indicated that they were K-*Ras*$^{V14I/V14I}$;*Trp53*$^{-/-}$. However, two embryos (2/24, 8%) were found at embryonic day E18.5 ***(Table 15 in Appendix I)***. One of these two K-*Ras*$^{V14I/V14I}$;*Trp53*$^{-/-}$ E18.5 embryos, a female, displayed cranial malformation. It has been described that a variable percentage (8-16%) of *Trp53*$^{-/-}$ females exhibited a variety of cranial malformation, including exencephaly, a neural tube defect in which the neural tube fails

to close during development. This developmental alteration results in a reduction in the number of females at weaning *(15, 178)*. All together suggest that the increased dosage effect of the K-*Ras*^{V14I} allele in a *Trp53 null* background may led to a late embryonic lethality probably due to a combination of the cranial malformation, typically found in *Trp53*$^{-/-}$ females and the heart defects associated to K-*Ras*$^{V14I/V14I}$ mice.

6.11.6 Somatic expression of the K-*Ras*^{V14I} mutation

We interrogated if the expression of the K-*Ras*^{V14I} mutation initiated in the adulthood could induce the oncogenic transformation of some specific cell types, as the expression of the typical K-*Ras* oncogenic mutations *(69, 90, 221)*. Following the same approach of the K-*Ras*$^{+/LSLG12Vgeo}$ mouse model generated in our laboratory *(69)*, the conditional K-*Ras*$^{+/LSLV14I}$ line was crossed with the tamoxifen inducible Cre strain, *RERTn*. The *RERTn* is a knock-in strain that expresses the inducible Cre recombinase under the control of the locus encoding the large subunit of the RNA polymerase II, thus providing its ubiquitous expression *(69)*. This Cre recombinase is merged to the binding domain of the steroid hormone estrogen receptor (ER), previously modified (ERT2) in a way that prevents its binding to the endogenous steroids *(30)*. The addition of the synthetic steroid 4-hydroxy-tamoxifen (4-OHT) provokes the dissociation of the Cre recombinase from the Heatshock protein 90 (Hsp90) that anchor it in the cytoplasm, resulting in the translocation of the enzyme to the nucleus. Therefore, treatment of K-*Ras*$^{+/LSLV14I}$; *RERTn*$^{ert/ert}$ mice with 4OHT or Tamoxifen results in the activation of the inducible Cre-ERT2 recombinase leading to removal of the STOP transcriptional sequences that prevent expression of the targeted K-*Ras*^{V14I} allele.

To induce the ubiquitous expression of our mutation in somatic cells, we treated K-*Ras*$^{+/LSLV14I}$; *RERTn*$^{ert/ert}$ (n=20) and K-*Ras*$^{+/+}$; *RERTn*$^{ert/ert}$ (n=10) mice with Tamoxifen (TAM-diet) for three months starting at weaning (P21). K-*Ras*$^{+/LSLV14I}$; *RERTn*$^{ert/ert}$ mice (n=7) survived for at least 16 months without any obvious alterations. Histological analysis 15 different tissues of a small group of mutant (n=7) and control (n=4) mice at 16 months of age did not reveal the presence of any neoplastic lesion (data not shown). No lung lesions were found, in contrast to the results obtained in the K-*Ras*$^{+/LSLG12Vgeo}$; *RERTn*$^{ert/ert}$ mice *(129)*. Furthermore, splenomegaly was found in four out of the six analyzed mice, indicative of the development of MPD or other hematological alterations. This data suggest that the expression of the K-*Ras*^{V14I} mutation in somatic cells is not sufficient to induce oncogenic transformation in most of the tissues and only the hematopoietic compartment seems to be susceptible to transformation by the postnatal somatic expression of the mutation

6.11.7 Cooperation between K-*Ras*^{V14I} mutation and the oncogenic mutation *PI3KCA*^{H1047R}

Mutations in genes that encode components of the PI3K signaling pathway are common in human cancer. The *PI3KCA* gene that encodes for the catalytic subunit p110α of class IA PI3 kinase, is frequently mutated in human tumors, including colon, brain, breast, ovarian and lung tumors. The majority of the reported mutations occur in three hotspots: two (E542K and E545K) in the helical domain and one (H1047R) in the kinase domain. The H1047R mutation results in an increased catalytic activity, with a subsequent enhancement of the downstream signaling and oncogenic transformation *in vitro (95)*.

To test if PI3K mutation could cooperate with the K-*Ras*^{V14I} mutation to promote tumor development, we used the *Pi3kca*^{LmgLH1047R} inducible knock-in mouse model (developed by the Experimental Therapeutic Unit at the CNIO). The *Pi3kca*^{LmgLH1047R} knock-in mouse model was generated by replacement of the exons 18, 19 and 20 by an equivalent cDNA flanked by loxP sites, followed by a cDNA containing exons 18, 19 and the 20 with the H1047R mutation. Therefore upon Cre recombinase activity, the floxed DNA fragment containing the wild type forms is deleted allowing the expression of the mutated cDNA (lox-minigene-lox; LmgL). This substitution can be monitored by the presence of IRES GFP-Luc reporter cassette ***(Figure 46)***. We found out that the germline expression of one mutant *Pi3kca*^{H1047R} allele is not compatible with embryo development, since no mutant mice were obtained from crosses between the *Pi3kca*$^{+/LmgLH1047R}$ mice and the *EIIaCre* strain. For this reason, to study the cooperation between *Pi3kca*^{H1047R} and K-*Ras*^{V14I} mutations, we decided to express both mutations from adulthood. To avoid premature mice death due to a strong cooperation between both mutations, in this pilot study we decided to express both mutations at P60. To this aim we crossed both conditional mouse models with the *RERTn* strain.

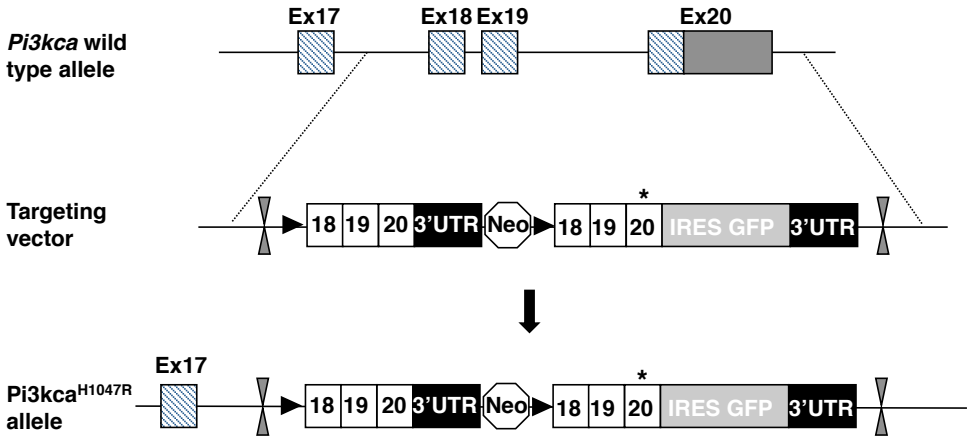

Figure 46. **PI3K targeting vector and modified PI3K allele by homologous recombination.** Stapled boxes represent the exon (Ex) 17, 18, 19 and 20; white boxes, the exons 18, 19 and 20 of the cDNA; black box, 3'UTR; octagonal box (Neo), Neomycin resistance cassette; gray box, IRES-GFP reporter cassette; gray triangles, Frt sites; black triangles, lox-P sites and asterisk, mutation in exon 20 (H1047R).

We treated K-*Ras*$^{+/LSLV14I}$; *RERTn*$^{ert/ert}$; *Pi3kca*$^{+/LmgLH1047R}$ mice (n=8) and the control K-*Ras*$^{+/+}$; *RERTn*$^{ert/ert}$; *Pi3kca*$^{+/LmgLH1047R}$ mice (n=4) Tamoxifen (Tam diet) starting at P60 for 1 month and mice were kept for survival studies. Double mutant and *Pi3kca* single mutant mice displayed the same survival rate indicating no cooperation between both mutations ***(Figure 47)***. Blood analysis ***(Table 16 in Appendix I)*** and preliminary histological characterization of 15 tissues revealed that K-*Ras*$^{+/LSLV14I}$; *RERTn*$^{ert/ert}$; *Pi3kca*$^{+/LmgLH1047R}$ and K-*Ras*$^{+/+}$; *RERTn*$^{ert/ert}$; *Pi3kca*$^{+/LmgLH1047R}$ mice developed hematological alterations. Since both single mutant and double mutant mice succumbed by hematological disorders and displayed the same survival rate, these preliminary results suggests that the hematological disorders induced by the expression of the K-*Ras*^{V14I} mutation is mainly done through the Pi3K pathway. More studies are needed to confirm these observations. Furthermore, the analysis of the alterations developed by K-*Ras*$^{+/LSLV14I}$; *RERTn*$^{ert/ert}$ treated with Tamoxifen starting at P60 for 1 month is also needed.

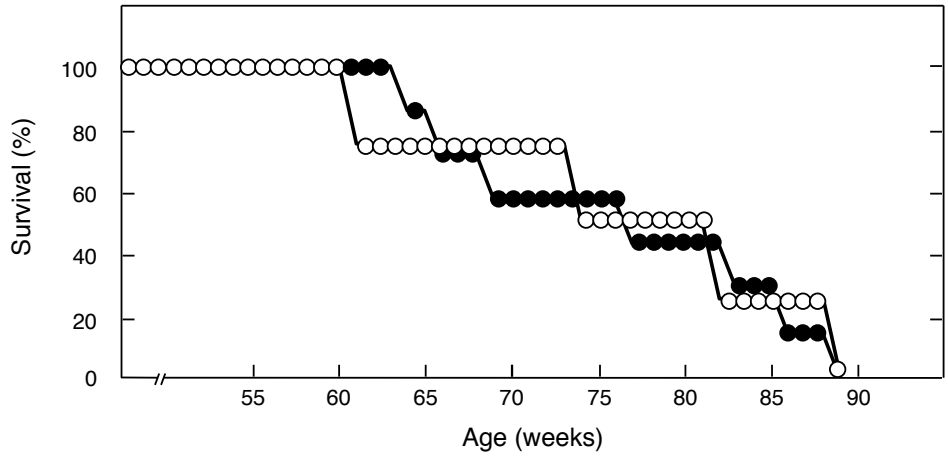

Figure 47. **K-*Ras*^{V14I} mutation does not cooperate with the *Pi3kca*^{H1047R} mutation.** Survival curve of K-*Ras*$^{+/+}$; *RERTn*$^{ert/ert}$; *Pi3kca*$^{+/LmgLH1047R}$ (n=4, open circles) and K-*Ras*$^{+/LSLV14I}$; *RERTn*$^{ert/ert}$; *Pi3kca*$^{+/LmgLH1047R}$ (n=8, solid circles) mice treated for 1 month with Tam diet at P60.

6.12 THERAPEUTIC STRATEGIES: MEK INHIBITOR TREATMENT OF K-*Ras*^{V14I} MICE AT DIFFERENT DEVELOPMENTAL STAGES

Since the Ras/MAPK pathway is frequently found mutated in human tumors, most efforts have been focused on the design of small-molecule inhibitors of the different members of the pathway. The NCFC syndromes result from germline mutations in these same targets. Thus, the same molecular inhibitors of the Ras/MAPK pathway being developed as cancer therapeutics may provide opportunities to therapeutically treat these developmental disorders or ameliorate disease progression of some symptoms *(165)*. Proof of principle for using MEK inhibitors in these syndromes has been demonstrated in Noonan mouse models that express *Raf1 (237)* or *Sos1 (39)* mutations.

We interrogated whether inhibition of K-*Ras* signaling using the MEK inhibitor PD0325901 could ameliorate the defects observed in K-*Ras*^{V14I} mice. PD0325901 is a non-ATP competitive MEK inhibitor that selectively binds to and inhibits both MEK1 and MEK2 kinases. MEK contains a unique inhibitor-binding pocket adjacent to the ATP-binding site. Binding of the inhibitor into this hydrophobic pocket induces conformational changes in unphosphorylated MEK that locks the kinase into a closed but catalytically inactive form, inhibiting the phosphorylation and activation of the downstream target ERK *(190)*.

To this aim, we performed three different treatment protocols ***(Figure 48)***:

1. *Prenatal treatment*: pregnant mothers were treated daily by i.p injection with 1mg/kg of MEK inhibitor PD0325901 or vehicle from E7.5 until P9. Starting at P10 the drug was injected to the pups at the same concentration every other day until P21. This treatment protocol was performed to determine whether the MEK inhibitor could prevent the defects observed in the K-*Ras*^{V14I} mice.
2. *Postnatal treatment:* mice were treated daily by i.p injection with 5mg/kg of MEK inhibitor PD0325901 or vehicle at P21 for 6 weeks to determine whether the MEK inhibitor could eliminate or ameliorate some of the typical alterations of the K-*Ras*^{V14I} mice.
3. *Adult treatment:* 4-month-old mice that already display signs of MPD, were treated daily by i.p injection with 5mg/kg of MEK inhibitor PD0325901 or vehicle for 1 month to determine whether MEK inhibitor might be of therapeutic value to treat the MPD.

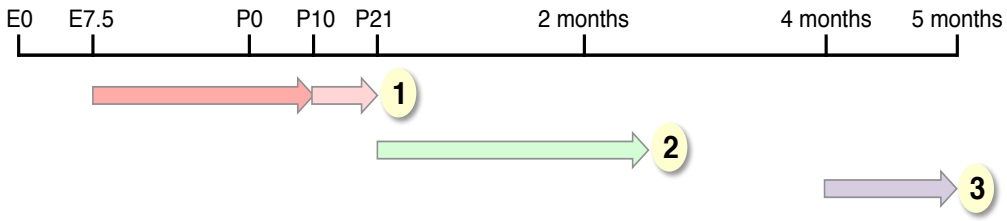

Figure 48. Treatment protocols. Arrows indicate the duration of the treatments. Pink arrows: prenatal treatment or treatment 1; green arrow: postnatal treatment or treatment 2; purple arrow: adult treatment or treatment 3.

6.12.1 Prenatal MEK inhibitor treatment prevents the developmental defects

In an initial experiment, pregnant mothers (n=8) were treated with the MEK inhibitor PD0325901 from E7.5 until P9 and starting at P10, the pups were directly injected. Two hours after the last injection tissues were taken from some mice (n=2) to determine the effect of the MEK inhibitor on K-Ras^{V14I} signaling using phosphorylation of the Erk1/2 kinases as a read out.

As illustrated in ***Figure 49A***, the MEK inhibitor efficiently inhibited Erk1/2 phosphorylation in both wild type and K-*Ras*$^{V14I/V14I}$ animals, albeit the inhibition in the homozygous mice was only partial. In spite of the incomplete inhibition of K-Ras signaling in K-*Ras*$^{V14I/V14I}$ mice, this treatment completely rescued the perinatal lethality. Whereas at weaning, the percentage of alive K-*Ras*$^{V14I/V14I}$ mice treated with vehicle was only 13% (4/31), in those exposed to the MEK inhibitor the percentage of K-*Ras*$^{V14I/14I}$ animals was the expected from Mendelian ratio (29%, 16/56). The rescue of the perinatal lethality was a consequence of the elimination of the heart defects in neonatal mice. Hearts of P0 K-*Ras*$^{V14I/V14I}$ mice exposed to the MEK inhibitor displayed the same size and morphology to their wild type littermates and vehicle treated controls ***(Figure 50A)***. Moreover, a small experiment treating C57BL/6J heterozygous mothers revealed that MEK inhibitor treatment also rescued the lethality observed in this genetic background. C57BL/6J K-*Ras*$^{V14I/V14I}$ mice (3/6) were born and survived for at least 6 months.

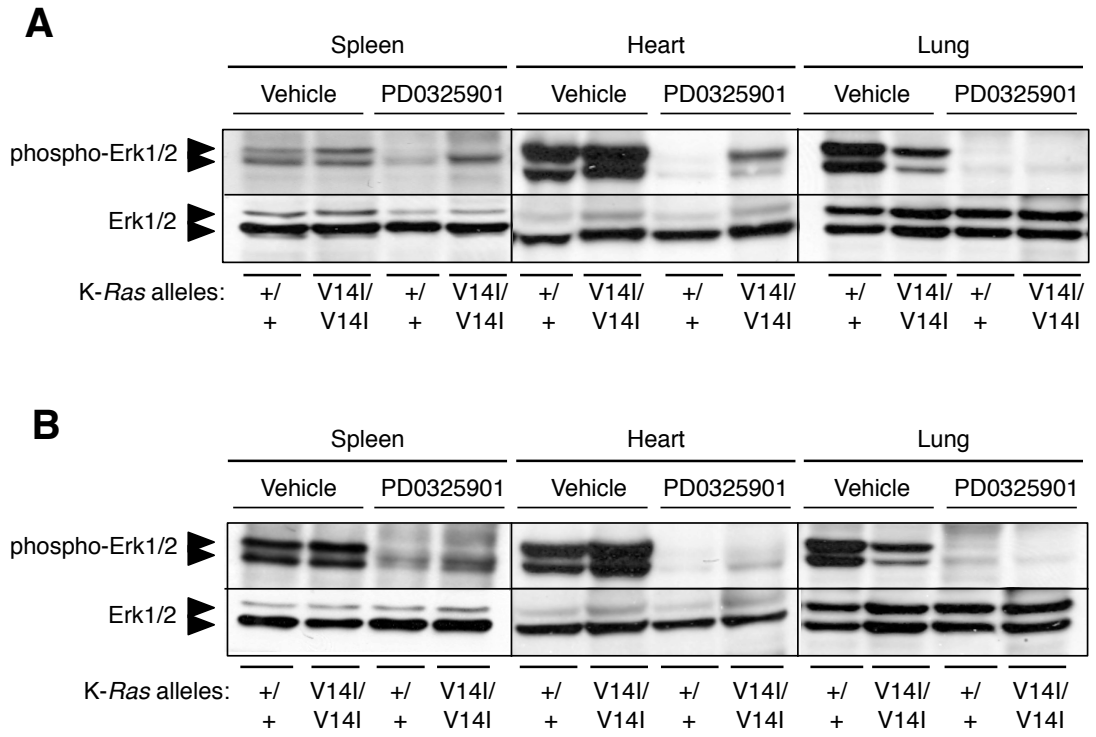

Figure 49. **Exposure of K-Ras^{V14I} mice to MEK inhibitor results in inhibition of Erk1/2 phosphorylation**. Protein extracts (40 µg) obtained from spleen, heart and lung of wild type (+/+) and K-*Ras*$^{V14I/V14I}$ (V14I/V14I) mice exposed to vehicle or PD0325901 **(A)** from E7.5 to P21 or **(B)** for 6 weeks starting at P21 and sacrificed two hours after the last injection were resolved by SDS-PAGE, transferred to nitrocellulose membranes and blotted with antibodies against Erk1/2 and phosphoErk1/2. The migration of the corresponding proteins is indicated by arrowheads.

Treatment with the MEK inhibitor PD0325901 also rescued the growth defects of mutant mice up to weaning (n=30), the time when the treatment was discontinued. However, four weeks later, the weight of the K-*Ras*$^{V14I/V14I}$ mice exposed to the MEK inhibitor was smaller (22.81±2.33 g; n=14) to that of wild type littermates (25.10±2.15 g; n=7) suggesting

that the effect in the body weight of the MEK inhibitor was reversible. However, at this time the body length remained comparable. Thus, in contrast to the body weight, MEK inhibitor completely rescued the reduced length of mutant mice ***(Figure 50B)***. In addition, 4-month-old K-*Ras*$^{V14I/V14I}$ mice (n=9), exposed to the MEK inhibitor displayed normal skulls ***(Table 17 in Appendix I)***. Similar results were obtained when we analyzed the cardiac phenotype. Four-month-old homozygous mice (n=13) displayed normal hearts with normal numbers of cardiomyocytes ***(Figure 51)***. Moreover, MEK inhibitor treatment also rescued the increase of Sca-1^{+}/PDGFRa^{+}/CD31^{-} cardiac stem cells in K-*Ras*$^{+/V14I}$ mice sacrificed from P10-P14 ***(Figure 6 in Appendix I)***. These observations indicate that the deleterious effects caused by abnormal K-*Ras*^{V14I} signaling does not affect bone development or heart homeostasis beyond weaning.

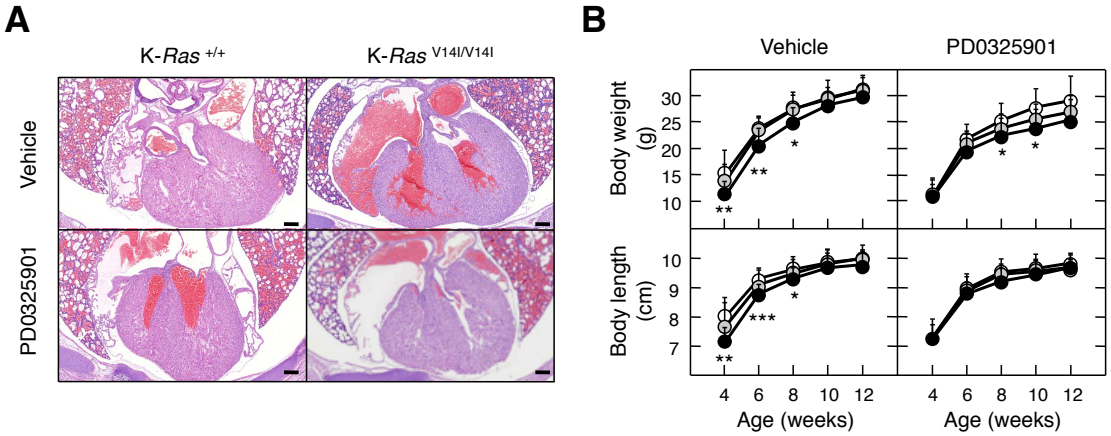

Figure 50. **Prenatal treatment with the MEK inhibitor PD0325901 prevents cardiac alteration at P0 and the development of growth defects**. **(A)** H&E stained paraffin transverse sections of neonatal (P0) wild type (+/+) and K-*Ras*$^{V14I/V14I}$ (V14I/V14I) mice exposed to vehicle or PD0325901 from E7.5. Scale bar, 200 μm. **(B)** Top: body weight of wild type (open bars), K-*Ras*$^{+/V14I}$ (gray bars) and K-*Ras*$^{V14I/V14I}$ (solid bars) male mice exposed from E7.5 to P21 to vehicle (n=8, n=11; n=10, respectively) or PD0325901 inhibitor (n=7, n=16; n=14, respectively) from E7.5 to P21. Bottom: body lenght of wild type (open bars), K-*Ras*$^{+/V14I}$ (gray bars) and K-*Ras*$^{V14I/V14I}$ (solid bars) male mice exposed from E7.5 to P21 to vehicle (n=8, n=11; n=10, respectively) or PD0325901 inhibitor (n=7, n=16; n=14, respectively) from E7.5 to P21. Error bars indicate SD. *P < 0.05; **P < 0.01; ***P < 0.001.

However, K-*Ras*$^{V14I/V14I}$ mice (n=13) treated with the MEK inhibitor had enlarged spleens and an expansion of myeloid cells (Gr1^{+} and CD11b^{+}/Gr1^{+}), similar to those animals treated with vehicle. Likewise, they also had increased numbers of LSK progenitor cells in BM. Similar results were obtained in K-*Ras*$^{+/V14I}$ mice (n=10) treated with the MEK inhibitor ***(Figure 52)***. These results indicate that treatment with the MEK inhibitor PD0325901 did not prevent the development of MPD. In spite of these results, K-*Ras*$^{V14I/V14I}$ mice (n=9) treated with the inhibitor during embryonic and postnatal development (E7.5 to P21) had a survival advantage with a median survival 30% longer than that of littermates treated with vehicle (48 *vs.* 37 weeks) (n=6). Similar results were observed in heterozygous K-*Ras*$^{+/V14I}$ mice (n=12) ***(Figure 53A)***. These observations indicate that MEK inhibitor slows progression but does not prevent

the hematological disorder. In addition, K-*Ras*^{V14I} mice succumbed by the development of MPD in combination with other hematological alterations (lymphomas, histiocytic sarcomas and leukemias). Therefore, these observations also indicate that the MEK inhibitor treatment reduces the progression of these secondary alterations, resulting in longer survival.

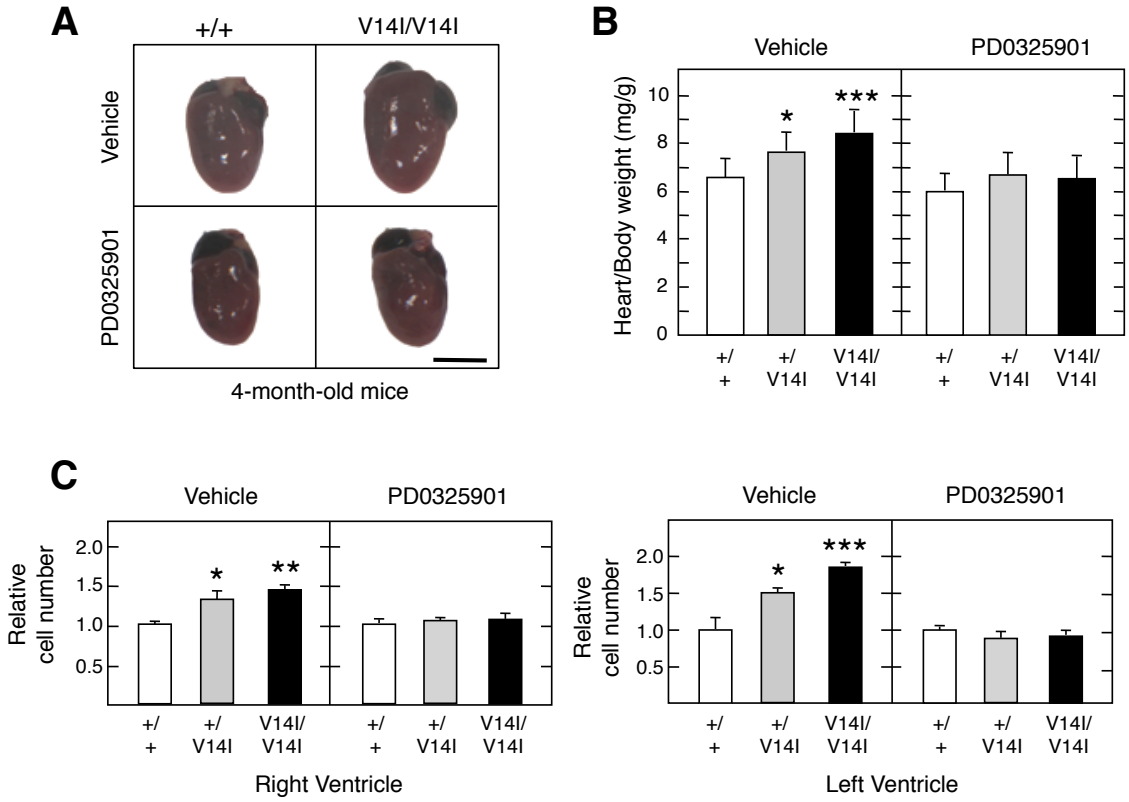

Figure 51. **Prenatal treatment with the MEK inhibitor PD0325901 prevents developmental defect in K-*Ras*^{V14I} mice**. **(A)** Representative hearts appearance of 4-month-old wild type (+/+) and K-*Ras*$^{V14I/V14I}$ (V14I/V14I) male mice exposed to vehicle or PD0325901 from E7.5 to P21. Scale bar, 5 mm. **(B)** Heart/Body weight ratio of 4-month-old wild type (+/+, open bars), K-*Ras*$^{+/V14I}$ (+/V14I, gray bars) and K-*Ras*$^{V14I/V14I}$ (V14I, solid bars) male mice exposed from E7.5 to P21 to vehicle (n=6, n=10; n=9, respectively) or PD0325901 inhibitor (n=5, n=10; n=13, respectively). **(C)** Relative number of cardiomyocytes in the right (left) and left (right) ventricle of 4-month-old wild type (+/+, open bars), K-*Ras*$^{+/V14I}$ (+/V14I, gray bars) and K-*Ras*$^{V14I/V14I}$ (V14I/V14I, solid bars) male mice exposed from E7.5 to P21 to vehicle (n=11, n=13; n=6, respectively) or PD0325901 (n=4, n=8; n=8, respectively). Error bars indicate SD. *P < 0.05; **P< 0.01; ***P < 0.001.

6.12.2 Postnatal MEK inhibitor treatment does not rescue any defects of K-*Ras*^{V14I} mice

Next, we examined the effect of interfering with K-*Ras*^{V14I} signaling in mice at postnatal stages when mice already showed growth defects, craniofacial dysmorphia and cardiac alterations. To this end, mice were treated with the PD0325901 inhibitor or vehicle at P21 for 6 weeks. Under these experimental conditions the MEK inhibitor also inhibited phosphorylation of the Erk1/2 kinases to the same extent as in mice treated during embryonic development ***(Figure 49B)***. However, this treatment did not ameliorate or correct any of the developmental defects characteristic of K-*Ras*^{V14I} mice, including decreased size and body weight (data not

shown), craniofacial dysmorphia ***(Table 18 in Appendix I)*** and cardiac defects ***(Figure 7 in Appendix I)***. Moreover, these treated mice also underwent the same expansion of myeloid cells in spleen and of LSK progenitor cells in the BM ***(Figure 8 in Appendix I)***. However, exposure to MEK inhibitors increased the medial survival of K-*Ras*$^{+/V14I}$ mice from an average of 50 weeks (n=11) to 72 weeks (n=13), a 44% increase. No such effect in survival was observed in homozygous K-*Ras*$^{V14I/V14I}$ mice (n=5) ***(Figure 9 in Appendix I)***.

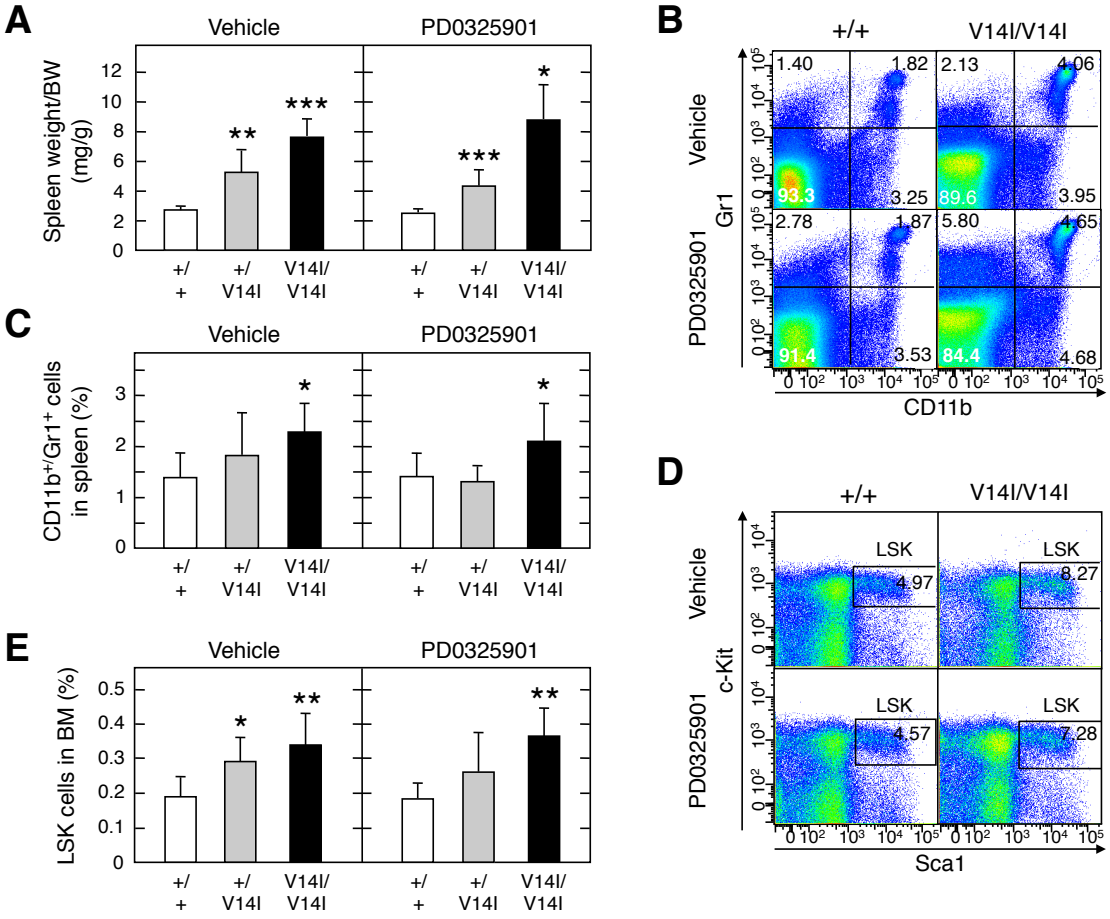

Figure 52. **Prenatal treatment with the MEK inhibitor PD0325901 does not prevent hematological disorders in K-*Ras*^{V14I} mice**. **(A)** Spleen/body weight ratio of 4-month-old wild type (+/+, open bars), K-*Ras*$^{+/V14I}$ (+/V14I, gray bars) and K-*Ras*$^{V14I/V14I}$ (V14I/V14I, solid bars) mice exposed from E7.5 to P21 to vehicle (n=6, n=10; n=9, respectively) or PD0325901 inhibitor (n=5, n=10; n=13, respectively). **(B)** Flow cytometry analysis of Gr1^{+} and CD11b^{+} cells in spleens obtained from 4-month-old mice wild type (+/+) and K-*Ras*$^{V14I/V14I}$ (V14I/V14I) mice exposed to vehicle or to PD0325901 from E7.5 to P21. **(C)** Percentages of Gr1^{+}/CD11b^{+} myeloid cells in spleens of 4-month-old wild type (+/+, open bars), K-*Ras*$^{+/V14I}$ (+/V14I, gray bars) and K-*Ras*$^{V14I/V14I}$ (V14I/V14I, solid bars) mice exposed from E7.5 to P21 to vehicle (n=6, n=8; n=8, respectively) or to PD0325901 inhibitor (n=6, n=10; n=10, respectively). **(D)** Flow cytometry analysis of HSCs of BM of 4-month-old of wild type (+/+) and K-*Ras*$^{V14I/V14I}$ (V14I/V14I) mice exposed from E7.5 to P21 to vehicle or PD0325901 inhibitor using antibodies against c-Kit and Sca-1. The percentage of LSK cells is indicated. **(E)** Percentage of LSK cells in 4 month-old wild type (+/+, open bars), K-*Ras*$^{+/V14I}$ (+/V14I, gray bars) and K-*Ras*$^{V14I/V14I}$ (V14I/V14I, solid bars) mice exposed from E7.5 to P21 to vehicle (n=6, n=8; n=8, respectively) or to PD0325901 inhibitor (n=6, n=10; n=10, respectively). Error bars indicate SD. *P < 0.05; **P < 0.01; ***P < 0.001.

6.12.3 Adult inhibitor treatment does not have any therapeutic effects to treat MPD

Finally, we used the MEK inhibitor to treat 4-month-old K-*Ras*$^{+/V14I}$ (n=11) and K-*Ras*$^{V14I/V14I}$ (n=2) mice already displaying signs of MPD to determine whether MEK inhibitors might be of therapeutic value to treat this disease. MPD was diagnosed by detection of enlarged spleens using CT scans as well as by altered blood counts (leukocytosis and anemia). Unfortunately, this treatment also failed to provide any significant decrease in spleen size as well as in average survival ***(Figure 53B)***. Thus, suggesting that additional pathways, other than the canonical Raf/Mek/Erk signaling cascade, must contribute to the development of MPD.

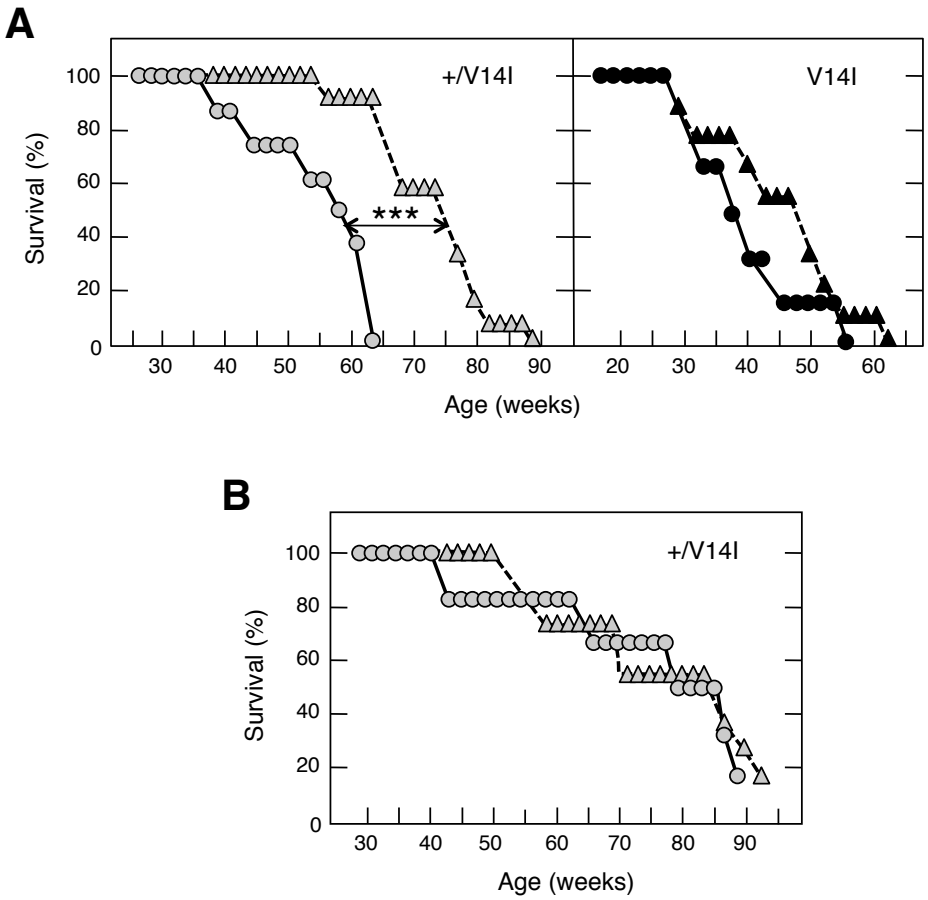

Figure 53. **Exposure of K-*Ras*^{V14I} mice to MEK inhibitor results in increased survival**. **(A)** Left: Survival of K-*Ras*$^{+/V14I}$ (+/V14I) mice exposed from E7.5 to P21 to vehicle (n=8, gray circles, solid line) or PD0325901 (n=12, gray triangles, dotted line). ***P < 0.001. Right: Survival of K-*Ras*$^{V14I/V14I}$ (V14I/V14I) mice exposed from E7.5 to P21 to vehicle (n=6, solid circles, solid line) or PD0325901 (n=9, solid triangles, dotted line). **(B)** Survival of K-*Ras*$^{+/V14I}$ (+/V14I) mice exposed from 4 to 5 months of age to vehicle (n=6, gray circles, solid line) or to PD0325901 (n=11, gray triangles, dotted line).

7. Discussion

Mutations in RAS genes and other members of the RAS signaling pathway have been implicated in a group of developmental disorders called Neuro-Cardio-Facio-Cutaneous (NCFC) syndromes or 'RASopathies'. These rare conditions share different phenotypic features and include, among others, the Noonan syndrome (NS). NS is an autosomal dominant disorder characterized by a broad number of alterations including facial dysmorphia, short stature, congenital heart disease, skeletal abnormalities and learning disabilities *(171)*. Six genes of the RAS-MAPK signaling pathway have been associated with NS including *PTPN11*, *SOS1*, K-*RAS*, N-*RAS*, *RAF1* and B-*RAF* and mutations in other two genes, *SHOC2* and *CBL,* have been discovered in closely related conditions *(165)*. Recently, mutations in *RIT1*, a member of the RAS subfamily, have been also described in Noonan patients *(10)*. The broad spectrum of phenotypic alterations and mutations, together with the low incidence of some of these mutations, make difficult to establish a good phenotype-genotype correlation *(171)*. The generation of genetically engineered mouse models (GEMMs) could help to better understand the role of each mutation in the development of this disorder. Role of *PTPN11*, *SOS1* and *RAF1* mutations in NS have been clarified by others groups by the generation of GEMMs *(14, 39, 237)*. All these mouse models display alterations characteristic of NS patients, although interestingly, each of these mutant mice show specific features, as described in NS patients *(14, 39, 237)*.

To better understand the role of K-*RAS* in NS we have generated a strain of mice carrying the K-*Ras*^{V14I} mutation. This mouse model faithfully reproduced the phenotypic abnormalities observed in NS patients, including smaller size, craniofacial dysmorphia as well as cardiac and hematopoietic defects. These alterations are reminiscent of the alterations described in the other NS mouse models *(13, 14, 39, 237)*.

7.1 K-*Ras*^{V14I} EXPRESSION IS COMPATIBLE WITH EMBRYO AND POSTNATAL DEVELOPMENT

Germline expression of the classical oncogenic K-*Ras* mutations, K-*Ras*^{G12V} or K-*Ras*^{G12D}, is not tolerated during development and embryos die due to placental, cardiovascular and hematopoietic defects *(69, 194, 221)*. Nevertheless, the expression of one copy of the mutated allele K-*Ras*^{V14I} was compatible with embryo and postnatal development, since the heterozygous mice were born at the expected Mendelian ratios and reached adulthood. Biochemical analysis using recombinant V14I proteins *(186, 188)* and our data with E13.5 embryos suggest that the K-Ras^{V14I} mutant protein resulted in an intermediate increase of the active Ras status compared to the wild type and the oncogenic protein. Our results further illustrate that this intermediate activation levels allows embryo development.

Interestingly, increased dosage of the mutant protein affects embryonic development since the number of homozygous mice was significantly lower than expected. Homozygous mice died at perinatal stages due to cardiovascular problems. These mice displayed cardiomegaly already evident at midgestation (E13.5). However, we did not detect any of the alterations found in the K-*Ras*^{G12D} embryos such as septal defects, valve malformation, DORV or excess endocardial cushion *(194)*.

This allele dose effect was also observed in other Noonan mouse models *(13, 14, 39, 237*). Homozygous *Ptpn11*$^{D16G/D61G}$ mice were not viable due to the development of severe cardiac defects, including septal defects, DORV and markedly enlarged outflow tract and atrioventricular valve primordial. And *Ptpn11*$^{+/D61G}$ mice also displayed high embryonic lethality *(14)*. Any of these alterations were found in our K-*Ras*^{V14I} mice. Thus, suggesting that the K-*Ras*^{V14I} mutation used in this study is less aggressive than this *Ptpn11* mutation. Interestingly, these differences can be attributed not only to the mutation but also to the different activation levels, since the expression of a less activated version of the Shp2 protein, the *Ptpn11*^{N308D}, results in complete viability of heterozygous mice and only small percentage of homozygous mice succumb by heart failure, similar to our model *(13)*. Like to the K-*Ras*^{V14I} mice, heterozygous *Sos1*$^{+/E846K}$ mice were viable and only a small percentage of *Sos1*$^{E846K/E846K}$ mice survive. These homozygous mice die at various stages from E10.5 to the neonate stage due to the development of cardiac defects including septal defects and aortic stenosis *(39)*. These alterations were not found in the K-*Ras*^{V14I} mice.

The incomplete penetrance of the perinatal lethality of K-*Ras*^{V14I} mice in a B6/129 mix background suggests the presence of modifiers alleles, in one or the other strain, that modulate the phenotypic consequences of the K-*Ras*^{V14I} expression. This incomplete penetrance disappeared when mutant mice were backcrossed to C57BL/6J background for five generations since homozygous C57BL/6J K-*Ras*^{V14I} mice were no longer viable at this generation. In contrast, no changes in the perinatal lethality were found when mutant mice were backcrossed to 129S2/Sv background. Similar results were obtained when the *Ptpn11*^{D16G} or the *Raf1*^{L613V} mice were backcrossed to C57BL/6J. In this background, after five and three generations respectively, the allele expression was lethal *(13, 237)*. However, in contrast to our results in the 129S2/Sv background, *Ptpn11*$^{+/D16G}$ mice backcrossed to 129S6/SvEv displayed nearly normal viability *(13)*. Thus suggesting than in the K-*Ras*^{V14I} mice there is also a small contribution of the 129S2/Sv background to the perinatal lethality.

7.2 GROWTH DEFECTS AND CRANIOFACIAL ALTERATIONS: TWO IMPORTANT FEATURES IN NCFC SYNDROMES

Similar to Noonan patients and to mouse models that express NS-associated mutations

in *Ptpn11, Sos1* and *Raf1 (13, 14, 39, 237)*, the K-*Ras*^{V14I} mice showed reduce body weight and size similar to Noonan patients. Moreover, the CFC mouse model carrying the B-*Raf*^{V600E} mutation *(223)* and mouse models that express a LEOPARD-associated *Ptpn11* substitution *(136)* or the Costello syndrome H-*Ras*^{G12V} mutation also display reduced body size at least in the first month of life *(40, 189)*. These results suggest a crucial role of the RAS-MAPK pathway in growth during early development.

Interestingly, in our mouse model, the body weight defect was due to a reduction in the fat and leans content. In addition, we found that the growth alterations were affected by genetic backgrounds. This phenotype became ameliorate in heterozygous C57BL/6J and 129S2/Sv mice, while in homozygous 129S2/Sv mice were more dramatic. These results suggest the presence of modifiers alleles in the 129S2/Sv strain that modulate the effect of the K-*Ras*^{V14I} expression in growth during the development.

The K-*Ras*^{V14I} mice also displayed a typical facial appearance reminiscent of NS patients and similar to those described in the *Ptpn11*^{D16G}, *Ptpn11*^{N308D}, *Sos1*^{E846K} and *Raf1*^{L613V} mouse models *(13, 14, 39, 237)*. As growth defects, this phenotype was also more dramatic in homozygous 129S2/Sv mice.

Therefore, two of the most common alterations found in Noonan patients, the craniofacial dysmorphia and the growth defect are common features of the NS mouse models. Interestingly, other frequent alteration, such as skeletal abnormalities, has not has no been described neither in our mouse model nor in the other NS mouse models *(14, 39, 237)*.

7.3 CARDIAC ALTERATIONS: DIFFERENTIAL EFFECTS OF THE SPECIFIC MUTATIONS

The K-*Ras*^{V14I} mice displayed heart hyperplasia due to increased cardiomyocyte proliferation associated with an increased thickening of the aortic valve. Indeed heart function in these mice appeared to be normal or enhanced as illustrated by the MRI studies. This phenotype is affected by the different genetic backgrounds and is significantly different from those observed in NS models carrying mutations in other loci. For instance, about 50% of the lower affected *Ptpn11*$^{+/D61G}$ *(14)* and the *Ptpn11*^{N380D} mice *(13)* display septal defects with no association to cardiac hypertrophy. *Sos1*$^{+/E846K}$ developed left ventricular hypertrophy with incomplete penetrance of aortic stenosis and ventricular fibrosis *(39)*. And *Raf1*$^{+/L613V}$ mice had normal valvuloseptal development but exhibit eccentric cardiac hypertrophy *(237)*. The variability in the cardiac alterations found in the NS mouse models suggests differential effects of each specific RAS-MAPK mutations alone or in combination with the presence of modifiers genes that remain to be indentified. This variability is also reminiscence of the Noonan patient-cardiac alterations. Approximately 20% of Noonan patients display HCM *(152)*. However, the

mutated NS alleles are differentially associated with HCM. For instance, HCM is found in approximately 95% of patients bearing *RAF1* mutations *(157, 168)*. However, K-*RAS* is rarely associated with HCM *(151, 188, 243)* and only 10% of patients with *PTPN11* mutation *(205)* and 20% of those with mutations in *SOS1* develop HCM *(211)*. Therefore, these alleles negatively associated to HCM in patients (K-*RAS* and *PTPN11*) have not been associated with the cardiac hyperthrophy development in mouse models. Neither *Ptpn11*^{D61G} *(14)* nor K-*Ras*^{V14I} mice exhibit this alteration.

This variability of the cardiac alterations can be also extended to the rest of 'Rasopathies'. In the case of HCM, while Noonan patients with K-*RAS* mutations are rarely associated to this alteration *(151, 188, 243)*, H-*RAS* causes HCM in most of the CS patients *(12, 121)*. Thus, the H-*Ras*^{G12V} mice generated in our laboratory, displayed concentric hypertrophy in the left ventricle associated with heart fibrosis *(189)*. In contrast to the *Sos1*^{E846K} *(39)* and *Raf1*^{L613V} NS-mouse models *(243)*, this hypertrophy is secondary to pressure overload caused by the AngII-dependent hypertension displayed by these mice. Interestingly, H-*Ras*^{G12V} mice also display an enlargement of the auricles and the right ventricle due to an increase in the number of cardiomyocytes similar to the K-*Ras*^{V14I} mice. This alteration is a cell autonomous effect induced by expression of H-*Ras*^{G12V} mutation and not a secondary effect of the hypertension *(237)*.

In the past ten years, the existence of cycling ventricular cardiomyocytes in normal and pathological adults mammalian hearts have been documented *(20, 94, 163)*. The existence of cardiac stem cells with proliferative and regenerative capacities in the myocardium of several species, including humans, has also been described *(9)*. Interestingly, we found an increase in the cardiac stem cells and in the cycling cardiomyocytes in our NS mouse model, as well as a promotion of a more undifferentiated state at postnatal stages (P10-P14). These results indicate that K-*Ras* might be an important role in the homeostasis of cardiac stem cells. In fact, *Xenopus* studies suggest that Ptpn11 is required for the maintaining of the cardiac precursor population. In the absence of the Shp2 signaling early cardiac markers are downregulated and cardiac stem cells fail to initiate cardiac differentiation *(110)*. Therefore, these studies together suggest a dependence of the cardiac stem cells to the RAS-MAPK pathway.

In addition, the cardiac hyperplasia found in the K-*Ras*^{V14I} mice is similar to that described in the B-*Raf*$^{+/V600E}$ model, which recapitulates some of the clinical features present in CFC patients developed heart hyperplasia similar to our model *(223)*.

7.3.1 K-*Ras*^{V14I} expression in adult myocardial cells does not induce an alteration of the heart development

The expression of the K-*Ras*^{V14I} mutation in adult myocardial cells did not induce the cardiac hyperplasia described in mice that germline expressed this mutation. No alterations in heart appearance or histology were found when K-*Ras*^{V14I} expression takes place in the adult cardiomyocytes. These results indicate that the expression of the NS-associated mutation cause cardiac alterations only during embryo development. Similar results were obtained when the oncogenic mutation K-*Ras*^{G12D} was expressed in the same cells types *(47)*. While the germline expression of the oncogenic K-*Ras*^{G12D} mutation results in cardiac abnormalities, the expression of the same mutation in adult myocardial cells does not cause cardiomyopathy in mice. In the case of *PTPN11*-NS associated mutation, mice that express the *Ptpn11*^{D61Y} mutation *(13)* and transgenic mice overexpressing the Shp2 Q79R mutant protein in adult myocardial cells do not display cardiac defects *(145)*. However, the overexpression of the Q79R mutation in the same type of cells during gestation led to the development of ventricular noncompaction and ventricular septal defects *(145)*. Therefore, these results indicate that expression of the different RAS-MAPK results in development of cardiac alterations only when they take place during heart organogenesis.

We cannot rule out the role of other type of cells, for instance endothelial cells, in the development of the cardiac hyperplasia of K-*Ras*^{V14I} mice. In fact, the expression of the *Ptpn11*^{D61Y} mutation in endothelial cells during embryonic development induced cardiac abnormalities, while any alterations were induced when the same mutation was expressed in myocardial cells *(13)*.

7.4 ROLE OF K-*Ras*^{V14I} AND K-*Ras*^{G12V} MUTATIONS IN THE DEVELOPMENT OF HEMATOLOGICAL ALTERATIONS

Somatic K-*RAS* and N-*RAS* mutations are found in myeloid malignancies including JMML *(112)*. Approximately 25% of JMML patients present mutation in these alleles. JMML is a myeloproliferative disorder characterized by leukocytosis with tissue infiltration and *in vitro* hypersensitivity of myeloid progenitors to GM-CSF *(112)*. Infants with NS show a spectrum of hematological abnormalities and are predisposed to JMML *(91)*. Interestingly, mice that expressed the oncogenic mutations K-*Ras*^{G12D} *(27, 37)* and N-*Ras*^{G12D} *(120)* in the hematopoietic compartment driven by the *Mx1*-Cre expression develop myeloid malignancies.

K-*Ras*^{V14I} mice developed MPD characterized by leukocytosis, anemia and thrombocytopenia. Mutant mice also displayed splenomegaly associated with an expansion of the myeloid cells and BM progenitors demonstrated hypersensitivity to cytokines. This

phenotype is affected by the different genetic backgrounds and is similar to the JMML developed by Noonan patients. In contrast, while K-*RAS* is found mutated in myeloid malignances, mice in which oncogenic K-*Ras* is activated germline by a *CMV*-Cre transgene did not develop myeloid. The expression of K-*Ras*^{G12V} resulted in frequent embryonic lethality, but a significant number of mice reached adulthood. These mice did not develop myeloid malignancies and succumb by breathing difficulties due to lung tumor development *(69)*. Subsequent studies performed in our laboratory, reveal that the efficiency of the *CMV*-Cre strain used in this experiments was very low allowing the survival of some mice. Therefore, it is not possible to determine the time and the percentage of the activation of this mutation in each cell type. For this reason, it is possible that the K-*Ras* allele was not activated in the susceptible-initiating cells and for this reason no myeloid malignancies were found in this mouse model.

Postnatal expression of the K-*Ras*^{G12V} mutation in mice using the *RERTn* strain also results in lung tumor development. In mice analyzed at 1 year of age, only *bona fide* tumors in lung tissues were detected. No myeloid malignancies were found in these mice *(129)*. However, unpublished data of our laboratory reveals that these mice, similar to our mouse model displayed leukocytosis due to an expansion of the neutrophils, eosinophils and basophils population. Therefore, it is possible that these mice do not live long enough to develop hematological alterations. To compare both substitutions in the same scenario, we used the same approach to induce the somatic expression of the K-*Ras*^{V14I} mutation. In this case, in contrast to the oncogenic mouse model, mice that expressed the K-*Ras*^{V14I} mutation postnatally live longer and only displayed hematopoietic alterations with slower progression than when the mutation were induced germline. Splenomegaly was found with low penetrance in a 67% (4/6) of 16-month-old mice. Therefore, it is possible that the susceptibility of the initiating-cell to the oncogenic K-*Ras* transformation in adult stages in mice is lower.

These results demonstrate that somatic expression of the K-*Ras*^{V14I} induces the development of myeloid malignancies. Therefore, the presence of this somatic substitution in patients with myeloid malignancies could be possible. In fact, high-throughput sequencing screening of patients with myeloid alterations revealed the presence of the K-*Ras*^{V14I} mutation in one patient with acute myeloid leukemia (AML) out of 329 analyzed patients. However, the etiology (germline or somatic) of this mutation is unknown, since the analysis of the presence of the mutation in other cell type was not evaluated *(222)*.

Finally, we expressed the K-*Ras*^{V14I} and the K-*Ras*^{G12V} mutations in the hematopoietic compartment using the inducible *Mx1*-Cre strain to clarify the role of these mutations in the development of hematological alterations. By this approach we were able to induce the development of myeloid malignancies in the case of the K-*Ras*^{G12V} mice and to accelerate the progression of the disease in the case of the K-*Ras*^{V14I} strain, in comparison with the results obtained with the *RERTn* strain. These different results obtained with both Cre lines can be

explain by the different targeted cells by these two strains. The *RERTn* line induces the expression of the mutation in most of the tissues *(69, 129)*. In contrast, the *Mx1*-Cre strain targets mostly the hematopoietic compartment and with low efficiency other tissues like heart, kidney, lung and duodenum *(107)*. An alternatively explanation is that the *Mx1*-Cre line is not a true inducible strain. In 2004, Chan and colleagues published that K-*Ras*$^{+/LSLG12D}$; *Mx1*-Cre$^{+/T}$ mice in absence of interferon administration also developed MPD *(37)*. This result suggests that with the *Mx1*-Cre, we induced the expression of the mutations before postnatal stages when the initiating-cells are more susceptible to tumor transformation. And at this stage, oncogenic K-*Ras* mutations can initiate the development of the myeloproliferative alterations.

7.5 THE HEMATOLOGICAL DISORDER DISPLAYED BY K-*Ras*^{V14I} MICE IS SIMILAR TO THOSE INDUCED IN MICE THAT EXPRESSED MUTATION OF THE RAS-MAPK PATHWAY

K-*Ras*^{V14I} mice developed MPD similar to that observed in *Nf1*$^{+/-}$ mice *(84)* or mice that expressed in the hematopoietic compartment the oncogenic mutations K-*Ras*^{G12D} *(27, 37)*, N-*Ras*^{G12D} *(120)* or *Ptpn11*^{D61Y} *(36)*; as well as mice carrying a null *Nf1* mutation of hematopoietic cells *(114)*. This MPD was also induced by the expression of the K-*Ras*^{V14I} mutation only in hematopoietic cells upon the expression of the *Mx1*-Cre strain. In both cases (germline or hematopoietic lineage expression), the MPD is less aggressive than those induced by the oncogenic K-*Ras*^{G12D} mutation, which induce as early as 3-4 months of age the death of mice *(27, 37)*. This difference in the aggressiveness may reflect the different activaty properties of both mutations. Our results illustrate that the K-Ras^{V14I} protein is less active than the oncogenic protein K-Ras^{G12V}. In fact, mice that express the oncogenic mutation N-*Ras*^{G12D} in the hematopoietic compartment developed an attenuated MPD phenotype compared to the K-*Ras*$^{+/LSLG12D}$; Mx1-Cre mouse model due to lower Ras protein expression and Ras-GTP levels in the Mac1^{+} cells *(120)*. The MPD observed in this strain was also attenuated compared to the K-*Ras*^{V14I} mice. Moreover, the myeloid malignancie developed by our K-*Ras*^{V14I} mouse model is similar to the hematological alterations described in the other NS mouse model, but the disease in these strains, in contrast to our mouse model, is well tolerated *(14, 39, 237)*.

In addition, the MPD displayed by the K-*Ras*^{V14I} mice was reproduced in primary transplanted mice, similarly to the *Ptpn11*^{D61G} mice *(239)* and mice carrying the oncogenic mutation K-*Ras*^{G12D} mutation *(27, 37)* or a null *Nf1* mutation of in hematopoietic cells *(114)*. This result indicates that the pathogenic effect of the K-*Ras*^{V14I} expression initiate at stem cell levels.

7.5.1 Aberrant hematopoiesis induced by K-*Ras*^{V14I} mutation: mutation specific or RAS-MAPK pathway specific?

The expression of the K-*Ras*^{V14I} mutation is associated with an expansion of the LSK cells similar to the mice that expressed the K-*Ras*^{G12D} in the hematopoietic compartment *(225)* and similar to the mice that express the N-*Ras*^{G12D} in hematopoietic cells *(120)*. The N-*Ras*^{G12D} mouse model displays an expansion of the multipotent progenitor population (MPP) (Lin$^-$, Sca-1$^+$, c-Kit$^+$, Flk2$^-$), but normal levels of the HSC-enriched LSKF$^-$ cells (Lin$^-$, Sca-1$^+$, c-Kit$^+$, Flk2$^-$). Both type of cells were gated from the LSK (Lin$^-$, Sca-1$^+$, c-Kit$^+$) cells *(120)*, the population that we analyzed in our mouse model. Therefore, we can assume that the LSK cells are also increased, since one subpopulation (MPP) is increased and the other (LSKF$^-$) is unchanged. Similar expansion of the LSK cells was also observed in the mice *Ptpn11*^{D61G} Noonan mice (239).

In our K-*Ras*^{V14I} mouse model, the expansion of the HSC is associated with an increase of the myeloid progenitors CMP and GMP, similar to the mice that expressed the K-*Ras*^{G12D} *(225)* and N-*Ras*^{G12D} mutation *(120)* in hematopoietic cells. However, while in our mouse model no alterations were found in the MEP progenitors, mice that express the oncogenic K-*Ras* and N-*Ras* mutations displayed an increase in this population *(120, 225)*. These mice express the mutation only in the hematopoietic cells and more efficiently upon interferon administration *(120, 225)*. Since, the K-*Ras*^{V14I} mouse model expresses germline the mutation in all type of cells, analysis of the progenitor population in the K-*Ras*$^{+/LSLV14I}$; *Mx1*-Cre mice could clarify if this difference reflects different properties of the mutations or it is due to an unlike patter of expression of the mutation due to different genetic strategies. Our results also differ from the data obtained with the *Ptpn11*^{D61G} mice, which displays an increase of GMPs and MEPs populations in combination with a decreased of CLP, while no alterations in the CMPs percentages were found *(239)*. These differences suggest a different role of these genes in hematopoietic development.

Finally, in the K-*Ras*^{V14I} mouse model the expansion of the HSC population was due to a decreased programmed cell death rather than to an enhanced cell proliferation. No information about apoptosis of the hematopoietic cell progenitors in the K-*Ras*^{G12D} mice was published. However, while in mice that express the K-*Ras*^{G12D} mutation in hematopoietic cells similar percentages of BrdU positive cells were found in total BM cells, the Mac1$^+$ fraction displayed an increased marked proliferation *(27)*. No information about the proliferation status of the LSK cells was found in this mouse model, although they described that the myeloid CMP, GMP and MEP progenitor displayed a significant increase in BrdU uptake *(120)*. These results suggest that K-*Ras*^{G12D} mice displayed an elevated proliferation rate only in myeloid lineage, no in other BM population. The different approaches used in the K-*Ras*^{G12D} mice and in our mouse model

makes us difficult to compare the unlike data. Analysis of the proliferation status and apoptosis of the LSK, GMP and CMP populations in mouse models that express the K-*Ras*^{V14I} or the K-*Ras*^{G12V} mutations in hematopoietic cells could clarify these results. Interestingly, in mice that express the oncogenic N-*Ras*^{G12D} mutation in hematopoietic cells the percentage of proliferating cells within myeloid progenitor populations (CMP, GMP and MEP) is similar to the control mice, but more cell divisions were found in the LSK fraction. Again, no information about the apoptosis status was published *(225)*. These results differ from the data obtained with the K-*Ras*^{V14I} and the K-*Ras*^{G12D} mouse model *(120)* and are indicative of a different role of the K-*Ras* and N-*Ras* genes in hematopoietic progenitors. Similar to our results, decreased programmed cell death in HSC population was also observed in the *Ptpn11*^{D61G} mice *(239)*. However, in this mouse model this decrease is also associated to an expansion of the cycling HSC. They found an enhanced entry of the quiescent stem cell (G_0 phase) into the cell cycle in the mutant mice *(239)*. Though the approaches used in both analyses are different, it seems that both mutations (K-*Ras*^{V14I} and *Ptpn11*^{D61G}) have different role in HSC homeostasis.

7.6 IS THE K-*RAS*^{V14I} MUTATION A MILD ONCOGENIC SUBSTITUTION?

Our study is the first evidence that the expression of the NS K-*Ras*^{V14I} mutation is associated with an increased risk of tumor development. K-*Ras*$^{+/V14I}$ and K-*Ras*$^{V14I/V14I}$ mice presented reduced life span with a half-life of 62 and 36 weeks, respectively mainly due to the development of hematopoietic alterations including lymphomas and histiocytic sarcomas. These hematological alterations were developed in combination with the MPD. Similar results were found in mice that express the oncogenic N-*Ras*^{G12D} mutation in the hematopoietic compartment. These mice developed an indolent MPD at 6 months of age that in some mice became fatal. The rest of the mice ultimately succumb due to a variety of hematologic cancers, which occur at approximately equal frequencies, including a disorder that was a reminiscent of human myelodysplastic syndrome (MDS), lymphoid expansion or lymphoproliferation and histiocytic sarcoma *(225)*.

Interestedly, K-*Ras*^{V14I} mice also developed adenomas and adenocarcinomas mainly in intestine, liver and lung. These lesions were only found in K-*Ras*$^{+/V14I}$ mice, probably due to their longer survival, but their incidence was very low compared to the K-*Ras*^{G12D} mice. Mouse models that express the oncogenic K-*Ras*^{G12D} or K-*Ras*^{G12V} mutation in adult stages develop lung tumor with complete penetrance *(69, 86, 221)*. A possible explanation for this differences is the unlike patter of expression of both mutations. The K-*Ras*^{V14I} substitution, in contrast to the oncogenic ones is expressed throughout development in all cell types. Therefore, during this time the cells can adapt to the mild activate signaling from the K-Ras^{V14I} protein and assume

this signal as the normal levels. On the other hand, it is possible that the intermediate active levels of the K-Ras^{V14I} protein were not enough to induce the oncogenic transformation.

Here, we demonstrated that, in contrast to the K-*Ras*^{G12D} or K-*Ras*^{G12V} mouse models *(69, 86, 221),* mice that expressed the K-*Ras*^{V14I} mutation at postnatal stages either in all cells or only in lung did not develop lung tumors. Moreover, any other type of solid tumors was not found when the K-*Ras*^{V14I} mutation was expressed in adult stages in all the cells. These results suggest that our NS-associated mutation does not have enough oncogenic potential to elicit lung tumors or any other tumor types in which K-*RAS* is preferentially mutated: pancreatic ductal adenocarcinoma (PDAC) and colorectal cancer. However, as the oncogenic K-*Ras* mutations *(70, 80)*, the K-*Ras*^{V14I} substitution cooperated with chronic pancreatitis to induce low-grade and high-grade intraepithelial neoplasias (PanIN), the preneoplastic lesions, observed during PDAC development. This cooperation was found either when the mutation was expressed germline in all the cells or only in 30% of acinar cells starting at embryonic day E16.5. The percentage of low- and high-grade PanIN lesions was bigger in the germline model, probably due to the bigger amount of acinar cells in which this mutation was expressed. Moreover, in contrast to the mouse models that express the oncogenic mutation *(69, 70, 80)*, no PDAC lesions were found in our K-*Ras*^{V14I} mouse model indicating the lower oncogenic capacity of the K-*Ras*^{V14I} mutation.

We also demonstrated that Nicotine administration induces the development of lung adenocarcinomas and with lower incidence, PDAC lesions in small cohort of K-*Ras*$^{V14I/V14I}$ mice. Unpublished studies performed by Hermann P.C. and colleagues demonstrated that, similar to our results, nicotine enhanced pancreatic tumorigenesis in mice that express the oncogenic K-*Ras*^{G12V} mutation in acinar cells. However, in contrast to our result, nicotine does not increase lung tumor number or size and does not affect overall survival *(128)* in mice that expressed a K-*Ras* oncogenic mutation by spontaneous recombination *(90)*.

Interestingly, K-*Ras*^{V14I} mutation was identified in 12 cases of human colorectal cancer *(5, 61, 76, 87, 159, 201, 214, 226, 238)*. In some patients (3/12) this mutation was detected in *trans* with the typical oncogenic mutation *(5, 76, 226)* and only in one of the cases the mutation was confirmed as a somatic one by the absence of this substitution in non-neoplastic tissues *(226)*. No lesions were found in large intestine of our K-*Ras*^{V14I} mouse model neither when the mutation was expressed germline nor when it was expressed in adult stages. Similar results were obtained in mice that express the oncogenic mutation by spontaneous recombination *(90)* or upon the inducible Cre recombinases: *RERTn (69)* or *Ah*-Cre *(179)*. None of these mouse models develop spontaneous colorectal adenomas and adenocarcinomas. These results are in agreement with the model of human colorectal tumor progression, in which loss of APC function initiates the formation of a benign lesions and followed oncogenic activation of K-*RAS*, loss of *TP53* and 18q locus altogether contribute to malignant disease progression *(57)*.

Therefore, the expression of the K-*Ras*^{V14I} mutation in absence of *Apc*, using conditional knock-out mouse model *(197)* may to clarify the role of this mutation in colorectal cancer progression. In fact, intestinal K-*Ras*^{G12V} expression accelerates intestinal tumorigenesis and confers invasive properties after *Apc* loss *(179)*.

Finally, in human, allelic loss of the wild type K-*Ras* allele is found in most of lung adenocarcinomas and large cells carcinomas samples which K-*Ras* oncogenic mutation *(119)*. Studies in chemically induced models of lung or skin tumorigenesis have demonstrated that the acquisition of activating mutations in the K-*Ras* or H-*Ras* allele is associated with loss the corresponding wild type alleles during tumor progression *(28, 78)*. Furthermore, Zhang and colleages demonstrated that loss of the wild type K-*Ras* allele enhanced mutant lung tumorigenesis *(244)*. Moreover, unpublished data of our laboratory indicates that the conditional elimination of the wild type allele in adult K-*Ras*$^{LSLG12V/lox}$ animals that express one copy of the oncogenic K-*Ras*^{G12V} mutation results in reduction of mice life span due to acceleration of lung and pancreatic tumorigenesis. In our mouse model (K-*Ras*$^{V14I/-}$), germline elimination of the wild type K-*Ras* allele had no effect in the mice survival. Hemizygous mice died due to hematological alterations, but displayed the same survival rate to the heterozygous mice. Therefore, in contrast to the results obtained in the lung context, the elimination of the wild type allele has not important effect in the progression of the hematological disorders. Since K-*Ras*$^{V14I/-}$ mice were born without the wild type copy of K-*Ras*, cells can adapt to this absence and maybe for this reason the loss of wild type allele does not cooperate with the activating mutation to accelerate tumor development or to induce other tumor types Generation a conditional K-*Ras*$^{LSLV14I/lox}$ mouse model that allow us eliminate the wild type copy in adult stages could prove this hypothesis.

7.6.1 The K-*Ras*^{V14I} mutation cooperated with loss of tumor suppressor genes but does not cooperate with activating *Pi3kca* mutation

The K-*Ras*^{V14I} mutation cooperated with loss of tumor suppressor genes including *p16Ink4a/p19Arf* and *Trp53*. Germline expression of K-*Ras*^{V14I} significantly accelerated tumor development in mice lacking the *p16Ink4a/p19Arf* tumor suppressor genes. Although no unpublished tumors were identified in these mice, the pattern of these lesions was different. For instance, the incidence of histiocytic sarcoma in K-*Ras*$^{V14I/V14I}$; *p16Ink4a/p19Arf* $^{-/-}$ mice was bigger than the percentage described in the *p16Ink4a/p19Arf* $^{-/-}$ strain. And, in contrast to the published results, we did not find any mesenchymal tumors, such as fibrosarcomas. Although a small percentage of these differences might be explained by the unlike genetic background of both strains, it seems that the loss *p16Ink4a/p19Arf* tumor suppressors cooperate with K-*Ras*^{V14I} mutation to promote the development of hematological abnormalities, preferentially histiocytic

sarcomas, more than mesenchymal tumors. Cooperation between *p16Ink4a/p19Arf* loss and K-*Ras* mutations were also found in pancreatic tumor mouse models. In these mice, loss of *p16Ink4a/p19Arf* tumor suppressor genes in early pancreatic precursor during embryo development *(4)* or in embryonic acinar cells *(68)* cooperates with K-*Ras* oncogenes to induce invasive and metastatic PDAC.

Gemline expression of K-*Ras*^{V14I} mutation also accelerated tumor development in mice lacking the *Trp53* tumor suppressor gene. K-*Ras*$^{+/V14I}$;*Trp53* $^{-/-}$ mice died significantly faster than *Trp53*$^{-/-}$ mice due to the development of more aggressive tumors. However, we found the same typical lesions described before in the *Trp53* null mice. Cooperation between *Trp53* loss and K-*Ras* mutation was also found in mice that expressed a K-*Ras* oncogenic mutation by spontaneous recombination *(90)*. In these mice, the elimination of *Trp53* significantly reduces their lifespan due to the development of more malignant lung tumors, thymic lymphomas and skin papillomas, the typical lesion associated with the expression of this oncogenic mutation. Moreover, haemangiosarcomas and fibrosarcomas were also described in about 30% of double mutant mice *(90)*. Moreover, cooperation between *Trp53* deficiency and the oncogenic mutations were also found in mice that expressed the K-*Ras*^{G12V} oncogene in embryonic acinar cells *(70)*. In these mice, the elimination of *Trp53* results in a reduction of the mice survival due to faster PDAC development *(70)*. Same results were found in mice that concomitant express the K-*Ras*^{G12D} mutation and the *Trp53*^{R172H} mutation in pancreatic cells, under the *Pdx1*-Cre expression *(81)*. In addition, *Trp53* loss promotes the progression of K-*Ras*^{G12D}-induced lung adenocarcinomas *(85)*.

In contrast, we performed a pilot experiment to address if there is cooperation between K-*Ras*^{V14I} and *Pi3kca*^{H1047R} mutations. Our results demonstrated that the concomitant activation of both mutations in adult stages did not accelerated tumor development. Interestingly, preliminary studies suggest that K-*Ras*$^{+/LSLV14I}$; *RERTn*$^{ert/ert}$; *Pi3kca*$^{+/LmgLH1047R}$ and K-*Ras*$^{+/+}$; *RERTn*$^{ert/ert}$; *Pi3kca*$^{+/LmgLH1047R}$ displayed hematological alterations, suggesting that the hematological disorders induced by expression of mutation of K-*Ras* signal through the Pi3K pathway. However, unpublished data from the Experimental Therapeutic Unit of CNIO indicate that, in contrast to our results, *Pi3kca*^{H1047R} cooperate with K-*Ras*^{G12V} accelerating lung tumor development. This difference might be explained by the unlike activating status of the oncogenic K-*Ras*^{G12V} and the NS-associated K-*Ras*^{V14I} mutations.

7.7 IS THE MEK INHIBITOR PD0325901 A GOOD DRUG TO PREVENT OR AMILORATE NOONAN SYNDROME ALTERATIONS?

Several studies suggest that targeting RAS/MAPK signaling might be a powerful therapeutic strategy to prevent or ameliorate some of the typical alterations found in Noonan

patients. First studies showed that genetic ablation of *Erk*1/2 in mice overexpressing the Shp2 Q79R mutation in myocardial cells during the gestation *(145)* or the elimination of *Erk*1 in mice overexpressing the same mutation in endothelial-derived cells *(105)* prevent the cardiac alteration and the endocardial cushion phenotype, respectively found in these strains. Moreover, prenatal treatment during the pregnancy with the U0126 MEK inhibitor abrogates the craniofacial abnormalities described in mice that express the *Ptpn11*^{D61G} mutation under the Wnt promoter *(146)*. Our results illustrate that exposure of the developing embryo to well tolerated doses of the PD0325901 MEK inhibitor rescued the perinatal lethality of homozygous mice and prevented the appearance of the growth and cardiac defects, as well as the facial dysmorphia. Similar experiments were carried out in the *Sos1*^{E846K} mice *(39)*. In this mouse model, same prenatal treatment with the PD0325901 MEK inhibitor rescued the embryonic lethality, as in the case of the K-*Ras*^{V14I} mice. By contrast, while in our mouse model this treatment completely normalizes the cardiac alterations at P0 and 4 months old, in the *Sos1*^{E846K} mice the same protocol of treatment only reduces the penetrance of heart defects. Some homozygous *Sos1*$^{E846K/E846K}$ treated mice succumbed due to the development of cardiac abnormalities. As we discussed before, the cardiac phenotype of both NS mouse model (*Sos1*^{E846K} and K-*Ras*^{V14I}) are different. While *Sos1*^{E846K} mice developed left ventricular hypertrophy with incomplete penetrance of aortic stenosis and ventricular fibrosis, our mouse model displayed cardiac hyperplasia with an increase in the thickening of the aortic valve. These differences might indicate the contribution of different effectors to the cardiac defects and might explain the different effect of the MEK inhibitor. For instance, in hearts, the *Sos1*^{E846K} mutation increases Rac activity inducing Stat3 activation through autocrine IL-6. This Stat3 activation persists in mice treated with the PD0325901 inhibitor and for this reason some of cardiac defects still exist in mice exposed to the inhibitor. The completely normalization of the heart hyperplasia in our mouse model might suggest the only contribution of the RAS/MAPK pathway to this phenotype. Moreover, in contrast to our results this prenatal treatment improves, although did not correct, size and craniofacial dysmorphia *(39)*. The complete normalization of the heart hyperplasia and facial dysmorphia in our mouse model suggests the only contribution of the RAS/MAPK pathway to this phenotype.

We also described that treatment with the MEK inhibitor of mice that already displayed all the NS typical features did not ameliorate or correct any of the developmental defects characteristic of K-*Ras*^{V14I} mice. Similarly, the same postnatal treatment does not rescue the facial dysmorphia in the *Raf1*^{L613V} mouse model. However, this phenotype was normalized when the treatment started at P0 *(237)*. These observations, taken together, indicate that an early identification of the developmental disorder, ideally by prenatal testing, is needed for the successfully treatment of cranial alteration with MEK inhibitors. In contrast, the same postnatal treatment normalized the cardiac and growth defects in the *Raf1*^{L613V} mouse model.

Although moving mice results to clinical trials is difficult, treatment of the germline phenotypic features of 'RASopathies' with pathway modulation or small-molecule inhibition in under way. The first randomized clinical trial examined the effect of simvastatin treatment on congnitive function in children with NF1. Simvastatin is a 3-hydroxy-3-methylglutamyl (HMG) coenzyme A (CoA) reductase inhibitor that interferes with the cholesterol biosynthesis pathway as well as RAS isoprenylation. Unfortunately, this treatment did not improve cognitive function in NF1 children *(102)*. A second clinical trial was performed with better outcome to evaluate the effect of lovastatin, another HMG-CoA reductase inhibitor, on the neourocognitive disabilities of NF1 patients *(1, 35)*. In addition to these clinical trials, a phase II trial is in progress to assess the safety and efficacy of MEK162 in adult NS HCM patients (NCT01556568 by Novartis).

7.8 EFFECT OF THE MEK INHIBITOR PD0325901 IN THE MDP DEVELOPMENT

About 10% of NS patients exhibit MPD, which are usually transient. Less frequently, these patients develop severe MPD, JMML or other forms of leukemia *(91)*. Moreover, somatic mutations in K-*RAS* and N-*RAS* oncogenes are identified in approximately 25% of patients with JMML *(112)* and mutations in other members of the RAS signaling pathway that also result in a hyperactivation of the pathway, were found in 90% of these patients *(56)*. Therefore, targeting RAS/MAPK signaling might be a good therapeutic strategy for these hematological disorders. The K-*Ras*^{V14I} mice developed MPD similar to JMML, thus it is an excellent tool to test the efficiency of different drugs, for instance the MEK inhibitor PD0325901 in the development of this hematological alteration.

Our results illustrate that MEK inhibitor PD0325901 treatment starting at embryo stages or at weaning had no effects in MPD as assessed in mice sacrificed at 4 months of age. Spleen weight as well as the expansion of the myeloid cells was comparable in mice treated with the MEK inhibitor or vehicle. Indeed, treated mice also underwent the same expansion of LSK cells in BM. However, exposure to MEK inhibitor increased the median survival of K-*Ras*^{V14I} mice in spite of the treatment protocol. In contrast, no benefit in survival was found in mice treated at 4 months of age, when the mice presented MPD. These results indicate that MEK inhibitor treatment slows the progression of the MPD or the secondary hematological alterations also found in this mouse model, but only when mice were treated at early stages of the disease.

Two recent studies demonstrated that MEK inhibitor PD0325901 treatment in mice that express the oncogenic K-*Ras*^{G12D} mutation *(126)* or a null *Nf1* mutation in hematopoietic cells *(38)* results in longer mice survival. In these experiments, similar to our third protocol of treatment, mice that display signs of the hematological alteration were daily treated (5 mg/kg). The different results that we found might be explained by the different via of administration and

duration of the treatment. While our mice were treated for 1 month by intraperitoneal injection, these studies were performed by oral gavage until mice became moribund. The different administration might determine the bio-disponibility of the compound and consequently the efficacy of the treatment. For instance, whereas CI-1040 MEK inhibitor administration was ineffective in *Nf1*$^{lox/lox}$; *Mx1*-Cre mice *(113)*, PD0325902 treatment induced a prolonged survival *(38)* due to the higher stabiliy of the last compound (12 hours vs the 4 hours of the CI-1040 inhibitor). On the other hand, these experiments were performed using mice that express the oncogenic mutation only in a percentage of hematopoietic cells and more efficiently at postnatal stages. Therefore, targeting mutant hematopoietic cells in this scenario might be easier and more effective than in our mice, which express the mutation in all the cells by germline, since the normal hematopoietic cells can replace the BM.

Furthermore, they showed that MEK inhibitor PD0325901 treatment results in a rapid improvement of the aberrant composition of peripheral blood as well as reduction of the spleen weight. However, in both cases the effects of the MEK inhibitor are associated with persistence of the mutant cells due to an incomplete elimination of the HSC *(38, 126)*. This incomplete elimination might explain why we did not see any benefits in the MPD features in mice treated at embryo stages or at 4 weeks age. These mice were analyzed at 4 months of age, several months (4 months in the case of the prenatal protocol and 1 and a half in the case of the postnatal protocol) after the end of the treatment. Since the MEK inhibitor treatment does not eliminate the HSC, this pool of resistance stem cell can repopulate again the BM and induce the development of the disease. Therefore, the small benefit in survival found in these studies may reflect only the slow progression of the disease during the treatment period. Combination with drugs that inhibit other additional pathway, for instance the PI3K pathway, might be required for elimination of the mutant cells and for the success of the treatment. The observation that mice that expressed the *Pi3kca*^{H1047R} mutation alone or in combination with the K-*Ras*^{V14I} mutation developed hematological disorders suggest that this pathway could be important for the initiation and/or the development of this disease. Take into account these results, a combination of PI3K and MEK inhibitor might be the election therapeutic combination for treatment of myeloproliferative disease.

8.Conclusiones/Conclusions

1. La mutación K-*Ras*^{V14I} tiene como resultado una activación intermedia de la proteína en comparación con la mutación oncogénica K-*Ras*^{G12V}, permitiendo que sea compatible con el desarrollo embrionario y postnatal. Sin embargo, la expresión de dos copias afecta al desarrollo embrionario resultando en una reducción significativa del número de ratones homozigotos obtenidos de cruces entre ratones heterocigotos, indicativo de que el efecto de esta mutación es dosis génica dependiente.

2. Los ratones que expresan la mutación K-*Ras*^{V14I} desde línea germinal reproducen fielmente muchas de las alteraciones del desarrollo asociadas al Síndrome Noonan (SN), entre las que se encuentran retraso de crecimiento, dismorfia cráneo-facial, alteraciones cardiacas y el desarrollo de un desorden mieloproliferativo.

3. La expresión de la mutación K-*Ras*^{V14I} desde línea germinal induce hiperplasia del corazón asociada con un engrosamiento de la válvula aórtica. Esta hiperplasia se debe a un incremento en el número de cardiomiocitos en división y a un incremento en el número de células madre cardiacas durante el desarrollo embrionario. Ninguna de esta alteraciones aparecen cuando la mutación se expresan en células del miocardio en estadios adultos. Sin embargo, esta alteraciones no se traducen en una disminución de la función cardiaca, como se puede deducir de los estudios de resonancia magnética.

4. La expresión de la mutación K-*Ras*^{V14I} desde línea germinal tiene como resultado el desarrollo de un desorden mieloproliferativo como consecuencia de una expansión de las células LSK, debido a la disminución en su muerte celular programada, así como una expansión en los progenitores mieloides. Este desorden mieloproliferativo se reproduce en estudios de transplantes primarios de médula ósea, lo que corrobora el origen de esta alteración en las células madre. Este desorden hematológico aparece también en ratones que expresan postnatalmente la mutación en células hematopoyéticas.

5. Los ratones K-*Ras*^{V14I} presentan una predisposición tumoral mayor. La supervivencia de los ratones mutantes se encuentra reducida debido al desarrollo de múltiples neoplasias, distintas al desorden mieloproliferativo, entre las que se encuentran linfomas, sarcomas histiocíticos y carcinomas. Además, esta mutación coopera con genes supresores de tumores como *Trp53* o *p16Ink4a/p19Arf*, acelerando la progresión tumoral.

6. Eventos de tipo no genético que causan daño tisular y/o respuesta inflamatoria también cooperan con el desarrollo de lesiones preneoplásicas y de tumores en los ratones que

expresan la mutación K-*Ras*^{V14I} desde línea germinal. Así, la pancreatitis crónica inducida por tratamiento con ceruleina indujo la aparición de lesiones pancreáticas pre-neoplásicas y la administración de nicotina propició el desarrollo de adenocarcinomas en pulmón y en páncreas.

7. La expresión postnatal de la mutación K-*Ras*^{V14I} en todos los tipos celulares únicamente induce el desarrollo de desórdenes hematológicos, pero no de lesiones típicas inducidas por la expresión de las mutaciones oncogénicas K-*Ras*^{G12V} y K-*Ras*^{G12D}, tales como lesiones pancreáticas o pulmonares. Las lesiones pulmonares tampoco se encontraron cuando la mutación se expresa en estadios postnatales en células pulmonares, indicando que las propiedades oncogénicas de la mutación K-*Ras*^{V14I} no son suficientes para inducir el desarrollo de tumores en pulmón.

8. La expresión embrionaria de la mutación K-*Ras*^{V14I} en células acinares en condiciones de pancreatitis crónica, induce el desarrollo de lesiones pancreáticas pre-neoplásicas, como en el caso de las mutaciones oncogénicas. Sin embargo, a diferencia de los ratones K-*Ras*^{G12V} o K-*Ras*^{G12D}, no se encontraron adenocarcinomas, indicando una menor propiedad oncogénica de la mutación K-*Ras*^{V14I}.

9. El tratamiento prenatal con el inhibidor de MEK PD0325901 rescata la letalidad perinatal, así como previene el desarrollo de los defectos en el crecimiento y las alteraciones cráneo-faciales y cardiacas, alteraciones características de los pacientes con SN descritas en el modelo K-*Ras*^{V14I}. Sin embargo, ninguna de estas alteraciones se previenen o mitigan en los ratones tratados al destete. Estos resultados sugieren que los tratamientos solo serán efectivos si se realizan durante el desarrollo embrionario; para lo que se hace indispensable disponer de diagnóstico prenatal en estos pacientes.

10. El tratamiento con el inhibidor de MEK PD0325901 no tiene ningún efecto en la prevención del desarrollo del desorden mieloproliferativo, independientemente del tiempo de inicio del tratamiento. Únicamente se observa un pequeño beneficio en la supervivencia en ratones tratados antes del desarrollo de la enfermedad (estadio prenatal y al destete) debido un retraso en la progresión de la misma.

1. K-*Ras*^{V14I} mutation induces an intermediate activation state of the protein compared to the K-*Ras*^{G12V} oncogenic substitution, property that allows embryonic and postnatal development. However, the expression of both copies of the mutated allele results in a reduccion of the number of homozygous mice obtained from crosses between heterozygous parentals, indicating that increased dosage of the mutant K-Ras^{V14I} protein affects embryonic development.

2. Mice that germline express the K-*Ras*^{V14I} mutation faithfully reproduced multiple NS-associated developmental defects such as growth delay, craniofacial dysmorphia, cardiac defects and development of MPD.

3. Germline K-*Ras*^{V14I} expression induces heart hyperplasia associated with an increased thickening of the aortic valve. This hyperplastic condition is due to an increase in the number of cycling cardiomyocytes and cardiac stem cells during embryonic development, since the expression of the mutation in adult myocardial cells had no consequences. However, theses alterations does not affect the heart function, as illustrated by MRI studies.

4. Germline K-*Ras*^{V14I} expression results in a MPD due to an expansion of the LSK cells by decreasing the programmed cell death, and an expansion of myeloid progenitor. This MPD was reproduced in primary bone marrow transplantation indicating this stem cell origin. Same hematological alteration is also induced by the expression of the K-*Ras*^{V14I} mutation only in hematopoietic cells at postnatal stages.

5. K-*Ras*^{V14I} mice display an increased predisposition to tumor development. Mutant mice present a reduced life span due to the development of multiple malignancies, different to MPD, mostly lymphomas, histiocytic sarcomas and carcinomas. Moreover, K-*Ras*^{V14I} mice efficiently cooperate with tumor suppressors genes such as *Trp53* and *p16Ink4a/p19Arf* accelerating the tumor development.

6. Non-genetic events involving tissue damage and/or an inflammatory response also cooperate with the development of neoplastic lesions and tumors in mice that express germline the K-*Ras*^{V14I} mutations. Thus, chronic pancreatitis, driven by caerulein treatment induces PanIN lesions and nicotine administration promotes the development of pancreatic and lung adenocarcinomas.

7. Postnatal expression of the K-*Ras*^{V14I} mutation in all type of cells induces the development of a hematological disorder, but not the typical lesions induced by the expression of the oncogenic K-*Ras*^{G12V} and K-*Ras*^{G12D} mutation, such as pancreatic and lung tumors. These lung lesions were not either found when the K-*Ras*^{V14I} mutation is expressed at postnatal stages in lung, indicating that this mutation does not have enough oncogenic properties to elicit lung tumors.

8. The expression of the K-*Ras*^{V14I} mutation in acinar cells at embryonic stages under chronic pancreatitis conditions induces the development of PanIN lesions, similar to the oncogenic mutations. However, in contrast to the K-*Ras*^{G12V} and K-*Ras*^{G12D} mice, no PDAC lesions were found indicating that the oncogenic properties of the K-*Ras*^{V14I} mutation are smaller than the oncogenic ones.

9. Treatment of pregnant mothers with the MEK inhibitor PD0325901 rescues the perinatal lethality and prevents the development of growth defects, craniofacial alterations and cardiac defects, the typical NS-associated features described in the K-*Ras*^{V14I}. However, any of these alterations were prevented or ameliorated when the treatment starts at weaning indicating that prenatal testing, that allow the initiation of the treatment at early stages, is needed for the success of this treatment.

10. MEK inhibitor PD0325901 has no effect in preventing MPD development independently of the time of the initiation of the treatment. Only a small benefit in the survival was found in mice treated before the development of the disease or at early stages (prenatal stages or at weaning, respectively) due to a delay in the progression of the disease.

9. Bibliography

1. Acosta, M. T., Kardel P. G., Walsh K. S., Rosenbaum K. N., Gioia G. A., and Packer R. J. 2011. Lovastatin as treatment for neurocognitive deficits in neurofibromatosis type 1: phase I study. *Pediatr Neurol* 45:241-5.

2. Agah, R., Frenkel P. A., French B. A., Michael L. H., Overbeek P. A., and Schneider M. D. 1997. Gene recombination in postmitotic cells. Targeted expression of Cre recombinase provokes cardiac-restricted, site-specific rearrangement in adult ventricular muscle in vivo. *J Clin Invest* 100:169-79.

3. Aggarwal, B. B. 2004. Nuclear factor-kappaB: the enemy within. *Cancer Cell* 6:203-8.

4. Aguirre, A. J., Bardeesy N., Sinha M., Lopez L., Tuveson D. A., Horner J., Redston M. S., and DePinho R. A. 2003. Activated Kras and Ink4a/Arf deficiency cooperate to produce metastatic pancreatic ductal adenocarcinoma. *Genes Dev* 17:3112-26.

5. Ahlquist, T., Bottillo I., Danielsen S. A., Meling G. I., Rognum T. O., Lind G. E., Dallapiccola B., and Lothe R. A. 2008. RAS signaling in colorectal carcinomas through alteration of RAS, RAF, NF1, and/or RASSF1A. *Neoplasia* 10:680-6,

6. Allanson, J. E. 1987. Noonan syndrome. *J Med Genet* 24:9-13.

7. Allanson, J. E. 2007. Noonan syndrome. *Am J Med Genet C Semin Med Gene*t 145C:274-9.

8. Allanson, J. E., Hall J. G., Hughes H. E., Preus M., and Witt R. D. 1985. Noonan syndrome: the changing phenotype. *Am J Med Genet* 21:507-14.

9. Anversa, P., and Nadal-Ginard B. 2002. Myocyte renewal and ventricular remodelling. *Nature* 415:240-3.

10. Aoki, Y., and Matsubara Y. 2013. Ras/MAPK syndromes and childhood hemato-oncological diseases. *Int J Hematol* 97:30-6.

11. Aoki, Y., Niihori T., Banjo T., Okamoto N., Mizuno S., Kurosawa K., Ogata T., Takada F., Yano M., Ando T., Hoshika T., Barnett C., Ohashi H., Kawame H., Hasegawa T., Okutani T., Nagashima T., Hasegawa S., Funayama R., Nakayama K., Inoue S., Watanabe Y., Ogura T., and Matsubara Y. 2013. Gain-of-function mutations in RIT1

cause Noonan syndrome, a RAS/MAPK pathway syndrome. *Am J Hum Genet* 93:173-80.

12. Aoki, Y., Niihori T., Kawame H., Kurosawa K., Ohashi H., Tanaka Y., Filocamo M., Kato K., Suzuki Y., Kure S., and Matsubara Y. 2005. Germline mutations in HRAS proto-oncogene cause Costello syndrome. *Nat Genet* 37:1038-40.

13. Araki, T., Chan G., Newbigging S., Morikawa L., Bronson R. T., and Neel B. G. 2009. Noonan syndrome cardiac defects are caused by PTPN11 acting in endocardium to enhance endocardial-mesenchymal transformation. *Proc Natl Acad Sci U S A* 106:4736-41.

14. Araki, T., Mohi M. G., Ismat F. A., Bronson R. T., Williams I. R., Kutok J. L., Yang W., Pao L. I., Gilliland D. G., Epstein J. A., and Neel B. G. 2004. Mouse model of Noonan syndrome reveals cell type- and gene dosage-dependent effects of Ptpn11 mutation. *Nat Med* 10:849-57.

15. Armstrong, J. F., Kaufman M. H., Harrison D. J., and Clarke A. R. 1995. High-frequency developmental abnormalities in p53-deficient mice. *Curr Biol* 5:931-6.

16. Bader, A. G., Kang S., Zhao L., and Vogt P. K. 2005. Oncogenic PI3K deregulates transcription and translation. *Nat Rev Cancer* 5:921-9.

17. Barbacid, M. 1987. ras genes. *Annu Rev Biochem* 56:779-827.

18. Bauler, T. J., Kamiya N., Lapinski P. E., Langewisch E., Mishina Y., Wilkinson J. E., Feng G. S., and King P. D. 2011. Development of severe skeletal defects in induced SHP-2-deficient adult mice: a model of skeletal malformation in humans with SHP-2 mutations. *Dis Model Mech* 4:228-39.

19. Bellacosa, A., de Feo D., Godwin A. K., Bell D. W., Cheng J. Q., Altomare D. A., Wan M., Dubeau L., Scambia G., Masciullo V., Ferrandina G., Benedetti Panici P., Mancuso S., Neri G., and Testa J. R. 1995. Molecular alterations of the AKT2 oncogene in ovarian and breast carcinomas. *Int J Cancer* 64:280-5.

20. Beltrami, A. P., Urbanek K., Kajstura J., Yan S. M., Finato N., Bussani R., Nadal-Ginard B., Silvestri F., Leri A., Beltrami C. A., and Anversa P. 2001. Evidence that human cardiac myocytes divide after myocardial infarction. *N Engl J Med* 344:1750-7.

21. Blasco, R. B., Francoz S., Santamaria D., Canamero M., Dubus P., Charron J., Baccarini M., and Barbacid M. 2011. c-Raf, but not B-Raf, is essential for development of K-Ras oncogene-driven non-small cell lung carcinoma. *Cancer Cell* 19:652-63.

22. Boettner, B., and Van Aelst L. 2002. The RASputin effect. *Genes Dev* 16:2033-8.

23. Bollag, G., Clapp D. W., Shih S., Adler F., Zhang Y. Y., Thompson P., Lange B. J., Freedman M. H., McCormick F., Jacks T., and Shannon K. 1996. Loss of NF1 results in activation of the Ras signaling pathway and leads to aberrant growth in haematopoietic cells. *Nat Genet* 12:144-8.

24. Bos, J. L. 1989. ras oncogenes in human cancer: a review. *Cancer Res* 49:4682-9.

25. Brannan, C. I., Perkins A. S., Vogel K. S., Ratner N., Nordlund M. L., Reid S. W., Buchberg A. M, Jenkins N. A., Parada L. F., and Copeland N. G.. 1994. Targeted disruption of the neurofibromatosis type-1 gene leads to developmental abnormalities in heart and various neural crest-derived tissues. *Genes Dev* 8:1019-29.

26. Brasil, A. S., Malaquias A. C., Kim C. A., Krieger J. E., Jorge A. A., Pereira A. C., and Bertola D. R.. 2012. KRAS gene mutations in Noonan syndrome familial cases cluster in the vicinity of the switch II region of the G-domain: report of another family with metopic craniosynostosis. *Am J Med Genet* A 158A:1178-84.

27. Braun, B. S., Tuveson D. A., Kong N., Le D. T., Kogan S. C., Rozmus J., Le Beau M. M., Jacks T. E., and Shannon K. M. 2004. Somatic activation of oncogenic Kras in hematopoietic cells initiates a rapidly fatal myeloproliferative disorder. *Proc Natl Acad Sci U S A* 101:597-602.

28. Bremner, R., and Balmain A.. *1990.* Genetic changes in skin tumor progression: correlation between presence of a mutant ras gene and loss of heterozygosity on mouse chromosome 7. Cell 61:407-17.

29. Brems, H., Chmara M., Sahbatou M., Denayer E., Taniguchi K., Kato R., Somers R., Messiaen L., De Schepper S., Fryns J. P., Cools J., Marynen P., Thomas G., Yoshimura A., and Legius E. 2007. Germline loss-of-function mutations in SPRED1 cause a neurofibromatosis 1-like phenotype. *Nat Genet* 39:1120-6.

30. Brocard, J., Warot X., Wendling O., Messaddeq N., Vonesch J. L., Chambon P., and Metzger D. 1997. Spatio-temporally controlled site-specific somatic mutagenesis in the mouse. *Proc Natl Acad Sci U S A* 94:14559-63.

31. Buhrman, G., Holzapfel G., Fetics S., and Mattos C. Allosteric modulation of Ras positions Q61 for a direct role in catalysis. *Proc Natl Acad Sci U S A* 107:4931-6.

32. Cai, W., Rudolph J. L., Sengoku T., and Andres D. A.. 2012. Rit GTPase regulates a p38 MAPK-dependent neuronal survival pathway. *Neurosci Lett* 531:125-30.

33. Carta, C., Pantaleoni F., Bocchinfuso G., Stella L., Vasta I., Sarkozy A., Digilio C., Palleschi A., Pizzuti A., Grammatico P., Zampino G., Dallapiccola B., Gelb B. D., and Tartaglia M. 2006. Germline missense mutations affecting KRAS Isoform B are associated with a severe Noonan syndrome phenotype. *Am J Hum Genet* 79:129-35.

34. Cawthon, R. M., O'Connell P., Buchberg A. M., Viskochil D., Weiss R. B., Culver M., Stevens J., Jenkins N. A., Copeland N. G., and White R. 1990. Identification and characterization of transcripts from the neurofibromatosis 1 region: the sequence and genomic structure of EVI2 and mapping of other transcripts. *Genomics* 7:555-65.

35. Chabernaud, C., Mennes M., Kardel P. G., Gaillard W. D., Kalbfleisch M. L., Vanmeter J. W., Packer R. J., Milham M. P., Castellanos F. X., and Acosta M. T. 2012. Lovastatin regulates brain spontaneous low-frequency brain activity in neurofibromatosis type 1. Neurosci Lett 515:28-33.

36. Chan, G., Kalaitzidis D., Usenko T., Kutok J. L., Yang W., Mohi M. G., and Neel B. G. 2009. Leukemogenic Ptpn11 causes fatal myeloproliferative disorder via cell-autonomous effects on multiple stages of hematopoiesis. *Blood* 113:4414-24.

37. Chan, I. T., Kutok J. L., Williams I. R., Cohen S., Kelly L., Shigematsu H., Johnson L., Akashi K., Tuveson D. A., Jacks T., and Gilliland D. G. 2004. Conditional expression

of oncogenic K-ras from its endogenous promoter induces a myeloproliferative disease. *J Clin Invest* 113:528-38.

38. Chang, T., Krisman K., Theobald E. H., Xu J., Akutagawa J., Lauchle J. O., Kogan S., Braun B. S., and Shannon K. 2013. Sustained MEK inhibition abrogates myeloproliferative disease in Nf1 mutant mice. *J Clin Invest* 123:335-9.

39. Chen, P. C., Wakimoto H., Conner D., Araki T., Yuan T., Roberts A., Seidman C., Bronson R., Neel B., Seidman J. G., and Kucherlapati R. 2010. Activation of multiple signaling pathways causes developmental defects in mice with a Noonan syndrome-associated Sos1 mutation. *J Clin Invest* 120:4353-65.

40. Chen, X., Mitsutake N., LaPerle K., Akeno N., Zanzonico P., Longo V. A., Mitsutake S., Kimura E. T., Geiger H., Santos E., Wendel H. G., Franco A., Knauf J. A., and Fagin J. A. 2009. Endogenous expression of Hras(G12V) induces developmental defects and neoplasms with copy number imbalances of the oncogene. *Proc Natl Acad Sci U S A* 106:7979-84.

41. Cirstea, I. C., Kutsche K., Dvorsky R., Gremer L., Carta C., Horn D., Roberts A. E., Lepri F., Merbitz-Zahradnik T., Konig R., Kratz C. P., Pantaleoni F., Dentici M. L., Joshi V. A., Kucherlapati R. S., Mazzanti L., Mundlos S., Patton M. A., Silengo M. C., Rossi C., Zampino G., Digilio C., Stuppia L., Seemanova E., Pennacchio L. A., Gelb B. D., Dallapiccola B., Wittinghofer A., Ahmadian M. R., Tartaglia M., and Zenker M. 2009. A restricted spectrum of NRAS mutations causes Noonan syndrome. *Nat Genet* 42:27-9.

42. Clark, C. E., Beatty G. L., and Vonderheide R. H. 2009. Immunosurveillance of pancreatic adenocarcinoma: insights from genetically engineered mouse models of cancer. *Cancer Lett* 279:1-7.

43. Cohen, M. M. Jr., and Gorlin R. J. 1991. Noonan-like/multiple giant cell lesion syndrome. *Am J Med Genet* 40:159-66.

44. Colicelli, J. 2004. Human RAS superfamily proteins and related GTPases. *Sci STKE* 2004:RE13.

45. Cordeddu, V., Di Schiavi E., Pennacchio L. A., Maayan A., Sarkozy A., Fodale V., Cecchetti S., Cardinale A., Martin J., Schackwitz W., Lipzen A., Zampino G., Mazzanti L., Digilio M. C., Martinelli S., Flex E., Lepri F., Bartholdi D., Kutsche K., Ferrero G. B., Anichini C., Selicorni A., Rossi C., Tenconi R., Zenker M., Merlo D., Dallapiccola B., Iyengar R., Bazzicalupo P., Gelb B. D., and Tartaglia M. 2009. Mutation of SHOC2 promotes aberrant protein N-myristoylation and causes Noonan-like syndrome with loose anagen hair. *Nat Genet* 41:1022-6.

46. Croonen, E. A., Nillesen W., Schrander C., Jongmans M., Scheffer H., Noordam C., Draaisma J. M., van der Burgt I., and Yntema H. G. 2013. Noonan syndrome: comparing mutation-positive with mutation-negative dutch patients. *Mol Syndromol* 4:227-34.

47. Dalin, M. G., Zou Z., Scharin-Tang M., Safari R., Karlsson C., and Bergo M. O. 2014. Myocardial KRAS(G12D) expression does not cause cardiomyopathy in mice. *Cardiovasc Res* 101:229-35.

48. Dasgupta, P., Rizwani W., Pillai S., Kinkade R., Kovacs M., Rastogi S., Banerjee S., Carless M., Kim E., Coppola D., Haura E., and Chellappan S. 2009. Nicotine induces cell proliferation, invasion and epithelial-mesenchymal transition in a variety of human cancer cell lines. *Int J Cancer* 124:36-45.

49. Davis, R., Rizwani W., Banerjee S., Kovacs M., Haura E., Coppola D., and Chellappan S. 2009. Nicotine promotes tumor growth and metastasis in mouse models of lung cancer. *PLoS One* 4:e7524.

50. De Ruiter, N. D., Burgering B. M., and Bos J. L. 2001. Regulation of the Forkhead transcription factor AFX by Ral-dependent phosphorylation of threonines 447 and 451. *Mol Cell Biol* 21:8225-35.

51. Digilio, M. C., Conti E., Sarkozy A., Mingarelli R., Dottorini T., Marino B., Pizzuti A., and Dallapiccola B. 2002. Grouping of multiple-lentigines/LEOPARD and Noonan syndromes on the PTPN11 gene. *Am J Hum Genet* 71:389-94.

52. Donehower, L. A., Harvey M., Slagle B. L., McArthur M. J., Montgomery C. A., Butel Jr. J. S., and Bradley A. 1992. Mice deficient for p53 are developmentally normal but susceptible to spontaneous tumours. *Nature* 356:215-21.

53. Downward, J. 2003. Targeting RAS signalling pathways in cancer therapy. *Nat Rev Cancer* 3:11-22.

54. Edouard, T., Montagner A., Dance M., Conte F., Yart A., Parfait B., Tauber M., Salles J. P., and Raynal P. 2007. How do Shp2 mutations that oppositely influence its biochemical activity result in syndromes with overlapping symptoms? *Cell Mol Life Sci* 64:1585-90.

55. Ehrhardt, A., Ehrhardt G. R., Guo X., and Schrader J. W. 2002. Ras and relatives--job sharing and networking keep an old family together. *Exp Hematol* 30:1089-106.

56. Emanuel, P. D. 2008. Juvenile myelomonocytic leukemia and chronic myelomonocytic leukemia. *Leukemia* 22:1335-42.

57. Fearon, E. R., and Vogelstein B. 1990. A genetic model for colorectal tumorigenesis. *Cell* 61:759-67.

58. Feig, L. A. 2003. Ral-GTPases: approaching their 15 minutes of fame. *Trends Cell Biol* 13:419-25.

59. Feig, L. A., Urano T., and Cantor S. 1996. Evidence for a Ras/Ral signaling cascade. *Trends Biochem Sci* 21:438-41.

60. Fernandez-Medarde, A., and Santos E. Ras in cancer and developmental diseases. *Genes Cancer* 2:344-58.

61. Ferraz, J. M., Zinzindohoue F., Lecomte T., Cugnenc P. H., Loriot M. A., Beaune P., Stucker I., Berger A., and Laurent-Puig P. 2004. Impact of GSTT1, GSTM1, GSTP1 and NAT2 genotypes on KRAS2 and TP53 gene mutations in colorectal cancer. *Int J Cancer* 110:183-7.

62. Gelb, B. D., and Tartaglia M. 2006. Noonan syndrome and related disorders: dysregulated RAS-mitogen activated protein kinase signal transduction. *Hum Mol Genet* 15 Spec No 2:R220-6.

63. Gonzalez-Garcia, A., Pritchard C. A., Paterson H. F., Mavria G., Stamp G., and Marshall C. J. 2005. RalGDS is required for tumor formation in a model of skin carcinogenesis. *Cancer Cell* 7:219-26.

64. Gorlin, R. J., Anderson R. C., and Blaw M. 1969. Multiple lentigenes syndrome. *Am J Dis Child* 117:652-62.

65. Gremer, L., Merbitz-Zahradnik T., Dvorsky R., Cirstea I. C., Kratz C. P., Zenker M., Wittinghofer A., and Ahmadian M. R. 2010. Germline KRAS mutations cause aberrant biochemical and physical properties leading to developmental disorders. *Hum Mutat* 32:33-43.

66. Gripp, K. W. 2005. Tumor predisposition in Costello syndrome. *Am J Med Genet C Semin Med Genet* 137C:72-7.

67. Gripp, K. W., and Lin A. E. 2012. Costello syndrome: a Ras/mitogen activated protein kinase pathway syndrome (rasopathy) resulting from HRAS germline mutations. *Genet Med* 14:285-92.

68. Guerra, C., Collado M., Navas C., Schuhmacher A. J., Hernandez-Porras I., Canamero M., Rodriguez-Justo M., Serrano M., and Barbacid M. 2011. Pancreatitis-induced inflammation contributes to pancreatic cancer by inhibiting oncogene-induced senescence. *Cancer Cell* 19:728-39.

69. Guerra, C., Mijimolle N., Dhawahir A., Dubus P., Barradas M., Serrano M., Campuzano V., and Barbacid M. 2003. Tumor induction by an endogenous K-ras oncogene is highly dependent on cellular context. *Cancer Cell* 4:111-20.

70. Guerra, C., Schuhmacher A. J., Canamero M., Grippo P. J., Verdaguer L., Perez-Gallego L., Dubus P., Sandgren E. P., and Barbacid M. 2007. Chronic pancreatitis is essential for induction of pancreatic ductal adenocarcinoma by K-Ras oncogenes in adult mice. *Cancer Cell* 11:291-302.

71. Hamad, N. M., Elconin J. H., Karnoub A. E., Bai W., Rich J. N., Abraham R. T., Der C. J., and Counter C. M. 2002. Distinct requirements for Ras oncogenesis in human versus mouse cells. *Genes Dev* 16:2045-57.

72. Hancock, J. F. 2003. Ras proteins: different signals from different locations. *Nat Rev Mol Cell Biol* 4:373-84.

73. Hancock, J. F., Magee A. I., Childs J. E., and Marshall C. J. 1989. All ras proteins are polyisoprenylated but only some are palmitoylated. *Cell* 57:1167-77.

74. Hanna, N., Montagner A., Lee W. H., Miteva M., Vidal M., Vidaud M., Parfait B., and Raynal P. 2006. Reduced phosphatase activity of SHP-2 in LEOPARD syndrome: consequences for PI3K binding on Gab1. *FEBS Lett* 580:2477-82.

75. Hasle, H. 2009. Malignant diseases in Noonan syndrome and related disorders. *Horm Res* 72 Suppl 2:8-14.

76. He, Y., Van't Veer L. J., Mikolajewska-Hanclich I., van Velthuysen M. L., Zeestraten E. C., Nagtegaal I. D., van de Velde C. J., and Marijnen C. A. 2009. PIK3CA mutations predict local recurrences in rectal cancer patients. *Clin Cancer Res* 15:6956-62.

77. Heeschen, C., Jang J. J., Weis M., Pathak A., Kaji S., Hu R. S., Tsao P. S., Johnson F. L., and Cooke J. P. 2001. Nicotine stimulates angiogenesis and promotes tumor growth and atherosclerosis. *Nat Med* 7:833-9.

78. Hegi, M. E., Devereux T. R., Dietrich W. F., Cochran C. J., Lander E. S., Foley J. F., Maronpot R. R., Anderson M. W., and Wiseman R. W. 1994. Allelotype analysis of mouse lung carcinomas reveals frequent allelic losses on chromosome 4 and an association between allelic imbalances on chromosome 6 and K-ras activation. *Cancer Res* 54:6257-64.

79. Hennessy, B. T., Smith D. L., Ram P. T., Lu Y., and Mills G. B. 2005. Exploiting the PI3K/AKT pathway for cancer drug discovery. *Nat Rev Drug Discov* 4:988-1004.

80. Hingorani, S. R., Petricoin E. F., Maitra A., Rajapakse V., King C., Jacobetz M. A., Ross S., Conrads T. P., Veenstra T. D., Hitt B. A., Kawaguchi Y., Johann D., Liotta L. A., Crawford H. C., Putt M. E., Jacks T., Wright C. V., Hruban R. H., Lowy A. M., and Tuveson D. A. 2003. Preinvasive and invasive ductal pancreatic cancer and its early detection in the mouse. *Cancer Cell* 4:437-50.

81. Hingorani, S. R., Wang L., Multani A. S., Combs C., Deramaudt T. B., Hruban R. H., Rustgi A. K., Chang S., and Tuveson D. A. 2005. Trp53R172H and KrasG12D cooperate to promote chromosomal instability and widely metastatic pancreatic ductal adenocarcinoma in mice. *Cancer Cell* 7:469-83.

82. Hogan B., Costantini F., and Lacy E. 1994. Manipulating the Mouse Embryo: A Laboratory Manual. *Second edition (Cold Spring Harbor, NY: Cold Spring Harbor Laboratory Press).*

83. Hynds, D. L., Spencer M. L., Andres D. A., and Snow D. M. 2003. Rit promotes MEK-independent neurite branching in human neuroblastoma cells. *J Cell Sci* 116:1925-35.

84. Jacks, T., Shih T. S., Schmitt E. M., Bronson R. T., Bernards A., and Weinberg R. A. 1994. Tumour predisposition in mice heterozygous for a targeted mutation in Nf1. *Nat Genet* 7:353-61.

85. Jackson, E. L., Olive K. P., Tuveson D. A., Bronson R., Crowley D., Brown M., and Jacks T. 2005. The differential effects of mutant p53 alleles on advanced murine lung cancer. *Cancer Res* 65:10280-8.

86. Jackson, E. L., Willis N., Mercer K., Bronson R. T., Crowley D., Montoya R., Jacks T., and Tuveson D. A. 2001. Analysis of lung tumor initiation and progression using conditional expression of oncogenic K-ras. *Genes Dev* 15:3243-8.

87. Jeon, C. H., Lee H. I., Shin I. H., and Park J. W. 2008. Genetic alterations of APC, K-ras, p53, MSI, and MAGE in Korean colorectal cancer patients. *Int J Colorectal Dis* 23:29-35.

88. Jiang, H., Luo J. Q., Urano T., Frankel P., Lu Z., Foster D. A., and Feig L. A. 1995. Involvement of Ral GTPase in v-Src-induced phospholipase D activation. *Nature* 378:409-12.

89. Johnson, L., Greenbaum D., Cichowski K., Mercer K., Murphy E., Schmitt E., Bronson R. T., Umanoff H., Edelmann W., Kucherlapati R., and Jacks T. 1997. K-ras is an essential gene in the mouse with partial functional overlap with N-ras. *Genes Dev* 11:2468-81.

90. Johnson, L., Mercer K., Greenbaum D.,. Bronson R. T, Crowley D., Tuveson D. A., and Jacks T. 2001. Somatic activation of the K-ras oncogene causes early onset lung cancer in mice. *Nature* 410:1111-6.

91. Jongmans, M. C., van der Burgt I., Hoogerbrugge P. M., Noordam K., Yntema H. G., Nillesen W. M., Kuiper R. P., Ligtenberg M. J., van Kessel A. G., van Krieken J. H., Kiemeney L. A., and Hoogerbrugge N. 2011. Cancer risk in patients with Noonan syndrome carrying a PTPN11 mutation. *Eur J Hum Genet* 19:870-4.

92. Jopling, C., van Geemen D., and den Hertog J. 2007. Shp2 knockdown and Noonan/LEOPARD mutant Shp2-induced gastrulation defects. *PLoS Genet* 3:e225.

93. Jurnak, F. 1988. The three-dimensional structure of c-H-ras p21: implications for oncogene and G protein studies. *Trends Biochem Sci* 13:195-8.

94. Kajstura, J., Leri A., Finato N., Loreto C. Di, Beltrami C. A., and Anversa P. 1998. Myocyte proliferation in end-stage cardiac failure in humans. *Proc Natl Acad Sci U S A* 95:8801-5.

95. Kang, S., Bader A. G., and Vogt P. K. 2005. Phosphatidylinositol 3-kinase mutations identified in human cancer are oncogenic. *Proc Natl Acad Sci U S A* 102:802-7.

96. Karin, M., Cao Y., Greten F. R., and Li Z. W. 2002. NF-kappaB in cancer: from innocent bystander to major culprit. *Nat Rev Cancer* 2:301-10.

97. Karnoub, A. E., and Weinberg R. A. 2008. Ras oncogenes: split personalities. *Nat Rev Mol Cell Bio*l 9:517-31.

98. Kelley, G. G., Reks S. E., Ondrako J. M., and Smrcka A. V. 2001. Phospholipase C(epsilon): a novel Ras effector. *EMBO J* 20:743-54.

99. Ko, J. M., Kim J. M., Kim G. H., and Yoo H. W. 2008. PTPN11, SOS1, KRAS, and RAF1 gene analysis, and genotype-phenotype correlation in Korean patients with Noonan syndrome. *J Hum Genet* 53:999-1006.

100. Koera, K., Nakamura K., Nakao K., Miyoshi J., Toyoshima K., Hatta T., Otani H., Aiba A., and Katsuki M. 1997. K-ras is essential for the development of the mouse embryo. *Oncogene* 15:1151-9.

101. Kontaridis, M. I., Swanson K. D., David F. S., Barford D., and Neel B. G. 2006. PTPN11 (Shp2) mutations in LEOPARD syndrome have dominant negative, not activating, effects. *J Biol Chem* 281:6785-92.

102. Krab, L. C., de Goede-Bolder A., Aarsen F. K., Pluijm S. M., Bouman M. J., van der Geest J. N., Lequin M., Catsman C. E., Arts W. F., Kushner S. A., Silva A. J., de Zeeuw C. I., Moll H. A., and Elgersma Y. 2008. Effect of simvastatin on cognitive functioning in children with neurofibromatosis type 1: a randomized controlled trial. *JAMA* 300:287-94.

103. Kratz, C. P., Rapisuwon S., Reed H., Hasle H., and Rosenberg P. S. 2011. Cancer in Noonan, Costello, cardiofaciocutaneous and LEOPARD syndromes. *Am J Med Genet C Semin Med Genet* 157C:83-9.

104. Kratz, C. P., Zampino G., Kriek M., Kant S. G., Leoni C., Pantaleoni F., Oudesluys-Murphy A. M., Di Rocco C., Kloska S. P., Tartaglia M., and Zenker M. 2009. Craniosynostosis in patients with Noonan syndrome caused by germline KRAS mutations. *Am J Med Genet A* 149A:1036-40.

105. Krenz, M., Gulick J., Osinska H. E., Colbert M. C., Molkentin J. D., and Robbins J. 2008. Role of ERK1/2 signaling in congenital valve malformations in Noonan syndrome. *Proc Natl Acad Sci U S A* 105:18930-5.

106. Kuan, C. T., Wikstrand C. J., and Bigner D. D. 2001. EGF mutant receptor vIII as a molecular target in cancer therapy. *Endocr Relat Cancer* 8:83-96.

107. Kuhn, R., Schwenk F., Aguet M., and Rajewsky K. 1995. Inducible gene targeting in mice. *Science* 269:1427-9.

108. Lakso, M., Pichel J. G., Gorman J. R., Sauer B., Okamoto Y., Lee E., Alt F. W., and Westphal H. 1996. Efficient in vivo manipulation of mouse genomic sequences at the zygote stage. *Proc Natl Acad Sci U S A* 93:5860-5.

109. Lambert, J. M., Lambert Q. T., Reuther G. W., Malliri A., Siderovski D. P., Sondek J., Collard J. G., and Der C. J. 2002. Tiam1 mediates Ras activation of Rac by a PI(3)K-independent mechanism. *Nat Cell Biol* 4:621-5.

110. Langdon, Y. G., Goetz S. C., Berg A. E., Swanik J. T., and Conlon F. L. 2007. SHP-2 is required for the maintenance of cardiac progenitors. *Development* 134:4119-30.

111. Largaespada, D. A., Brannan C. I., Jenkins N. A., and Copeland N. G. 1996. Nf1 deficiency causes Ras-mediated granulocyte/macrophage colony stimulating factor hypersensitivity and chronic myeloid leukaemia. *Nat Genet* 12:137-43.

112. Lauchle, J. O., Braun B. S., Loh M. L., and Shannon K. 2006. Inherited predispositions and hyperactive Ras in myeloid leukemogenesis. *Pediatr Blood Cancer* 46:579-85.

113. Lauchle, J. O., Kim D., Le D. T., Akagi K., Crone M., Krisman K., Warner K., Bonifas J. M., Li Q., Coakley K. M., Diaz-Flores E., Gorman M., Przybranowski S., Tran M., Kogan S. C., Roose J. P., Copeland N. G., Jenkins N. A., Parada L., Wolff L., Sebolt-Leopold J., and Shannon K. 2009. Response and resistance to MEK inhibition in leukaemias initiated by hyperactive Ras. *Nature* 461:411-4.

114. Le, D. T., Kong N., Zhu Y., Lauchle J. O., Aiyigari A., Braun B. S., Wang E., Kogan S. C., Le Beau M. M., Parada L., and Shannon K. M. 2004. Somatic inactivation of Nf1 in hematopoietic cells results in a progressive myeloproliferative disorder. *Blood* 103:4243-50.

115. Lee, B. H., Kim J. M., Jin H. Y., Kim G. H., Choi J. H., and Yoo H. W. 2011. Spectrum of mutations in Noonan syndrome and their correlation with phenotypes. *J Pediatr* 159:1029-35.

116. Leevers, S. J., Paterson H. F., and Marshall C. J. 1994. Requirement for Ras in Raf activation is overcome by targeting Raf to the plasma membrane. *Nature* 369:411-4.

117. Leon, J., Guerrero I., and Pellicer A. 1987. Differential expression of the ras gene family in mice. *Mol Cell Biol* 7:1535-40.

118. Leventopoulos, G., Denayer E., Makrythanasis P., Papapolychroniou C., and Fryssira H. 2010. Noonan syndrome and systemic lupus erythematosus in a patient with a novel KRAS mutation. *Clin Exp Rheumatol* 28:556-7.

119. Li, J., Zhang Z., Dai Z., Plass C., Morrison C., Wang Y., Wiest J. S., Anderson M. W., and You M. 2003. LOH of chromosome 12p correlates with Kras2 mutation in non-small cell lung cancer. *Oncogene* 22:1243-6.

120. Li, Q., Haigis K. M., McDaniel A., Harding-Theobald E., Kogan S. C., Akagi K., Wong J. C., Braun B. S., Wolff L., Jacks T., and Shannon K. 2011. Hematopoiesis and leukemogenesis in mice expressing oncogenic NrasG12D from the endogenous locus. *Blood* 117:2022-32.

121. Lin, A. E., Alexander M. E., Colan S. D., Kerr B., Rauen K. A., Noonan J., Baffa J., Hopkins E., Sol-Church K., Limongelli G., Digilio M. C., Marino B., Innes A. M., Aoki Y., Silberbach M., Delrue M. A., White S. M., Hamilton R. M., O'Connor W., Grossfeld P. D., Smoot L. B., Padera R. F., and Gripp K. W. 2011. Clinical, pathological, and molecular analyses of cardiovascular abnormalities in Costello syndrome: a Ras/MAPK pathway syndrome. *Am J Med Genet A* 155A:486-507.

122. Lo, F. S., Lin J. L., Kuo M. T., Chiu P. C., Shu S. G., Chao M. C., Lee Y. J., and Lin S. P. 2009. Noonan syndrome caused by germline KRAS mutation in Taiwan: report of two patients and a review of the literature. *Eur J Pediatr* 168:919-23.

123. Lohmann, S., Wollscheid U., Huber C., and Seliger B. 1996. Multiple levels of MHC class I down-regulation by ras oncogenes. *Scand J Immunol* 43:537-44.

124. Lowy, D. R., and Willumsen B. M. 1993. Function and regulation of ras. *Annu Rev Biochem* 62:851-91.

125. Luo, J. Q., Liu X., Frankel P., Rotunda T., Ramos M., Flom J., Jiang H., Feig L. A., Morris A. J., Kahn R. A., and Foster D. A. 1998. Functional association between Arf and RalA in active phospholipase D complex. *Proc Natl Acad Sci U S A* 95:3632-7.

126. Lyubynska, N., Gorman M. F., Lauchle J. O., Hong W. X., Akutagawa J. K., Shannon K., and Braun B. S. 2011. A MEK inhibitor abrogates myeloproliferative disease in Kras mutant mice. *Sci Transl Med* 3:76ra27.

127. Mack, T. M., Yu M. C., Hanisch R., and Henderson B. E. 1986. Pancreas cancer and smoking, beverage consumption, and past medical history. *J Natl Cancer Inst* 76:49-60.

128. Maier, C. R., Hollander M. C., Hobbs E. A., Dogan I., Linnoila R. I., and Dennis P. A. 2011. Nicotine does not enhance tumorigenesis in mutant K-ras-driven mouse models of lung cancer. *Cancer Prev Res (Phila)* 4:1743-51.

129. Mainardi, S., Mijimolle N., Francoz S., Vicente-Duenas C., Sanchez-Garcia I., and Barbacid M.. 2013. Identification of cancer initiating cells in K-Ras driven lung adenocarcinoma. *Proc Natl Acad Sci U S A* 111:255-60.

130. Maisonneuve, P., and Lowenfels A. B. 2010. Epidemiology of pancreatic cancer: an update. *Dig Dis* 28:645-56.

131. Malliri, A., van der Kammen R. A., Clark K., van der Valk M., Michiels F., and Collard J. G. 2002. Mice deficient in the Rac activator Tiam1 are resistant to Ras-induced skin tumours. *Nature* 417:867-71.

132. Malumbres, M., and Barbacid M. 2003. RAS oncogenes: the first 30 years. *Nat Rev Cancer* 3:459-65.

133. Mao, X., Fujiwara Y., and Orkin S. H. 1999. Improved reporter strain for monitoring Cre recombinase-mediated DNA excisions in mice. *Proc Natl Acad Sci U S A* 96:5037-42.

134. Marais, R., Y. Light, H. F. Paterson, and C. J. Marshall. 1995. Ras recruits Raf-1 to the plasma membrane for activation by tyrosine phosphorylation. EMBO J 14:3136-45.

135. Marcus, K. A., Sweep C. G., van der Burgt I., and Noordam C. 2008. Impaired Sertoli cell function in males diagnosed with Noonan syndrome. *J Pediatr Endocrinol Metab* 21:1079-84.

136. Marin, T. M., Keith K., Davies B., Conner D. A., Guha P., Kalaitzidis D., Wu X., Lauriol J., Wang B., Bauer M., Bronson R., Franchini K. G., Neel B. G., and Kontaridis M. I. 2011. Rapamycin reverses hypertrophic cardiomyopathy in a mouse model of LEOPARD syndrome-associated PTPN11 mutation. *J Clin Invest* 121:1026-43.

137. Martinelli, S., De Luca A., Stellacci E., Rossi C., Checquolo S., Lepri F., Caputo V., Silvano M., Buscherini F., Consoli F., Ferrara G., Digilio M. C., Cavaliere M. L., van Hagen J. M., Zampino G., van der Burgt I., Ferrero G. B., Mazzanti L., Screpanti I., Yntema H. G., Nillesen W. M., Savarirayan R., Zenker M., Dallapiccola B., Gelb B. D., and Tartaglia M. 2010. Heterozygous germline mutations in the CBL tumor-suppressor gene cause a Noonan syndrome-like phenotype. *Am J Hum Genet* 87:250-7.

138. Massarano, A. A., Wood A., Tait R. C., Stevens R., and Super M. 1996. Noonan syndrome: coagulation and clinical aspects. *Acta Paediatr* 85:1181-5.

139. Mazzanti, L., Cacciari E., Cicognani A., Bergamaschi R., Scarano E., and Forabosco A. 2003. Noonan-like syndrome with loose anagen hair: a new syndrome? *Am J Med Genet A* 118A:279-86.

140. Mendelsohn, J., and Baselga J. 2000. The EGF receptor family as targets for cancer therapy. *Oncogene* 19:6550-65.

141. Mendez, H. M., and Opitz J. M. 1985. Noonan syndrome: a review. *Am J Med Genet* 21:493-506.

142. Mitin, N., Rossman K. L., and Der C. J. 2005. Signaling interplay in Ras superfamily function. *Curr Biol* 15:R563-74.

143. Momi, N., Ponnusamy M. P., Kaur S., Rachagani S., Kunigal S. S., Chellappan S., Ouellette M. M., and Batra S. K. 2013. Nicotine/cigarette smoke promotes metastasis of pancreatic cancer through alpha7nAChR-mediated MUC4 upregulation. *Oncogene* 32:1384-95.

144. Nagy, A., Rossant J., Nagy R., Abramow-Newerly W., and Roder J. C. 1993. Derivation of completely cell culture-derived mice from early-passage embryonic stem cells. *Proc Natl Acad Sci U S A* 90:8424-8.

145. Nakamura, T., Colbert M., Krenz M., Molkentin J. D., Hahn H. S., Dorn G. W., and Robbins J. 2007. Mediating ERK 1/2 signaling rescues congenital heart defects in a mouse model of Noonan syndrome. *J Clin Invest* 117:2123-32.

146. Nakamura, T., Gulick J., Pratt R., and Robbins J. 2009. Noonan syndrome is associated with enhanced pERK activity, the repression of which can prevent craniofacial malformations. *Proc Natl Acad Sci U S A* 106:15436-41.

147. Nava, C., Hanna N., Michot C., Pereira S., Pouvreau N., Niihori T., Aoki Y., Matsubara Y., Arveiler B., Lacombe D., Pasmant E., Parfait B., Baumann C., Heron D., Sigaudy S., Toutain A., Rio M., Goldenberg A., Leheup B., Verloes A., and Cave H. 2007. Cardio-facio-cutaneous and Noonan syndromes due to mutations in the RAS/MAPK signalling pathway: genotype-phenotype relationships and overlap with Costello syndrome. *J Med Genet* 44:763-71.

148. Neel, B. G., Gu H., and Pao L. 2003. The 'Shp'ing news: SH2 domain-containing tyrosine phosphatases in cell signaling. *Trends Biochem Sci* 28:284-93.

149. Neumann, T. E., Allanson J., Kavamura I., Kerr B., Neri G., Noonan J., Cordeddu V., Gibson K., Tzschach A., Kruger G., Hoeltzenbein M., Goecke T. O., Kehl H. G., Albrecht B., Luczak K., Sasiadek M. M., Musante L., Laurie R., Peters H., Tartaglia M., Zenker M., and Kalscheuer V. 2009. Multiple giant cell lesions in patients with Noonan syndrome and cardio-facio-cutaneous syndrome. *Eur J Hum Genet* 17:420-5.

150. Niemeyer, C. M., Kang M. W., Shin D. H., Furlan I., Erlacher M., Bunin N. J., Bunda S., Finklestein J. Z., Sakamoto K. M., Gorr T. A., Mehta P., Schmid I., Kropshofer G., Corbacioglu S., Lang P. J., Klein, C. Schlegel P. G., Heinzmann A., Schneider M., Stary J., van den Heuvel-Eibrink M. M., Hasle H., Locatelli F., Sakai D., Archambeault S., Chen L., Russell R. C., Sybingco S. S., Ohh M., Braun B. S., Flotho C., and Loh M. L. 2010. Germline CBL mutations cause developmental abnormalities and predispose to juvenile myelomonocytic leukemia. *Nat Genet* 42:794-800.

151. Niihori, T., Aoki Y., Narumi Y., Neri G., Cave H., Verloes A., Okamoto N., Hennekam R. C., Gillessen-Kaesbach G., Wieczorek D., Kavamura M. I., Kurosawa K., Ohashi H., Wilson L., Heron D., Bonneau D., Corona G., Kaname T., Naritomi K., Baumann C., Matsumoto N., Kato K., Kure S., and Matsubara Y. 2006. Germline KRAS and BRAF mutations in cardio-facio-cutaneous syndrome. *Nat Genet* 38:294-6.

152. Nishikawa, T., Ishiyama S., Shimojo T., Takeda K., Kasajima T., and Momma K. 1996. Hypertrophic cardiomyopathy in Noonan syndrome. *Acta Paediatr Jpn* 38:91-8.

153. Nosan, G., Bertok S., Vesel S., Yntema H. G., and Paro-Panjan D. 2013. A lethal course of hypertrophic cardiomyopathy in Noonan syndrome due to a novel germline mutation in the KRAS gene: case study. *Croat Med* J 54:574-8.

154. Nystrom, A. M., Ekvall S., Berglund E., Bjorkqvist M., Braathen G., Duchen K., Enell H., Holmberg E., Holmlund U., Olsson-Engman M., Anneren G., and Bondeson M. L. 2008. Noonan and cardio-facio-cutaneous syndromes: two clinically and genetically overlapping disorders. *J Med Genet* 45:500-6.

155. O'Reilly, A. M., Pluskey S., Shoelson S. E., and Neel B. G. 2000. Activated mutants of SHP-2 preferentially induce elongation of Xenopus animal caps. *Mol Cell Biol* 20:299-311.

156. Pacold, M. E., Suire S., Perisic O., Lara-Gonzalez S., Davis C. T., Walker E. H., Hawkins P. T., Stephens L., Eccleston J. F., and Williams R. L. 2000. Crystal structure and functional analysis of Ras binding to its effector phosphoinositide 3-kinase gamma. *Cell* 103:931-43.

157. Pandit, B., Sarkozy A., Pennacchio L. A., Carta C., Oishi K., Martinelli S., Pogna E. A., Schackwitz W., Ustaszewska A., Landstrom A., Bos J. M., Ommen S. R., Esposito G., Lepri F., Faul C., Mundel P., Lopez Siguero J. P., Tenconi R., Selicorni A., Rossi C., Mazzanti L., Torrente I., Marino B., Digilio M. C., Zampino G., Ackerman M. J., Dallapiccola B., Tartaglia M., and Gelb B. D. 2007. Gain-of-function RAF1 mutations cause Noonan and LEOPARD syndromes with hypertrophic cardiomyopathy. *Nat Genet* 39:1007-12.

158. Perez, B., Mechinaud F., Galambrun C., Ben Romdhane N., Isidor B., Philip N., Derain-Court J., Cassinat B., Lachenaud J., Kaltenbach S., Salmon A., Desiree C., Pereira S., Menot M. L., Royer N., Fenneteau O., Baruchel A., Chomienne C., Verloes A., and Cave H. 2010. Germline mutations of the CBL gene define a new genetic syndrome with predisposition to juvenile myelomonocytic leukaemia. *J Med Genet* 47:686-91.

159. Pinto, P., Rocha P., Veiga I., Guedes J., Pinheiro M., Peixoto A., Pinto C., Fragoso M., Sanches E., Araujo A., Alves F., Coutinho C., Lopes P., Henrique R., and Teixeira M. R. Comparison of methodologies for KRAS mutation detection in metastatic colorectal cancer. *Cancer Genet* 204:439-46.

160. Polakis, P., and McCormick F. 1993. Structural requirements for the interaction of p21ras with GAP, exchange factors, and its biological effector target. *J Biol Chem* 268:9157-60.

161. Pruitt, K., and Der C. J. 2001. Ras and Rho regulation of the cell cycle and oncogenesis. *Cancer Lett* 171:1-10.

162. Pylayeva-Gupta, Y., Grabocka E., and Bar-Sagi D. 2011. RAS oncogenes: weaving a tumorigenic web. *Nat Rev Cancer* 11:761-74.

163. Quaini, F., Urbanek K., Beltrami A. P., Finato N., Beltrami C. A., Nadal-Ginard B., Kajstura J., Leri A., and Anversa P. 2002. Chimerism of the transplanted heart. *N Engl J Med* 346:5-15.

164. Rauen, K. A. 2007. HRAS and the Costello syndrome. *Clin Genet* 71:101-8.

165. Rauen, K. A. 2013. The RASopathies. *Annu Rev Genomics Hum Genet* 14:355-69.

166. Rauen, K. A., Banerjee A., Bishop W. R., Lauchle J. O., McCormick F., McMahon M., Melese T., Munster P. N., Nadaf S., Packer R. J., Sebolt-Leopold J., and Viskochil D. H. 2011. Costello and cardio-facio-cutaneous syndromes: Moving toward clinical trials in RASopathies. *Am J Med Genet C Semin Med Genet* 157C:136-46.

167. Razzaque, M. A., Komoike Y., Nishizawa T., Inai K., Furutani M., Higashinakagawa T., and Matsuoka R. 2012. Characterization of a novel KRAS mutation identified in Noonan syndrome. *Am J Med Genet* A 158A:524-32.

168. Razzaque, M. A., Nishizawa T., Komoike Y., Yagi H., Furutani M., Amo R., Kamisago M., Momma K., Katayama H., Nakagawa M., Fujiwara Y., Matsushima M., Mizuno K., Tokuyama M., Hirota H., Muneuchi J., Higashinakagawa T., and Matsuoka R. 2007. Germline gain-of-function mutations in RAF1 cause Noonan syndrome. *Nat Genet* 39:1013-7.

169. Repasky, G. A., Chenette E. J., and Der C. J. 2004. Renewing the conspiracy theory debate: does Raf function alone to mediate Ras oncogenesis? *Trends Cell Biol* 14:639-47.

170. Roberts, A., Allanson J., Jadico S. K., Kavamura M. I., Noonan J., Opitz J. M., Young T., and Neri G. 2006. The cardiofaciocutaneous syndrome. *J Med Genet* 43:833-42.

171. Roberts, A. E., Allanson J. E., Tartaglia M., and Gelb B. D. 2013. Noonan syndrome. *Lancet* 381:333-42.

172. Roberts, A. E., Araki T., Swanson K. D., Montgomery K. T., Schiripo T. A., Joshi V. A., Li L., Yassin Y., Tamburino A. M., Neel B. G., and Kucherlapati R. S. 2007. Germline gain-of-function mutations in SOS1 cause Noonan syndrome. *Nat Genet* 39:70-4.

173. Rodriguez-Viciana, P., and McCormick F. 2005. RalGDS comes of age. *Cancer Cell* 7:205-6.

174. Rodriguez-Viciana, P., Tetsu O., Tidyman W. E., Estep A. L., Conger B. A., Cruz M. S., McCormick F., and Rauen K. A. 2006. Germline mutations in genes within the MAPK pathway cause cardio-facio-cutaneous syndrome. *Science* 311:1287-90.

175. Rodriguez-Viciana, P., Warne P. H., Dhand R., Vanhaesebroeck B., Gout I., Fry M. J., Waterfield M. D., and Downward J. 1994. Phosphatidylinositol-3-OH kinase as a direct target of Ras. *Nature* 370:527-32.

176. Rojas, A. M., Fuentes G., Rausell A., and Valencia A. The Ras protein superfamily: evolutionary tree and role of conserved amino acids. *J Cell Biol* 196:189-201.

177. Runtuwene, V., van Eekelen M., Overvoorde J., Rehmann H., Yntema H. G., Nillesen W. M., van Haeringen A., van der Burgt I., Burgering B., and den Hertog J. 2011. Noonan syndrome gain-of-function mutations in NRAS cause zebrafish gastrulation defects. *Dis Model Mech* 4:393-9.

178. Sah, V. P., Attardi L. D., Mulligan G. J., Williams B. O., Bronson R. T., and Jacks T. 1995. A subset of p53-deficient embryos exhibit exencephaly. *Nat Genet* 10:175-80.

179. Sansom, O. J., Meniel V., Wilkins J. A., Cole A. M., Oien K. A., Marsh V., Jamieson T. J., Guerra C., Ashton G. H., Barbacid M., and Clarke A. R. 2006. Loss of Apc allows phenotypic manifestation of the transforming properties of an endogenous K-ras oncogene in vivo. *Proc Natl Acad Sci U S A* 103:14122-7.

180 Sarkozy, A., Carta C., Moretti S., Zampino G., Digilio M. C., Pantaleoni F., Scioletti A. P., Esposito G., Cordeddu V., Lepri F., Petrangeli V., Dentici M. L., Mancini G. M., Selicorni A., Rossi C., Mazzanti B., Marino B., Ferrero G. B., Silengo M. C., Memo L., Stanzial F., Faravelli F., Stuppia L., Puxeddu E., Gelb B. D., Dallapiccola B., and Tartaglia M. 2009. Germline BRAF mutations in Noonan, LEOPARD, and cardiofaciocutaneous syndromes: molecular diversity and associated phenotypic spectrum. *Hum Mutat* 30:695-702.

181. Sarkozy, A., Digilio M. C., and Dallapiccola B. 2008. Leopard syndrome. *Orphanet J Rare Dis* 3:13.

182. Saxton, T. M., Henkemeyer M., Gasca S., Shen R., Rossi D. J., Shalaby F., Feng G. S., and Pawson T. 1997. Abnormal mesoderm patterning in mouse embryos mutant for the SH2 tyrosine phosphatase Shp-2. *EMBO J* 16:2352-64.

183. Scheffzek, K., Ahmadian M. R., Kabsch W., Wiesmuller L., Lautwein A., Schmitz F., andWittinghofer A. 1997. The Ras-RasGAP complex: structural basis for GTPase activation and its loss in oncogenic Ras mutants. *Science* 277:333-8.

184. Scheidig, A. J., Burmester C., and Goody R. S. 1999. The pre-hydrolysis state of p21(ras) in complex with GTP: new insights into the role of water molecules in the GTP hydrolysis reaction of ras-like proteins. *Structure* 7:1311-24.

185. Schramm, C., Fine D. M., Edwards M. A., Reeb A. N., and Krenz M. 2012. The PTPN11 loss-of-function mutation Q510E-Shp2 causes hypertrophic cardiomyopathy by dysregulating mTOR signaling. *Am J Physiol Heart Circ Physiol* 302:H231-43.

186. Schubbert, S., Bollag G., Lyubynska N., Nguyen H., Kratz C. P., Zenker M., Niemeyer C. M., Molven A., and Shannon K. 2007. Biochemical and functional characterization of germ line KRAS mutations. *Mol Cell Biol* 27:7765-70.

187. Schubbert, S., Shannon K., and Bollag G. 2007. Hyperactive Ras in developmental disorders and cancer. *Nat Rev Cancer* 7:295-308.

188. Schubbert, S., Zenker M., Rowe S. L., Boll S., Klein C., Bollag G., van der Burgt I., Musante L., Kalscheuer V., Wehner L. E., Nguyen H., West B., Zhang K. Y.,

Sistermans E., Rauch A., Niemeyer C. M., Shannon K., and Kratz C. P. 2006. Germline KRAS mutations cause Noonan syndrome. *Nat Genet* 38:331-6.

189. Schuhmacher, A. J., Guerra C., Sauzeau V., Canamero M., Bustelo X. R., and Barbacid M. 2008. A mouse model for Costello syndrome reveals an Ang II-mediated hypertensive condition. *J Clin Invest* 118:2169-79.

190. Sebolt-Leopold, J. S. 2008. Advances in the development of cancer therapeutics directed against the RAS-mitogen-activated protein kinase pathway. *Clin Cancer Res* 14:3651-6.

191. Serrano, M., Lee H., Chin L., Cordon-Cardo C., Beach D., and DePinho R. A. 1996. Role of the INK4a locus in tumor suppression and cell mortality. *Cell* 85:27-37.

192. Sharland, M., Burch M., McKenna W. M., and Paton M. A. 1992. A clinical study of Noonan syndrome. *Arch Dis Child* 67:178-83.

193. Shaw, A. C., Kalidas K., Crosby A. H., Jeffery S., and Patton M. A. 2007. The natural history of Noonan syndrome: a long-term follow-up study. *Arch Dis Child* 92:128-32.

194. Shaw, A. T., Meissner A., Dowdle J. A., Crowley D., Magendantz M., Ouyang C., Parisi T., Rajagopal J., Blank L. J., Bronson R. T., Stone J. R., Tuveson D. A., Jaenisch R., and Jacks T. 2007. Sprouty-2 regulates oncogenic K-ras in lung development and tumorigenesis. *Genes Dev* 21:694-707.

195. Shi, G. X., and Andres D. A. 2005. Rit contributes to nerve growth factor-induced neuronal differentiation via activation of B-Raf-extracellular signal-regulated kinase and p38 mitogen-activated protein kinase cascades. *Mol Cell Biol* 25:830-46.

196. Shi, G. X., Jin L., and Andres D. A. 2011. A rit GTPase-p38 mitogen-activated protein kinase survival pathway confers resistance to cellular stress. *Mol Cell Biol* 31:1938-48.

197. Shibata, H., Toyama K., Shioya H., Ito M., Hirota M., Hasegawa S., Matsumoto H., Takano H., Akiyama T., Toyoshima K., Kanamaru R., Kanegae Y., Saito I., Nakamura Y., Shiba K., and Noda T. 1997. Rapid colorectal adenoma formation initiated by conditional targeting of the Apc gene. *Science* 278:120-3.

198. Shibatohge, M., Kariya K., Liao Y., Hu C. D., Watari Y., Goshima M., Shima F., and Kataoka T. 1998. Identification of PLC210, a Caenorhabditis elegans phospholipase C, as a putative effector of Ras. *J Biol Chem* 273:6218-22.

199. Siegel, R., Naishadham D., and Jemal A. 2013. Cancer statistics, 2013. *CA Cancer J Clin* 63:11-30.

200. Simpson, A. J., Wallace W. A., Marsden M. E., Govan J. R., Porteous D. J., Haslett C., and Sallenave J. M. 2001. Adenoviral augmentation of elafin protects the lung against acute injury mediated by activated neutrophils and bacterial infection. *J Immunol* 167:1778-86.

201. Solassol, J., Ramos J., Crapez E., Saifi M., Mange A., Vianes E., Lamy P. J., Costes V., and Maudelonde T. KRAS Mutation Detection in Paired Frozen and Formalin-Fixed Paraffin-Embedded (FFPE) Colorectal Cancer Tissues. *Int J Mol Sci* 12:3191-204.

202. Song, C., Hu C. D., Masago M., Kariyai K., Yamawaki-Kataoka Y., Shibatohge M., Wu D., Satoh T., and Kataoka T. 2001. Regulation of a novel human phospholipase C, PLCepsilon, through membrane targeting by Ras. *J Biol Chem* 276:2752-7.

203. Sparks, J. A., and Pauly J. R. 1999. Effects of continuous oral nicotine administration on brain nicotinic receptors and responsiveness to nicotine in C57Bl/6 mice. *Psychopharmacology (Berl)* 141:145-53.

204. Stevenson, D. A., and Yang F. C. The musculoskeletal phenotype of the RASopathies. *Am J Med Genet C Semin Med Genet* 157C:90-103.

205. Sznajer, Y., Keren B., Baumann C., Pereira S., Alberti C., Elion J., Cave H., and Verloes A. 2007. The spectrum of cardiac anomalies in Noonan syndrome as a result of mutations in the PTPN11 gene. *Pediatrics* 119:e1325-31.

206. Tarantino, C., Paolella G., Cozzuto L., Minopoli G., Pastore L., Parisi S., and Russo T. 2010. miRNA 34a, 100, and 137 modulate differentiation of mouse embryonic stem cells. *FASEB* J 24:3255-63.

207. Tartaglia, M., and Gelb B. D. 2010. Disorders of dysregulated signal traffic through the RAS-MAPK pathway: phenotypic spectrum and molecular mechanisms. *Ann N Y Acad Sci* 1214:99-121.

208. Tartaglia, M., and Gelb B. D. 2005. Noonan syndrome and related disorders: genetics and pathogenesis. *Annu Rev Genomics Hum Genet* 6:45-68.

209. Tartaglia, M., Kalidas K., Shaw A., Song X., Musat D. L., van der Burgt I., Brunner H. G., Bertola D. R., Crosby A., Ion A., Kucherlapati R. S., Jeffery S., Patton M. A., and Gelb B. D. 2002. PTPN11 mutations in Noonan syndrome: molecular spectrum, genotype-phenotype correlation, and phenotypic heterogeneity. *Am J Hum Genet* 70:1555-63.

210. Tartaglia, M., Martinelli S., Stella L., Bocchinfuso G., Flex E., Cordeddu V., Zampino G., Burgt I., Palleschi A., Petrucci T. C., Sorcini M., Schoch C., Foa R., Emanuel P. D., and Gelb B. D. 2006. Diversity and functional consequences of germline and somatic PTPN11 mutations in human disease. *Am J Hum Genet* 78:279-90.

211. Tartaglia, M., Mehler E. L., Goldberg R., Zampino G., Brunner H. G., Kremer H., van der Burgt I., Crosby A. H., Ion A., Jeffery S., Kalidas K., Patton M. A., Kucherlapati R. S., and Gelb B. D. 2001. Mutations in PTPN11, encoding the protein tyrosine phosphatase SHP-2, cause Noonan syndrome. *Nat Genet* 29:465-8.

212. Tartaglia, M., Pennacchio L. A., Zhao C., Yadav K. K., Fodale V., Sarkozy A., Pandit B., Oishi K., Martinelli S., Schackwitz W., Ustaszewska A., Martin J., Bristow J., Carta C., Lepri F., Neri C., Vasta I., Gibson K., Curry C. J., Siguero J. P., Digilio M. C., Zampino G., Dallapiccola B., Bar-Sagi D., and Gelb B. D. 2007. Gain-of-function SOS1 mutations cause a distinctive form of Noonan syndrome. *Nat Genet* 39:75-9.

213. Tartaglia, M., Zampino G., and Gelb B. D. 2010. Noonan syndrome: clinical aspects and molecular pathogenesis. *Mol Syndromol* 1:2-26.

214. Teng, H. W., Huang Y. C., Lin J. K., Chen W. S., Lin T. C., Jiang J. K., Yen C. C., Li A. F., Wang H. W., Chang S. C., Lan Y. T., Lin C. C., Wang H. S., and Yang S. H. 2012. BRAF mutation is a prognostic biomarker for colorectal liver metastasectomy. *J Surg Oncol* 106:123-9.

215. Tidyman, W. E., and Rauen K. A. 2009. The RASopathies: developmental syndromes of Ras/MAPK pathway dysregulation. *Curr Opin Genet Dev* 19:230-6.

216. Todaro, G. J., and Green H. 1963. Quantitative studies of the growth of mouse embryo cells in culture and their development into established lines. *J Cell Biol* 17:299-313.

217. Trahey, M., and McCormick F. 1987. A cytoplasmic protein stimulates normal N-ras p21 GTPase, but does not affect oncogenic mutants. *Science* 238:542-5.

218. Tran, H., Brunet A., Griffith E. C., and Greenberg M. E. 2003. The many forks in FOXO's road. *Sci STKE* 2003:RE5.

219. Travis WD., B. E., Muller-Hermelin H.K., and Harris C.C.E. 2004. world health organization. Classification of tumors. Pathology and Genetics of tumours of the lung, pleura, thymus and heart. *IARC Press*.

220. Turner, A. M. 2011. Noonan syndrome. *J Paediatr Child Health.*

221. Tuveson, D. A., Shaw A. T., Willis N. A., Silver D. P., Jackson E. L., Chang S., Mercer K. L., Grochow R., Hock H., Crowley D., Hingorani S. R., Zaks T., King T., Jacobetz M. A., Wang L., Bronson R. T., Orkin S. H., DePinho R. A., and Jacks T. 2004. Endogenous oncogenic K-ras(G12D) stimulates proliferation and widespread neoplastic and developmental defects. *Cancer Cell* 5:375-87.

222. Tyner, J. W., Erickson H., Deininger M. W., Willis S. G., Eide C. A., Levine R. L., Heinrich M. C., Gattermann N., Gilliland D. G., Druker B. J., and Loriaux M. M. 2009. High-throughput sequencing screen reveals novel, transforming RAS mutations in myeloid leukemia patients. *Blood* 113:1749-55.

223. Urosevic, J., Sauzeau V., Soto-Montenegro M. L., Reig S., Desco M., Wright E. M., Canamero M., Mulero F., Ortega S., Bustelo X. R., and Barbacid M. 2011. Constitutive activation of B-Raf in the mouse germ line provides a model for human cardio-facio-cutaneous syndrome. *Proc Natl Acad Sci U S A* 108:5015-20.

224. van der Burgt, I. 2007. Noonan syndrome. *Orphanet J Rare Dis* 2:4.

225. Van Meter, M. E., Diaz-Flores E., Archard J. A., Passegue E., Irish J. M., Kotecha N., Nolan G. P., Shannon K., and Braun B. S. 2007. K-RasG12D expression induces hyperproliferation and aberrant signaling in primary hematopoietic stem/progenitor cells. *Blood* 109:3945-52.

226. Vaughn, C. P., Zobell S. D., Furtado L. V., Baker C. L., and Samowitz W. S. Frequency of KRAS, BRAF, and NRAS mutations in colorectal cancer. 2011. *Genes Chromosomes Cancer* 50:307-12.

227. Vivanco, I., and Sawyers C. L. 2002. The phosphatidylinositol 3-Kinase AKT pathway in human cancer. *Nat Rev Cancer* 2:489-501.

228. Vogt, P. K., Jiang H., and Aoki H. 2005. Triple layer control: phosphorylation, acetylation and ubiquitination of FOXO proteins. *Cell Cycle* 4:908-13.

229. Wakioka, T., Sasaki A., Kato R., Shouda T., Matsumoto A., Miyoshi K., Tsuneoka M., Komiya S., Baron R., and Yoshimura A. 2001. Spred is a Sprouty-related suppressor of Ras signalling. *Nature* 412:647-51.

230. Weiss, B., Bollag G., and Shannon K. 1999. Hyperactive Ras as a therapeutic target in neurofibromatosis type 1. *Am J Med Genet* 89:14-22.

231. Wennerberg, K., Rossman K. L., and Der C. J. 2005. The Ras superfamily at a glance. *J Cell Sci* 118:843-6.

232. West, K. A., Brognard J., Clark A. S., Linnoila I. R., Yang X., Swain S. M., Harris C., Belinsky S., and Dennis P. A. 2003. Rapid Akt activation by nicotine and a tobacco carcinogen modulates the phenotype of normal human airway epithelial cells. *J Clin Invest* 111:81-90.

233. Willemer, S., Elsasser H. P., and Adler G. 1992. Hormone-induced pancreatitis. *Eur Surg Res* 24 Suppl 1:29-39.

234. Willumsen, B. M., Norris K., Papageorge A. G., Hubbert N. L., and Lowy D. R. 1984. Harvey murine sarcoma virus p21 ras protein: biological and biochemical significance of the cysteine nearest the carboxy terminus. *EMBO* J 3:2581-5.

235. Wittinghofer, A., and Pai E. F. 1991. The structure of Ras protein: a model for a universal molecular switch. *Trends Biochem Sci* 16:382-7.

236. Wood, A., Massarano A., Super M., and Harrington R. 1995. Behavioural aspects and psychiatric findings in Noonan's syndrome. *Arch Dis Child* 72:153-5.

237. Wu, X., Simpson J., Hong J. H., Kim K. H., Thavarajah N. K., Backx P. H.,. Neel B. G, and Araki T. 2011. MEK-ERK pathway modulation ameliorates disease phenotypes in a mouse model of Noonan syndrome associated with the Raf1(L613V) mutation. *J Clin Invest* 121:1009-25.

238. Xu, C., Liu Y. L., Huang J., He D. M., Hou Y. Y., Ji Y., Hou J., Lu S. H., Xu J. F., Hu Q., Shi Y., Zhao L. J., and Tan Y. S. 2012. Detection of KRAS gene mutation and its clinical significance in colorectal adenocarcinoma. *Zhonghua Bing Li Xue Za Zhi* 41:667-70.

239. Xu, D., Wang S., Yu W. M., Chan G., Araki T., Bunting K. D., Neel B. G., and Qu C. K. 2010. A germline gain-of-function mutation in Ptpn11 (Shp-2) phosphatase induces myeloproliferative disease by aberrant activation of hematopoietic stem cells. *Blood* 116:3611-21.

240. Yin, J., Pollock C., Tracy K., Chock M., Martin P., Oberst M., and Kelly K. 2007. Activation of the RalGEF/Ral pathway promotes prostate cancer metastasis to bone. *Mol Cell Biol* 27:7538-50.

241. Yoo, B. M., Oh T. Y., Kim Y. B., Yeo M., Lee J. S., Surh Y. J., Ahn B. O., Kim W. H., Sohn S., Kim J. H., and Hahm K. B. 2005. Novel antioxidant ameliorates the fibrosis and inflammation of cerulein-induced chronic pancreatitis in a mouse model. *Pancreatology* 5:165-76.

242. Yordy, J. S., and Muise-Helmericks R. C. 2000. Signal transduction and the Ets family of transcription factors. *Oncogene* 19:6503-13.

243. Zenker, M., Lehmann K., Schulz A. L., Barth H., Hansmann D., Koenig R., Korinthenberg R., Kreiss-Nachtsheim M., Meinecke P., Morlot S., Mundlos S., Quante A. S., Raskin S., Schnabel D., Wehner L. E., Kratz C. P., Horn D., and Kutsche K.

2007. Expansion of the genotypic and phenotypic spectrum in patients with KRAS germline mutations. *J Med Genet* 44:131-5.

244. Zhang, Z., Wang Y., Vikis H. G., Johnson L., Liu G., Li J., Anderson M. W., Sills R. C., Hong H. L., Devereux T. R., Jacks T., Guan K. L., and You M. 2001. Wildtype Kras2 can inhibit lung carcinogenesis in mice. *Nat Genet* 29:25-33.

APPENDIX I

Supplemental Figures and Tables

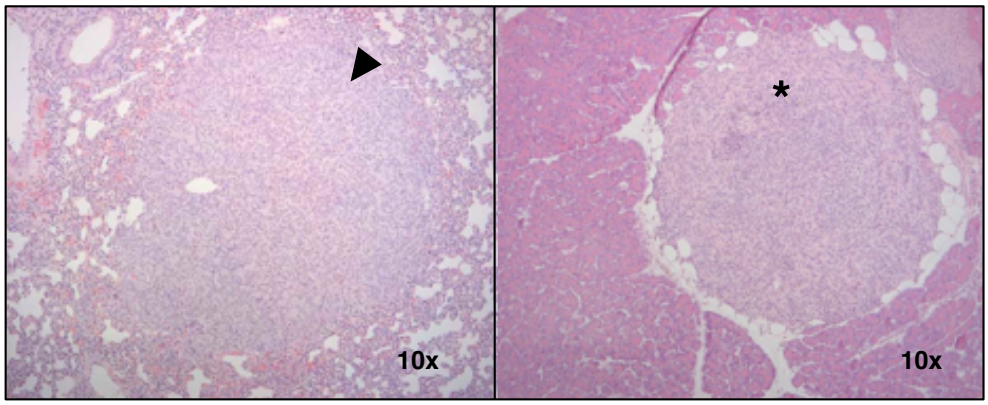

Figure 1 K-*Ras*$^{V14I/V14I}$ mice develop lung and pancreatic lesions upon nicotine administration. H&E stained paraffin section representative lung type III adenocarcinoma (left) and sarcomatoid PDAC (right) from a K-*Ras*$^{V14I/V14I}$ exposed to nicotine from P60. Arrowhead points to lung type III adenocarcinoma and asterisk points ot PDAC lesions.

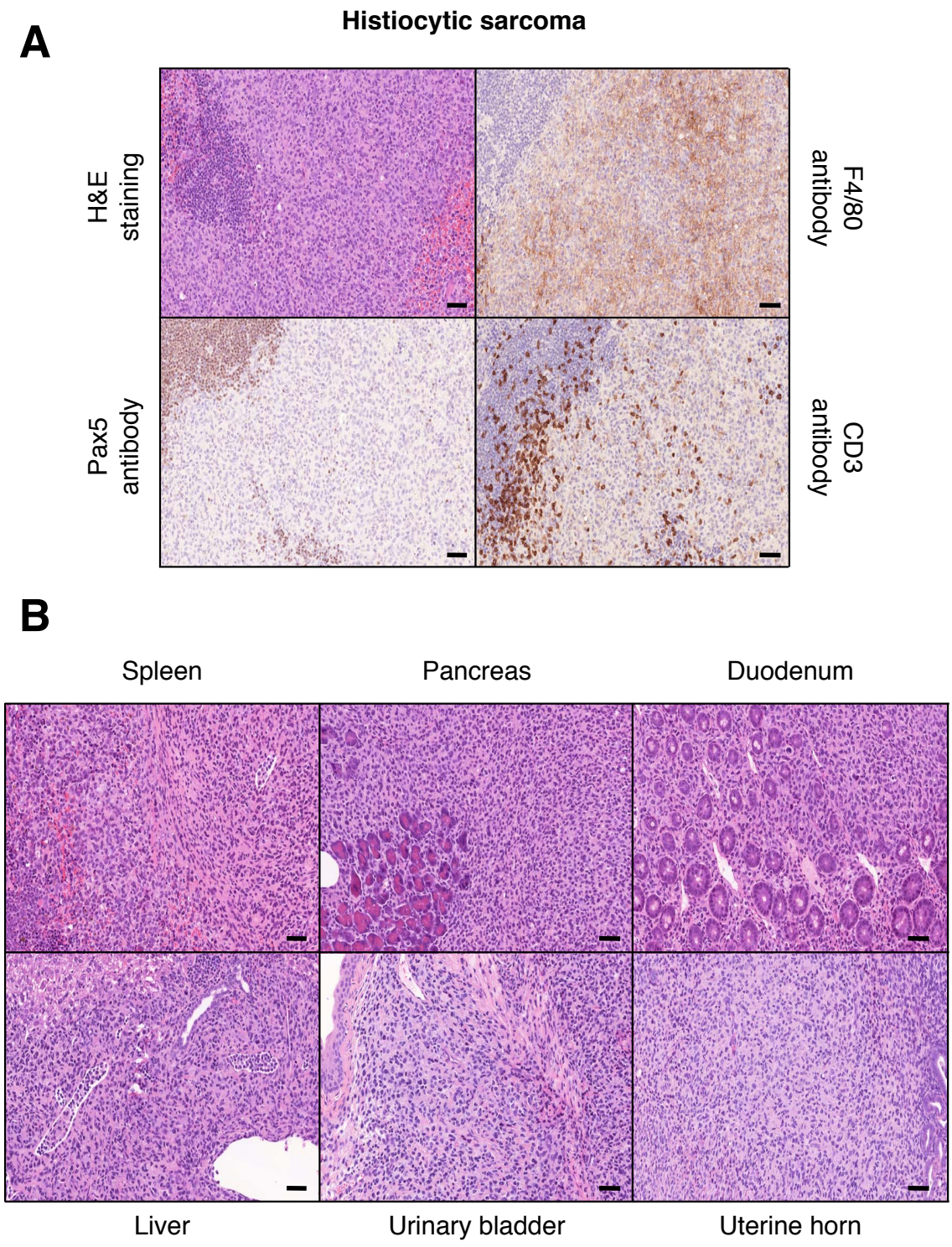

Figure 2 K-*Ras*^{V14I};*p16Ink4a/p19Arf*$^{-/-}$ mice develop histiocytic sarcomas. (A) H&E stained paraffin section and F4/80, Pax5 and CD3 immunostaining of a representative histiocytic sarcoma from a K-*Ras*$^{V14I/V14I}$; *p16Inka/p19Arf*$^{-/-}$Scale bars: 50 μm. **(B)** H&E stained paraffin sections spleen, pancreas, duodenum, liver, urinary bladder and uterine horn infiltrates for a histiocytic sarcoma from a K-*Ras*$^{+/V14I}$; *p16Inka/p19Arf*$^{-/-}$ mouse. Scale bars: 50 μm.

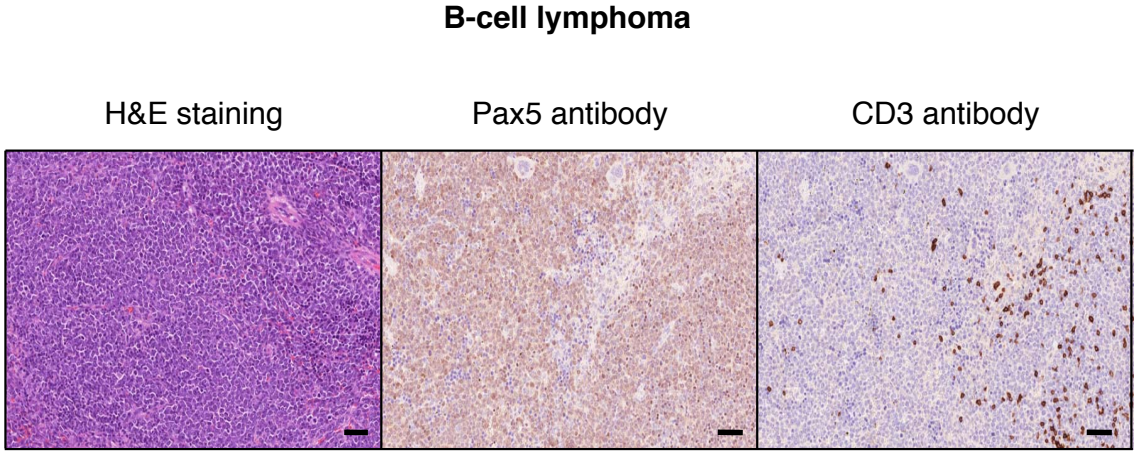

Figure 3 K-*Ras*^{V14I}; *p16Ink4a/p19Arf*$^{-/-}$ mice develop B cell lymphomas. H&E stained section and Pax5 and CD3 immunostaining of a representative B cell lymphoma from K-*Ras*$^{V14I/V14I}$; p16INK4a/p19ARF$^{-/-}$ mouse. Scale bars: 50 μm.

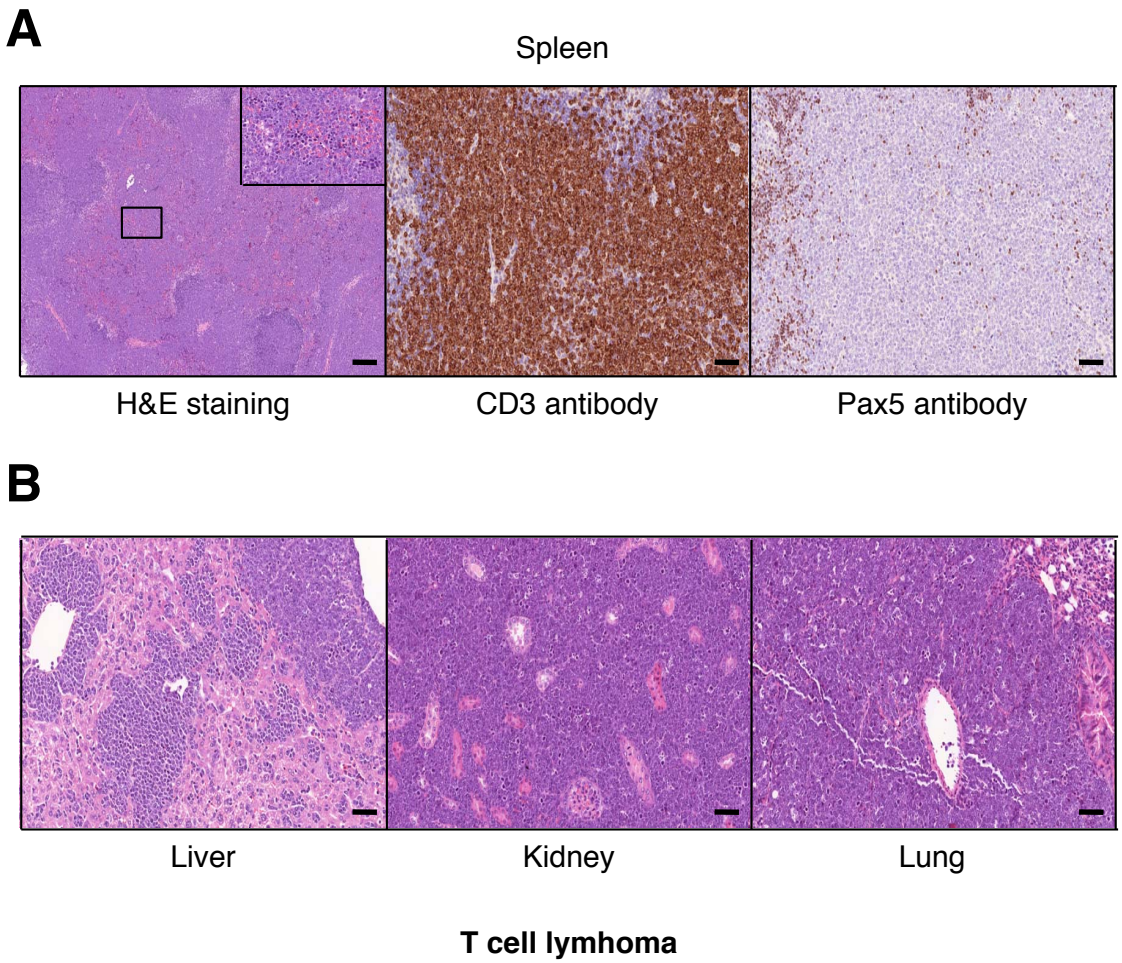

Figure 4 K-*Ras*^{V14I}; p53$^{-/-}$ mice develop T cell lymphomas. (A) H&E stained section and CD3 and Pax5 immunostainig of a T cell lymphoma from K-*Ras*$^{+/V14I}$; *Trp*53$^{-/-}$ mouse. Inset shows detail area of spleen. Spleen scale bars: 200 μm. Immunostaining scale bar: 50 μm**. (B)** H&E stained sections of liver, kidney and lung infiltrate for the T cell lymphoma from K-*Ras*$^{+/V14I}$; p53$^{-/-}$ mouse. Scale bars: 50 μ

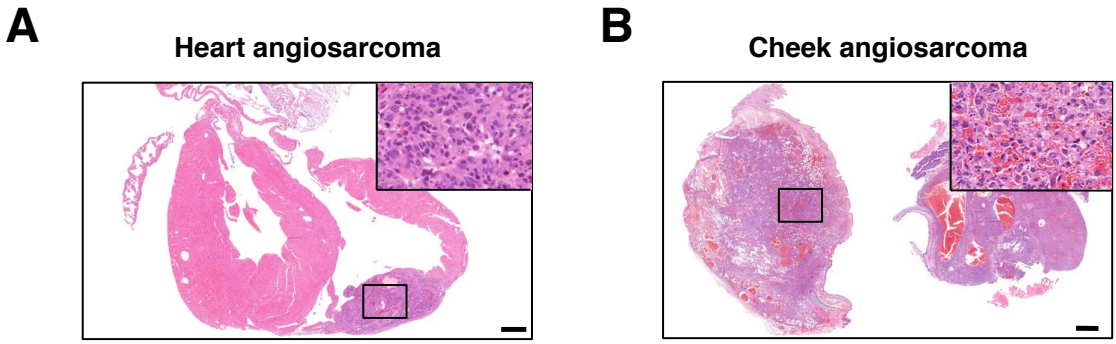

Figure 5 K-*Ras*^{V14I}; p53$^{-/-}$ mice develop angiosarcoma. (A) H&E stained section of a heart from a K-*Ras*$^{+/V14I}$; *Trp53*$^{-/-}$ mouse with a representative angiosarcoma. . Inset shows detail area of the angiosarcoma. Scale bars: 500 μm. **(B)** H&E stained section of a cheek angiosarcoma from a K-*Ras*$^{+/V14I}$; *Trp53*$^{-/-}$ mouse. Inset shows detail area of the angiosarcoma. Scale bars: 1000 μm.

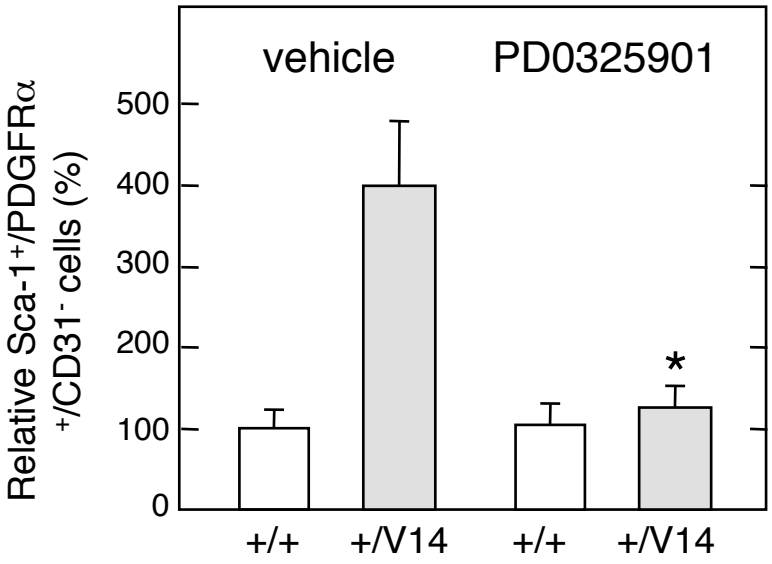

Figure 6 Prenatal treatment with MEK inhibitor PD0325901 prevents the expansion of cardiac stem cells. Relative percentage of Sca-1^{+}/PDGFRα^{+}/CD31^{-} cells in hearts from wild type (+/+, open bars) and K-*Ras*$^{+/V14I}$ (+/V14I, gray bars) P10-14 pups exposed from E7.5 to sacrificed time to vehicle (n=7, n=8, respectively) or PD0325901 (n=3, n=4, respectively)

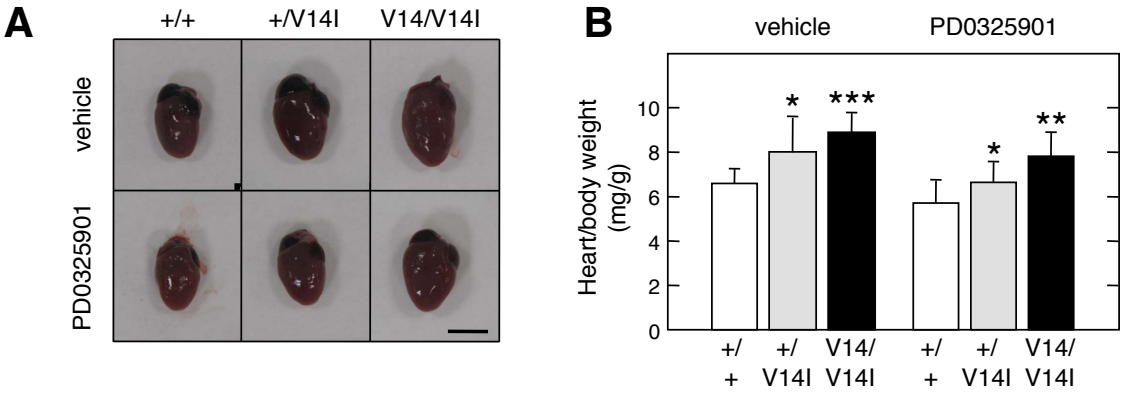

Figure 7 Postnatal treatment with the MEK inhibitor PD0325901 does not correct the cardiac abnormalities in K-*Ras*^{V14I} mice (A) Representative hearts appearance of 4-month-old wild type (+/+), K-*Ras*$^{+/V14I}$ (+/V14I) and K-*Ras*$^{V14I/V14I}$ (V14I/V14I) male mice exposed to vehicle or PD0325901 for 6 weeks starting at P21. Scale bar, 5mm. **(B)** Heart/Body weight ratio of 4-month-old wild type (+/+, open bars), K-*Ras*$^{+/V14I}$ (+/V14I, gray bars) and K-*Ras*$^{V14I/V14I}$ (V14I, solid bars) male mice exposed for 6 weeks starting at P21 to vehicle (n=9, n=10; n=10, respectively) or PD0325901 inhibitor (n=9, n=11; n=10, respectively). Error bars indicate SD. *P < 0.05; **P< 0.01; ***P < 0.001.

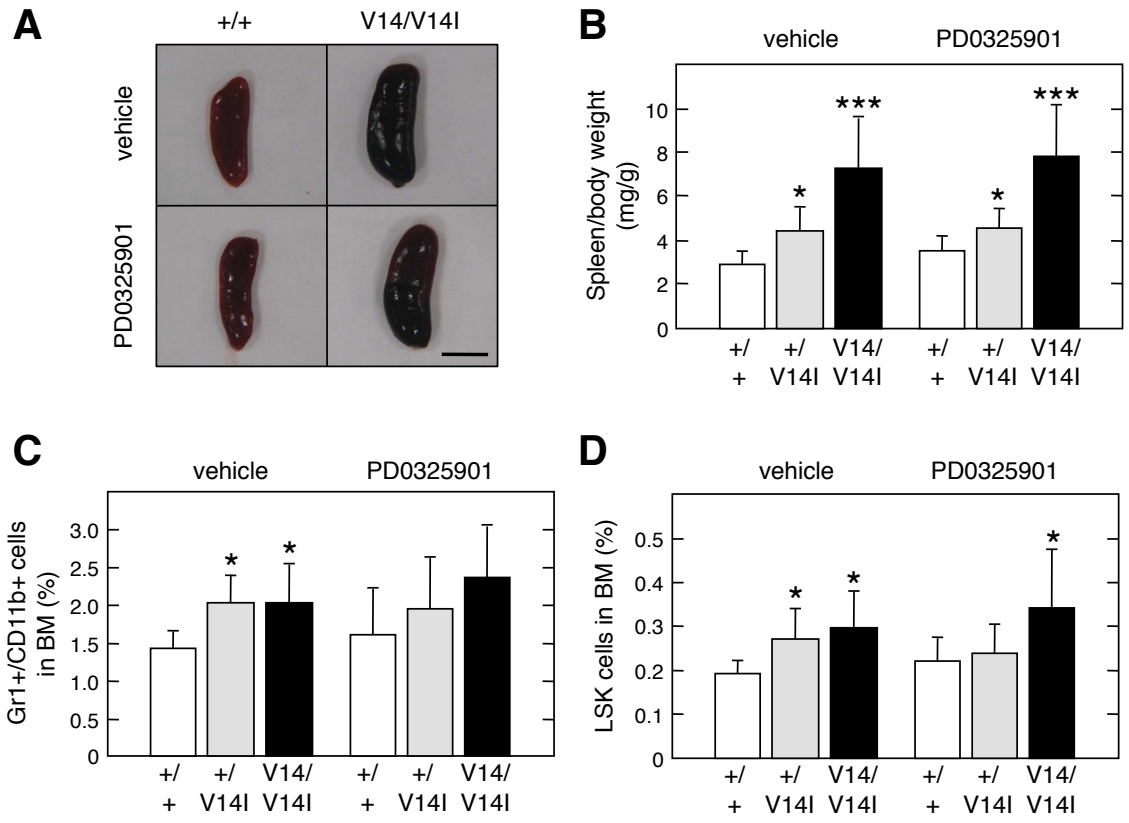

Figure 8 Postnatal treatment with the MEK inhibitor PD0325901 does not correct the hematological disorders in K-*Ras*^{V14I} mice (A) Representative spleen appearance of 4-month-old wild type (+/+) and K-*Ras*$^{V14I/V14I}$ (V14I/V14I) mice exposed to vehicle or PD0325901 for 6 weeks starting at P21. Scale bar, 5mm. **(B)** Spleen/body weight ratio of 4-month-old wild type (+/+, open bars), K-*Ras*$^{+/V14I}$ (+/V14I, gray bars) and K-*Ras*$^{V14I/V14I}$ (V14I/V14I, solid bars) mice exposed for 6 weeks starting at P21 to vehicle (n=9, n=10; n=10, respectively) or PD0325901 inhibitor (n=9, n=11; n=10, respectively). **(C)** Percentages of Gr1^{+}/CD11b^{+} myeloid cells in spleens of 4-month-old wild type (+/+, open bars), K-*Ras*$^{+/V14I}$ (+/V14I, gray bars) and K-*Ras*$^{V14I/V14I}$ (V14I/V14I, solid bars) mice exposed for 6 weeks starting at P21 (n=9, n=8; n=10, respectively) or PD0325901 inhibitor (n=9, n=9; n=10, respectively). **(D)** Percentage of LSK cells in 4 month-old wild type (+/+, open bars), K-*Ras*$^{+/V14I}$ (+/V14I, gray bars) and K-*Ras*$^{V14I/V14I}$ (V14I/V14I, solid bars) mice exposed for 6 weeks starting at P21to vehicle (n=9, n=7; n=8, respectively) or PD0325901 inhibitor (n=8, n=8; n=8, respectively). Error bars indicate SD. *P < 0.05; ***P < 0.001.

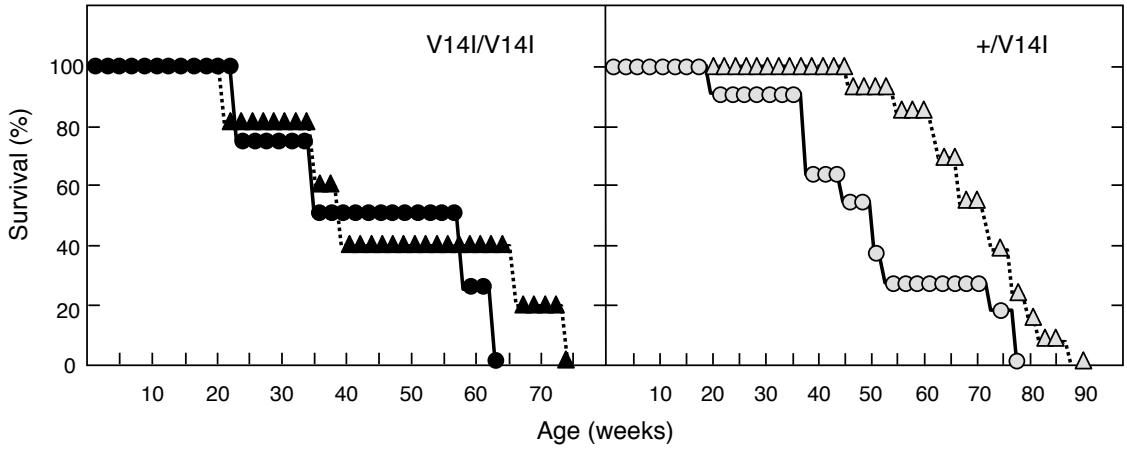

Figure 9. **Postnatal treatment with the MEK inhibitor PD0325901 results in an increased survival in K-*Ras*$^{+/V14I}$ mice**. Left: Survival of K-*Ras*$^{V14I/V14I}$ (V14I/V14I) mice exposed to vehicle for 6 weeks starting at P21 (n=4, solid circles, solid line) or PD0325901 for 6 weeks starting at P21 (n=5, solid triangles, dotted line). Right: Survival of K-*Ras*$^{+/V14I}$ (+/V14I) mice exposed to vehicle for 6 weeks starting at P21 (n=11, gray circles, solid line) or PD0325901 for 6 weeks starting at P21 (n=13, gray triangles, dotted line).

TABLE 1. **Distribution and frequency of RAS mutations in human tumors**

Organ/Tissue	K-*RAS*	H-*RAS*	N-*RAS*
Billiary tract	**25.70%**	0%	2.04%
Breast	1.56%	0.34%	0.58%
Cervix	7.13%	**8.21%**	1.32%
Endometrium	14.64%	0.63%	2.58%
Ganglia (autonomic)	0.49%	0.16%	1.37%
Leukemias & Lymphomas	4.86%	0.25%	**9.64%**
Large intestine	**34.74%**	N/A	3.84%
Liver	3.38%	0.16%	1.32%
Lung	**16.36%**	0.61%	0.66%
Ovary	12.50%	0%	0.86%
Pancreas	**57.52%**	0%	0.76%
Prostate	5.67%	3.34%	0.91%
Skin	2.17%	**7.43%**	**15.54%**
Small intestin	**20.65%**	0%	0%
Soft tissue	4.68%	4.09%	3.93%
Stomach	6.26%	2.01%	1.13%
Testis	3.82%	3.85%	2.83%
Thyroid	2.05%	3.84%	6.42%
Urinary tract	4.34%	**9.85%**	1.16%
Total tumor samples	130480	33460	56321
Positive tumor samples	21,75%	2,86%	5,74%

Data obtained from the Sanger Catalogue of Somatic Mutation in Cancer: http://sangeer.ac.uk/cosmic (September 2013). Values presented as the total percentage of clinical samples analyzed for that particular tumor type. Boldface corresponds to most frequent mutated organ/tissue. N/A=not available.

TABLE 2. **K-*RAS* mutations found in Noonan patients**

Exon	NT substitution	Aa substitution	Diagnosis	References
1	40 G>A	V14I	10 NS	46, 99, 115, 122, 147, 188, 243
1	65 A>G	Q22R	1 NS/severe 1 NS	115, 243
1	77 A>T	N26I	1 NS + lupus erythematosus	118
1	101 C>T	P34L	1 NS	243
1	101 C>A	P34Q	1 NS	243
1	108 A>G	I36M	3 NS	115, 122, 243
2	173 C>T	T58I	1 NS /JMML 1 NS 1NS/ craniosynostosis	104, 147, 188
2	178 G>A	G60S	1 NS/ craniosynostosis	104
2	179 G>T	G60V	NS lethal course	153
3	214 A>C	M72L	1 NS/craniosynostosis 2 NS	26
3	347 A>G	N116S	1 NS	167
4B	455 T>G	V152G	1 NS/CS	33
4B	458 A>T	D153V	1 NS/CFC syndrome 1 NS	33, 188
4B	460 A>T	D153V	2 NS	243
4B	466 T>A	F156I	1 NS/CFC syndrome 1 NS	147, 243

NS: Noonan syndrome; *JMML*: Juvenile Myelomonocytic leukemia; *CS*: Costello syndrome; *CFC syndrome*: cardiofaciocutaneous syndrome.

TABLE 3. Fat and lean content measured using densitometer analysis

		Lean content (g)			
	n	1 month	2 month	3 month	4 month
K-*Ras*$^{+/+}$	4	12.45 ± 3.02	19.42 ± 0.62	22.25 ± 1.09	23.75 ± 0.07
K-*Ras*$^{+/V14I}$	10	9.36 ± 0.84	19.00 ± 1.50	22.53 ± 1.94	24.29 ± 2.23
K-*Ras*$^{V14I/V14I}$	5	7.64 ± 1.30*	17.56 ± 1.01*	21.40 ± 0.74	24.68 ± 1.88
		Fat content (g)			
	n	1 month	2 month	3 month	4 month
K-*Ras*$^{+/+}$	4	1.42 ± 0.55	2.90 ± 0.26	4.00 ± 1.04	6.25 ± 1.58
K-*Ras*$^{+/V14I}$	10	0.95 ± 0.19	2.79 ± 0.50	3.68 ± 0.97	4.77 ± 1.47
K-*Ras*$^{V14I/V14I}$	5	0.76 ± 0.26 *	2.28 ± 0.26	2.46 ± 0.49 *	2.98 ± 0.75 **

Numbers shown are the media ± SD. Statistical significance was assessed by two-tailed Student's test. *P < 0.05.

TABLE 4. Bone Mineral Density (BMD) and Bone Mineral content (BMC) measured using densitometer analysis

	Bone Mineral Density (g/cm^2)				
	n	1 month	2 month	3 month	4 month
K-*Ras*$^{+/+}$	4	0.03 ± 0.004	0.05 ± 0.003	0.05 ± 0.001	0.52 ± 0.001
K-*Ras*$^{+/V14I}$	10	0.03 ± 0.002	0.04 ± 0.002	0.05 ± 0.002	0.05 ± 0.002
K-*Ras*$^{V14I/V14I}$	5	0.03 ± 0.002	0.04 ± 0.002	0.05 ± 0.002	0.05 ± 0.001
	Bone Mineral Content (g)				
	n	1 month	2 month	3 month	4 month
K-*Ras*$^{+/+}$	4	0.16 ± 0.05	0.34 ± 0.03	0.41 ± 0.01	0.43 ± 0.04
K-*Ras*$^{+/V14I}$	10	0.11 ± 0.01	0.35 ± 0.04	0.42 ± 0.03	0.45 ± 0.04
K-*Ras*$^{V14I/V14I}$	5	0.09 ± 0.02 *	0.31 ± 0.02	0.40 ± 0.03	0.46 ± 0.02

Numbers shown are the media ± SD. Statistical significance was assessed by two-tailed Student's test. *P < 0.05.

TABLE 5. Hearing threshold for click stimulation in 4-month-old mice

	n	Hearing threshold for click stimulation (dB SPL)
K-*Ras*$^{+/+}$	8	24 ± 3
K-*Ras*$^{+/V14I}$	7	25 ± 4
K-*Ras*$^{V14I/V14I}$	4	29 ± 5

Numbers shown are the media ± SD. dB SPL, decibel Sound Pressure Levels.

TABLE 6. MRI heart parameters of 4-month-old males

	4 months						
	K-*Ras*$^{+/+}$ (n=5)	**K-*Ras*$^{+/V14I}$ (n=4)**	**K-*Ras*$^{V14I/V14I}$ (n=3)**	**p value +/+ *vs* +/V14I**		**p value +/+ *vs* V14I/V14I**	
LVM (mg)	68.40 ± 19.06	84.75 ± 23.10	112 ± 10.82	0.2815	NS	0.0120	*
WTd (mm)	0.85 ± 0.08	0.86 ± 0.37	0.90 ± 0.13	0.5952	NS	0.5024	NS
WTs (mm)	1.32 ± 0.13	1.35 ± 0.22	1.59 ± 0.20	0.7763	NS	0.0152	*
WTn (%)	46.68 ± 7.46	48.03 ± 16.52	68.48 ± 9.18	0.8733	NS	0.0079	**
EDV (µl)	44.40 ± 13.89	55.25 ± 15.78	74 ± 10.39	0.3084	NS	0.0196	**
ESV (µl)	13.40 ± 5.37	17.75 ± 9.64	20.33 ± 3.51	0.4160	NS	0.0968	NS
FS (%)	55.09 ± 6.84	55.59 ± 19.06	79.07 ± 19.75	0.9583	NS	0.0458	*
EF (%)	70.2 ± 5.17	69.50 ± 8.06	73.00 ± 2.65	0.8782	NS	0.4256	NS
HR (bpm)	411.2 ± 39.11	394 ± 60.42	466.67 ± 20.43	0.6196	NS	0.0671	NS
CO (ml/min)	12.5 ± 2.91	14.9 ± 4.66	24.97 ± 2.65	0.4228	NS	0.0011	**

LVM: left ventricle mass; WTd: wall thicknesses in diastole, WTs: wall thicknesses in systole; WTn: systolic wall thickening; EDV: end diastolic volume; ESV: end systolic volume; FS: fractional shortening; EF: ejection fraction; HR: hear rate; CO: cardiac output. Numbers shown are the media ± SD. Statistical significance was assessed by two-tailed Student's t-test. *P < 0.05; **P < 0.01; ***P < 0.001; NS, not significant.

TABLE 7. Blood cell counts of 4-month-old mice

	K-*Ras*$^{+/+}$ (n=10)	**K-*Ras*$^{+/V14I}$** (n=15)	**K-*Ras*$^{V14I/V14I}$** (n=10)	**p value +/+ *vs* +/V14I**		**p value +/+ *vs* V14I/V14I**	
WBC (10^9/l)	9.76 ± 3.12	12.16 ± 2.15	16.77 ± 5.57	0.0825	NS	0.0100	**
LYM (10^9/l)	8.43 ± 2.91	8.53 ± 1.86	7.37 ± 2.94	0.9363	NS	0.5148	NS
MID (10^9/l)	0.43 ± 0.26	0.53 ± 0.31	0.83 ± 0.87	0.5316	NS	0.3306	NS
GRA (10^9/l)	0.81 ± 0.39	2.28 ± 2.14	8.87 ± 4.97	0.0747	NS	0.0122	*
RBC (10^{12}/l)	9.36 ± 0.33	9.07 ± 1.47	6.21 ± 2.08	0.1441	NS	0.0010	***
PLT (10^9/l)	714 ± 265	547.7 ± 276	344.5 ± 129	0.2557	NS	0.1009	NS

WBC: white blood cells; LYM: lymphocytes; MID: monocytes and some eosinophiles; GRA: granulocytes; RBD: red blood cells; PLT: platelets. Numbers shown are the media ± SD. Statistical significance was assessed by two-tailed Student's t-test. *P < 0.05; **P < 0.01; ***P < 0.001; NS, not significant.

TABLE 8. Blood cell counts of animals transplanted with BM cells

	K-*Ras*$^{+/+}$ (n=20)	K-*Ras*$^{+/V14I}$ (n=14)	p value +/+ *vs* V14I	
WBC (10^9/l)	8.85 ± 3.69	10.17 ± 2.88	0.2737	NS
LYM (10^9/l)	6.53 ± 2.89	5.17 ± 1.88	0.1228	NS
MID (10^9/l)	0.30 ± 0.37	0.28 ± 0.19	0.9046	NS
GRA (10^9/l)	2.12 ± 0.83	4.72 ± 1.75	<0.0001	***
RBC (10^{12}/l)	8.66 ± 1.09	5.96 ± 1.77	<0.0001	***
PLT (10^9/l)	766 ± 382	209 ± 211	0.0006	***

Values from mice sacrificed between 30 to 34 weeks after transplantation. WBC: white blood cells; LYM: lymphocytes; MID: monocytes and some eosinophils; GRA: granulocytes; RBD: red blood cells; PLT: platelets. Animals transplanted with wild-type cells were sacrificed at the same age. Numbers shown are the media ± SD. Statistical significance was assessed by two-tailed Student's t-test. ***P < 0.001; NS, not significant.

TABLE 9. Viable progeny from matings between K-*Ras*$^{+/V14I}$ mice in the different pure genetic backgrounds

Stage	n	K-*Ras*$^{+/+}$	K-*Ras*$^{+/V14I}$	K-*Ras*^{V14I}
		C57BL/6J (F5)		
P0	14	4 (28%)	10 (71%)	0 (0%)
P21	50	21 (42%)	29 (58%)	0 (0%)
		129S2/Sv (F5)		
P21	100	33 (33%)	54 (54%)	13 (13%)

TABLE 10. Morphometric measurements of skulls from 4-month-old C57BL/6J and 129S2/Sv mice

	C57BL/6J mice (F5)			
	K-*Ras*$^{+/+}$ (n=6)	**K-*Ras*$^{+/V14I}$** (n=7)	**p value +/+ *vs* +/V14I**	
Length (mm)	23.72 ± 0.28	23.51 ± 0.50	0.3798	NS
Width (mm)	9.59 ± 0.15	9.77 ± 0.25	0.1585	NS
Height (mm)	5.71 ± 0.09	6.06 ± 0.35	0.0458	*
Volume (mm^3)	367.08 ± 16.6	425.48 ± 18.71	<0.0001	***

	129S2/Sv mice (F5)						
	K-*Ras*$^{+/+}$ (n=5)	**K-*Ras*$^{+/V14I}$** (n=4)	**K-*Ras*$^{V14I/V14I}$** (n=7)	**p value +/+ *vs* +/V14I**		**p value +/+ *vs* V14I/V14I**	
Length (mm)	22.77 ± 0.27	23.01 ± 0.68	20.97 ± 0.90	0.4779	NS	0.0013	**
Width (mm)	9.42 ± 0.12	9.70 ± 0.32	10.22 ± 0.21	0.1191	NS	<0.0001	***
Height (mm)	5.81 ± 0.19	6.02 ± 0.34	6.56 ± 0.18	0.2692	NS	<0.0001	***
Volume (mm^3)	337.58 ± 28.5	395.37 ± 27.4	394.93 ± 16.4	0.0179	*	0.0013	**

Morphometric measurements from micro-CT scans of the skulls of a cohort of 4-month-old mice (see Figure 1D for skull images). Numbers shown are the media ± SD. Statistical significance was assessed by two-tailed Student's t-test. *P < 0.05; **P < 0.01; ***P < 0.001; NS, not significant.

TABLE 11. Blood cells counts of 4-month-old C57BL/6J and 129S2/Sv mice

	C57BL/6J mice (F5)			
	K-*Ras*$^{+/+}$ (n=6)	**K-*Ras*$^{+/V14I}$** (n=11)	**p value +/+ *vs* +/V14I**	
WBC (10^9/L)	9.96 ± 0.14	13.80 ± 5.56	0.1413	NS
LYM (10^9/L)	8.42 ± 2.96	10.71 ± 5.36	0.3505	NS
MID (10^9/L)	0.38 ± 0.44	0.38 ± 0.18	0.9969	NS
GRA (10^9/L)	1.17 ± 0.41	2.71 ± 1.56	0.0089	**
RBC (10^{12}/L)	10.62 ± 1.03	8.38 ± 1.26	0.0022	**
PLT (10^9/L)	959.6 ± 425.1	230.0 ± 163.3	0.0142	*

	129S2/Sv mice (F5)					
	K-*Ras*$^{+/+}$ (n=9)	**K-*Ras*$^{+/V14I}$** (n=10)	**K-*Ras*$^{V14I/V14I}$** (n=6)	**p value +/+ *vs* +/V14I**		**p value +/+ *vs* V14I/V14I**	
WBC (10^9/L)	7.33 ± 2.19	9.07 ± 2.76	15.64 ± 7.04	0.1510	NS	0.0332	*
LYM (10^9/L)	6.13 ± 1.73	7.57 ± 2.78	8.84 ± 3.83	0.1995	NS	0.1530	NS
MID (10^9/L)	0.19 ± 0.12	0.29 ± 0.15	0.90 ± 0.74	0.1369	NS	<0.0981	NS
GRA (10^9/L)	1.02 ± 0.69	1.21 ± 0.59	6.04 ± 5.17	0.5173	NS	0.0630	NS
RBC (10^{12}/L)	10.43 ± 1.68	10.85 ± 0.88	10.36 ± 0.67	0.9241	NS	0.4952	NS
PLT (10^9/L)	305.0 ± 153.7	363.89 ± 190.7	182.67 ± 147	0.3721	NS	0.2247	NS

WBC: white blood cells; LYM: lymphocytes; MID: monocytes and some eosinophiles; GRA: granulocytes; RBD: red blood cells; PLT: platelets. Numbers shown are the media ± SD. Statistical significance was assessed by two-tailed Student's t-test.

*P < 0.05; **P < 0.01; ***P < 0.001; NS, not significant.

TABLE 12 Summary of pathological alterations found in K-*Ras*$^{V14I/V14I}$ and K-*Ras*$^{+/V14I}$ mice

K-*Ras*$^{+/V14I}$ mice (AVB line)

Mouse ID	Sex	Age at death (weeks)	Spleen/ BW	WBC (10^9/L)	LYM (10^9/L)	MID (10^9/L)	GRA (10^9/L)	RBC (10^{12}/L)	PLT (10^9/L)	Pathology
218	M	109	31.9	8.36	4.65	0.72	2.99	2.35	1173	Lymphoma, lung adenoma and adenocarcinoma
172	F	97	24.8	12.94	3.49	0.56	8.89	7.85	274	Histiocytic sarcoma
162	M	90	7.1	ND	ND	ND	ND	ND	ND	Lung adenocarcinoma. Adenoma and adenocarcinoma in liver
224	M	83	5.2	7.54	1.65	0.41	5.84	8.97	1489	Lymphoma
207	F	83	30.0	ND	ND	ND	ND	ND	ND	Lymphoma and histiocytic sarcoma
384	F	83	46.1	ND	ND	ND	ND	ND	ND	Lymphoma
247	F	82	42.4	9.53	2.93	0.58	6.01	6.73	593	Histiocytic sarcoma
271	M	78	10.7	17.66	11.10	0.41	6.16	8.94	1429	Tubular adenoma in duodenum. Hydronephrosis
230	M	77	8.5	ND	ND	ND	ND	ND	ND	Lymphoma and hepatocarcinoma. Adenoma in epididymis
354	M	77	9.5	16.53	9.52	0.12	6.89	8.99	786	Lymphoma and vasculitis
199	M	76	3.2	5.86	3.65	0.12	2.09	9.3	1371	B cell lymphoma
345	F	75	41.8	16.4	9.52	0.10	6.78	3.88	472	Lymphoma and intestinal adenoma
216	M	73	53.2	14.5	8.14	0.52	5.83	3.87	283	Myeloproliferative disorder (MPD)
310	F	68	43.8	6.11	2.89	0.51	2.71	1.34	45	Histiocytic sarcoma
279	F	65	26.1	10.65	2.92	0.62	7.11	5.72	450	Lymphoma
276	M	63	34.6	11.66	6.4	0.31	4.96	6.19	565	Lymphoma and angiosarcoma. Areas of infarctation in the heart
333	M	62	43.9	ND	ND	ND	ND	ND	ND	Histiocytic sarcoma
357	F	60	18.0	12.22	7.16	0.29	4.77	6.86	336	B cell lymphoma and systemic vasculitis
342	F	59	35.2	ND	ND	ND	ND	ND	ND	Lymphoma
222	F	57	11.1	16.21	10.46	0.66	5.09	7.14	877	B cell lymphoma and systemic vasculitis
329	F	37	8.1	8.08	5.98	0.13	1.98	6.54	460	Lymphoma
595	F	32	161.7	29.79	12.49	1.47	15.83	3.88	49	Myeloid Leukemia
509	M	31	37.0	18.97	9.16	1.51	8.31	5.28	786	Myeloproliferative disorder (MPD)
344	F	27	40.2	32.22	3.37	1.14	27.7	5.96	174	Myeloid Leukemia. Acute glomerulonephritis. Adenoma in doudenum
487	F	26	29.6	ND	ND	ND	ND	ND	ND	Lymphoblastic lymphoma
766	F	26	22.5	20.52	9.33	0.32	10.87	9.10	646	Lymphoma. Areas of infarctation in the heart

Table 12 continuation

K-*Ras*$^{V14I/V14I}$ mice (AVB line)										
Mouse ID	**Sex**	**Age at death (weeks)**	**Spleen/ BW**	**WBC (10^9/L)**	**LYM (10^9/L)**	**MID (10^9/L)**	**GRA (10^9/L)**	**RBC (10^{12}/L)**	**PLT (10^9/L)**	**Pathology**
275	M	65	36.9	23.8	14.57	1.28	7.94	6.95	472	Lymphoma and myeloproliferative disorder. Hydronephrosis
349	F	55	30.5	24.9	11.51	1.55	11.83	7.86	289	Lymphoma. Hydronephrosis
246	M	52	34.5	38.01	9.98	2.88	25.15	6.55	472	Myeloproliferative disorder. Areas of infarctation in the heart. Pyelonephritis
640	M	51	34.2	ND	ND	ND	ND	ND	ND	Histiocytic sarcoma and lymphoma.
402	F	41	49.2	ND	ND	ND	ND	ND	ND	Histiocytic sarcoma
374	F	37	154.6	39.35	16.32	2.08	20.95	3.31	280	Lymphoma and myeloproliferative disorder. Tumor in adenohypophysis
579	F	33	46.5	36.90	12.65	2.13	22.12	4.01	550	Lymphoma
683	M	30	9.6	ND	ND	ND	ND	ND	ND	Lymphoma. Pyelonephritis and nephropathy
448	M	26	14.3	9.49	3.77	0.34	5.38	7.7	675	Pyelonephritis and hydronephrosis
455	M	26	19.7	11.46	2.82	0.35	8.29	4.6	200	Lymphoma. Pyelonephritis
846	M	19	54.4	ND	ND	ND	ND	ND	ND	Histiocytic sarcoma and lymphoma
426	F	17	32.6	7.93	2.89	0.26	4.78	6.77	498	Myeloproliferative disorder. Glomerulonephritis and pyelonephritis

M: male; F: female. Spleen/BW: spleen weight (mg)/ body weight (g). WBC: white blood cells [4-12]; LYM: lymphocytes [2-9]; MID: monocytes and some eosinophils [<0.6]; GRA: granulocytes [0.7-6]; RBD: red blood cells [9-15]; PLT: platelets [250-750]. ND: not determined. Numbers inside the brackets are the reference values.

TABLE 13. Summary of tumors observed in K-*Ras*^{V14I}; *p16Ink4a/p19Arf*$^{-/-}$ and K-*Ras*$^{+/V14I}$; *p16Ink4a/p19Arf*$^{-/-}$mice

K-*Ras*^{V14I}; *p16Ink4a/p19Arf*$^{-/-}$ mice (BYP line)				
Mouse ID	**Sex**	**Age at death (weeks)**	**Spleen/BW**	**Tumor type**
191	F	23	42.4	Histiocytic sarcoma
170	F	23	34.2	Histiocytic sarcoma
174	M	20	30.6	Histiocytic sarcoma and lymphoma
181	F	20	28.5	Histiocytic sarcoma
179	M	19	39.5	Histiocytic sarcoma
167	M	18	56.9	Histiocytic sarcoma and B-cell lymphoma
199	F	17	60.1	Histiocytic sarcoma and thymus lymphangioma
189	F	16	51.7	Lymphoma

Table 13 continuation

K-*Ras*$^{+/V14I}$; *p16Ink4a/p19Arf*$^{-/-}$ mice (BYP line)				
Mouse ID	**Sex**	**Age at death (weeks)**	**Spleen/BW**	**Tumor type**
148	F	37	40.7	Histiocytic sarcoma
154	F	30	4.9	Histiocytic sarcoma and lymphoma
159	M	30	48.2	Histiocytic sarcoma and B cell lymphoma
123	F	27	66.4	Histiocytic sarcoma
128	F	27	93.9	Histiocytic sarcoma
149	F	25	34.7	Histiocytic sarcoma
109	M	23	32.8	Fibrosarcoma
183	F	23	62.4	Histiocytic sarcoma and lymphoma
144	M	22	45.3	Histiocytic sarcoma
184	F	22	51.7	Sarcoma

M: male; F: female. Spleen/BW: spleen weight (mg)/ body weight (g).

TABLE 14. Summary of tumors observed in the K-*Ras*$^{+/V14I}$; *Trp53*$^{-/-}$ mice

K-*Ras*$^{+/V14I}$; *Trp53*$^{-/-}$ mice (BOG line)				
Mouse ID	**Sex**	**Age at death (weeks)**	**Spleen/BW**	**Tumor type**
133	M	20	12.8	Lymphoma and angiosarcoma
136	M	19	74.2	Lymphoma and angiosarcoma
128	F	18	60.3	B cell lymphoma and angiosarcoma
40	M	16	36.9	Lymphoma, heart angiosarcoma and PIN
67	M	15	21.8	Angiosarcoma
110	M	15	25.7	B cell lymphoma, lymphoblastic lymphoma in thymus and brain tumor
38	M	15	40.6	Lymphoma and heart angiosarcoma
162	M	15	5.6	Lymphoblastic lymphoma, angiosarcoma and hemangioma
138	M	14	18.1	Lymphoma and angiosarcoma
125	M	11	51.3	T cell lymphoma

M: male and F: female. Spleen/BW: spleen weight (mg)/ body weight (g).

TABLE 15 Progeny from matings between K-*Ras*$^{+/V14I}$; p53$^{-/-}$ and K-*Ras*$^{+/V14I}$; p53$^{+/-}$ mice

Stage	n	Progeny from matings between K-*Ras*$^{+/V14I}$; p53$^{-/-}$ and K-*Ras*$^{+/V14I}$; p53$^{+/-}$ mice					
		K-*Ras*$^{+/+}$; p53$^{+/-}$	K-*Ras*$^{+/V14}$; p53$^{+/-}$	K-*Ras*$^{V14I/V14I}$; p53$^{+/-}$	K-*Ras*$^{+/+}$; p53$^{-/-}$	K-*Ras*$^{+/V14}$; p53$^{-/-}$	K-*Ras*$^{V14I/V14I}$; p53$^{-/-}$
E18.5	24	2 (8%)	10 (42%)	4 (17%)	2 (8%)	4 (17%)	2 (8%)
P0	23	2 (9%)	6 (26%)	3 (13%)	4 (17%)	6 (26%)	2 (DIC) (9%)
P21	103	27 (26%)	29 (28%)	3 (3%)	16 (16%)	28 (27%)	0 (0%)

Progeny is indicated. Numbers in parentheses indicate the percentage of embryos or mice compared with the analyzed total number.

DIC: Dead in cage.

TABLE 16 Blood cells counts of K-*Ras*$^{+/LSLV14I}$; *RERTn*$^{ert/ert}$; *Pi3kca*$^{+/LmgLH1047R}$ and K-*Ras*$^{+/+}$; *RERTn*$^{ert/ert}$; *Pi3kca*$^{+/LmgLH1047R}$ sacrificed at humane end point

K-*Ras*$^{+/LSLV14I}$; *RERTn*$^{ert/ert}$; *Pi3kca*$^{+/LmgLH1047R}$ mice (MJA line)								
Mouse ID	Sex	Age at death (weeks)	WBC (10^9/L)	LYM (10^9/L)	MID (10^9/L)	GRA (10^9/L)	RBC (10^{12}/L)	PLT (10^9/L)
52	M	86	3.75	2.27	0.03	1.45	8.55	1316
37	M	83	9.82	4.55	0.24	5.03	11.27	1528
44	M	77	11.70	8.68	0.27	2.75	9.73	580
53	F	69	15.53	4.88	0.13	10.52	7.76	102
K-*Ras*$^{+/+}$; *RERTn*$^{ert/ert}$; *Pi3kca*$^{+/LmgLH1047R}$ mice (MJA line)								
Mouse ID	Sex	Age at death (weeks)	WBC (10^9/L)	LYM (10^9/L)	MID (10^9/L)	GRA (10^9/L)	RBC (10^{12}/L)	PLT (10^9/L)
36	M	83	9.44	3.50	1.08	4.86	7.13	741
57	F	82	10.38	7.94	0.07	2.37	8.30	40
46	F	61	17.36	13.03	0.53	3.80	6.10	116
53	F	69	15.53	4.88	0.13	10.52	7.76	102

M: male; F: female. WBC: white blood cells [4-12]; LYM: lymphocytes [2-9]; MID: monocytes and some eosinophils [<0.6]; GRA: granulocytes [0.7-6]; RBD: red blood cells [9-15]; PLT: platelets [250-750]. Numbers inside the brackets are the reference values.

TABLE 17. Morphometric measurements of skulls of 4-month-old mice treated from E7.5 to P21 with either vehicle or the MEK inhibitor PD0325901

	Vehicle						
	K-*Ras*$^{+/+}$ (n=4)	**K-*Ras*$^{+/V14I}$** (n=5)	**K-*Ras*$^{V14I/V14I}$** (n=5)	**p value +/+ *vs* +/V14I**		**p value +/+ *vs* V14I/V14I**	
Length (mm)	24.10 ± 0.52	24.19 ± 0.21	22.73 ± 0.72	0.7561	NS	0.0154	*
Width (mm)	9.66 ± 0.09	9.65 ± 0.18	9.99 ± 0.26	0.9769	NS	0.0411	*
Height (mm)	5.62 ± 0.13	5.61 ± 0.04	6.48 ± 0.30	0.9155	NS	0.0012	*
Volume (mm^3)	359.41 ± 22.8	372.84 ± 29.6	418.47 ± 8.37	0.4816	NS	0.0009	***
	PD0325901						
	K-*Ras*$^{+/+}$ (n=5)	**K-*Ras*$^{+/V14I}$** (n=6)	**K-*Ras*$^{V14I/V14I}$** (n=9)	**p value +/+ *vs* +/V14I**		**p value +/+ *vs* V14I/V14I**	
Length (mm)	23.59 ± 0.30	23.64 ± 0.40	23.39 ± 0.41	0.8249	NS	0.2431	NS
Width (mm)	9.50 ± 0.08	9.51 ± 0.26	9.54 ± 0.31	0.8808	NS	0.8651	NS
Height (mm)	5.52 ± 0.23	5.64 ± 0.26	5.65 ± 0.21	0.4233	NS	0.9445	NS
Volume (mm^3)	343.06 ± 29.0	360.38 ± 36.4	345.19 ± 45.6	0.3998	NS	0.4759	NS

Morphometric measurements from micro-CT scans of a cohort of 4-month-old mice treated with vehicle and MEK inhibitor PD0325901 from E7.5 to P21. Numbers shown are the media ± SD. Statistical significance was assessed by two-tailed Student's t-test. *P < 0.05; **P < 0.01; NS, not significant.

TABLE 18. Morphometric measurements of skulls from 4 month-old mice treated either with vehicle or with the MEK inhibitor PD0325901 from P21 during 6 weeks.

	Vehicle						
	K-*Ras*$^{+/+}$ (n=5)	**K-*Ras*$^{+/V14I}$** (n=7)	**K-*Ras*$^{V14I/V14I}$** (n=6)	**p value +/+ *vs* +/V14I**		**p value +/+ *vs* V14I/V14I**	
1. Length (mm)	24.12 ± 0.45	23.78 ± 0.29	22.72 ± 0.65	0.1460	NS	0.0079	**
2. Width (mm)	9.65 ± 0.08	9.73 ± 0.18	9.96 ± 0.24	0.3530	NS	0.0228	*
3. Height (mm)	5.63 ± 0.11	5.68 ± 0.23	6.51 ± 0.29	0.6531	NS	0.0001	***
4. Volume (mm^3)	358.23 ± 19.9	375.31 ± 27.4	410.64 ± 28.3	0.2650	NS	0.0074	**
	PD0325901						
	K-*Ras*$^{+/+}$ (n=5)	**K-*Ras*$^{+/V14I}$** (n=9)	**K-*Ras*$^{V14I/V14I}$** (n=4)	**p value +/+ *vs* +/V14I**		**p value +/+ *vs* V14I/V14I**	
1. Length (mm)	23.92 ± 0.21	23.93 ± 0.24	22.42 ± 0.92	0.9404	NS	0.0448	*
2. Width (mm)	9.37 ± 0.27	9.52 ± 0.29	9.93 ± 0.37	0.3794	NS	0.0346	*
3. Height (mm)	5.50 ± 0.16	5.50 ± 0.20	6.36 ± 0.28	0.9668	NS	0.0006	***
4. Volume (mm^3)	329.04 ± 30.0	358.32 ± 36.7	389.31 ± 36.5	0.1914	NS	0.0609	NS

Morphometric measurements from micro-CT scans of a cohort of 4 month-old mice treated with vehicle and PD0325901 MEK inhibitor from P21 during 6 weeks. Numbers shown are the media ± SD. Statistical significance was assessed by two-tailed Student's t-test. *P < 0.05; **P < 0.01; NS, not significant.

APPENDIX II

Publications